

PHOTOSTABILITY AND THE BOPHY ARCHITECTURE



Owen Woodford

Molecular Photonics Laboratory

School of Natural and Environmental Sciences (Chemistry)

Newcastle University

Project Supervisor: Prof. Anthony Harriman

This dissertation is submitted in fulfilment of the degree:

Doctor of Philosophy

April 2018

Abstract

Organic molecules offer the potential to harvest solar energy and underpin diverse optoelectronic applications, including fluorescent imaging techniques, OLEDs and chemical sensing. A critical factor in such technological advances concerns the stability of the dyes under continuous exposure to light. Indeed, photobleaching of fluorescence dyes is exploited in super-resolution microscopy and in measuring diffusion coefficients by way of FRAP. In other cases, such as photodynamic therapy, it is desirable that the organic sensitizer is destroyed at the conclusion of the operation. In general, however, photobleaching hinders innovative and progressive developments in the field of applied photochemistry. An important premise of this thesis is that the logical design of improved systems requires a deep understanding of the kinetics and mechanisms of photobleaching events.

To begin to understand photodegradation a model compound, Erythrosine, which is known to bleach quickly is studied. It is a water-soluble, halogenated xanthene dye used in foodstuffs that has a near unity quantum yield for triplet formation. Further interest in this dye stems from the cost of approving new materials through regulatory testing, which can be prohibitive for consumer products. The solution is to use commercial reagents already on the market. Erythrosine bleaches rapidly under monochromatic illumination, allowing determination of the effects of temperature and concentration on the efficacy of the bleaching step and identification of rate-limiting conditions. It has been possible to estimate a quantum yield for bleaching under illumination at 523 nm. The mechanism appears fully consistent with singlet oxygen playing a key role in the bleaching chemistry.

To be usefully photostable, logically, dyes should be resistant to intersystem crossing to the triplet manifold. We first detail the photophysical properties of such a dye, BOPHY, a new class of organic dyes derived from the ever-popular BODIPY family. Advantages of BOPHY include facile synthesis, easy derivatization and the ability to extend the conjugation length. The parent BOPHY shows poor mirror symmetry between absorption and fluorescence spectra, which was unexpected for such a simple chromophore displaying very high levels of fluorescence. Temperature dependence studies, high-resolution NMR and the use of polymeric host materials have been exploited to explain the underlying optical transitions associated with simple BOPHY derivatives. Using iodomethane as external heavy-atom spin perturber, phosphorescence could be detected at 77K.

The BOPHY chromophore can be extended to produce linear molecules with widely-spaced terminals. One such derivative (BOPHY-DMA), having *N,N*-dimethylamino groups at both ends, has been examined to establish the level of electronic communication along the molecular backbone. A difference was found for the pK_a values for successive protonation of

the amino sites while partial oxidation of the dye allows further characterisation of the electronic properties. Other BOPHY derivatives studied here include a conjugated BOPHY equipped with polyethylene glycol solubilizing functions and a BOPHY-perylene dyad. The latter compound is an attempt to expand the conjugation pathway by fusing together BOPHY with ethynylperylene with the objective of establishing if the resultant supermolecule possesses individual or composite electronic properties.

Returning to the issue of photostability, critical examination was made of the parent BOPHY dye and also of BOPHY-DMA in both plastic films and organic solvents. Broadband illumination was used to simulate exposure to sunlight. Disparate behaviour was found according to the nature of the compound and the surrounding medium. In plastic films, the bleaching mechanism involves a contribution from auto-catalysis. The extended BOPHY-DMA bleaches at a significantly faster rate than does the parent BOPHY. This situation continues in cyclohexane solution where the rate of bleaching of BOPHY-DMA is some 700-fold greater than that of the parent. Reducing the fluorescence lifetime offers a route to increasing stability of the dye. This is realized for BOPHY-DMA because of the inherent dipolar characteristics of this dye. Thus, the rate of bleaching is some 900-fold slower in acetonitrile compared to cyclohexane. Remarkably, both BOPHY and BOPHY-DMA are stabilised by toluene and NMR spectroscopy was used to aid understanding of this effect. Stacking between solvent and chromophore minimises close contact between solute molecules and thereby eliminate the auto-catalytic step.

Industry makes heavy use of stabilisers and has developed a range of anti-oxidants for protecting fragile molecules against attack by free radicals. For the stabilizer to be effective with excited states, we need covalently-linked molecular dyads. This was achieved by attaching butylated hydroxyl toluene (BHT) groups to BOPHY. Rates of photobleaching of the chromophore can be related to the photophysical properties recorded in a series of solvents. Our results implicate light-induced charge transfer from BHT to BOPHY as being responsible for shortening the excited-state lifetime. There is a beneficial effect of the anti-oxidant in terms of photostability in polar environments. A complex autocatalytic mechanism is found in non-polar solvents.

Acknowledgements

This thesis is dedicated to the memory of my grandfather Prof. John Willmott.

I would like to acknowledge the support of my family of the past three years. My parents for their help and my own family for their understanding throughout this process. I could not have done without them.

I would also like to thank my uncle, Prof. Philip Willmott and his family for their added support, it was greatly appreciated.

This work would not have been possible without the help of colleagues and collaborators who are noted throughout the text. Dr Raymond Ziessel is especially thanked for providing many of the materials. Fellow MPL members, Patrycja Stachelek and in particular Joshua Karlsson were a great help and it was a pleasure to work with them over these three years. Again, it would not have been possible to achieve all of this without their help. Dr. Dumitru Sirbu, also of the MPL is also thanked in the highest possible manner. He provided new materials and gave me much assistance in the most basic techniques of chemistry which are beyond my skills and knowledge and for entering into many lively discussions.

Lastly, I will remain forever indebted to Professor Anthony Harriman for, first, this opportunity and then his supervision over these three years. He provides endless wisdom and knowledge both with regards to photophysics and to the academic process and of course I could not have completed this work without his guidance.

Publications Associated with this Thesis

Chapter 3. Karlsson, J. K., Woodford, O. J., Al-Aqar, R. A. and Harriman, A., 2017. Effects of Temperature and Concentration on the Rate of Photo-bleaching of Erythrosine in Water. *The Journal of Physical Chemistry A*. 121 (45), pp. 8569-8576.

Chapter 5. Woodford, O. J., Harriman, A. et al. End-to-end communication in a linear supermolecule with a BOPHY centre and N,N-dimethylanilino-based terminals. 2018. *New Journal of Chemistry*, 42, 4835-4842.

Chapter 6. Woodford, O. J., Wills, C., McFarlane, W., Harriman, A. Dramatic Effect of Solvent on the Rate of Photobleaching of Organic Pyrrole-BF₂ (BOPHY) Dyes. 2018. *ChemPhotoChem*. 1 (7), pp. 317-325.

Chapter 7. (Submitted). Woodford, O.J., Ziesel, R., Harriman, A. Photo-fading of an extended BOPHY Chromophore Dispersed in PMMA as a Chemical Actinometer. *ChemPhotoChem*.

Chapter 8. Sirbu, D., Woodford, O. J., Benniston, A., Harriman, A. Photocatalysis and Self-catalyzed Photobleaching with Covalently-Linked Chromophore-Quencher Conjugates Built Around BOPHY. 2018. *Photochemical and Photobiological Sciences*.

Further Publications Associated with these Studies

Karlsson, J.K., Woodford, O.J., Mustroph, H. and Harriman, A., 2018. Cyanine dyes as ratiometric fluorescence standards for the far-red spectral region. *Photochemical & Photobiological Sciences*, 17 (1), pp. 99-106.

Hall, MJ. et al. Circularly Polarised Luminescence from Helically Chiral "Confused" N,N,O,C-Boron-Chelated Dipyrromethenes (BODIPYs). 2017. *ChemPhotoChem*, 1 (11), pp. 513-517

Table of Contents

Abstract.....	i
Acknowledgements.....	iii
Publications Associated with this Thesis.....	iv
Chapter 1: Introduction.....	p1
1.1 Poor Photostability Creates Opportunities for Novel Research	
1.2 Photosynthesis – Lessons from Nature	
1.2.1 Non-Photochemical Quenching in Photosynthesis	
1.2.2 Reactive Oxygen Species (ROS) in Oxygen	
1.2.3 Self-Repair	
1.3 Bio-Hybrid Systems	
1.4 Examples of Artificial systems	
1.4.1 Application 1 - Luminescent Solar Collectors	
1.4.2 Application 2 - Organic Photovoltaics	
1.4.3 Application 3 - Fluorescence Microscopy	
1.5 Photostability in the Context of this Thesis	
Chapter 2: Experimental Methods.....	p23
2.1 Absorption Spectroscopy	
2.2 Fluorescence Measurements	
2.2.1 Steady-State Fluorescence Measurements	
2.2.2 Temperature Controlled Spectroscopy	
2.3 Fluorescence Lifetime Measurements	
2.3.1 Time Correlated, Single Photon Counting	
2.3.2 Frequency Domain Lifetime Measurements	
2.4 Transient Absorption Spectroscopy	
2.5 Photobleaching Protocols	
2.5.1 Photostability under Continuous Illumination	
2.5.2 Fluorescence Recovery after Photobleaching	
2.5.3 Preparation of Samples in Solid Matrices	
2.6 Electrochemistry	
2.7 Nuclear Magnetic Resonance Spectroscopy	

2.8 IR Spectroscopy
2.9 Thermal Blooming
2.10 Mass Spectroscopy
2.12 Analytical Methods
2.13 Materials

Chapter 3: Probing the Photostability of Erythrosine.....p41

3.1 Introduction
3.2 Photophysical Properties of Erythrosine
3.3 Photobleaching of Erythrosine
3.3.1 Broadband Bleaching
3.3.2 Monochromatic Bleaching
3.3.3 Concentration Dependence under Monochromatic Illumination
3.3.4 Autocatalysis at Higher Concentrations
3.3.5 Temperature dependence under Monochromatic Illumination
3.3.6 Variation of Experimental Conditions
3.4 Bleaching in the Solid Phase
3.5 Conclusion

Chapter 4: Violation of the Mirror Symmetry Rule in the BOPHY Architecture.....p63

4.1 Introduction
4.2 Photophysical Properties of BOPHY Dyes
4.3 Temperature Controlled Spectroscopy
4.3.1 Low-Temperature Spectra Recorded for TM-BOPHY
4.3.2 Analysis of TM-BOPHY Fluorescence Spectra
4.3.3 High Temperature Spectroscopy of TM-BOPHY
4.3.4 TM-BOPHY Excitation Analysis
4.3.5 Electronic Spectra of TM-BOPHY in a Stretched Film

- 4.4 Revealing the Second Transition
- 4.5 Effect on Non-Radiative Rate
- 4.6 The Second Transition in BOPHY
- 4.7 Conclusion

Chapter 5: Electronic communication in Linear BOPHY Supermolecule.....p97

- 5.1 Introduction
- 5.2 Photophysical Properties of BOPHY-DMA
- 5.3 Probing Electronic Communication by Measurement of the pK_a of the Termini
 - 5.3.1 Protonation of BOPHY-DMA
 - 5.3.2 Titration of BOPHY-DMA with HCL
- 5.4 Oxidation of the Dye
 - 5.4.1 Cyclic Voltammetry
 - 5.4.2 Photochemical Oxidation
 - 5.4.3 Search for an Intervalence Charge-Transfer (IVCT) Absorption Band
- 5.5 Use a Photo-Acid Generator
- 5.6 Conclusion

Chapter 6: The Photostability of the BOPHY Architecture.....p123

- 6.1 Introduction
- 6.2 Photostability of TM-BOPHY
 - 6.2.1 Photostability in a Solid Medium
 - 6.2.2 Photostability in Solution
- 6.3 Photostability of BOPHY-DMA
 - 6.3.1 Photon Considerations
 - 6.3.2 Photostability in a Solid Medium
 - 6.3.3 Photostability in Solution
 - 6.3.3 Photostability of the BOPHY-DMA Dication in Solution
- 6.4 Understanding the effect of Toluene

6.4.1 Toluene as an Additive Stabiliser and use of anti-Oxidants	
6.4.2 TM-BOPHY-Solvents interactions Probed by NMR Spectroscopy	
6.5 Conclusion	
Chapter 7: Covalently-Modified BOPHY Derivatives	p153
7.1 Introduction	
7.2 Photophysical Properties of PEG-BOPHY	
7.3 Photobleaching of PEG-BOPHY	
7.3.1 Photobleaching in Solid Medium	
7.3.2 Photobleaching in Solution	
7.4 BOPHY-Perylene Dyad	
7.4.1 Photophysical Properties of the Dyad	
7.4.2 Photobleaching of the Dyad in Solution	
7.5 Conclusion	
Chapter 8: Photo-Processes of a Chromophore-Quencher-Conjugate based on BOPHY	p177
8.1 Introduction	
8.2 Photophysical Properties of CQCs	
8.3 Photobleaching of CQCs	
8.3.1 Photobleaching of P2B in Polar Solvents	
8.3.2 NMR Spectroscopy for P1B	
8.3.3 Photobleaching in Non-Polar Solvents	
8.3.4 Quantum Yield of Photobleaching	
8.3.5 Photobleaching in Solid Medium	
8.4 Effect of Additives	
8.5 Properties of Condensed P1B	
8.6 CQC as a Photocatalyst	
8.7 Conclusion	

Appendix 1: Boron and fluorine NMR of TM BOPHY.....	p207
Appendix 2: Table of oxygen solubility in common solvents.....	p208
Appendix 3: Mass spectrum of P1B-OOH intermediate.....	p208

Chapter 1 – Introduction

1.1 - Poor Photostability Creates Opportunities for Novel Research

This thesis is primarily concerned with the photostability, or more precisely the photofading, of organic chromophores. As a research field, the topic lacks glamour and relevant publications rarely appear in the top journals. Yet the subject is of immense importance, especially for industry and whenever it is claimed that certain compounds have important applications for some kind of light-driven purpose. Few chromophores have been tested for photostability under standardised conditions. Is there such a thing as a standardised test for photostability? What do we expect for the stability of a new dye when exposed to sunlight? If we buy a Ferrari sports car, we would not be happy if the famous red colour faded inside of a decade. Figure 1.1 illustrates a few examples where photofading occurs. There are no universal solutions to prevent photofading. Indeed, Nature seems to have reached the conclusion that it is not possible to prevent photochemical destruction of organic chromophores under persistent exposure to sunlight. Thus, the photosynthetic machinery collapses and is rebuilt for a new season. Even so, and accepting the inevitable breakdown of the chromophores, Nature builds in various levels of protection against photochemical damage (*vide infra*). We are unable to work out how to do the same with artificial analogues. Here, we attempt to build an improved platform for better understanding the photofading processes and, in so doing, indicate ways for introducing photostability. One final thought: many research publications will highlight fluorophores as being highly emissive with quoted fluorescence quantum yields of 0.2 or similar. We are looking at samples where the quantum yield for photobleaching is around 10^{-7} or less. These compounds are deemed to be susceptible to photofading. How do we establish the reaction mechanism when the process of interest is caused by one rogue photon in 10 million?

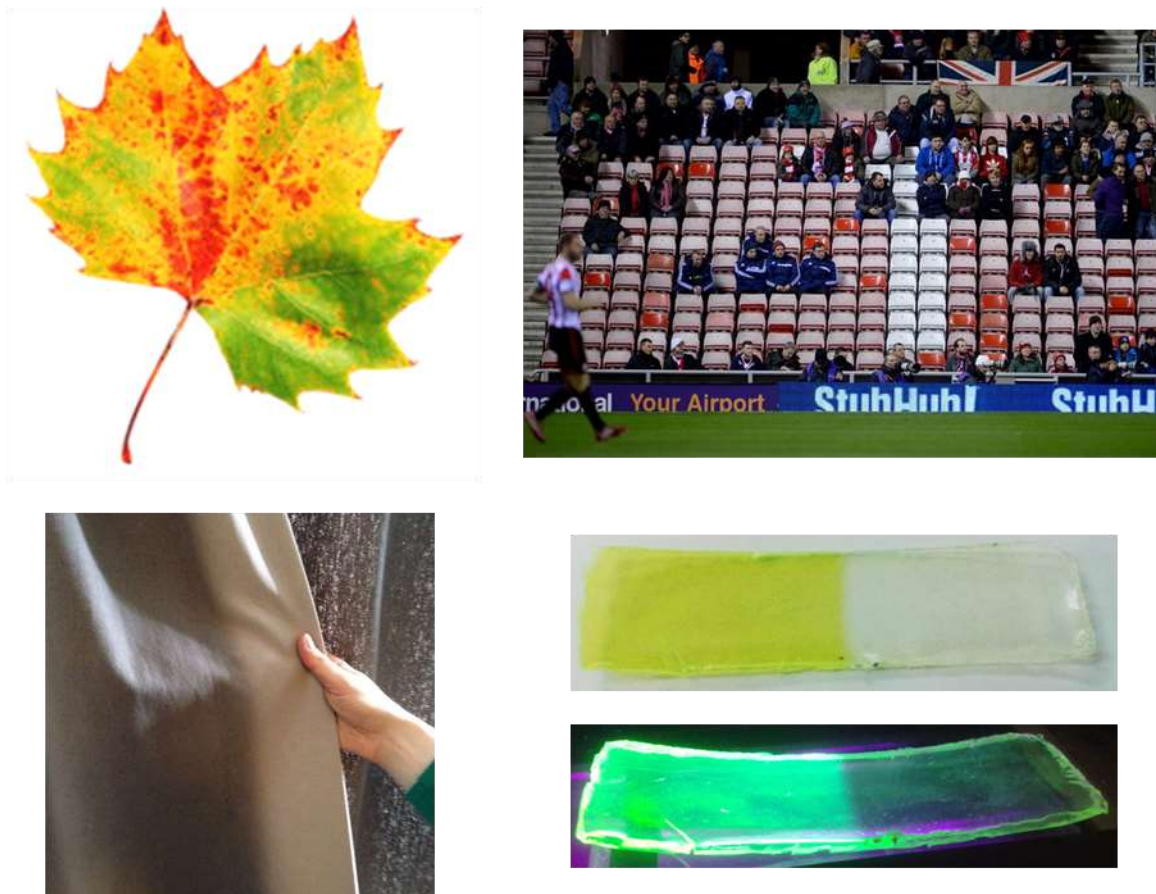


Figure 1.1 – Examples of how light degrades certain chromophores. Nature stops the self-repair process and the leaf takes on the colour of the carotenoids. Red pigments are known to fade when exposed to sunlight. Household curtains can show major loss of colour after only a couple of years. Also shown is an example of photo-fading of a dye that does not undergo intersystem crossing to the triplet manifold.

A search of the scientific literature will quickly bring up any number of articles that state a certain class of organic chromophore displays *good, exceptional, or high* photostability^[1-4]. Usually this comes as an unqualified statement during the introduction. Systematic, quantitative studies on the photostability of chromophores are rare even though the area has concerned researchers for at least 85 years^[5]. There are myriad applications for which luminophores have found use, ranging from energy harvesting^[6], anti-forgery^[7] and sensors^[8], to their use in biological imaging^[9]. By-and-large the photostability of a material will be a determining factor in which applications it may be used. Organic fluorophores are of particular interest compared to other luminophores because of the relatively cheap, abundant starting materials, the infinite synthetic possibilities and the desirable photophysical properties such as high absorptivity and fluorescence quantum yields^[10] that can be achieved. It is evident that there is a need for photostable chromophores and the deleterious effect of light is demonstrated by the images shown in Figure 1.1. If we are to ever fully realise the potential

of organic-based opto-electronic devices for light-harvesting and energy-based applications then we need to fully understand the photostability of chromophores. Only by fully understanding the photofading processes will we be able to develop suitably long-lived analogues. Of course, we can anticipate complementary advances from engineering that will help protect sophisticated blends of chromophores but these will work only if the compounds perform well. A recent research seminar at Newcastle University saw Prof. Ifor Samuel, of the University of St. Andrews, claim that certain conjugated polymers suffered no degradation over 50,000 hours of operation. A rather long extrapolation was involved!

Throughout this thesis, a detailed introduction is given to each chapter. To put our research into perspective, we first give a short overview of natural photosynthetic engines. These are the ultimate photochemical devices and have been perfected over several billion years. We then look at some of the applications of organic chromophores and how photofading affects such examples.

1.2 Photosynthesis – Lessons from Nature

Natural photosynthetic systems are some of the most elaborate machines on Earth, developed over billions of years by evolution. The basic principles of photosynthesis are very well-known and we shall not dwell on them here, a crude scheme is given in Figure 1.2 for the output of photosynthesis and how humans use these outputs. Replicating Nature has distracted researchers for years. Water-splitting, for example, is a multi-electron process, developing a synthetic system that can transport four electrons quickly enough to mimic the process requires sacrificial electron and hole donors to achieve a reasonable internal quantum efficiency^[11, 12]. Natural systems feature a complex light-harvesting arrangement with many chromophores working in unison to direct photons to the reaction centre. In terms of stored energy, the maximum achievable efficiency of photosynthesis is 4.5%^[13], some 10^5 TW of energy in the form of sunlight is incident on Earth and 0.2% of this is converted by all forms^[14] of photosynthesis. Human global energy demand is rising and the rate of consumption was estimated to be 13TW in 2015^[15]. Clearly, a huge amount of energy remains unharnessed and the desire to capture more sunlight for human power consumption is understandable.

Photosynthetic systems are adaptable to both long-term and short-term changes in light conditions. These might involve intermittent cloud cover, for example, and can regulate the amount of light they harness and use. In the longer-term acclimation to variable light conditions, the antenna size can be regulated^[16]. To be able to capture sufficient light in low-light conditions there will be, during times of intense light, harvesting of more energy than can be used for photosynthetic processes (Figure 1.2). The system needs to expend this excess

energy without sustaining damage. Aerobic photosynthesis in particular creates highly oxidising species and unwanted reactive oxygen species (ROS)^[17], as the price paid for the ability to split water. When excess energy is absorbed, more ROS will be created unless the energy can be effectively dissipated. Within photosynthetic systems, there exist a number of photo-protective methods to keep photosynthesis running smoothly until such time as the organism needs to regenerate the photosynthetic system. Whilst many of the mechanisms of photosynthesis, including protective ones, are well characterised, finding quantitative data, such as the turnover number of the chlorophyll molecules in-situ is somewhat difficult but Green plants accept that the chlorophyll will ultimately degrade in-situ and are equipped with an unexpected solution to the problem. In the autumn, the system closes down thereby enabling the useful parts to be recycled. The rest of the organic matter is allowed to fall to the ground as fertilizer. If damage to the system occurs during operation, the photosynthetic processes are impaired and a state called photoinhibition^[18] is entered. Through evolution, many protective mechanisms have developed to protect photosynthetic systems.

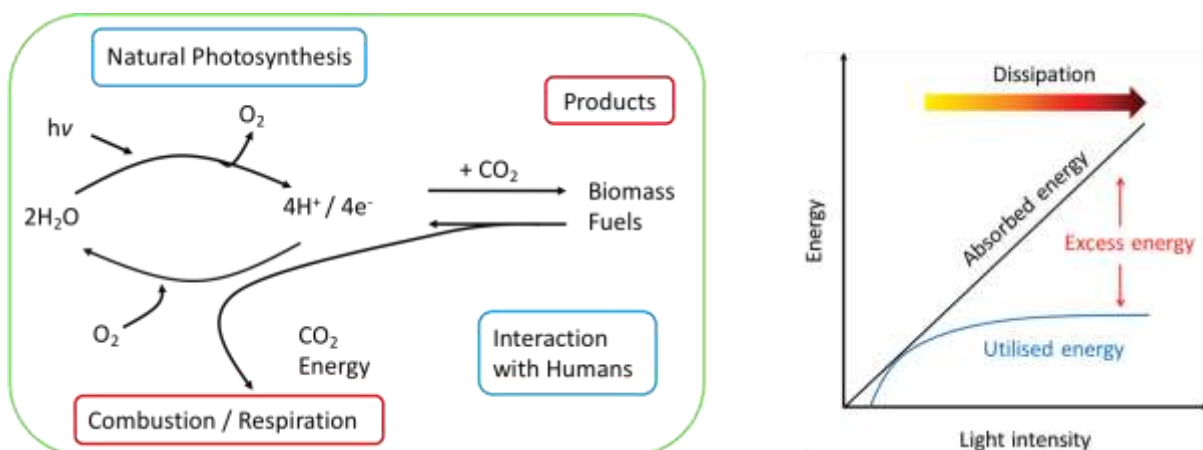


Figure 1.2 – Left, schematic showing the natural energy cycle and the interaction with humans, adapted from ref [14]. Right, adapted from ref [19], photosynthesis can only use a certain fraction of absorbed light, the rest must be dissipated in some way.

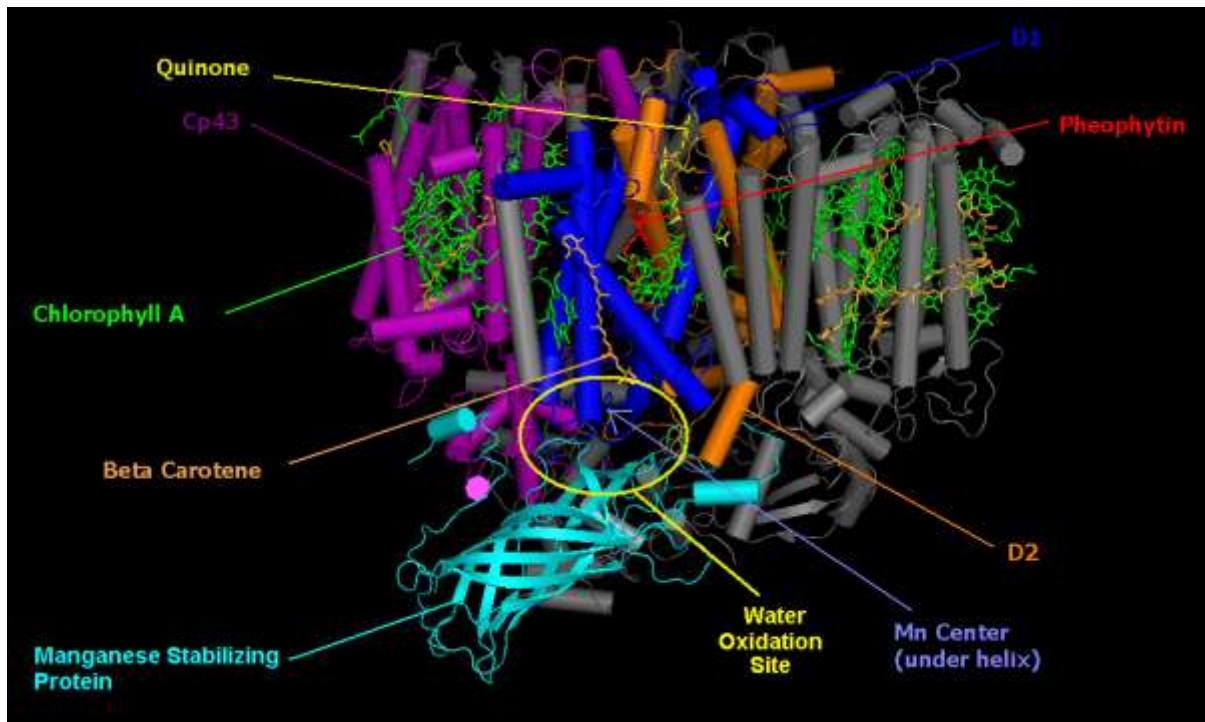


Figure 1.3 – The structure of Photosystem II, note in particular the large number of chromophores per reaction centre and also the β -carotene which provides important photo-protection. (Image taken from Wikipedia)

1.2.1 Non-Photochemical Quenching in Photosynthesis

Under conditions of intense sunlight, more photons are absorbed than can be transferred to the reaction centres. Some of the excited-state chlorophylls are not quenched by the electron-transfer steps that are part of the photosynthetic processes. They may then undergo intersystem crossing to the triplet state from where damaging chemistry may ensue. Non-Photochemical Quenching (NPQ) is employed to stop this^[19]. There are at least three aspects to NPQ^[20], one of which is allowing the system to go into a photoinhibitor state^[21], in purple bacteria, the conformation of the light-harvesting complex can be transformed by pH from the quenched state to a highly fluorescent state^[22]. This highly innovative route allows the chlorophyll to return to the ground state. In green plants, the main component of NPQ, and that of most interest for artificial analogues, is the dissipation of excess excitation energy in the form of distributed heat.

In most light-harvesting complexes there are carotenoids present. These residues fulfil multiple functions, such as providing structural support, functioning as ancillary light harvesters and participating in NPQ. In Photosystem II (PSII), for example, the method is called the xanthophyll cycle^[23] and it utilises a pH gradient for initiation^[24]. Excess light causes the pH to drop in the lumen^[25], thereby causing a conformational change in the structure of the protein known as PsbS^[26]. The xanthophylls present are a set of three structurally related

carotenoids in PSII. During NPQ, these pigments undergo de-epoxidation and by this method transform to different conformations in a reversible cycle that results in degradation of excitation energy to heat. One of the de-epoxidised forms, zeaxanthin^[27], may couple to the excited-state of chlorophyll^[28] at certain sites allowing for energy transfer from the chlorophyll and eventually the degradation of this energy to heat. Despite the xanthophyll cycle, some small amount of singlet oxygen is still produced^[27] so further protective mechanisms are required.

1.2.2 Reactive Oxygen Species (ROS) in Photosynthesis

In Photosystems I and II, electron transfer to molecular oxygen can result in the formation of superoxide ions which in turn may lead to the production of hydrogen peroxide and hydroxyl radicals^[29]. Superoxide ions disproportionate to H₂O₂ and O₂ in a reaction catalysed enzymatically by superoxide dismutase. The H₂O₂ produced is reduced to water by ascorbate mainly forming monodehydroascorbate^[30] which is eventually reduced back to ascorbate. This process is known as the water-water cycle.

The species that creates most concern is the pernicious reagent, singlet molecular oxygen. This is molecular oxygen in its lowest-excited singlet state and is a well-known cause of damage in natural systems^[31]. Singlet oxygen is mainly formed by sensitisation *via* triplet-excited states of chromophores. In the PSII antenna, molecular oxygen is sensitised by the chlorophyll a triplet-state which forms directly by way of intersystem crossing from the singlet-state of chlorophyll a^[32] for those excited states not quenched by the usual energy- and electron-transfer steps. In the reaction centre, singlet oxygen is formed by energy transfer from the triplet state of P680, a chlorophyll dimer that is the primary donor^[33] in PSII. The triplet state is formed by charge recombination of the primary radical pair [P680^{•+}...Pheophytin^{•-}]^[32]. Although singlet oxygen is not as strong an oxidant as is P680⁺, it is long lived and free to diffuse so it will be uncontrolled within the system. Within PSII there resides 36 chlorophyll a molecules and 7 β-carotene molecules^[14], the configuration of these are shown in Figure 1.2. The carotenoids play an important role in protecting the system from singlet oxygen attack. In the antenna, they may quench the chlorophyll triplet-excited states by electronic energy transfer, where orbital contact is required. In the reaction centre, the carotenoid cannot be too close to the highly oxidative P680⁺ state as this could lead to damage of the carotenoid^[34], therefore the intermolecular distance is too great to allow direct quenching of the triplet state. The carotenoid must deactivate any singlet oxygen formed via electronic energy transfer. This particular reaction makes use of the very low triplet excitation energy inherent to the carotenoids.

1.2.3 Self-Repair

Despite these protective measures photodamage stills take place, particularly at the reaction centre in PSII. The chemistry of water-splitting involves highly oxidising species and the generation of ROS and there is damage to the D₁-polypeptide that comprises the reaction centre. Within PSII, there is autoproteolytic behaviour^[35], new protein is synthesised and the active complexes are reassembled. Singlet molecular oxygen, for example, preferentially attacks chlorophyll and then the polypeptide^[36]. Efficient turnover of the polypeptide seems to be the solution to the problem, the turnover half-life for the process is only about 1 hour^[37].

Replication of some of these mechanisms has been considered in isolation but not in a concerted fashion. The conformation of LHCII immobilised onto oxide surfaces was controlled by nano-patterning^[38], which allows control of whether the complex is present in fluorescent or quenched states. Molecular switches can be used to change the properties of complicated systems and a successful attempt to introduce photoregulation into a system is the case of an elaborate pentad^[39]. The system featured electron transfer from a porphyrin moiety to a fullerene and a photo-isomerizable dihydroindolizine unit. In the closed form, absorption due to the unit lies in the near-UV region but in the open, betaine, form absorption occurs across the visible spectrum. At low light levels, the quantum yield for electron transfer is constant but, as the light intensity increases, this yield decreases as photons are intercepted by the betaine. The use of covalent attachment of triplet quenchers or using triplet energy transfer is quite common^[40, 41] and has been used for different applications^[42]. The more complicated xanthophyll cycle has not been replicated^[43] but the use of protons as a switching mechanism that can change the photophysical properties of a systems has been explored^[44]. Self-repair in organometallic photo-catalysts has been described, such as the cobalt-phosphate catalyst, CoPI^[45]. Particularly interesting systems have been reported involving carbon nanotubes (CNT). One such system^[46] favours the self-assembly of CNT and purple bacteria reaction centres. Assembly was triggered by removal of a surfactant and its reintroduction caused disassembly, the cycle could be repeated ad infinitum. A light-harvesting antenna based on gallium protoporphyrin^[47] attached to CNT by DNA oligonucleotides could be refreshed after oxidative damage to the porphyrin. Inactive units were removed by H₂O₂ and fresh porphyrin could be introduced, and light-harvesting performance restored. Despite the multiple in-built protection mechanisms, summarised in Figure 1.4, Nature still regenerates the photosynthetic system *en masse* on an annual basis, also there is a natural daily dark/light cycle. Annual rebuilds are surely not feasible in an artificial system but perhaps the daily cycle could provide inspiration.

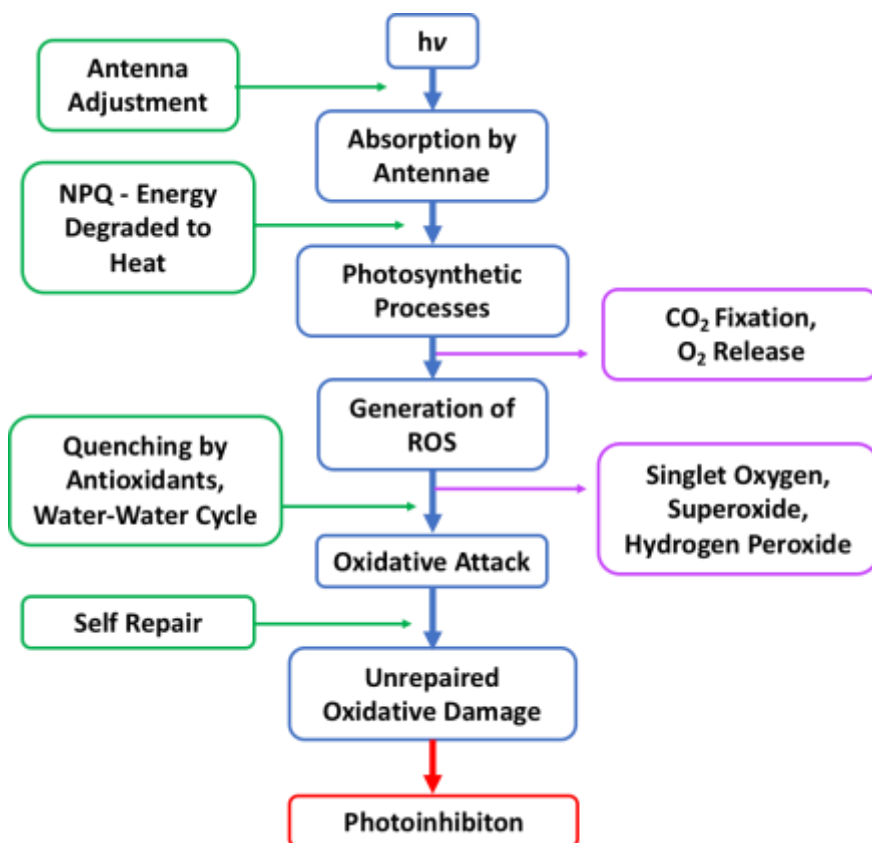


Figure 1.4 – Steps on the eventual path to photoinhibition of an aerobic photosynthetic system. The protective processes in green boxes can extend the time that a system remains viable.

1.3 Bio-Hybrid Systems

So-called bio-hybrid systems, where the architecture or mechanisms of nature are combined with synthetic molecules, is an elegant way to exploit light for our use. Bio-hybrid devices have been used for numerous applications, including photo-electrochemical cells^[48], bio-light-emitting diodes^[49] and bio-inspired artificial photosynthesis. Organic transformations have been achieved by attaching chromophores to bacteria^[50] and transferring electrons into the bacterial systems, essentially causing them to perform their enzymatic functions in reverse and thus working as photo-catalysts. The bio-hybrid strategy of most interest to us is their function as light-harvesting antennae^[51-54]. To achieve absorption across the entire solar spectrum requires a large number of chromophores working in unison and this presents a massive synthetic challenge. Fully synthetic antennae require both the scaffold and the chromophore to be built from starting materials. Use of the bio-hybrid allows one to insert chromophores at specific attachment sites of short proteins with up to 50 amino acids^[55], see Figure 1.5. Subsequent self-assembly of the units allows replication of natural antennae. Electronic energy transfer efficiencies of up to 95% have been achieved with the absorption

spectral profile penetrating well into the far-red part of the spectrum with this method. The usual mode of operation has bacteriochlorin chromophores transferring excitation energy to bacteriochlorophyll *a* and with up to 31 chromophores being integrated into the overall system^[55]. This is a modular approach meaning that other organic chromophores such as Oregon Green and Rhodamine Red can be appended. Although electronic energy transfer from the bacteriochlorophylls is efficient, direct transfer from the synthetic chromophores is less effective with, for example, Oregon Green giving an efficiency of only 30%^[52].

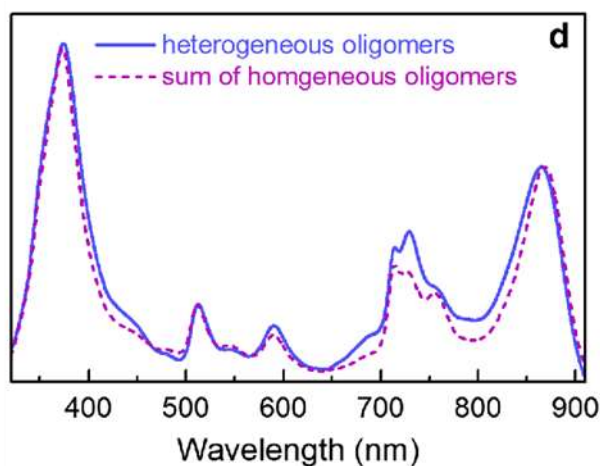
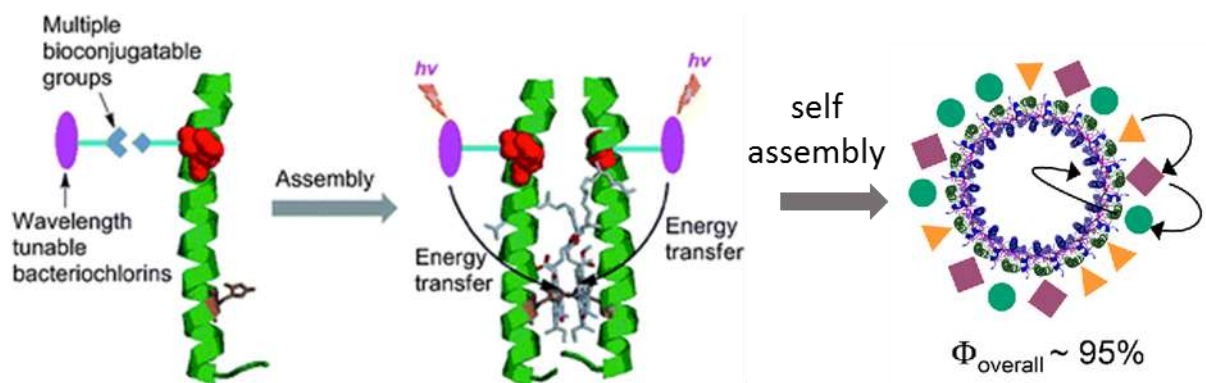


Figure 1.5 – Adapted from refs [52, 53], chromophores are attached to proteins which self-assemble. Shapes in the self-assembled unit are different sub-units featuring different bacteriochlorophylls. The spectra demonstrate the fact that there are absorption bands across the spectrum from near UV to near IR.

1.4 Examples of Artificial Systems and Applications

We can learn important lessons from natural photosynthesis but any real attempt to build artificial analogues able to harvest sunlight will doubtless take a different form from that of

plants and photosynthetic algae. Will there be a role for organic chromophores in such devices? The answer is not at all clear. So far, there have been few successful versions of a purely organic artificial photosynthetic device. Most research along the bio-inspired route involves sacrificial redox agents to minimise the importance of back reactions and to avoid problems associated with coupling together the necessary pair of half-reactions. After almost 50 years of research effort, we are still far from meeting even the most basic demands. Areas where organic chromophores are playing an essential role can be summarised in the topics illustrated below.

1.4.1 Application 1 - Luminescent Solar Collectors (LSCs)

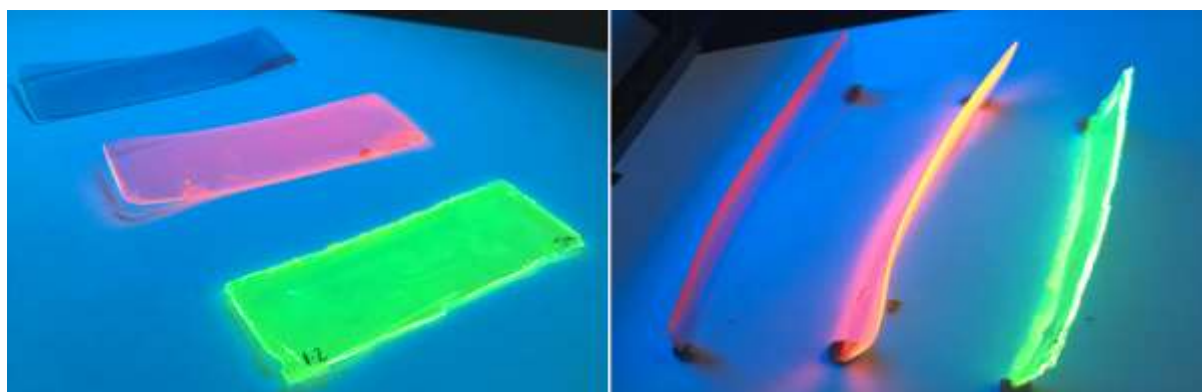


Figure 1.6 – Highly emissive chromophores in polymer matrices under UV illumination. From left to right, a pentacene-based dye, a BODIPY derivative and a BOPHY derivative. Note the enhanced emission from the edges.

The simplest system that can be imagined for using organic chromophores for light-harvesting purposes is in Luminescent Solar Collectors^[56] (LSCs), also known as luminescent solar concentrators^[57]. This approach takes the form of a chromophore dispersed in a transparent medium. The chromophore absorbs incoming light then emits fluorescence that impinges the internal boundary between the medium and air. If the incident angle at the interface is greater than the critical angle, as determined by Snell's law, fluorescence will be reflected and can only escape through the edges of the collector. This is evident in Figure 1.6 where the plastic films prepared in our laboratory are seen to show intense emission from the edges. The edge of the film may be coupled to some device to allow sensitisation; for example, the film might be coupled to a silicon photocell^[58]. This allows a large collection area to concentrate the photons down to a much smaller area. As of 2008, the external efficiency record for an LSC system was 7.1%^[59]. The schematic given in Figure 1.7 demonstrates the working principal and loss mechanisms. It is the least sophisticated form that an LSC can take, having a single chromophore in the media with no additional engineering. In this form, the LSC features some

significant loss mechanisms. Firstly, for a single chromophore only a rather limited portion of the total solar spectrum will be absorbed. Much of the light will be transmitted through the device and some absorbed light will be lost by non-radiative return to the ground state. A percentage of the emission will be emitted at an angle such that it escapes the collector while some will be scattered by the matrix. To absorb a high percentage of incoming light, a high concentration of chromophore is required and this might lead to aggregation and self-absorption^[60].

A time-dependent loss mechanism is the photobleaching of the chromophore. Eventually, the dyes will be degraded by some photo-oxidation process and will no longer be able to absorb light. The device described can be improved by physical engineering solutions including a diffusing mirror^[61] at the bottom to stop transmission losses while a photonic band gap^[62] filter can be used to stop the emitted light escaping. More complex collectors based on multiple layers of different chromophores^[63] can allow for greater spectral collection. To avoid the problems of self-absorption, multiple chromophores can be mixed together^[64], the distribution will be random but some chromophores will be located at sufficiently close contact to allow energy transfer by the Förster mechanism. More elegant chemical solutions, such as dyads, triads or multi-chromophoric systems, have been developed^[65] which result in panchromatic absorption profiles. Excitation energy will be funnelled to the lowest-energy chromophore, which is typically red-emitting. Such dyes are given further consideration in Chapter 7.

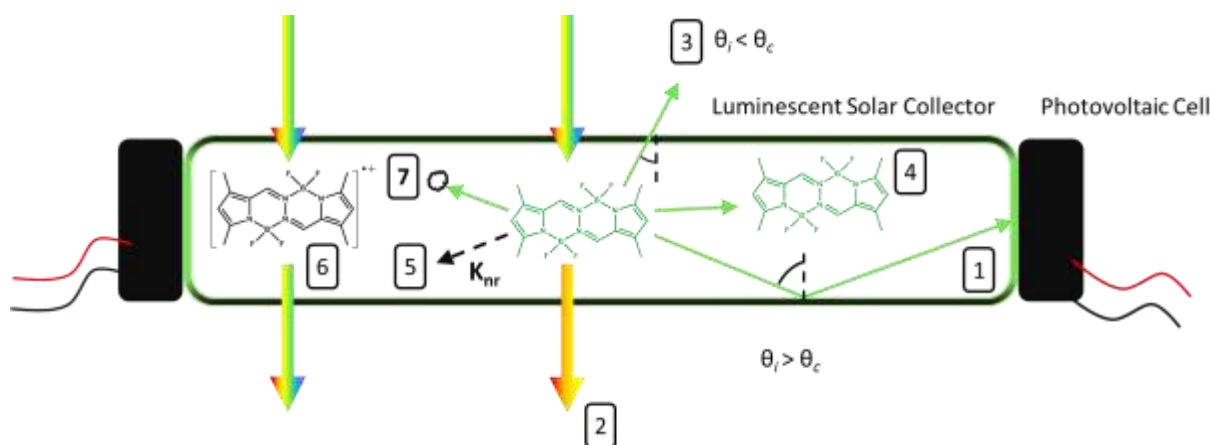


Figure 1.7 – Schematic view of an LSC. The various fates of absorbed photons are shown. 1 – sensitisation of the coupled PV device, 2 – transmitted light, 3 – emitted light escaping the collector, 4- emitted light absorbed by another chromophore, 5 – non-radiative decay of the chromophore, 6 – transmission of light due to degradation of chromophore, 7 – scattering or absorption by the matrix.

A cost-benefit analysis of using an LSC compared to direct use of a silicon photovoltaic cell would need to consider the effective lifetime of the device. Mono-crystalline silicon cells have a degradation rate around 0.5% per year^[66] so should operate for more than 20 years. An LSC

subject to exterior illumination by sunlight will surely degrade over a relatively short time. The stability of organic chromophores has been considered and the lifetime should be greater than 10 years^[56] to be economically viable. Some consideration has been given to the stability of LSCs. Perylene diimide dyes in a sol-gel matrix were found to retain 65% of the initial fluorescence after 5 years of exposure^[67]. It has been found that the stability is strongly dependent on the dye–matrix choice when polymerisation^[68] of some monomer is the method for making the matrix. Monomer residues have been blamed for the instability which can be improved by polymer engineering; e.g. using a styrene methyl methacrylate copolymer improved stability^[69] of Coumarin 6 some 5-fold compared to a poly(methyl methacrylate) (PMMA) matrix. Thermal polymerisation^[70] of the monomer, as opposed to solvent casting of PMMA, also improved stability. Degradation of a perylene dye was accelerated in methyl isobutyrate solution by the presence of the methyl pyruvate^[71] a ketone that is a common impurity in methyl methacrylate. Addition of the singlet molecular oxygen quencher^[72] 1,4-diazabicyclo[2.2.2]octane improved photostability when the ketone was not present but compounded the instability in the presence of the ketone. Attempts to reveal the mechanism of the degradation of another perylene dye showed that it initiated the disruption of lateral phenyl substituents^[73]. This reaction is due to free radicals so it was proposed that hindered amine radical scavengers could be used to promote stability and also fluorinated polymers would improve the barrier properties toward O₂. Indeed, such matrices were shown to improve stability^[74, 75] compared to PMMA after up to 1,000 hours of accelerated testing in a weather-o-meter. The kinetics for photodegradation of phthalocyanine^[76] based LSCs were fitted to first-order reactions when exposed to sunlight (in Egypt), although a cursory examination of the data would indicate a bi-exponential process might be more appropriate.

The LSC is a simple concept but, although it has been around more than 40 years, has not been developed into a commercial product. The advantages come in the form of the simplicity of production, installation and utilisation. The problem is that no single chromophore has the capacity to harvest a sufficiently high fraction of the solar spectrum for the device to be viable. Multiple chromophores are needed and so the expense increases and the design features become more complex. To solve all the intrinsic problems with respect to the photophysical processes it is necessary to use an elaborate, multi-chromophore harvesting unit that has been designed specifically for the purpose. Sufficient knowledge exists for a successful prototype to be produced. The synthesis of such a molecule on an industrial scale would be a monumental task and would require strict regulatory control. The photostability of the resultant network would need to be very high.

Collection devices have been constructed with luminophores other than organic dyes, including transition metal complexes^[77] and semi-conducting polymers^[78]. After organic dyes

the next largest area of interest is in using quantum dots^[79, 80] as the luminophore. Quantum dots emitting the red and IR region of the spectrum typically have fluorescence quantum yields of 0.3^[81] or greater; for example, lead-selenide quantum dots have been reported with fluorescence quantum yields up of 80%^[82], and feature broad absorption spectra making them viable LSC candidates. Such materials are expected^[10] to be more stable than organic chromophores. Core-shell structures^[83] are used so they are surface passivated, photooxidation is suppressed as the surface inorganic layer acts to protect the core although attack by singlet molecular oxygen has been recorded when used in microscopy^[84]. A selection of CdSe/ZnS quantum dots stored in solution were shown to degrade over time^[85] with a blue shift in the absorption and emission spectra and this was also seen for CdS dots in films^[86]. Improved stability could be achieved using multi-shell configurations^[87]. In accelerated testing of LSCs, these quantum dots have shown only minor fading^[88]. For example, CdSe/ZnS dots were compared to a perylene dye, both dyes fade *via* biexponential kinetics^[89]. The dominant slow phase, once corrected for photon absorption, was more than 10 times slower for the quantum dot than for the organic dye. The most remarkable finding however was that full recovery of the quantum dots was seen under a dark cycle but no mechanism was proposed for this amazing claim.

1.4.2 Application 2 – Organic Photovoltaics (OPV)

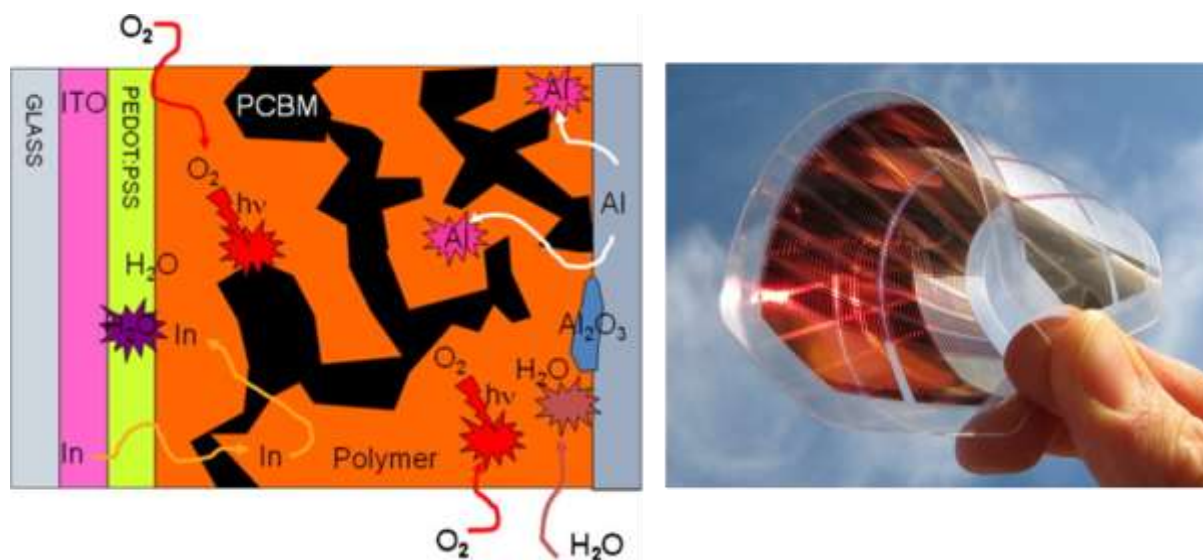


Figure 1.8 – Schematic diagram of an OPV showing ways in which the cell can degrade, adapted from ref [93], right shows the flexible nature of organic cells.

A more advanced approach for using organic materials is in the direct conversion of photon absorption to electricity within an organic photovoltaic (OPV) device. The best efficiency recorded for an OPV was about 11.5%^[90] as of 2016 which is low compared to the best inorganic photovoltaic cells. The energy required to promote an electron from the highest

occupied molecular orbital (HOMO) to the lowest unoccupied molecular orbital (LUMO) is equivalent to the band gap in semiconductors. This tends to be larger in OPV^[91], which means that less of the solar spectrum can be used and also lowers the theoretical efficiency limit. Commercial viability is approached when the conversion efficiency is 10-15%^[92], due to lower production costs compared to inorganics. The stability of the OPV device is a major drawback, with working lifetimes of only a few years^[93]. Although this is openly stated in almost every report on OPVs, specific studies into the stability are scarce and only become important as the system approaches commercial exploitation. Most research is still concentrated on raising the power conversion^[94-96]. However, due to the emergence of this field some standardisation of characterising OPV stability has been proposed^[97]. Methods such as encapsulation^[91] improve the stability of the cell but a fair number of studies on the stability due to the active layer have been undertaken^[98-100].

The basic working principle of a conventional OPV is that the organic donor, usually a conjugated polymer formed from organic chromophores^[101], absorbs the incident photons. Absorption causes an electron to be raised to the LUMO, thereby leaving a hole in the HOMO. This exciton pair can diffuse through the polymer until it reaches a junction where the free carriers migrate to the electrodes, producing electricity. The stability is compromised in a number of ways, including degradation of the electrodes and of the active layer. The donor materials include polyphenylene vinylene^[102], fluorene-containing polymers^[103], phthalocyanines^[104], and thiophene-based polymers^[105]. The usual choice of acceptor is a fullerene-based molecule^[106]. Fluorene-based polymers are considered unstable while dithienothiophene materials are amongst the most stable^[93]. It was generally accepted that the degradation mechanism involves singlet molecular oxygen, but other work has implicated superoxide ions and the formation of ozone^[107]. The degradation of a stable thiophene-based polymer, P3HT, was believed to be due to singlet oxygen addition across the aromatic ring but has now been shown to be due to side-chain oxidation due to hydroperoxide formation^[108]. The degradation of fluorene based systems to fluorenone has been studied and results from oxidation of the side chains at the 9-position^[109]. A particularly useful study^[110] involved the degradation of various conjugated polymers under white-light illumination. This established some relationships between structure and stability, kinetic information is provided but detailed analysis of this is missing. The traditional PPV-based polymers with a double bond within the backbone are particularly unstable. The addition of alkyl chains to the chromophore is seen to cause poorer stability so the use of units with thermo-cleavable chains is recommended and quaternary sites are to be avoided.

1.4.3 Application 3 - Fluorescence Microscopy

The greatest demand for fluorescent molecules is surely in bio-imaging^[111]. There is now a bewildering range of instrumental techniques available, some of which are very demanding in terms of the performance of the fluorescent tags used. As well as the wide-field epifluorescence^[112] and confocal^[113] techniques, there are many modern forms of high-performance microscopy that allow for resolution beyond the diffraction limit^[114], often employing single-molecule detection (SMD) methods^[115]. To achieve such resolution, it is important to be able to detect many photons over a relatively long period of time. If the dye is irreversibly bleached it will no longer emit and resolution is lost. There is a related problem called photo-blinking which is considered in Chapter 8. Some contemporary microscopy techniques include Total Internal Reflectance Microscopy (TIRF)^[116], Stochastic Optical Reconstruction Microscopy (STORM)^[117], and Stimulated Emission Depletion (STED)^[118]. The improvement in resolution of these techniques is demonstrated in Figure 1.9. TIRF uses the evanescent wave of a laser beam that is totally internally reflected from the substrate on which the sample sits, the wave penetrates into the sample by only about 100nm^[119] allowing surfaces to be imaged. STORM uses the random blinking of chromophores^[120] due to dark states, which can be switched on and off by light of different wavelengths. In this way, not all chromophores are illuminated at once. STED is conceptually similar to STORM but uses stimulated emission to depopulate the excited state^[115]. Now, the stimulating source must be of lower energy than the excitation source and relaxation is to a vibronic band. In a typical arrangement, a central focused region is not depleted so emits spontaneously while red-shifted stimulated emission appears as a ring embracing the focus.

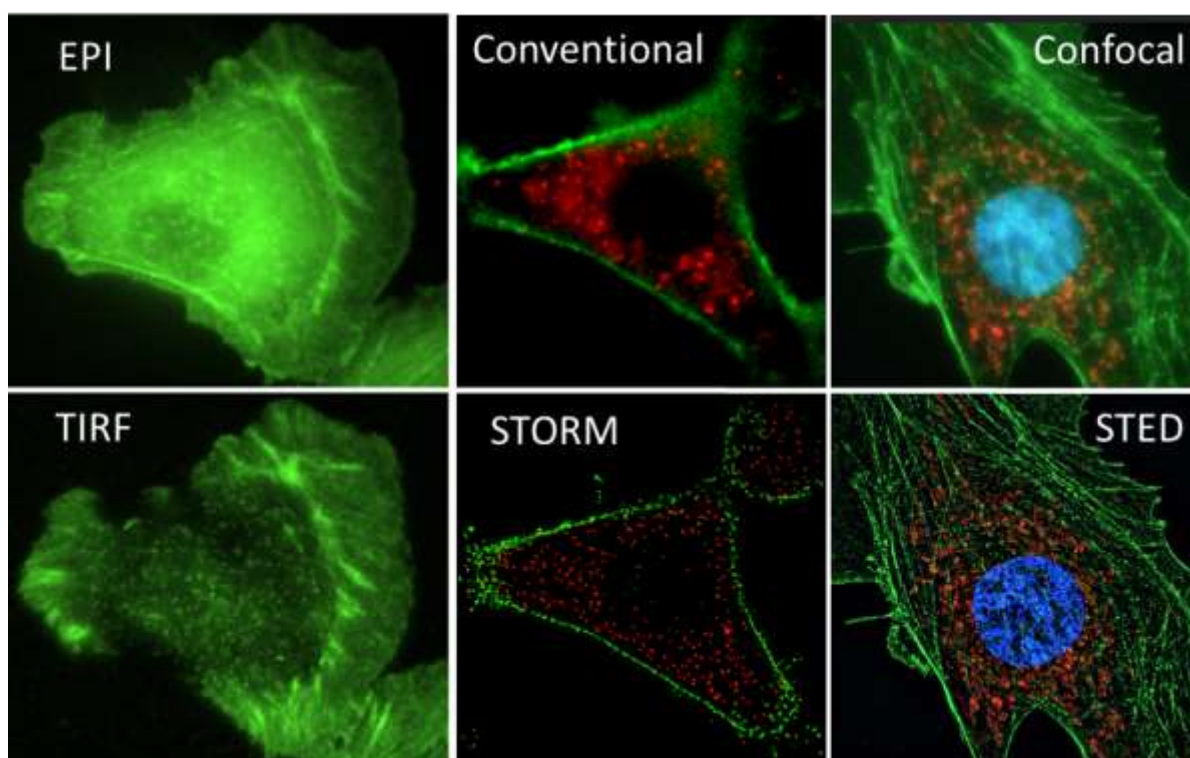


Figure 1.9 – Comparison of various SMD techniques compared to more conventional methods.

The benefits of these various experimental techniques are improved resolution, the ability to discover new environments^[121] and the opportunity to understand the distribution of time-dependent processes as opposed to ensemble averages^[122]. To achieve good images in SMD it is necessary to be able to accurately measure a single point and a very high signal-to-noise ratio is required^[123]. To achieve this feat, a fluorescent tag must have a large absorption cross-section, minimal crossing to dark states and be highly photostable^[123]. In the area of microscopy, the number of photons emitted before loss of signal is used as measure of photostability. In broad terms, for the classes of markers available, this figure is for fluorescent proteins^[124] $\sim 10^4$, for organic chromophores^[125] 10^5 - 10^6 and for quantum dots^[126] up to 10^8 photons may be emitted before degradation. The commercial availability, higher fluorescent yields and relative low toxicity mean that organic chromophores remain popular. Degradation of organic chromophores by singlet molecular oxygen is a significant problem. Enzymatic oxygen scavengers^[42] are employed while anti-oxidants, redox buffers and triplet state quenchers are used as secondary measures^[127] to protect chromophores. Recent advances have seen the covalent attachment^[128] of protecting units to chromophores and the use of scaffolds^[129] to co-locate them. Such methods have been shown to yield improvements in the numbers of emitted photons by up to three orders of magnitude^[125] in short-term microscopy studies.

In the single molecule techniques, high photostability is prized, conversely bleaching of chromophores can be used in microscopy advantageously in a set of techniques called Fluorescence Recovery After Photobleaching (FRAP)^[130], Fluorescence Loss in Photobleaching (FLIP) and Fluorescence Localisation after Photobleaching (FLAP)^[131]. Early use of FRAP measured diffusion coefficients in the cell membrane but is now applied to many cell environments. A spot on a sample is subjected to a short period of intense illumination causing the localised fluorophores to become irreversibly bleached. The same spot is then monitored over time with the fluorescence intensity recorded. In this manner, the mobility of the fluorophores in the cell membrane may be characterised. In FLIP, a region of interest is monitored while a different area is continuously bleached^[132], this allows characterisation of the mobile and immobile fractions of tagged targets. To fully characterise all the targets in a system, FLAP uses a double tagging method whereby one fluorophore is bleached while the other is a reference^[133] that allows bleached chromophores to be monitored as well as unbleached ones. This raises an important point, the photostability of chromophores can be a useful tool in the right hands. The possible uses of a chromophore are set by the stability needed for the application. Indeed in some situations a lack of photostability is desirable. Such cases, apart from the microscopy techniques just described, include the need to remove a sensitiser after it has performed some task and the development of solid-state actinometers for photon absorption.

1.5 Photostability in the Context of this Thesis

The main emphasis running throughout this work concerns examining the stability of organic molecules under continuous exposure to light. A variety of molecular systems is used to probe these effects. In Chapter 3, we explore the photochemistry of Erythrosine. This compound differs from all other systems studied herein in that it is a commercially available food dye that has been used for many centuries and is considered to be relatively non-toxic. It is a well-established photosensitiser, having a high quantum yield for formation of the triplet-excited state, which has been shown to generate singlet molecular oxygen under illumination in aerated water. It is known to undergo photobleaching. Our contribution has been to measure activation parameters for the bleaching reaction and also to determine the quantum yield for photofading in water. Even for such a seemingly simple system, the bleaching mechanism is complex and, under certain conditions, features an auto-catalytic element. In fact, auto-catalysis causes problems throughout our work!

Chapter 4 describes the photophysical properties of a relatively new family of dipyrromethene based dyes, bis(difluoroboron)1,2-bis((1H-pyrrol-2-yl)methylene)hydrazine (BOPHY). The

BOPHY class is closely related to the ubiquitous boron dipyrromethene (BODIPY) group of highly fluorescent dyes. A notable feature of BOPHY is that all the derivatives synthesised thus far exhibit a broad absorption spectrum compared to BODIPY which has the general appearance of overlapping electronic transitions. The emission spectra display a more typical vibronic structure so there is poor mirror symmetry between absorption and fluorescence spectral profiles. Because much of our photochemical work relates to BOPHY, it seems prudent to seek a better understanding of the underlying photophysics.

The photophysical properties of a significantly red-shifted BOPHY derivative are reported in Chapter 5. The generic structure of the BOPHY platform facilitates isolation of long, essentially planar molecules with extended π -systems. The question then arises as to the extent of intramolecular communication between the widely-spaced terminals. To address this question, we introduce a charge at one extreme end of the molecule and measure how this affects the opposite end. The essentially unique topology and electronic structure of this push-pull-push molecule do not appear to favour long-range through-bond electronic coupling.

Having established the basic properties of these BOPHY-based chromophores, the next phase of our work was to address their ability to resist photo-degradation under exposure to white light. This is the focus of Chapter 6. The main difference between BOPHY and Erythrosine relates to the relative effectiveness for forming the triplet-excited state. The poor spin-orbital coupling properties for BOPHY, and the relatively wide singlet-triplet energy gap, do not favour triplet formation. Instead, photobleaching occurs from the excited-singlet state. Now, we see a pronounced influence of solvent polarity on the rates of photobleaching which permits the introduction of a simple "rule" correlating the fluorescence quantum yield to the rate of photo-fading in solution. We also observe a remarkable example of photoprotection by aryl hydrocarbons.

Practical outlets for fluorescent dyes are most likely to involve solid-state devices. Throughout this work we have given some consideration to incorporating the chromophore in a thin plastic film and making a critical comparison with solution-phase results. In Chapter 7 we explore this difference in some detail using an extended BOPHY dye equipped with terminal poly(ethylene glycol) units to assist dispersibility. Photo-fading is accompanied by the appearance of a well-defined intermediate that is moderately fluorescent. The net result is a simple, easy-to-use chemical actinometer for recording exposure times.

In Chapter, 8, we design a new type of chromophore whereby an anti-oxidant residue is covalently linked to the dye. Light-induced, intramolecular charge transfer occurs on illumination of the BOPHY chromophore, followed by rapid geminate charge recombination. This behaviour shortens the excited-singlet state lifetime and serves to minimise the

importance of photo-fading. Again, there is an accompanying dependence on solvent polarity because of thermodynamic factors. For the first time, it proved possible to isolate the reactive intermediate, which was identified by NMR spectroscopy as being a specific organic hydroperoxide. This intermediate could be used as a photo-catalyst to drive useful organic transformations and to destroy organic dyes in solution. In this way, a harmful predator was put to good use.

References

- [1] G. Ulrich, R. Ziessel, A. Harriman, *Angew. Chem. Int. Ed.* **2008**, 47, 1184-1201.
- [2] N. A. Kuznetsova, O. L. Kaliya, *J. Porphyr. Phthalocyanines.* **2012**, 16, 705-712.
- [3] R. P. Haugland et al. *Tetrahedron Lett.* **2003**, 44, 4355-4359.
- [4] M. Beija, C. A. M. Afonso, J. M. G. Martinho, *Chem. Soc. Rev.* **2009**, 38, 2410-2433.
- [5] H. F. Blum, C. R. Spealman, *J. Phys. Chem.* **1933**, 37, 1123-1133.
- [6] M. R. Wasielewski, *Acc. Chem. Res.* **2009**, 42, 1910-1921.
- [7] R. A. Mustalish, *Stud. Conserv.* **2000**, 45, 133-136.
- [8] T. Gunnlaugsson, F. M. Pfeffer et al. *Coord. Chem. Rev.* **2006**, 250, 3094-3117.
- [9] R. Y. Tsien, A. Waggoner in *Fluorophores for confocal microscopy*, Springer, **1995**, pp.267-279.
- [10] U. Resch-Genger, T. Nann et al. *Nat. Methods.* **2008**, 5, 763.
- [11] Y. Tachibana, L. Vayssieres, J. R. Durrant, *Nat. Photonics.* **2012**, 6, 511.
- [12] K. Maeda, K. Domen, *J. Phys. Chem. Lett.* **2010**, 1, 2655-2661.
- [13] E. H. Thorndike, *Energy and the Environment: A Primer for Scientists and Engineers*, Reading Ma. **1976**.
- [14] J. Barber *Chem. Soc. Rev.* **2009**, 38, 185-196.
- [15] *International Energy Agency.* **2017**.
- [16] R. Croce et al. *Biochim. Biophys. Acta, Bioenerg.* **2013**, 1827, 420-426.
- [17] A. Telfer, J. Barber et al. *J. Biol. Chem.* **1994**, 269, 13244-13253.
- [18] S. B. Powles, *Annu. Rev. Plant. Physiol.* **1984**, 35, 15-44.
- [19] M. Landi et al, *Chlorophyll (Chapter 3)*, IntechOpen, **2017**.
- [20] W. P. Quick, M. Stitt, *Biochim. Biophys. Acta, Bioenerg.* **1989**, 977, 287-296.
- [21] R. Goss, B. Lepetit, *J. Plant. Physiol.* **2015**, 172, 13-32.
- [22] R. J. Cogdell et al. *J. Phys. Chem. B*, **2016**, 120, 951-956.
- [23] W. Bilger, O. Björkman, *Photosynth. Res.* **1990**, 25, 173-185.
- [24] G. H. Krause, B. Ursula, *FEBS Lett.* **1986**, 200, 298-302.
- [25] G. H. Krause, *Physiol. Plant.* **1988**, 74, 566-574.
- [26] K. K. Niyogi, X.-P. Li, V. Rosenberg, H.-S. Jung, *J. Exp. Bot.* **2004**, 56, 375-382.
- [27] P. Jahns, A. R. Holzwarth, *Biochim. Biophys. Acta, Bioenerg.* **2012**, 1817, 182-193.
- [28] N. E. Holt, G. R. Fleming et al. *Science.* **2005**, 307, 433-436.
- [29] K. Asada, *Annu Rev. Plant Biol.* **1999**, 50, 601-639.
- [30] L. Rizhsky, H. Liang, R. Mittler, *J. Biol. Chem.* **2003**.
- [31] I. R. Politzer, G. W. Griffin, J. L. Laseter, *Chem. -Biol. Interact.* **1971**, 3, 73-93.
- [32] A. Krieger-Liszkay, *J. Exp. Bot.* **2005**, 56, 337-346.
- [33] J. R. Durrant, G. Porter et al. *Proc. Natl. Acad. Sci. U.S.A.* **1995**, 92, 4798-4802.
- [34] A. Telfer, J. De Las Rivas, J. Barber, *Biochim. Biophys. Acta, Bioenerg.* **1991**, 1060, 106-114.
- [35] B. Andersson, E.-M. Aro, *Photodamage and D1 protein turnover in PSII, Vol2.*, Springer, **2001**
- [36] C. Triantaphylidès, M. Havaux, *Trends Plant Sci.* **2009**, 14, 219-228.
- [37] J. Barber, B. Andersson, *Trends Biochem. Sci.* **1992**, 17, 61-66.

- [38] C. Vasilev, C. N. Hunter et al. *Langmuir*. **2014**, 30, 8481-8490.
- [39] S. D. Straight, D. Gust et al. *Nat. Nanotechnol.* **2008**, 3, 280.
- [40] H. Tian, S. Yang, *J. Photochem. Photobiol. C*. **2002**, 3, 67-76.
- [41] Q. Zheng, S. C. Blanchard et al. *Photochem. Photobiol. Sci.* **2016**, 15, 196-203.
- [42] C. E. Aitken, R. A. Marshall, J. D. Puglisi, *Biophys. J.* **2008**, 94, 1826-1835.
- [43] D. Gust, T. A. Moore, A. L. Moore *Faraday Discuss.* **2012**, 155, 9-26.
- [44] D. Hablot, A. Harriman, R. Ziessel, *Angew. Chem. Intl. Ed.* **2011**, 50, 7833-7836.
- [45] S. Cobo, S. Palacin et al. *Nat. Mat.* **2012**, 11, 802.
- [46] M. H. Ham, M. S. Strano et al. *Nat. Chem.* **2010**, 2, 929-936.
- [47] H. Y. Zhang, J. H. Choi et al. *ACS Appl. Mater. Interfaces*, **2015**, 7, 7833-7837.
- [48] P. N. Ciesielski, G. K. Jennings et al. *Bioresour. Technol.* **2010**, 101, 3047-3053.
- [49] M. S. P. Reddy, C. Park, *Sci. Rep.* **2016**, 6, 32306.
- [50] S. F. Rowe, D. J. Richardson et al. *ACS Catal.* **2017**, 7, 7558-7566.
- [51] F. Milano, M. Trotta et al. *Angew. Chem. Intl. Ed.* **2012**, 51, 11019-11023.
- [52] J. S. Lindsey, D. Holten et al. *Photosynth. Res.* **2014**, 121, 35-48.
- [53] K. R. Reddy, P. S. Parkes-Loach et al. *Chem. Sci.* **2013**, 4, 2036-2053.
- [54] Y. Yoneda, T. Dewa et al. *J. Am. Chem. Soc.* **2015**, 137, 13121-13129.
- [55] J. W. Springer, D. F. Bocian et al. *J. Am. Chem. Soc.* **2012**, 134, 4589-4599.
- [56] B. S. Richards et al. *IEEE J. Sel. Top. Quantum Electron.* **2008**, 14, 1312-1322.
- [57] P. S. Friedman *Opt. Eng.* **1981**, 20, 206887.
- [58] M. D. Hughes, S.-Y. Wang, D.-A. Borca-Tasciuc, D. A. Kaminski *Sol. Energy.* **2015**, 122, 667-677.
- [59] L. H. Slooff, A. Büchtemann et al. *Phys. Status Solidi RRL.* **2008**, 2, 257-259.
- [60] J. R. Lakowicz, *Principles of Fluorescence Spectroscopy*, Springer. **2006**.
- [61] L. H. Slooff, A. R. Burgers, M. G. Debije, *Proc. SPIE 7043*, **2008**, 6-13.
- [62] L. Xu, Y. Yao, N. D. Bronstein, L. Li, A. P. Alivisatos, R. G. Nuzzo, *ACS Photonics*, **2016**, 3, 278-285.
- [63] A. A. Earp, G. B. Smith, J. Franklin, P. Swift, *Sol. Energy Mater. Sol. Cells*, **2004**, 84, 411-426.
- [64] S. T. Bailey, Y.-Z. Zhang et al. *Sol. Energy Mater. Sol. Cells*, **2007**, 91, 67-75.
- [65] O. Altan Bozdemir, E. U. Akkaya et al. *Angew. Chem. Intl. Ed.* **2011**, 50, 10907-10912.
- [66] D. C. Jordan, S. R. Kurtz, *Prog. Photovol.* **2013**, 21, 12-29.
- [67] R. Reisfeld, D. Shamrakov, C. Jorgensen, *Sol. Energy Mater. Sol. Cells*, **1994**, 33, 417-427.
- [68] R. Kinderman, L. H. Slooff et al. *J. Sol. Energy Eng.* **2007**, 129, 277-282.
- [69] A. F. Mansour, H. M. A. Killa, S. A. El-Wanees, M. Y. El-Sayed, *Polym. Test.* **2005**, 24, 519-525.
- [70] A. F. Mansour, M. Hammam et al. *Polym. Intl.* **2002**, 51, 393-397.
- [71] A. A. Earp, T. Rawling, J. B. Franklin, G. B. Smith, *Dyes Pigm.* **2010**, 84, 59-61.
- [72] S. Beutner, B. Bloedorn, T. Hoffmann, H. D. Martin, *Methods Enzymol.* **2000**, 319, 226-241.
- [73] G. Griffini, S. Turri et al. *Sol. Energy Mater. Sol. Cells*, **2013**, 111, 41-48.
- [74] G. Griffini, M. Levi, S. Turri, *Sol. Energy Mater. Sol. Cells*, **2013**, 118, 36-42.
- [75] G. Griffini, M. Levi, S. Turri, *Prog. Org. Coat.* **2014**, 77, 528-536.
- [76] S. M. Reda, *Sol. Energy.* **2007**, 81, 755-760.
- [77] D. J. Robbins et al. *J. Chem. Soc. Perkins Trans.* **1984**, 1293-1301.
- [78] V. Sholin, J. D. Olson, S. A. Carter, *J. Appl. Phys.* **2007**, 101, 123114.
- [79] S. Ghosh et al. *Appl. Phys. Lett.* **2010**, 96, 191901.
- [80] M. A. Malik et al. *Semiconductors.* **2004**, 38, 909-917.
- [81] M. Grabolle et al. *Anal. Chem.* **2009**, 81, 6285-6294.
- [82] J. Silcox et al. *Nano Lett.* **2002**, 2, 1321-1324.
- [83] H. Peng, L. Zhang, C. Soeller, J. Trivas-Sejdic, *J. Lumin.* **2007**, 127, 721-726.
- [84] W.-L. Yang et al. *J. Am. Chem. Soc.* **2006**, 128, 13396-13401.
- [85] S. J. Gallagher, B. C. Rowan, J. Doran, B. Norton *Sol. Energy.* **2007**, 81, 540-547.
- [86] S. M. Reda, *Acta Mater.* **2008**, 56, 259-264.
- [87] R. Xie, U. Kolb, J. Li, T. Basché, A. Mews, *J. Am. Chem. Soc.* **2005**, 127, 7480-7488.
- [88] R. Koole et al. *Sol. Energy Mater. Sol. Cells*, **2011**, 95, 2087-2094.

- [89] M. G. Hyldahl, S. T. Bailey, B. P. Wittmershaus, *Sol. Energy*. **2009**, 83, 566-573.
- [90] J. Zhao, Y. Li, G. Yang, K. Jiang, H. Lin, H. Ade, W. Ma, H. Yan, *Nat. Energy*, **2016**, 1, 15027.
- [91] M. V. Jacob et al. *Renew. Sust. Energ. Rev.* **2013**, 27, 104-117.
- [92] T. P. Osedach, T. L. Andrew, V. Bulović, *Energy Environ. Sci.* **2013**, 6, 711-718.
- [93] M. C. Krebs et al. *Adv. Mater.* **2012**, 24, 580-612.
- [94] Y. Xie et al. *J. Mater. Sci.* **2018**, 53, 7715-7724.
- [95] S. N. Duan, C. Dall'Agnese, H. Ojima, X. F. Wang, *Dyes Pigm.* **2018**, 151, 110-115.
- [96] S. Nho, D. H. Kim, S. Park, H. N. Tran, B. Lim, S. Cho, *Dyes Pigm.* **2018**, 151, 272-278.
- [97] E. A. Katz et al. *Sol. Energy Mater. Sol. Cells*, **2011**, 95, 1253-1267.
- [98] J. Schafferhans et al. *Org. Electron.* **2010**, 11, 1693-1700.
- [99] J. Hauch et al. *Sol. Energy*. **2011**, 85, 1238-1249.
- [100] H. Hintz, H. J. Egelhaaf, H. Peisert, T. Chassé, *Polym. Degrad. Stab.* **2010**, 95, 818-825.
- [101] C. J. Brabec, *Sol. Energy Mater. Sol. Cell.* **2004**, 83, 273-292.
- [102] C. Li, M. Liu, N. G. Pschirer, M. Baumgarten, K. Mullen, *Chem. Rev.* **2010**, 110, 6817-6855.
- [103] E. Bundgaard, F. C. Krebs, *Sol Energy Mater. Sol. Cells.* **2007**, 91, 954-985.
- [104] W. Wang, D. Placencia, N. R. Armstrong, *Org. Electron.* **2011**, 12, 383-393.
- [105] C.-P. Chen, S.-H. Chan, T.-C. Chao, C. Ting, B.-T. Ko, *J. Am. Chem. Soc.* **2008**, 130, 12828-12833.
- [106] P. Cheng, G. Li, X. W. Zhan, Y. Yang, *Nat. Photonics.* **2018**, 12, 131-142.
- [107] S. Guillerez et al. *Polym. Degrad. Stab.* **2010**, 95, 278-284.
- [108] D. E. Motaung, G. F. Malgas, C. J. Arendse, *J. Mater. Sci.* **2011**, 46, 4942-4952.
- [109] R. Grisorio, G. Allegretta, P. Mastrorilli, G. P. Suranna, *Macromolecules.* **2011**, 44, 7977-7986.
- [110] M. Manceau et al. *J. Mater. Chem.* **2011**, 21, 4132-4141.
- [111] J. W. Lichtman, J.-A. Conchello, *Nat. Methods.* **2005**, 2, 910.
- [112] J. Hašek, E. Streiblová, *Fluorescence Microscopy Methods, Vol.1*, Springer, **1996**, 391-405.
- [113] T. Wilson, *Confocal Microscopy*, Academic Press: London, **1990**, 426, 1-64.
- [114] B. Huang, M. Bates, X. Zhuang, *Annu. Rev. Biochem.* **2009**, 78, 993-1016.
- [115] B. O. Leung, K. C. Chou, *Appl. Spectrosc.* **2011**, 65, 967-980.
- [116] D. Axelrod, *Total Internal Reflection Fluorescence Microscopy, Vol.30*, Elsevier, **1989**, 245-270.
- [117] M. J. Rust, M. Bates, X. Zhuang, *Nat. Methods.* **2006**, 3, 793.
- [118] P. Tinnefeld et al. *Small*, **2010**, 6, 1379-1384.
- [119] M. L. Martin-Fernandez, C. J. Tynan, S. E. D. Webb, *J. Microsc.* **2013**, 252, 16-22.
- [120] B. Huang, *Curr. Opin. Chem. Biol.* **2010**, 14, 10-14.
- [121] W. E. Moerner, M. Orrit, *Science.* **1999**, 283, 1670-1676.
- [122] E. Barkai, Y. Jung, R. Silbey, *Annu. Rev. Phys. Chem.* **2004**, 55, 457-507.
- [123] W. E. Moerner, D. P. Fromm, *Rev. Sci. Instrum.* **2003**, 74, 3597-3619.
- [124] R. Y. Tsien et al. *Nat. Biotechnol.* **2004**, 22, 1567.
- [125] P. Tinnefeld et al. *ChemPhysChem.* **2010**, 11, 2475-2490.
- [126] A. M. Smith, H. Duan, A. M. Mohs, S. Nie, *Adv. Drug Deliv. Rev.* **2008**, 60, 1226-1240.
- [127] J. Dobrucki et al. *Photobleaching, Vol. 1*, Springer, **2006**, pp.690-702.
- [128] S. C. Blanchard et al. *Nat. Methods*, **2012**, 9, 68.
- [129] T. Cordes et al. *Nat. Commun.* **2016**, 7, 10144.
- [130] D. Axelrod et al. *Biophys. J.* **1976**, 16, 1055-1069.
- [131] H. C. Ishikawa-Ankerhold, R. Ankerhold, G. P. C. Drummen, *Molecules.* **2012**, 17, 4047-4132.
- [132] J. Lippincott-Schwartz et al. *Science.* **1996**, 273, 797-801.
- [133] D. Zicha et al. *J. Microsc.* **2002**, 205, 109-112.

Chapter 2 - Experimental Methods and Data Analysis

2.1 Absorption Spectroscopy

The most intensely used technique throughout the course of the research presented here is also perhaps the most modest. All measurements up to 1100nm were made using double beam spectrophotometers, either a Perkin-Elmer Lambda 35 or a Hitachi U3310. These instruments were used for both solution phase samples and also for samples distributed in solid matrices. The decadic absorption of a sample is related the molar absorption coefficient, ϵ , of the molecule of interest by the Beer-Lambert law, which gives us the following expression:

$$\text{Log} \left(\frac{I}{I_0} \right) = A = \epsilon \cdot c \cdot l \quad (2.1)$$

Here I is the intensity of the light transmitted through the sample. A is the absorbance and c the molar concentration of the solute. The molar absorption coefficient, ϵ , is related to the absorption cross-sectional area, $\epsilon = \sigma \cdot N_a / 2.303 \times 10^3$. Although it is entirely feasible to work in transmission mode, it is preferential to work in terms of absorbance as this value is linear with concentration.

Absorption spectroscopy is a robust measurement due to the double beam setup, a schematic of which is shown in Figure 2.1. The light source, deuterium and tungsten filament in our case, passes through a monochromator to select the wavelength and then passes through a beam splitter. The two beams then impinge on either the sample or the reference. The transmitted light is then detected by either separate detectors or the same detector in conjunction with a chopper. The amount of light transmitted by the sample is found by examining the ratio of the two signals.

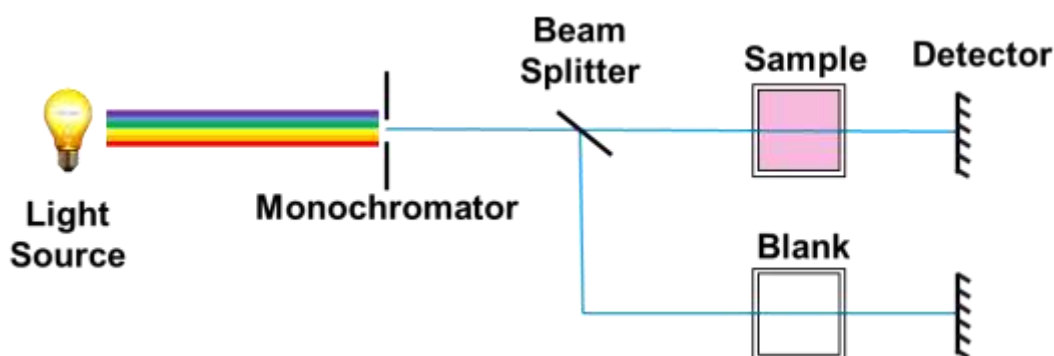


Figure 2.1 – Schematic diagram outlining the operating method of a dual-beam absorption spectrophotometer.

To effectively remove solvent or cuvette artefacts, a pair of matched quartz or glass cuvettes is used, and a suitable baseline recorded. Slit widths were minimised for proper resolution of spectra, except in the case of films where opening the slits allows for effective averaging of the signal and makes it easier to measure the same spot if a sample has to be moved. Scan rates and wavelength divisions are considered carefully in order to achieve high quality spectra in a reasonable time.

Absorption spectroscopy was used extensively to characterise the rate of loss of chromophores during photobleaching experiments. It was used also to measure molar absorption coefficients of new samples. To do this, samples were weighed out in triplicate using a four-figure balance of 0.1mg resolution and stock solutions were made in 25ml volumetric flasks. These stock solutions were diluted in a known fashion to construct Beer-Lambert plots. It is worth mentioning that careful selection of sample absorbance is of great importance. An absorbance of 2 equates to only 1% of the light being transmitted through the sample. At such values, stray light entering the system or fluorescence from the sample could cause errors in the measurement.

Routine use of dual-beam spectrometers is unhindered up to (a working) limit of 1000nm. With a trend toward evermore applications in the far-red and NIR regions of the spectrum, it is becoming more important to work outside the visible range. Specialised instruments are needed for this that work in the same manner but with a selection of detectors, typically InGaAs and PbS, to measure up to 3300nm. To attempt to measure an intervalence charge-transfer band in one of our materials it was necessary to make a measurement up to such values. We are indebted to the University of Leeds for access to their instrument.

To measure samples at high concentration, a variable path length absorbance cell, pictured in Figure 2.2, was designed and constructed in our machine shop. It consists of a threaded brass barrel with quartz windows at each end. The cell could be adjusted to any desired length down to a stopper at 200 μ m and a maximum at 4 cm. Solutions are introduced to the cell using the PTFE Luer lock ports shown in Figure 2.2. To calibrate the cell, a stock solution of Rhodamine 6G of known concentration was used to determine the path length of the cell. Turn markings were used to define the cell distance, with one turn increasing the cell length by 1mm.



Figure 2.2 – Variable path length cell used to measure high concentrations or alternatively long path lengths.

2.2 Fluorescence Measurements

2.2.1 Steady-State Fluorescence Spectroscopy

To measure the light emitted by molecules, fluorescence spectroscopy is employed. Unlike absorption spectroscopy, fluorescence spectroscopy is notoriously vulnerable to artefacts and errors, both instrumental and those induced by the user. The typical setup for measuring fluorescence involves selection of an excitation wavelength by a monochromator. The light is absorbed in part by the sample and the excited molecules then emit fluorescence. The detector is usually situated at a right angle to the sample but the actual position can be varied as required. It is sometimes useful to illuminate the sample with light delivered from some external source, such as a laser diode, and to couple the sample to the instrument through optical fibres.

Due to changes in lamp power, and also monochromator and detector variations across the spectral range, the spectrum reported by the instrument is the technical spectrum and is subject to the errors. For example, a typical fluorimeter may be equipped with an R928 PMT detector. The sensitivity of such a detector drops as we move from 400nm to longer wavelengths, decreasing rapidly in the range 700-800nm. Additionally, these inaccuracies may change over time. To report the true spectrum, correction must be made for all these possible errors. When reporting emission spectra, it is usually sufficient to provide the technical spectra as most measurements are repetitive and concerned with changes in intensity. What allows us to make quantitative comparison is the fact that the intensity of light emitted will depend linearly on the number of molecules emitting, as long as precautions are taken not to work at concentrations where the absorbance is too high. When reporting excitation spectra, it is more important to employ spectral corrections as it is typical to compare excitation spectra with the corresponding absorption spectra. In this case, a quantum counter

is needed. In principle, the emission wavelength is set to 680nm and sweeping the excitation range should give equal intensity from all excitation wavelengths. The quantum counter used was a highly concentrated solution (8mg/ml) of Rhodamine B in ethanol which is generally accepted to give the closest match between a quantum counter and a thermopile. The drawback is that the upper limit for excitation is 600nm. Quantum counters for longer wavelengths are known but the intensity deviation from the mean is much greater.

To an overwhelming extent, modern fluorescence spectrophotometers operate on a wavelength basis since the researcher and reader tend to be more comfortable interpreting results in this manner. It is important to understand that this representation of spectra is not ideal. Quanta of energy are not linear on a wavelength scale as we know from the relationship, $\lambda = hc/\nu$. For many purposes, it is acceptable to present spectra on a wavelength scale but if we need to delve deeper it is necessary to present data on an energy / quanta of energy basis, hence reduced spectra are required.

Making a fluorescence measurement seems to be a simple process but there is significant scope to introduce further artefacts by user error. These potential problems have been well documented in text books and include, but are not limited to, false signals from Rayleigh and Raman scattering and signals from trace amounts of highly emissive impurities. A particular source of user-introduced error comes from using solutions that are too concentrated. Even when a molecule is well solvated it is important to keep the absorption below 0.1 at the excitation wavelength. At this low concentration one can be confident that there will be no problem from self-absorption as long as the excitation wavelength has been selected properly. Self-absorption, or inner-filter effects, arise due to spectral overlap, photons emitted by the molecules are reabsorbed elsewhere in the solution. The result is distorted spectra that affect quantitative measurements such as the determination of the fluorescence quantum yield. It is worth describing that most abused of measurements in a little detail. Quantum yields of fluorophores are determined by the ratiometric method. The integrated emission intensity of an unknown sample is measured by excitation at a wavelength where the fraction of absorbed light has been measured accurately. A fluorophore with a well-established quantum yield is then excited at the same wavelength and the integrated emission and fraction of absorbed light recorded from the absorbance ($I_{abs} = 1 - 10^{-A}$). The quantum yield is given by the ratio of the integrated emissions, n refers to the refractive index of the solvent used and Φ_f^R is the fluorescence quantum yield of the reference.

$$\Phi_f^S = \frac{I_{abs}^R \int Fl^S}{I_{abs}^S \int Fl^R} \cdot \frac{n_S^2}{n_R^2} \cdot \Phi_f^R \quad (2.2)$$

To avoid errors in the measurement, the absorbance should not exceed 0.1 at the excitation wavelength, at higher concentration self-absorption effects begins to become important and some of the emitted light is reabsorbed by the sample. Where possible, the same solvent should be used for sample and reference but Equation 2.2 allows correction for different refractive indices.

All samples were measured at four different concentrations to ensure accuracy of the derived quantum yields. The excitation wavelength must be the same for sample and reference as lamp intensity and monochromator efficiency may depend on wavelength. This can be a source of error as the excitation wavelength may be far from the absorption maximum and as such the absorbance measurement at the excitation wavelength may be very low and subject to high error. Care should be taken to ensure there is good overlap between the emission range of the sample and reference. Again, due to monochromator and detector performances, if the spectra are located in different parts of the light spectrum then the integrated emissions will be subject to error. A final source of error of note is the value of the yield given for the reference. We are reliant on the absolute quantum yield having been determined accurately, often within the literature conflicting values are found for the same material. A specific example is the extensively used reference Rhodamine 6G, this molecule is now believed to have a quantum yield of 94% however many contemporary papers will refer to a previous value reported for this compound of 78%. Unity quantum yields have been reported for samples compared to Rhodamine 6G using this value, which would suggest there is some significant problem with those measurements.

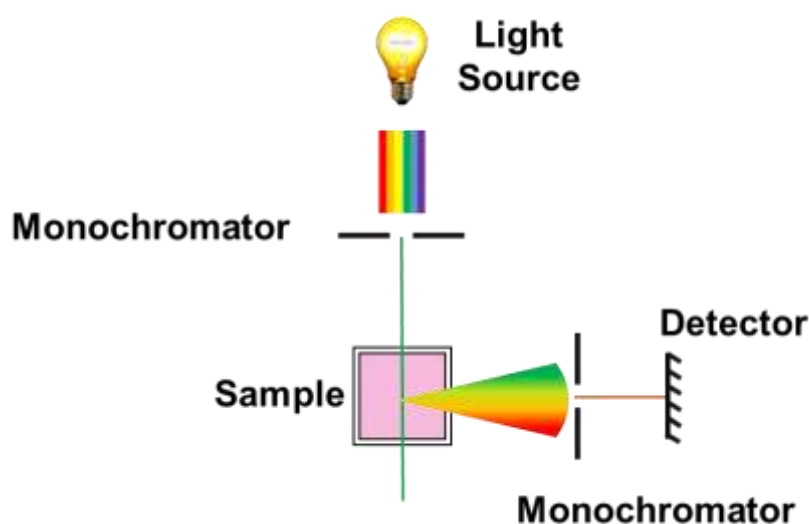


Figure 2.3 - A schematic view of a typical fluorescence setup. This arrangement was used for solution measurements using standard 10mm cuvettes. Where irregular samples such as films or cryogenics are studied, specialist fixtures were used but the generic arrangement is much the same.

Figure 2.3 shows a generic layout for a typical fluorescence spectrophotometer. For our work, most fluorescence measurements were carried out using Hitachi F4500 or F2500 model instruments depending on whether it was necessary to measure beyond 650nm or if specialised fittings were required. The measurement range could be extended beyond 800nm by using a Fluorolog Tau-3 modular instrument equipped with a R2658 PMT. Again, minimised monochromator slit widths were used to ensure proper resolution of spectral features. Typically, this was 2.5nm for both excitation and emission slits but was varied according to the need for more signal. As for the absorption measurements, scan rates were selected to provide a reasonable balance between quality of spectra and effective use of time.

2.2.2 Temperature-Controlled Spectroscopy

A more complete understanding of the photophysical properties of fluorophores can be garnered by understanding how these properties change with a variation in temperature. It is well known that temperature provides the impetus to cross barriers and can have an effect on environmental factors such as solvent viscosity. Temperature control is of particular significance for emission measurements but was also applied to absorption spectroscopy, transient absorption spectroscopy and photostability measurements. To record spectra at low temperature an Oxford Instruments Optistat DN was used with an ITC temperature controller and with liquid nitrogen as the coolant. For elevated temperatures, up to 80°C, a stabilised, circulating liquid bath was used. A thermocouple was placed at the sample surface to ensure accurate measurement of the temperature. Additionally, temperatures above 100°C were accessible using a high temperature cell, designed for IR measurements but adapted for fluorescence. In this case, samples were crystalline materials or powders dispersed in dried KBr and pressed into a transparent disc.

2.3 Fluorescence Lifetime Measurements

While steady-state fluorescence and excitation spectra are rich in information, it is essential to have time-resolved emission data too. In the first instance, this allows us to establish a rate constant for the radiative decay of an excited state according to: $k_r = \Phi_f / \tau_f$, where τ_f is the emission lifetime. The fluorescence lifetime of a molecule is a statistical measure of the time taken for a population of excited-state molecules to return to the ground state. It is defined as the time taken for the population to reach the point where 1/e of the molecules remain in the excited state. Lifetimes are vital for understanding the nature of any fluorescence quenching events and to better characterise samples where fluorophores may reside in multiple environments or conformations. Once the lifetime data have been recorded, the decay curves can be analysed by several different models. A single type of fluorophore in a uniform

environment should show a first-order decay but many other cases are possible. In our work, two different instrumental methods were used for lifetime measurements.

2.3.1 Time-Correlated, Single Photon Counting (TCSPC)

The modern preference for making lifetime measurements is to use time-correlated, single photon counting, TCSPC, methods. This technique involves exciting the sample with an appropriate pulsed source and using a gating method to count photons arriving at the detector. The time taken for the signal to reach the detector is found by setting a large number of channels to record photons arriving at different temporal delays. A pulsed excitation source repeatedly excites the sample, allowing photons to be counted at each delay and an intensity at each time is recorded. This accumulated curve is the fluorescence decay trace. To extract the lifetime from this trace, it is necessary to apply deconvolution procedures using an instrument response function (IRF), as can be seen in Figure 2.4. In this case, a scattering sample such as Ludox dispersed in water is used. There is no lifetime associated with this scattering pulse, so the intensity profile is a function of rise time of the detector.

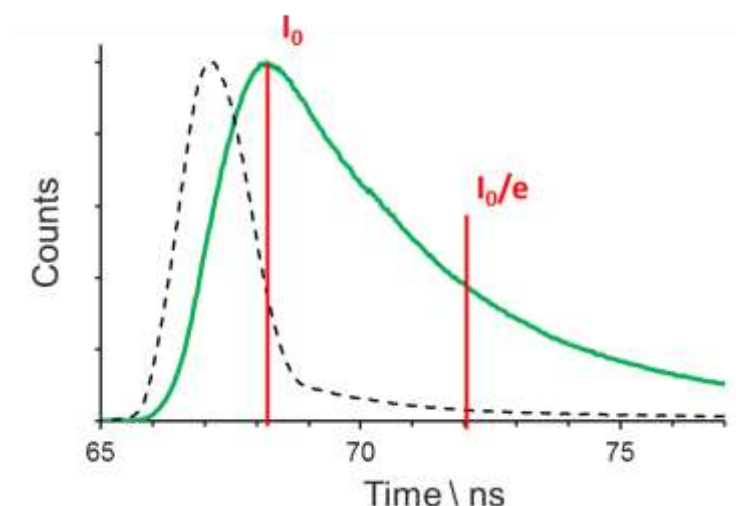


Figure 2.4 – TCSPC example for a BOPHY fluorophore with a ns lifetime, showing the fluorescence intensity (—) and the IRF (---)

The lower limit on TCSPC measurements is set by the duration of the excitation pulse and the rise time of the detector. In the work reported here, the temporal resolution of the basic set-up is 120ps, depending on the actual sample and the fluorescence characteristics. The upper limit is on the order of microseconds which is not generally relevant to S_1 emission in the organic fluorophore realm but can be useful for measuring delayed fluorescence and phosphorescence.

2.3.2 Frequency Domain Lifetime Measurements

This technique involves the modulation of the excitation signal and the subsequent modulation of the emission to calculate the lifetime of a sample. A sinusoidal modulation is applied to the intensity of the excitation source, which in turn causes the emission intensity to vary in intensity. To measure the fluorescence lifetime, a sweep across a frequency range is required. When the signal is modulated at long times relative to the lifetime under study, the phase angle between the signals will be (close to) zero as the emission will be almost instantaneous compared to the modulation of the signal. As the frequency increases, there is a relative delay in the emission maximum intensity due to the finite lifetime of the sample. Similarly, there is a decrease in the modulation of the emission signal. As the excitation signal reaches a maximum before the population has finished fluorescing the minimum in signal is never reached. More correctly this is called the demodulation of the emission intensity. Due to delays in the electronics, the phase angles and modulations seen by the spectrometer will not be correct so a reference is also required. This is usually achieved by using a scattering sample or a sample with a well-known, short lifetime. The upper limit on measuring the lifetime is set by the difficulty in measuring signals with a modulation greater than 200MHz.

The modulation of the intensity is found by $M = j/J/i/I$ which is demonstrated in the schematic in Figure 2.5. The lifetime of the sample is then calculated as a function of frequency from the following equations, if the lifetime under study is a single exponential, the two equations will yield the same value. The data are fitted by standard statistical protocols as for the TCSPC method, an example being given in Figure 2.6.

$$\tan\phi_\omega = \omega\tau_f \quad (2.3)$$

$$M_\omega = [1 + \omega^2\tau_f^2]^{-1/2} \quad (2.4)$$

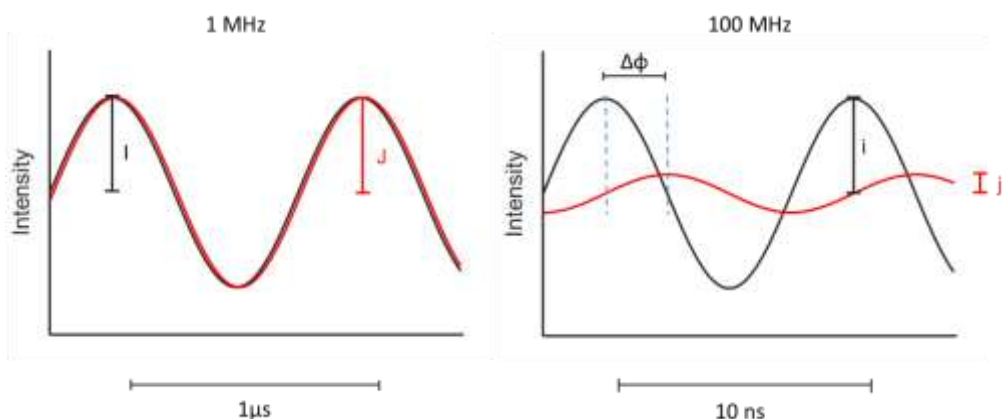


Fig 2.5 - Effect of modulation on the excitation (—) intensity and emission (—) signal at relatively low and high frequencies, the peak-to-peak time is shown for each frequency. At 1 MHz there is little or no demodulation of the signal or change in phase angle, unlike the high frequency signal.

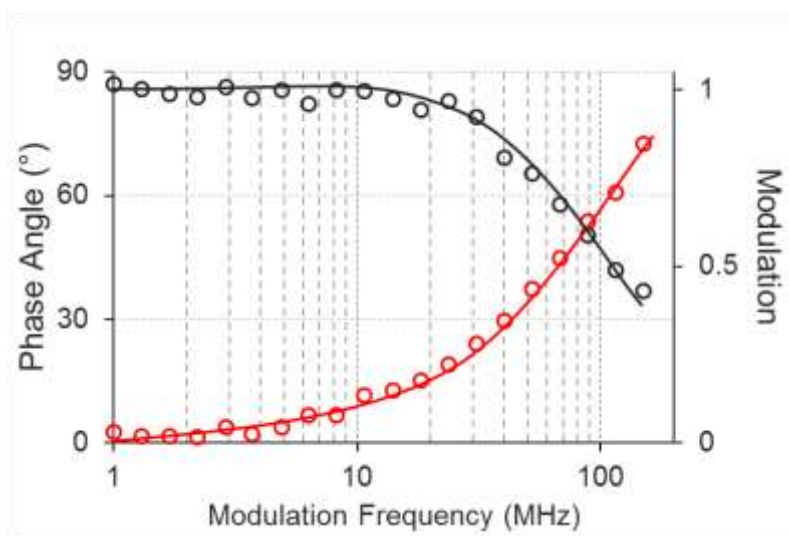


Figure 2.6 - Example of lifetime data recorded for a BOPHY sample with a ns lifetime: black points being the modulation and red points representing the phase angle. Solid lines refer to the best fit to Equations 2.3 and 2.4.

2.4 Transient Absorption Spectroscopy

An additional time-resolved instrumental method used extensively in this work was transient absorption spectroscopy (TAS). The technique is also known as ‘flash-photolysis’, related to the genesis of the technique where a flash lamp was used to excite the sample, or ‘pump-probe’ spectroscopy. In this technique an intense, pulsed, light source, usually monochromatic and delivered with a laser, is used to promote the sample to the excited state. A probe light is then used to measure the absorption spectrum of transient species so formed, such as triplet-excited states, photo-isomers or other meta-stable species or to probe the ground-state

bleach. In our work, TAS was performed using an Applied Photophysics LKS-70 instrument. This set-up is equipped with a Quantel Brilliant Nd:YAG laser emitting at 1064nm. The pulse duration is around 4ns and operates at a repetition rate of 10Hz with an energy of up to 250mJ. Additionally, second and third harmonic generators are used to produce 532nm and 355nm excitation, respectively. The excitation may also be coupled to an optical parametric oscillator (OPO), which allows the source to be further tuned. This allows excitation of the sample at almost any wavelength from the near-UV to the near-IR, although this comes at the cost of lost intensity. A timing gate records the laser pulse as it travels to the sample and allows the analysing broadband light to be pulsed so it arrives just after excitation of the sample. To record the decay kinetics of the transient of interest, a monochromator is used to isolate the wavelength at which the transient absorbs. The probe light is detected by a conventional PMT and the signal is monitored until recovery of the pre-pulse baseline. The monochromator may be varied sequentially, and a pump-probe experiment performed at each wavelength. This allows us to find absorption spectra for all species present at different times. Global analysis can be used to extract information about the number of species present and of their individual kinetic profiles.

The lower limit in time resolution is set by the pulse duration of the excitation source, which in our case is approximately 4ns, processes complete in shorter times than this will not be seen. The upper limit depends mainly on probe lamp stability and the occurrence of other artefact, a working limit in the millisecond range was encountered where the analysing light is not pulsed. The setup is effective over the range of ten nanoseconds to tens of milliseconds. To measure faster processes such as electronic energy transfer requires more specialised instruments. Typical output from our setup is illustrated by way of Figure 2.7.

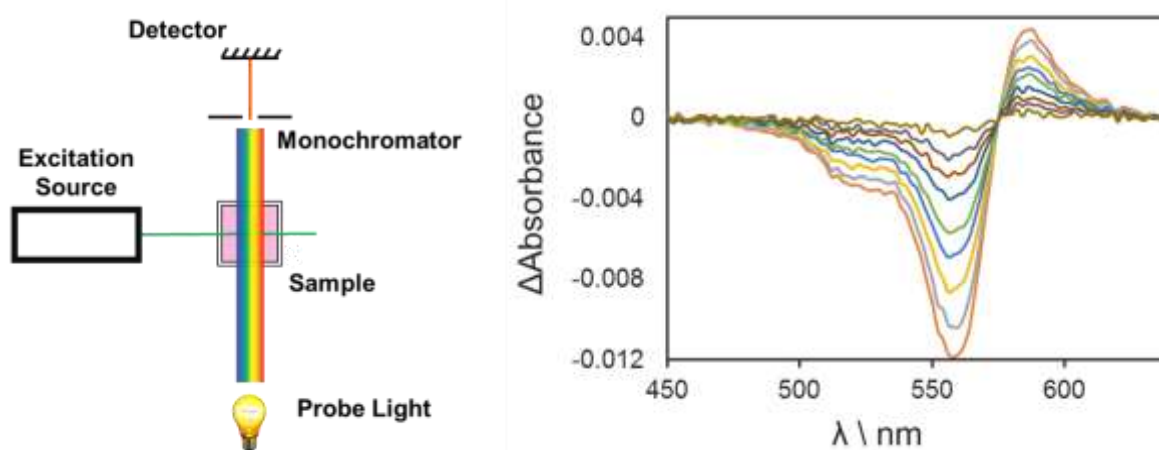


Figure 2.7 – Left, transient absorption spectroscopy schematic and right an example of spectroscopic data showing the isomerisation of a merocyanine dye. The individual traces are at regular time intervals up to 40ms.

2.5 Photobleaching Protocols

2.5.1 Photostability under Continuous Illumination

Much of the original research described in this thesis is concerned with the loss of photoactive material under illumination. Standard tests and protocols do not exist by which to compare rates of photo-fading so it is left to the researcher to select the most appropriate conditions for such experiments. Two separate approaches can be identified, namely the use of monochromatic or broadband illumination. We utilised both approaches, often for the same sample. Since we are invariably working with chromophores recognised as having good photostability, it follows that long illumination periods are required. This, in itself, introduces experimental difficulties and uncertainties.

The use of monochromatic light may be favoured when quantitative information, such as quantum yields for photobleaching, is needed and when we want to control which species is being subjected to illumination. The main approach used for studying photobleaching under monochromatic light was to focus a high-powered LED onto a solution contained in a standard cuvette. The cuvette was housed in a fixture allowing temperature control and includes a stirrer so that we are not reliant on diffusion to move bleached molecules out of the beam. Alternatively, laser sources were used, in particular for measuring the bleaching of films. This was performed using an in-house built bleaching rig, coupled to a photodiode as detector, which is shown in Figure 2.8. Samples could also be removed to perform spectroscopic measurements during the photobleaching process.

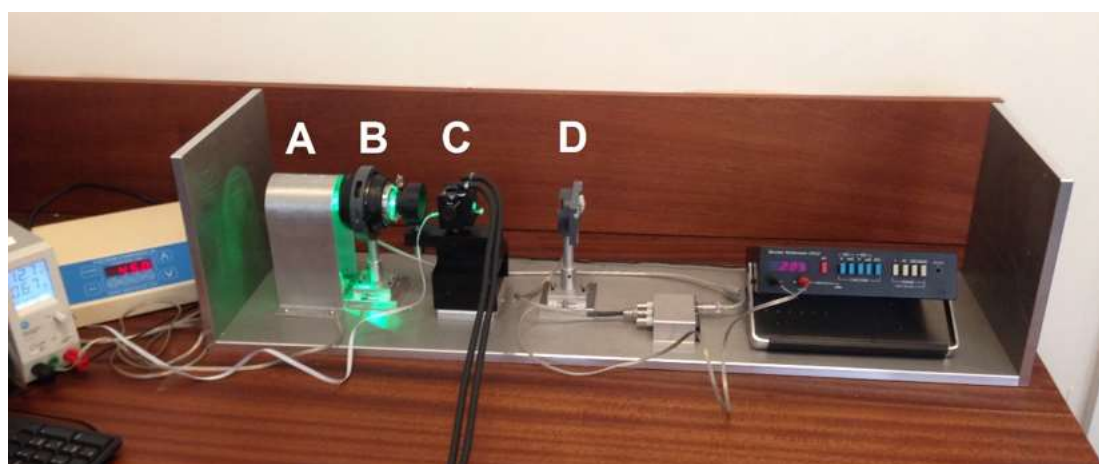


Figure 2.8 – Monochromatic bleaching rig, (A) is the replaceable LED, (B) the lens, (C) the temperature controlled cell holder and (D) a photodiode.

Monochromatic examination of the samples allows quantitative characterisation of the dye, we know how many photons are being absorbed and we should understand which species is absorbing those photons. However, the ultimate aim is to understand the stability of molecules

that will be used in devices for exploitation of the huge energy source given to us in the form of sunlight. Thus, it is appropriate to see how bleaching proceeds under conditions that equate to bleaching by sunlight. A broadband, 400W HQI floodlamp was used as the source for these studies. Samples were placed 50cm from the centre of the source to bathe the samples in light. A thick glass screen was used to absorb near-UV and IR radiation from the lamp to prevent excessive heating of the sample. The course of bleaching was monitored by absorption and/or emission spectroscopy. A further advantage of this method is that it allows multiple samples to be bleached simultaneously so that the molecule can be studied in various environments. Chromophores dispersed in solid media, typically plastic films, were studied in the same manner. Figure 2.9 shows the output from the lamp compared to standard sunlight. The inset to the figure shows the output profile for one of the high-power LEDs used for monochromatic illumination.

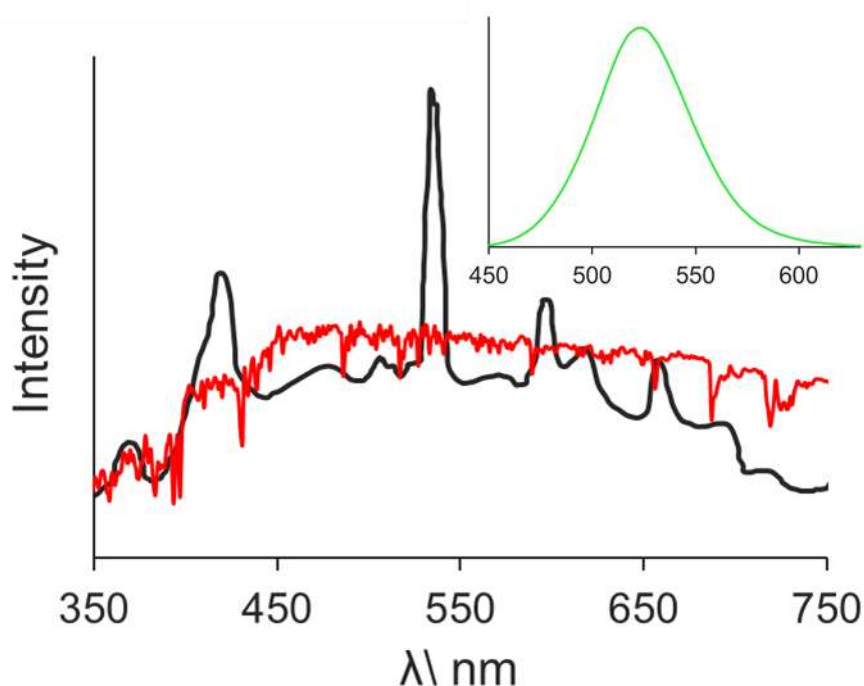


Figure 2.9 - The intensity output of the flood lamp used for bleaching experiment (–) compared to AM1.5G (—), a standardised spectrum for solar simulation. The lamp used is reasonably flat across the visible spectrum although some sharp peaks are evident. The intensity axis is arbitrary. Inset: The 523nm LED used for bleaching of samples (FWHM=50nm) under “monochromatic” excitation.

2.5.2 Fluorescence Recovery after Photobleaching (FRAP)

The Newcastle Medical School is very well equipped with an array of modern microscopes, including the latest version of super-resolution and single-molecule instruments. We have had occasional access to this resource, courtesy of Dr Alex Laude. One set of measurements made at the Newcastle Microscopy Centre involved using Fluorescence Recovery After

Photobleaching (FRAP) techniques to determine the diffusion coefficients for fluorescent dyes. Here, a solution of the fluorophore is drawn into a microscope slide holder by capillary forces. The sample is bleached by exposure to an intense laser of an appropriate wavelength directed to a fixed location. The same spot is interrogated by excitation with weak laser beam and the intensity of the fluorescence is monitored in real time. The fluorescence intensity recovers to a value close to that recorded prior to bleaching as the molecules diffuse into the region of interest. This allows the diffusion coefficient to be found by standard treatment of the kinetic data. There are clear analogies between photobleaching and FRAP and more use might be made of these modern microscope-based protocols in order to better understand some aspects of the bleaching chemistry.

A second technique offered by the Newcastle Microscopy Centre is known as Total Internal Reflectance Microscopy (TIRF). This is a new instrumental method that allows the surface layer to be monitored by way of total internal reflectance. This means that the chemistry of molecules at the interface can be monitored selectively and, in principle, this could have important implications for photobleaching studies. The technique is not well known in the field and, in our experience, it is useful only in cases where rates of photobleaching are quite fast.

2.5.3 Preparation of Samples in Solid Matrices

Typically, the photophysical properties of organic dyes are studied with the sample dissolved in a suitable solvent. This allows for easy determination of the properties and allows for control of environment properties such as polarity or viscosity. It is of ever-increasing interest to better understand the properties of dyes when distributed in some solid or pseudo-solid matrix. For most potential light-harvesting or opto-electronic devices, the dye will need to be incorporated into a transparent solid. Recognising this likelihood it follows that it is important to measure the chemical and physical properties of the dyes after the fabrication of the solid device. It is possible that, in certain cases, immobilisation of the dye can have significant effects on the properties. It is also important to make a critical comparison of stability of dyes in solid matrices and the fluid solution.

Much of our work was based on the use of poly(methyl methacrylate) with a molecular weight of 120,000 as the host material. The dye was dissolved at high concentration in some suitable solvent such as dichloromethane. Aliquots of the stock solution were diluted with either toluene or methoxybenzene (anisole). These solutions were placed in a water bath at around 45 °C and agitated with a magnetic stirrer. A weighted amount of PMMA was added gradually to the solvent to a maximum w/w ratio of 3:1 solvent to polymer. This mixture was then left until all the polymer had dissolved and was then poured into rectangular molds of 7.5x2.5mm which were 1mm deep. The samples were left in the dark to allow the solvent to evaporate. After at

least 24 hours standing, the films were removed and annealed at 80 °C for around 15 minutes so that flat films result. The choice of solvent is important for the effective dissolution of the polymer but more critically for the quality of the dried film. It is important that the vapour pressure is sufficiently low to ensure slow evaporation. Drying stress in films is of the order of MPa, the pressure changes result in expulsion of air from the drying solution. The result is bubbles in the film.

Other polymers, such as Zeonex and polyethylene, were used and fabricated in the same manner. Chromophores were also incorporated into optical-quality glasses formed from sucrose octaacetate, by dissolving the matrix in a water-ethanol mixture with dye added. The solution is recrystallized before being melted at 80°C. On cooling, a clear solid is formed.

2.6 Electrochemistry

Cyclic voltammetry was performed using a conventional 3-electrode setup. The working electrode used was glassy carbon and the counter electrode was a platinum wire. The reference electrode of choice was Ag/Ag⁺. Measurements were performed in nitrogen-purged solutions of anhydrous solvents, usually dichloromethane, with an electrolyte, normally tetrabutylammonium tetrafluoroborate, at a concentration of 0.1M. All measurements were performed using a CH Instruments 600 potentiostat.

2.7 Nuclear Magnetic Resonance Spectroscopy

¹H, spectra were recorded at either 400 or 700MHz and ¹³C, ¹¹B and ¹⁹F NMR were performed with the frequencies adjusted for the gyromagnetic ratios using Bruker Avance II 400 or Avance III HD 700 MHz instruments. The latter was exclusively in cases when it was important to work at low concentrations. Spectra were also recorded at cryogenic temperature in support of Chapter 4. Two-dimensional, cross-correlation methods, NOSY, HSQC and HMBC were used to confirm assignment of chemical shifts when samples were measured in different solvent environments. We are indebted to the help provided by Dr Corinne Wills, with assistance from Prof W. McFarlane, in interpreting NMR spectra.

2.8 IR Spectroscopy

Vibrational spectra were measured using a Varian 800 FT-IR spectrometer utilising an attenuated total reflectance (ATR) crystal. Samples were mixed with optical grade KBr and

discs prepared under high pressure. The positioning arm is used to ensure good contact between the sample and the crystal

2.9 Thermal Blooming

Accurate determination of fluorescence quantum yields is notoriously difficult to achieve. For routine work, when using liquid phase samples, it is usually most straightforward to use the ratiometric method described previously. As well as judicious choice of reference for one's excitation and emission needs, there is also a problem in that the stated quantum yields for many references are not wholly trustworthy. It is the case that as one moves toward the far-red and NIR regions, this becomes even more of a problem due to spectrometer limitations.

Absolute measurements of fluorescence quantum yields are required to establish reference materials emitting in the red-near IR. Absolute measurements are also obligatory for measuring non-standard samples such as in solid films where the precise number of molecules excited cannot be known. There are a number of techniques for measuring absolute fluorescence quantum yields, the most well-known being the use of an integrating sphere. Perhaps the main downside to the integrating sphere is the cost. We have set up our own capability to measure absolute, or more precisely *pseudo*-absolute quantum yields, by building an instrument that uses a technique called thermal blooming. The technique was developed in the 1970's and some of the established quantum yield standards were confirmed using this methodology. However, the technique never gained widespread usage. Thermal blooming uses the fact that power not emitted as light must be deposited into the medium as heat (Equation 2.5):

$$P_{Total} = P_{Tr} + P_L + P_{Th} \quad (2.5)$$

A laser is used to illuminate a solution in a standard cuvette. The light that impinges, P_{total} , the sample may be either absorbed or transmitted, P_{Tr} , the absorbed power may then either be emitted as luminescence, P_L , or degraded to heat, P_{Th} , which is then deposited in the solvent. The deposited heat causes localised heating of the solvent on a μK scale and in turn this changes the refractive index. This causes the solvent to act as a lens, expanding the laser beam. A shutter is used and a plano-convex lens is used to focus the laser beam, the detector is positioned at some large distance so that the initial beam size is greater than the size of the detector, and the cuvette is placed at the Rayleigh distance. The shutter is opened for some hundreds of milliseconds, power deposited in the sample heats the solvent and the beam expands at the detector. The signal reaching the detector decreases. This drop in signal

intensity with time is recorded using an oscilloscope until an equilibrium is reached and then fitted to Equation 2.6.

$$I(t) = I_o \left[1 - \theta \left(1 + \frac{t_c}{2t} \right)^{-1} + \frac{1}{2} \theta^2 \left(1 + \frac{t_c}{2t} \right)^{-2} \right]^{-1} \quad (2.6)$$

Here, θ is a parameter directly related to the power deposited and t_c is characteristic time related to thermal diffusivity of the solvent. The technique is *pseudo*-absolute in that it requires a non-emissive reference that absorbs the excitation source. Finding such a material with good solubility in the solvents of interest was not as simple a task as might be anticipated but Brilliant Green was found to be an acceptable chromophore. A rapid isomerisation quenches any fluorescence but it is not photostable so the solution needs to be regularly refreshed. A feature of the technique is that the reference and sample need not be absorbing in the same part of the spectrum, it is only necessary that the reference absorbs the excitation source so there are no complications with entering higher excited states. The reference gives a theta value with only transmitted and thermal power ($P_L = P_{Tr} + P_{TH}$). The quantum yield is then found by applying Equation 2.7.

$$\Phi_f = \left[1 - \frac{A_R \theta_S}{A_S \theta_R} \right] \frac{\nu_{ex}}{\nu_f} \quad (2.7)$$

Here A_s is the power absorbed by sample and A_R is the corresponding value for the reference. The factor at the end is the excitation energy of the laser divided by the emission maximum, which is needed to account for energy deposited due to the Stokes' shift. It is important that the amount of heat deposited is strictly controlled as excessive heating causes convection currents in the solvent. For methanol, this power limit is 0.6mW and can be controlled by laser intensity and sample concentration. A schematic outline of the set-up is shown as Figure 2.10.

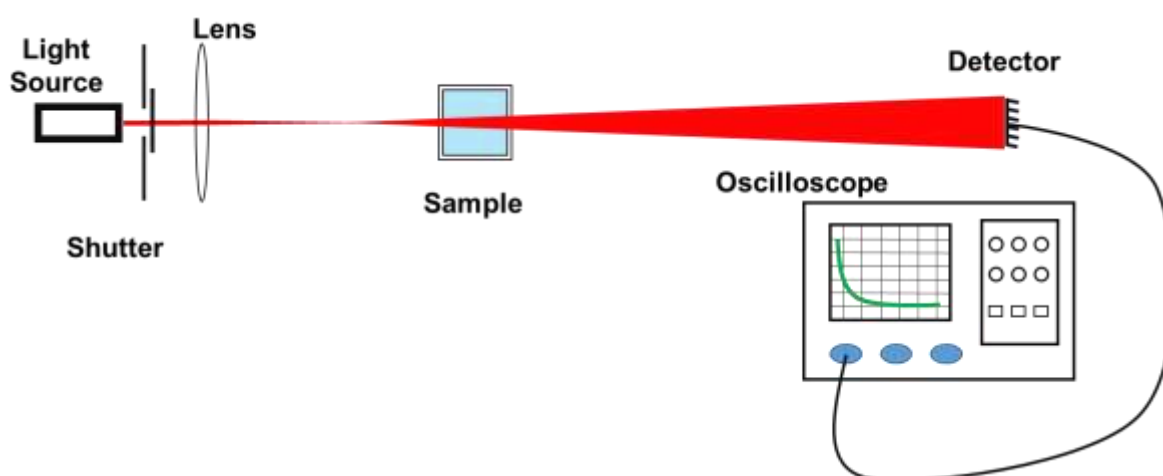


Figure 2.10 - Thermal blooming schematic, detection is by a silicon photodiode, the laser used for red emitting samples was a 635nm of TEM₀₀ mode with a Gaussian beam intensity profile.

2.10 Mass Spectroscopy

Mass spectroscopy was performed at the EPSRC National Research facility based at Swansea and we are grateful for access to this resource. Compounds, and some photobleaching reaction products, were analysed by electrospray ionization (ESI) methods using an LTQ Orbitrap XL-1. Where stability of was a concern, atmospheric pressure chemical ionization (APCI) / atmospheric solids analysis probe (ASAP) methods were employed using an Xevo G2-S instrument.

2.11 Analytical Methods

As a matter of routine, data were recovered from the instrument and analysed using purpose-built software routines. The fitting of data was performed, in all cases, using non-linear, least squares (NLLS) algorithms using facilities developed with Matlab, Scientist and PSI Plot. Mostly, data manipulation of this kind was routine and involved simple operations such as removing background signals, applying correction factors, converting between units, generating reduced spectra, fitting to various analytical models and extracting individual spectra from composite data. Wherever appropriate, subsequent modelling of the behaviour was carried out to test the robustness of the model. Mostly, this involved developing a model with Scientist and performing a series of simulations.

One notable exception to routine data management concerns the deconstruction of absorption, excitation and fluorescence spectra into a series of Gaussian-shaped components. This procedure is done in order to expose the set of vibronic modes coupled to the electronic transition. Our laboratory has considerable experience of this practice using the PeakFit software marketed by Jandel Scientific. Proper representation of spectra is required for this analysis, which means converting spectra to an energy scale and using reduced spectra (i.e., absorption intensity must be divided by the frequency and fluorescence by the third power of frequency). Spectra were fitted using the minimum number of Gaussian bands whilst maintaining a goodness-of-fit greater than 0.99. An example is shown in Figure 2.11. Such analysis allows determination of many parameters such as an exact value for the Stokes' Shift, the Huang-Rhys factor and the energy of the vibronic bands.

Efforts were made at all times to minimizing experimental uncertainty. Reported error values represent standard deviations of multiple experiments. This is the case for routine spectroscopic measurements such fluorescence quantum yield and fluorescence decay lifetimes. Fluorescence lifetimes and yields were often compared across different instruments

and techniques. In addition to running multiple measurements at different concentrations of dye in solution, as per a typical ratiometric fluorescence measurement. It is notable that greatest source of uncertainty in a quantum yield method probably comes from the literature value of the reference. Where values are obtained from fitting data to a model, the quality of the result is judged against visual inspection of model vs data, chi-squared values and by minimising residuals.

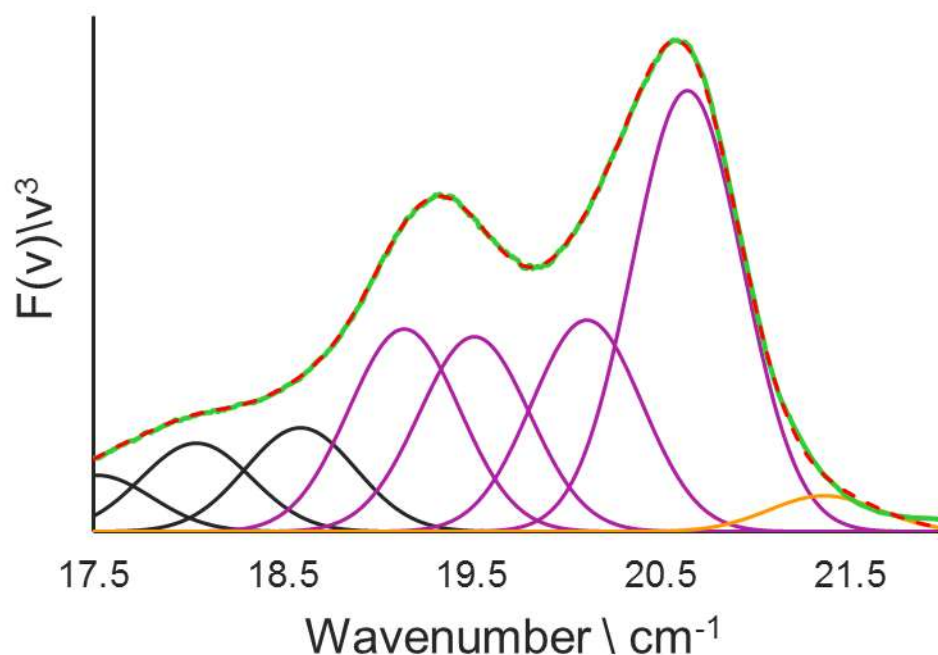


Figure 2.11 – Gaussian fitting of the room temperature fluorescence spectrum of a BOPHY molecule.

2.12 Materials

The new molecules studied here were provided by our collaborators and were used as received. We are greatly indebted to Raymond Ziesel, Julian Knight and Dumitru Sirbu for providing these materials. Where necessary compounds were further purified by preparative-scale -TLC until only a single component was observed on the plate. Certain other materials, such as quantum yield reference standards and established chemicals, were purchased from commercial sources and used as received. Samples of cyanine dyes were generously supplied free-of-charge by FEW Chemicals Ltd. Solvents used for spectroscopic measurements were of the highest grade available, either HPLC or spectroscopic grade and were stored in the dark at 4°C. All solvents were checked for the presence of fluorescent impurities. If in doubt, a fresh bottle was opened. Certain solvents, such as the alkane nitriles, were purified by vacuum distillation before use. Solvents for electrochemistry were refluxed and freshly distilled from drying agents.

Chapter 3 – Probing the Photostability of Erythrosine

3.1 Introduction

If we wish to obtain an improved understanding of how to design intrinsically stable dyes then a good place to start is with the photobleaching of a suitable model system. It is important to characterise to what extent common parameters, such as temperature, environment and concentration, affect the stability. In order to monitor the effects of these experimental variables, we need to identify a chromophore that undergoes relatively fast photobleaching. A dye that bleaches quickly might be expected to demonstrate a relatively simple mechanism. On a separate note, it is becoming ever more evident that huge costs are associated with bringing new commercial products to the market. This is especially so for chemical-based consumer products. In many cases, the regulatory barriers are prohibitive. As such, there is a strong case to be made for, wherever possible, using compounds that have already been tested over long periods and declared safe. For these various reasons, we have studied the photobleaching of Erythrosine. Erythrosine is the disodium salt, tetraiodo derivative of the xanthene class, as shown in Figure 3.1, that is commonly used as a food colourant^[1] (E127), as a^[2] dental plaque disclosing agent and a printing ink^[3]. It is an effective photosensitiser and has been proposed for use in photodynamic therapy^[4-6]. Xanthene dyes exhibit significant triplet yields and are known to generate singlet molecular oxygen under visible light illumination in water. Some photobleaching studies have been reported but important mechanistic details are missing.

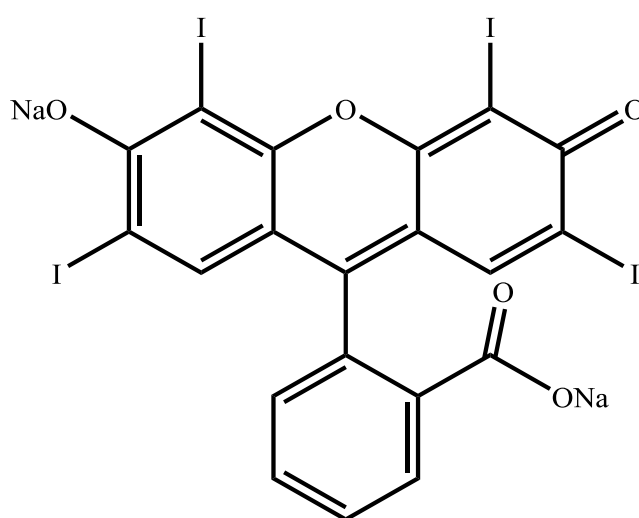


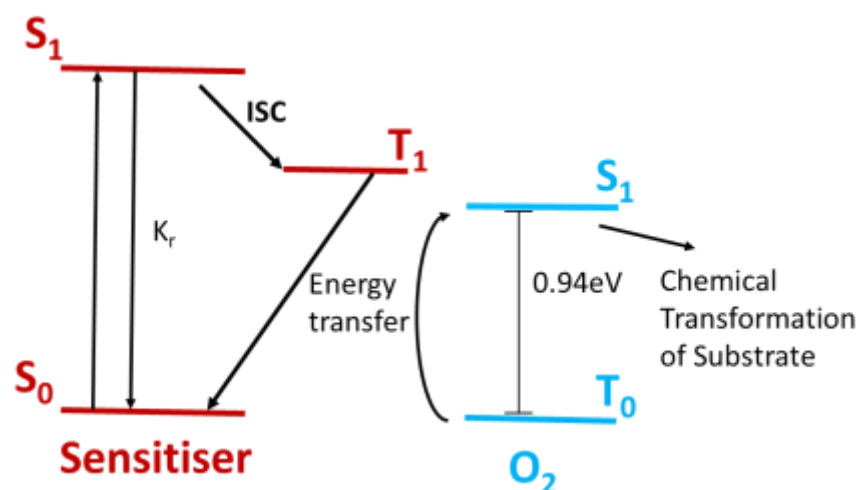
Figure 3.1 – Chemical structure of Erythrosine.

The majority of examples of dye photobleaching is believed^[7, 8] to proceed *via* the triplet-excited state of the dye. For the most part, this bleaching chemistry involves formation of the first-excited singlet state of molecular oxygen, known as singlet oxygen ($^1\Delta_g$). The oxygen electronic levels were established in 1928^[9], the ground state is triplet in nature ($^3\Sigma_g^-$) and an excited state of slightly higher energy ($^3\Sigma_g^+$) is also found. The lifetime of singlet oxygen is 45 minutes in the gas phase whilst for the other excited state it is around 10 seconds^[10]. This second excited state relaxes quickly to singlet oxygen. In solution, the lifetime of singlet oxygen is of the order of milliseconds to microseconds and is solvent-dependent^[11]. The species can be identified by its weak luminescence at 1270nm and an encounter pair of $^1\Delta_g$ molecules can pool their energy to produce red emission at twice this frequency. Singlet oxygen, therefore, is a *meta*-stable state that can encounter other species by diffusion. Singlet oxygen is a stronger oxidant than is ground-state molecular oxygen by about 1V^[12] and relatively long-lived so it is capable of performing organic modifications. On one hand, $^1\Delta_g$ can be considered a highly destructive, unwanted side-product of photoprocesses. Conversely, it can be a useful reactant for chemical transformations^[13] when employed with a photosensitiser. Singlet oxygen is particularly useful in photodynamic therapy where it is used in conjunction with a bio-compatible photosensitiser and the singlet oxygen can be used to attack cancer cells. Other interesting applications are the treatment of wastewater^[14] from domestic or industrial processes or use as an insecticide ^[15].

Singlet oxygen may be formed in a variety of ways, such as the excitation of oxygen in the gas phase by the electrical discharge of microwaves, the decomposition of hydrogen peroxide by reaction with hypochlorite ions, and energy transfer from an excited-state sensitiser which is the mechanism of interest to us. Singlet excited states may be quenched in some molecules by oxygen at diffusion controlled rates to yield $^1\Delta_g$ and an excited triplet state of the dye. This latter state in turn may be quenched by molecular oxygen to yield ground-state dye and a further crop of $^1\Delta_g$. By this process, quantum yields that exceed unity for the production of singlet oxygen have been reported^[16]. To be an effective sensitiser, the triplet state must have sufficient energy to excite molecular oxygen (i.e., the triplet excitation energy must exceed 0.98 eV). The excited-triplet state forms an encounter complex with ground-state oxygen. Assuming there is no intersystem crossing within the complex, spin statistics are used to argue that the quenching rate constant will be one-ninth of the diffusion-controlled rate limit.

Once free in solution, singlet oxygen is able to encounter substrates by way of diffusion and enter into chemical transformation, the process from excitation of the dye to the transformations is shown in Scheme 3.1. In terms of common solvents, water is an effective quencher of $^1\Delta_g$, the lifetime being 4 μ s while in chloroform the lifetime is increased to 230 μ s^[17]. Solvent deactivation is controlled by the vibronic levels of $^1\Delta_g$ which can couple to the

overtones of O-H and C-H vibrations. A useful consequence of this is that deuteration of the solvent can be used to prolong the lifetime. This is a useful tool when determining whether singlet oxygen plays an important role in a particular reaction mechanism.



Scheme 3.1 – Energy level diagram outlining how excitation of a sensitizer leads to chemical transformation of some substrate which may in fact be the sensitizer itself. The triplet energy of the sensitizer must be greater than the energy of singlet oxygen.

As already stated, $^1\Delta_g$ may be quenched by a suitable substrate. This quenching may be either physical or chemical in nature. Wholly physical quenching involves energy transfer from $^1\Delta_g$ to the substrate. An example of a physical quencher is β -carotene^[18], as employed in natural light-harvesting systems. For energy transfer to proceed, the excitation energy of the substrate must be below that of singlet oxygen. Bimolecular rate constants^[19] for such quenching steps can be on the order of $10^{10} \text{ M}^{-1}\text{s}^{-1}$ for certain carotenoids. The extent to which physical or chemical quenching will take place depends on the partitioning of the precursor complex. The reaction expected with highly conjugated π -networks is a 1,4-addition of O_2 to form an endoperoxide. Such products have been seen with tetracene^[20] or tryptophan^[13]. It is anticipated that reaction between organic chromophores, such as xanthene dyes, and oxygen will proceed in the same manner. Singlet Oxygen Sensor Green (SOSG), a commercially available sensor based on fluorescein linked to anthracene, apparently uses this transformation as a marker for the presence of $^1\Delta_g$ ^[21]. In the presence of singlet oxygen, there is oxygen addition across the anthracene^[22] switching off electron transfer such that fluorescein emission is restored, this process is shown in Figure 3.2.

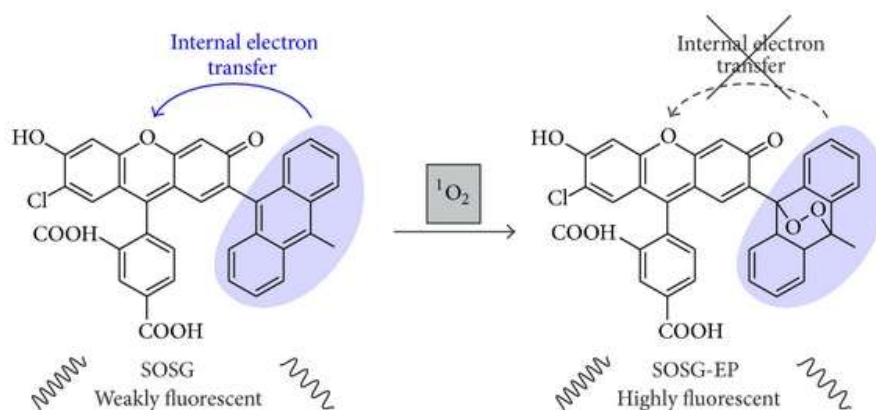


Figure 3.2 – Addition of singlet oxygen to the anthracene-fluorescein dyad, fluorescence is restored which signifies the presence of singlet oxygen. Figure adapted from ref [21].

Many different chromophores may be used as photosensitisers for the activation of molecular oxygen. These include transition metal complexes^[23], semiconductors^[24] and the porphyrin^[25] class of molecules. The porphyrin-type chromophores are of interest for bio-applications given that they are related to the chromophores present in natural systems and feature absorption within the 'biological window'. The xanthene class of dyes are well-established photosensitisers. They feature strong absorption bands and high yields of triplet states with excitation energies in the range of 1.5-2.0 eV. The parent form of this dye is fluorescein, which is one of the oldest known fluorescent dyes. Of particular interest are the tetraiodo-substituted forms, Rose Bengal and Erythrosine. Due to the presence of the four heavy atoms, these dyes have close to unity yield for the triplet-excited state. These highly conjugated systems can be vulnerable to addition of O₂ causing the conjugation path to be disturbed, which will lead to loss of the compound^[26].

Fluorescein, due to its widespread use in microscopy^[27], has been of interest in relation its photostability. Indeed, studies going back as far as the 1950's report on the stability of these chromophores under illumination^[28]. It is well known that these dyes are somewhat sensitive towards exposure to visible-light. It has been estimated, for example, that when used as photosensitisers they show turnover numbers with respect to singlet molecular oxygen in the order of 10³-10⁵ before degradation. Studies in various solvents and solid matrices have been undertaken^[29]. The formation of superoxide ions by way of light-induced electron transfer has also been implicated^[30]. Whilst studies exist, there is no standardised method to address the photobleaching and quantitative details are scarce. The bleaching is generally believed to be by way of first-order kinetics and a *pseudo*-unimolecular mechanism involving singlet oxygen has been implicated^[31]. Self-bleaching was suggested as a means by which to measure the extent of singlet oxygen formation^[32]. Although photostability has received limited attention,

there are no reports of how temperature affects the rate of reaction and indeed there is little real information about the bleaching mechanism. Here, we focus on one dye – Erythrosine – and undertake a systematic examination of the photobleaching process. This compound is readily available, water-soluble, cheap and non-toxic. It absorbs in a convenient part of the visible region, where high-intensity LEDs are available for excitation. The triplet-excited state is formed in high yield and is most likely associated with the bleaching chemistry. We have selected this compound for our initial studies on photobleaching and have given particular attention to recording how temperature affects the rate of photofading. Whilst the temperature would be controlled in microscopy this is not the usual case for a solar device. As such, the activation parameters could be of some significance but are essentially unknown for any photobleaching system.

3.2 Photophysical Properties of Erythrosine

The sample of Erythrosine used for these studies was provided by The Procter & Gamble Co. Preparative TLC, together with 700MHz ^1H and ^{13}C NMR spectroscopy, showed it to be of excellent purity. The photophysical properties of Erythrosine are well established and our measurements were largely in line with previous values. Dissolved in water, Erythrosine displays a sharp absorption transition with a peak at around 526nm (Figure 3.3), the measured molar absorption coefficient at the peak maximum was $75,000 \text{ M}^{-1}\text{cm}^{-1}$.^[33] The emission maximum is at 548nm, giving a Stokes' shift of 750cm^{-1} . It should be noted that these spectroscopic values are in accordance with previous reports^[34]. Emission from the singlet-excited state was recorded with a lifetime of 250ps which is somewhat longer than reported values of 140ps^[35] or less^[36].

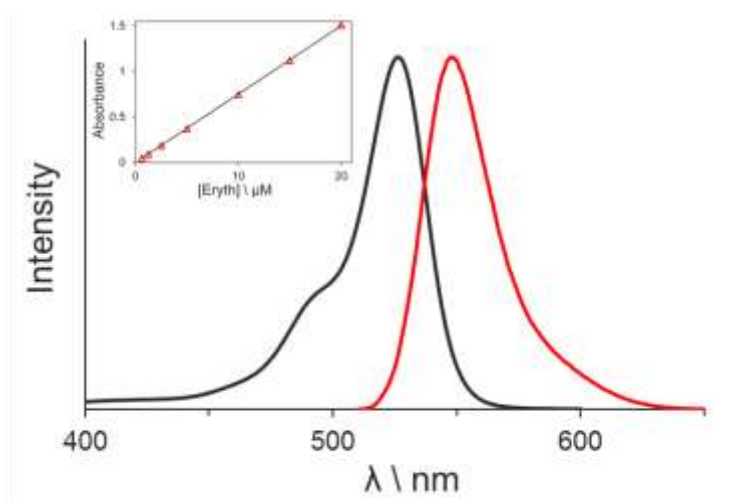


Figure 3.3 – Absorbance and emission of Erythrosine, inset shows a Beer-Lambert plot over the concentration range covered by the bleaching study.

The measured fluorescence quantum yield was 0.03, which is in line with literature values^[37] and the photon balance is achieved by crossing to the triplet state ($\Phi_t=0.97$)^[38]. Over the likely range of concentrations that are applicable to photobleaching studies, the dyes does not aggregate and a Beer-Lambert plot exhibits an excellent linear fit. These properties are collated in Table 3.1.

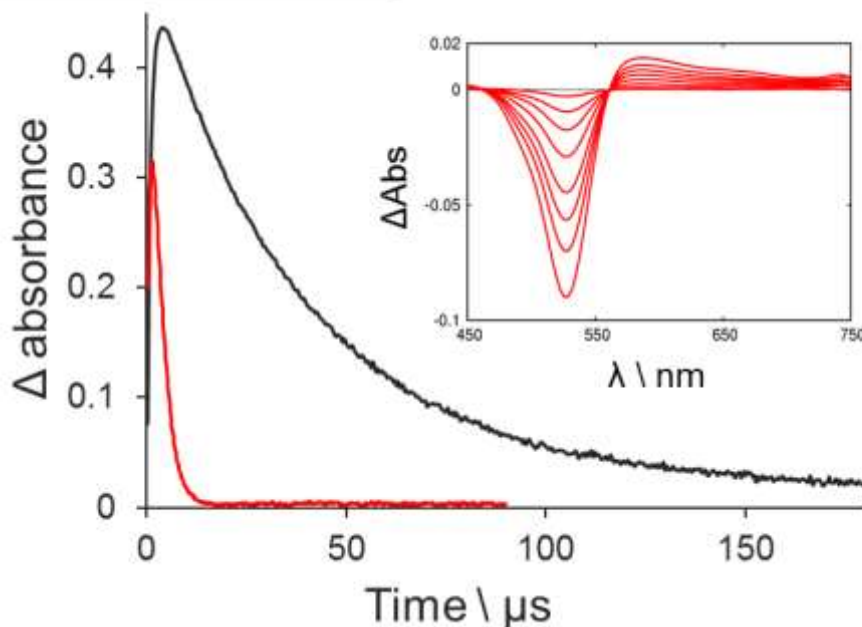


Figure 3.4 – Ground-state bleach decays in the presence of O_2 (—) and when purged with N_2 (—). Inset shows the transient spectrum of Erythrosine in deoxygenated solution at times from 30 to 130 μs

The triplet lifetime, in air-equilibrated and deoxygenated aqueous solutions, seen in Figure 3.4, was found to be 3 μs and 150 μs respectively; a triplet lifetime of 196 μs ^[39] has been reported elsewhere. Molecular oxygen quenches the triplet-excited state with a bimolecular rate constant of $1.4 \times 10^9 M^{-1} s^{-1}$. It is known that the product of this quenching is mainly singlet molecular oxygen, although superoxide ions might also be formed. We were able to record phosphorescent emission (Figure 3.5) at 77K in an ethanol:ethylene glycol mixture (80:20) with a maximum at 663nm. Reports of phosphorescence at room temperature in oxygen-free ethanol at 694nm^[40] have appeared in the literature but we could not replicate this effect. The properties of Erythrosine are not sensitive to proton concentrations at pH above 4^[41].

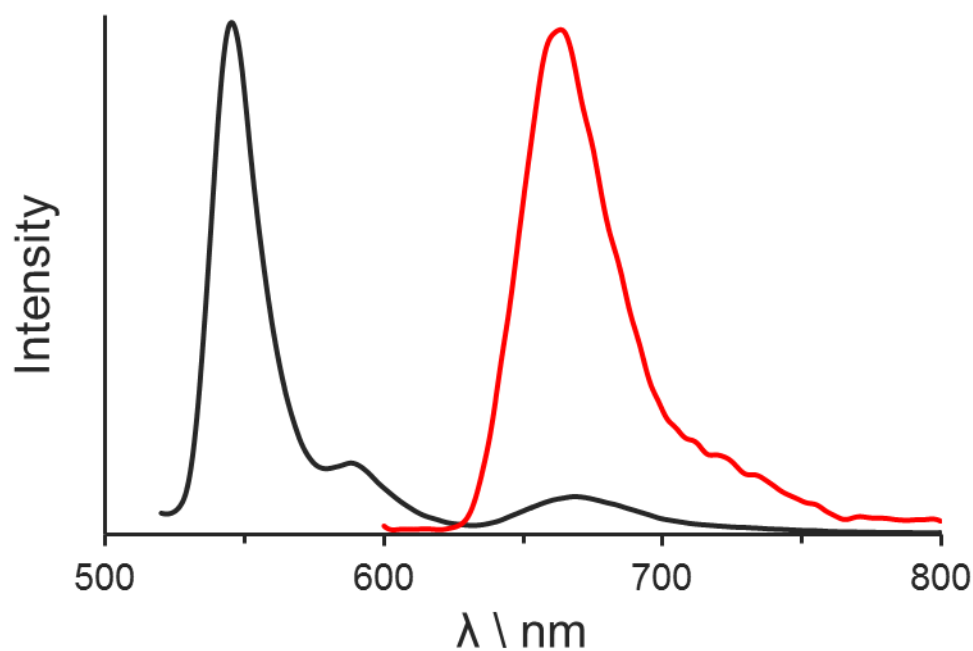


Figure 3.5 – Fluorescence (—) and Phosphorescence (—) of Erythrosine at 77K.

<i>Property</i>	<i>Measured</i>	<i>Literature</i>
$\lambda_{abs} \setminus \text{nm}$	526	527
$\lambda_{fluc} \setminus \text{nm}$	548	545
$SS \setminus \text{cm}^{-1}$	750	630
Φ_f	0.03	0.02
$\tau_f \setminus \text{ns}$	0.25	0.14
$\lambda_{phos} \setminus \text{nm}$	663	694
$\tau_f \setminus \mu\text{s}$	150	196

Table 3.1 – Collated photophysical properties as measured for our sample of Erythrosine and comparison with literature values.

3.3 Photobleaching of Erythrosine

3.3.1 Broadband Photobleaching

Initial assessment of the photodegradation of Erythrosine was made by exposing an air-equilibrated aqueous solution with a concentration of around 20 μM to broadband illumination. The compound was found to bleach rapidly with no build-up of a coloured product, although there does appear to be some UV product. Purging the solution with N_2 was found to reduce the bleaching rate although the degradation is still appreciable. In both cases, the bleaching kinetics were found to give excellent fits to first-order processes, as shown in Figure 3.6, the

rate is some 4 times faster in the presence of O₂. The bleaching observed under N₂ could be due to incomplete removal of oxygen but transient spectroscopy has shown that in oxygen-free solutions the triplet decay is dependent on the concentration of Erythrosine. This self-quenching mechanism has a bimolecular rate constant, k_{dd} , of $4 \times 10^8 \text{ M}^{-1} \text{ s}^{-1}$ [39]. Concentration quenching of this type is not unusual[42] and it is plausible that a dye-dye reaction could take place resulting in loss of chromophore. Given the relative abundance of oxygen and the high bimolecular quenching rate, reaction of triplet dye with a ground-state molecule will account for less than 2-3% of triplet deactivation even at the highest concentration. The change in concentration of Erythrosine with exposure time was measured by monitoring the absorbance at the band maximum. The quantum yield for formation of singlet oxygen with Erythrosine as a sensitizer, Φ_{Δ} , is 0.68[43] in water at 20°C.

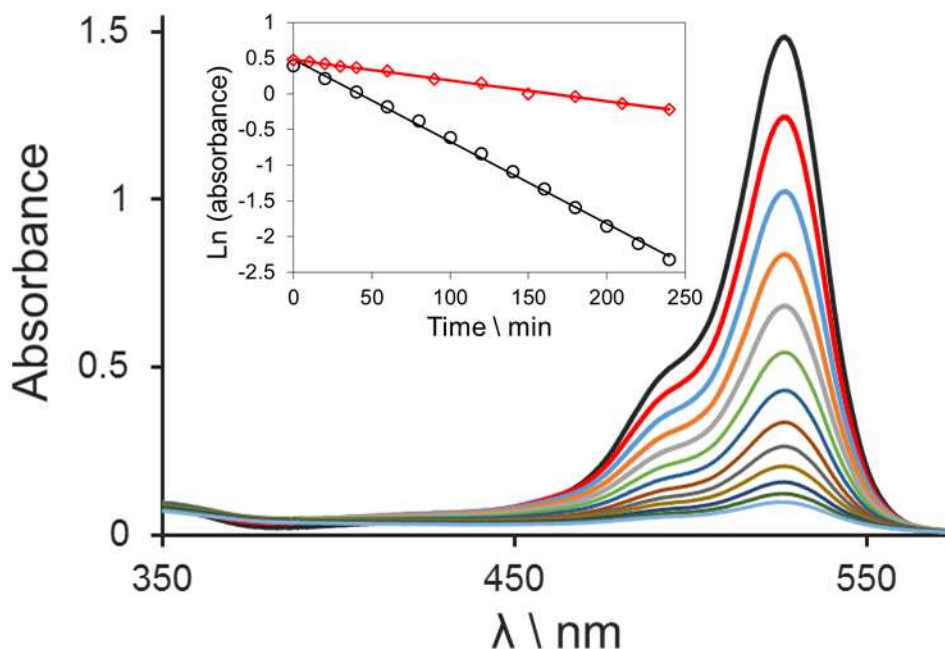


Figure 3.6 – Broadband bleaching of Erythrosine in water, inset shows the bleaching kinetics in air-equilibrated (O) and N₂ (◇) purged solutions

3.3.2 Monochromatic Photobleaching

Illumination by the way of the broadband source is an effective means to cause photobleaching of Erythrosine and is, to some extent, a simulation of exposure to sunlight. To gain a better understanding of the reaction kinetics, yields and mechanisms, a sample was illuminated using a high powered LED with output centred at 523nm. All results henceforth were collected in this mode. As demonstrated in Figure 3.7, the bleaching of Erythrosine under these conditions allowed characterisation of the illumination source! Thus, a piece of filter paper was soaked in a solution of Erythrosine and allowed to dry. The impregnated paper was

placed in the light beam then left until sufficient bleaching had occurred which, because of the intensity dependence, emphasized the dimensions of the individual LED units. The incident power was subsequently measured using a silicon photodiode detector calibrated for the response curve of the detector.

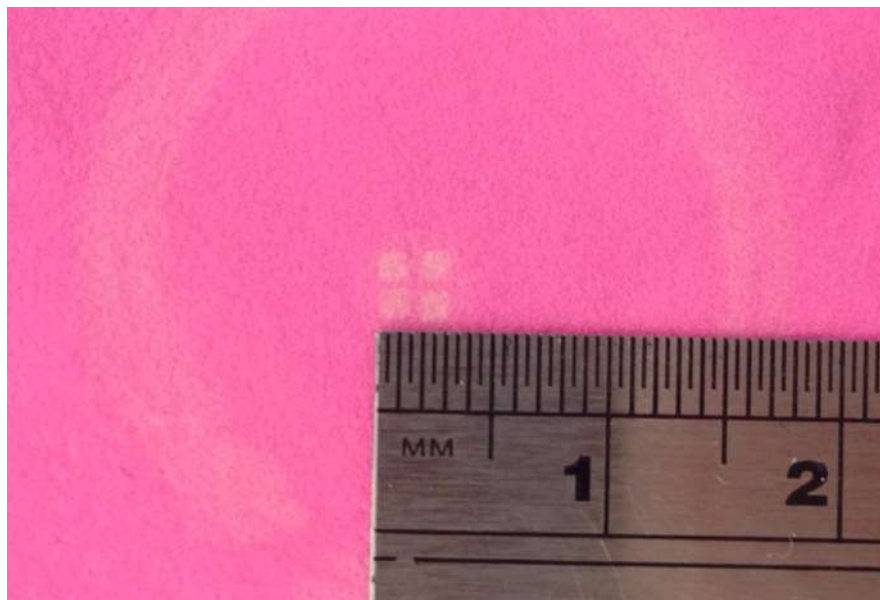


Figure 3.7 – Profile of the LED illumination source as incident on a piece of filter paper.

Under monochromatic illumination at room temperature, Erythrosine bleached quickly. Illumination of a stock solution of Erythrosine showed that the reproducibility of the bleaching rate was $\pm 5\%$ for a given LED power. An initial difference, shown in Figure 3.8, between the two forms of illumination is that we now see the growth of a product that forms in the UV to blue region of the spectrum, this product appears broad and featureless. This product must be either of low molar absorption coefficient or is one of a number of products. The isosbestic point is not maintained suggesting formation of more than one product. Given that the product is not seen under broadband illumination it must be unstable towards light. There is also a difference in the bleaching kinetics, the absorbance data no longer fit to a first-order process and is seen to accelerate over time. The implication of this is that the already efficient bleaching reaction is further catalysed by products that develop from the breakdown of Erythrosine. This concept is expanded upon later (*vide infra*).

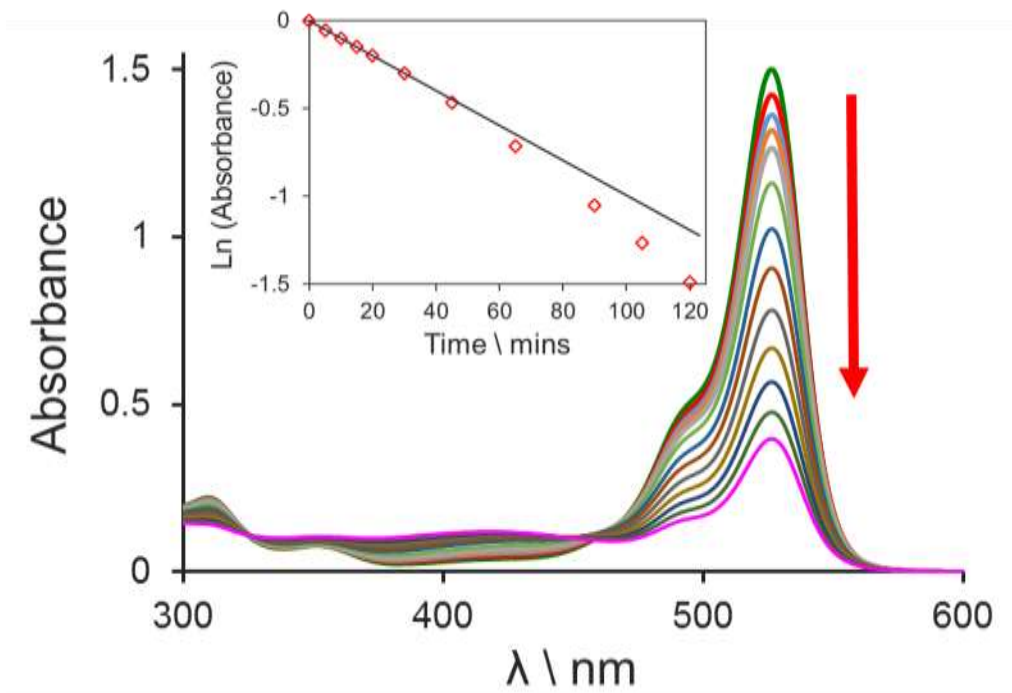


Figure 3.8 – Overlaid bleaching spectra of Erythrosine when subject to 523nm illumination. Inset shows the bleaching kinetics measured from the absorbance at λ_{max} . Solid black line is a first order fit to the initial bleaching rate, demonstrating the deviation.

3.3.3 Concentration Dependence under Monochromatic Illumination

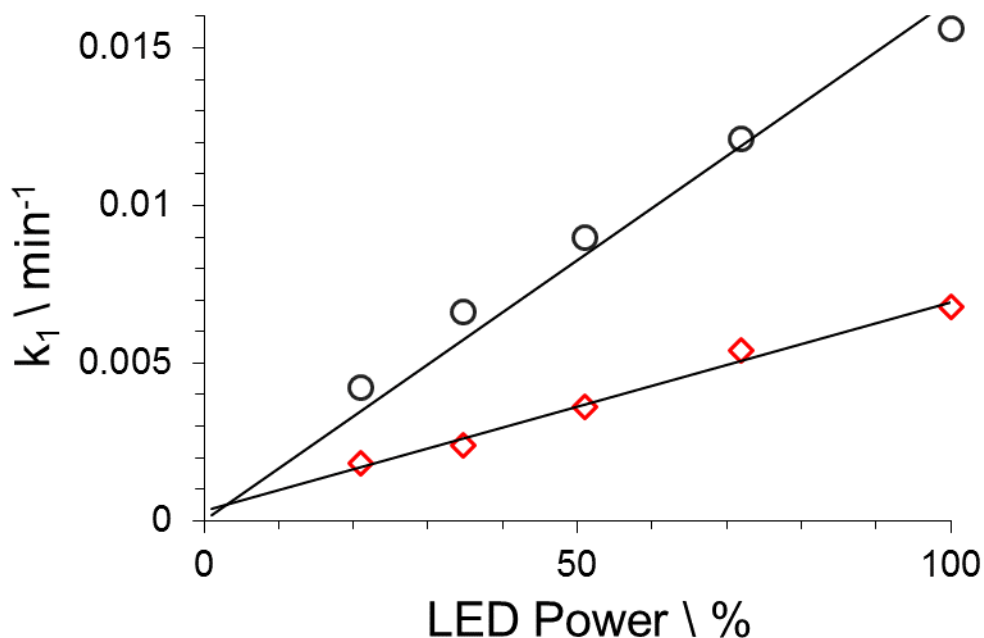


Figure 3.9 – Bleaching rate as LED transmitted power is varied

At relatively high concentration of Erythrosine, the bleaching rate was close to first-order but with some acceleration towards the end of the experiment. The bleaching rate was

subsequently measured over a range of lower concentrations. At the lowest concentration used, i.e. 0.9 μM , the rate corresponds to a first-order reaction with respect to Erythrosine. In fact, acceptable fits to first-order processes were found at all concentrations below 10 μM . For these studies, the reaction was carried out at 20°C. The bleaching data is shown in Figure 3.10.

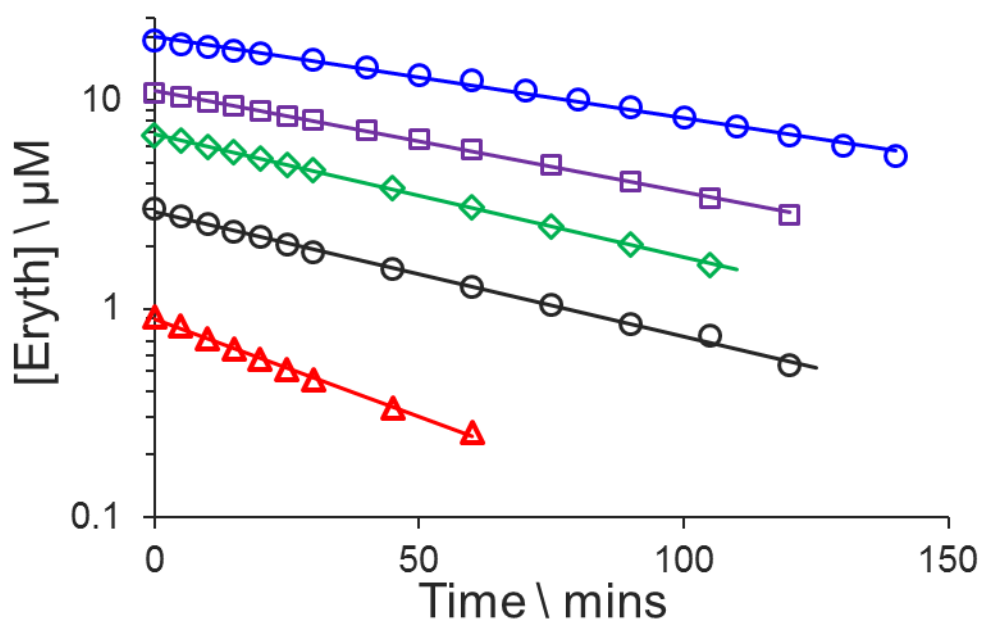


Figure 3.10 – Semi logarithmic plot of bleaching rate with a variety of starting concentrations fitted to a first-order decay, concentrations are found in table 3.2

$[Eryth]_0 \ \mu\text{M}$	$I_{obs} \ \%$	$\omega_0 \ \mu\text{M min}^{-1}$	$k_b \ \text{min}^{-1}$	R^2
0.91	14.5	0.0192	0.0216	0.9998
3.03	40.7	0.0515	0.0138	0.9997
6.77	68.9	0.0838	0.0136	0.9992
10.8	84.5	0.1	0.0112	0.9984
19.5	96.6	0.127	0.009	0.9971

Table 3.2 – Derived bleaching rates at concentrations studied.

The apparent first-order fits to the data are inversely dependent on the initial concentration of Erythrosine $[Eryth]_0$, which points towards a more complex mechanism. On the basis of Equation 3.1, estimates for the corresponding first-order rate constant, k_b , can be obtained and are listed in Table 3.2. The unusual dependence on Erythrosine concentration indicates that the first-order approximation is merely coincidental and arises because of some other factor.

$$\text{Ln}[Eryth] = \text{Ln}[Eryth]_0 - k_b t \quad (3.1)$$

At the lower concentrations, the initial rate of photobleaching, ω_0 , varies linearly with light intensity, I_λ , as shown in Figure 3.9. The light intensity is varied using neutral density filters placed in front of the sample cuvette. In principle, the rate should also depend on the total output power of the LED but this was not attempted. The rate should also depend on the number of photons absorbed by Erythrosine and this, of course, is a function of the absorbance of the sample at the excitation wavelength.

The initial rate, ω_0 , depends on the probability that molecular oxygen quenches the triplet state, P_{ox} . This term depends on k_Q , the bimolecular quenching rate constant, measured to be $1.4 \times 10^9 \text{ M}^{-1} \text{ s}^{-1}$, the concentration of dissolved oxygen, and the decay rate constant for the triplet-excited state in the absence of oxygen. The triplet lifetime in deoxygenated solution is $150 \mu\text{s}$ so that, in air-equilibrated solution, P_{ox} is close to unity.

$$P_{ox} = \frac{k_Q [O_2]}{k_Q [O_2] + k_D + k_{DD} [Eryth]} \quad (3.2)$$

Interaction between the triplet-excited state and molecular oxygen gives singlet molecular oxygen as the main product but the yield is not quantitative. In fact, in D_2O the quantum yield for production of singlet oxygen is 0.68, compared to a triplet quantum yield of 0.97. The probability that the triplet state leads to the formation of singlet oxygen is now given by Equation 3.3.

$$P_\Delta = \frac{\Phi_\Delta}{P_T} \quad (3.3)$$

Once formed, singlet oxygen can diffuse through the solution until encountering Erythrosine. At this point, chemical trapping of singlet oxygen occurs and leads to modification of the substrate. The probability for this trapping event, P_Q , depends on k_{trap} , and the non-radiative decay rate constant of singlet oxygen in water, k_Δ , which is $2.5 \times 10^5 \text{ s}^{-1}$. The rate k_{trap} , cannot be directly measured but the literature would indicate that this will not exceed $10^7 \text{ M}^{-1} \text{ s}^{-1}$. At the μM concentrations of Erythrosine used in our work P_Q is effectively zero.

$$P_Q = \frac{k_{trap} [Eryth]}{k_{trap} [Eryth] + k_\Delta} \quad (3.4)$$

This leads us to a generic expression for the rate constant for photobleaching of Erythrosine at modest sensitizer concentrations, as shown in Equation 3.5. It was observed that, at constant incident light intensity, the rate of photo-bleaching of Erythrosine could be well described in terms of this expression, where γ is a factor for converting the incident light intensity into photons per minute. This expression, with the partition coefficient κ reflecting the likelihood that triplet quenching will lead to product formation, was found to hold under all

conditions except for long exposure times at high Erythrosine concentrations. It will be noted that Equation 3.5 does not include the concentration of Erythrosine in any form other than its role as an absorber

$$\omega_0 = (I_\lambda I_{abs} \gamma) \cdot P_T \cdot P_{ox} \cdot \kappa \quad (3.5)$$

The chemical modification is assumed to be due to the singlet oxygen reacting immediately with the sensitizer after energy transfer has taken place. Such transfer should occur by the Dexter mechanism, i.e. electron transfer, as such there would need to be orbital contact between O₂ and Erythrosine and then a reaction within the geminate pair must take place before they can separate. The separation is controlled by diffusion with a rate k_{sp} , the excited state singlet oxygen eventually returning non-radiatively to the ground state. If reaction takes place in the geminate pair, a product is formed, [ErythOO], at a rate k_{pr} . If the quantum yield of singlet oxygen formation (0.68) is compared to the quantum yield for photo-bleaching then the probability for reaction within the ion pair is 0.1%.

3.3.4 – Autocatalysis at Higher Concentrations

Above Erythrosine concentrations of 10 μM, positive deviation from first-order kinetics was observed. Such deviations have been noted for other xanthene dyes^[44] although this was at mM concentrations. This behaviour was explained as competition between dye-oxygen reactions and dye-dye reactions but logically this should retain exponential kinetics. The intrinsic bleaching is fast and the deviation is only minor so the typical sigmoidal shape that would indicate auto-catalysis is not seen. A product must be formed that is able to cause bleaching of a second molecule of Erythrosine leading to elevated bleaching rates. Should this be the case the data may be analysed by an equation^[45] allowing for auto-catalysis, where ω_B is the observed bleaching rate for a given concentration of Erythrosine.

$$\frac{\omega_B}{[Eryth]} = (k_1 + k_{cat} \cdot [Eryth]_0) - k_{cat} \quad (3.6)$$

The occurrence of auto-catalysis is of great concern where the stability of organic chromophores is concerned. It is worth a detailed consideration of auto-catalytic kinetics as they are a recurring theme in our studies. To understand such kinetics, *pseudo*-first-order conditions are imposed. There must be an initial process that causes the first wave of bleaching, thereby creating the subsequent product, controlled by the rate constant k_1 . The second process uses the product (*Pro*) to cause accelerated bleaching of the chromophore (*Chro*). If the processes are all first-order with respect to each species, then:

$$rate = \omega_B = k_1[Chro] + k_{cat}[Chro][Pro] \quad (3.7)$$

$$\omega_B = k_1 \cdot c + k_{cat} \cdot c \cdot \xi \cdot (c_0 - c) \quad (3.8)$$

The factor ξ accounts for the stoichiometry, this can then be divided through by c and rearranged to give equation 3.6 and is of the form $y = mx + c$ so that the plot of $\omega_B/[Eryth]$ against $[Eryth]$ will give the rate k_{cat} by the gradient and the intercept will be $k_1 + k_{cat} \cdot [Eryth]_0$.

The rate of bleaching, ω_B , may be found tangentially from the bleaching data averaged over all the wavelengths where the bleaching shows the same kinetics i.e. it is not affected by the growth of the product spectrum, which is roughly the band relating to the 0-0 transition. Data was analysed for the two samples with concentrations above $10\mu\text{M}$. At 20°C and a concentration of $20\mu\text{M}$ a first-order rate of 0.0069min^{-1} was found and k_{cat} of $0.46\text{ nM}^{-1}\text{min}^{-1}$, the fits to equation 3.6, in Figure 3.11 are seen to be excellent.

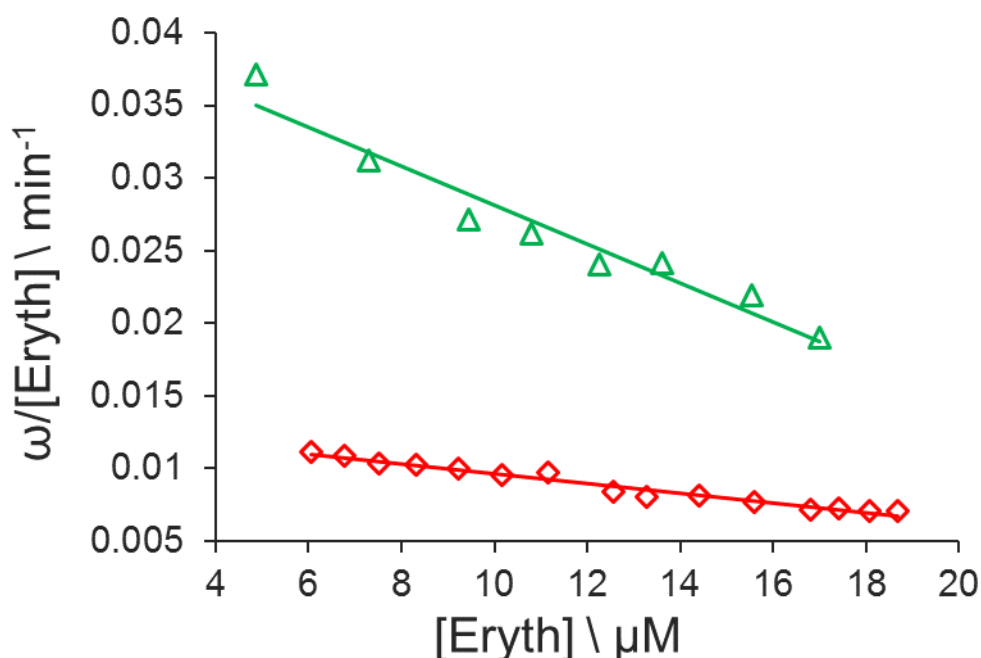


Figure 3.11 – Bleaching rates plotted against concentration, as per equation 3.6, of $20\mu\text{M}$ solutions at 20°C (◇) and 70°C (△), the gradient of the linear fit describes the catalytic rate k_{cat} , while the intercept gives the intrinsic rate k_1

3.3.5 Temperature Dependence under Monochromatic Illumination

$[Eryth]_0 \ \mu M$	$T \ ^\circ C$	$[O_2] \ mM$	$k_1 \ min^{-1}$	$k_{cat} \ nM^{-1}min^{-1}$
10.8	20	0.232	0.0093	0.39
19.5	10	0.285	0.0049	0.31
19.5	20	0.232	0.0069	0.46
19.5	30	0.196	0.0082	0.63
19.5	40	0.172	0.0091	0.82
19.5	50	0.156	0.0122	0.92
19.5	60	0.145	0.0137	1.01
19.5	70	0.138	0.0172	1.34

Table 3.3 – Intrinsic and catalytic bleaching rates under a variety of conditions.

For a fixed Erythrosine concentration of 20 μ M the temperature was varied from 10 $^\circ$ C to 70 $^\circ$ C and photobleaching was recorded under otherwise identical conditions. The bleaching kinetics of Figure 3.12 fit to Equation 3.6 to give the parameters given in Table 3.3. It is assumed that the mechanism for irreversible chromophore loss does not change with temperature over this range. We can consider that the terms associated with k_b are invariant to temperature other than factors dependent on the concentration of dissolved molecular oxygen. The oxygen concentration decreases with increasing temperature but the probability of quenching the triplet-excited state by O_2 remains high, reaching a minimum of 0.93 at the highest temperature. The rate of bleaching doubles over the temperature range. The spectral changes are not sensitive to temperature, with the same absorption changes appearing in the near-UV region.

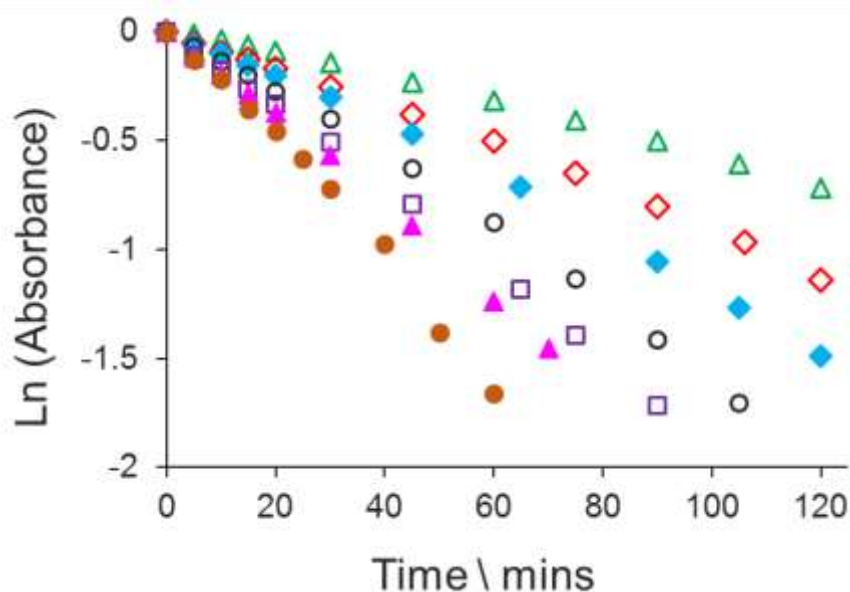


Figure 3.12 - Bleaching kinetics for 20 μ M solutions of Erythrosine at 10 (Δ), 20 (\diamond), 30 (\blacklozenge), 40 (\circ), 50 (\square), 60 (\blacktriangle), & 70 $^\circ$ C (\bullet)

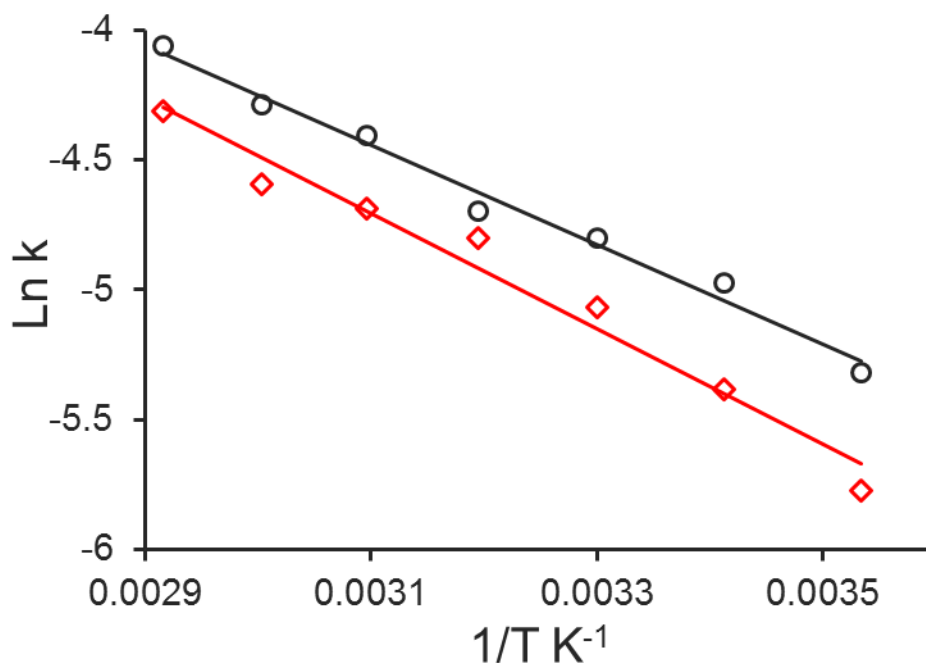
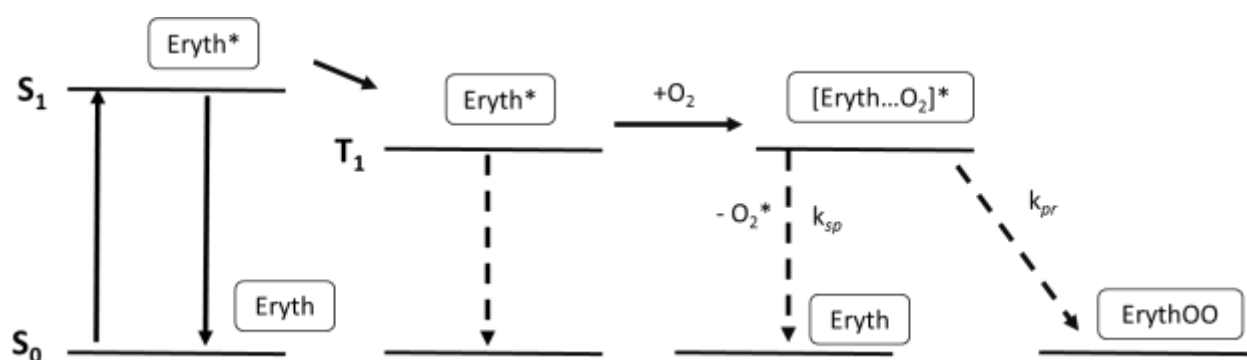


Figure 3.13 – Arrhenius plot for the k_1 (○) and k_{cat} (◇)

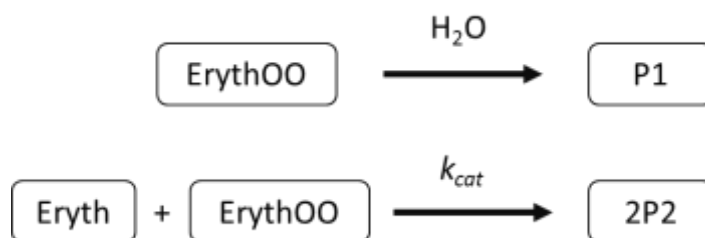
The rate constants were found to conform to Arrhenius-type behaviour, shown in Figure 3.13. For k_1 , an activation energy of $16.0 \pm 0.1 \text{ kJmol}^{-1}$ and a pre-exponential factor of 15.6 min^{-1} is derived. Comparing the observed rate constants with this pre-exponential factor indicates that the experimental conditions used are far from optimised, primarily due to the very low concentration of Erythrosine. This latter point is a consequence of using Erythrosine as the photosensitiser. The derived activation energy seems quite low but there are no literature values for any system that could be used for comparison. It is likely that this parameter is associated with addition of O_2 across a double bond of the Erythrosine molecule when part of the geminate pair. The intermediate, ErythOO, is expected to hydrolyse in water to form a further product and there is some indication for the release of the halide ions (*vide infra*). It has been shown^[46] that addition of singlet oxygen in simple alkene rings has an activation energy close to zero, which seems fairly consistent with our findings. Furthermore the lifetime of singlet oxygen does not change with temperature^[47].

A key step in the overall reaction sequence involves partitioning, κ , of the molecule- O_2 complex which was indicated in Equation 3.5. To a first approximation, this partitioning factor represents competition between separation of the geminate pair, k_{sp} , and reaction to form the product ErythOO, k_{pr} . The density of water will only change by a few percent^[48] over the temperature range studied so k_{sp} should be essentially insensitive to temperature. As such, the activation energy is associated with the product formation denoted by k_{pr} .

The temperature dependence noted for the bimolecular auto-catalytic reaction at an Erythrosine concentration of $20\mu\text{M}$ corresponds to an activation energy of 18.5 kJmol^{-1} with a pre-exponential factor of $0.9\ \mu\text{M}^{-1}\text{min}^{-1}$. This reaction must involve diffusional encounter between an undamaged chromophore and a photochemical breakdown product. Other auto-catalytic processes such as the growth of silica particles^[49] or conversion of formamide^[50] are activated processes so our finding seems reasonable. The two activation energies are similar in magnitude, which might indicate similarity in their chemical nature. As a model, addition of furfuryl alcohol was studied allowing us to speculate that the autocatalytic processes involves peroxy radicals which would indeed have a small activation energy^[51]. The processes involved are shown in the schemes 3.2 and 3.3.



Scheme 3.2 - The formation of the Erythrosine based intermediate from the geminate pair.



Scheme 3.3 – Formation of final products by way of the Erythrosine intermediate.

3.3.5 Variation of Experimental Conditions

The removal of oxygen was found to inhibit the rate of photobleaching, as was also seen in the case of broadband illumination. Indeed, the rate was seen to decrease progressively during illumination, shown in figure 3.14, which may indicate that there is a small amount of residual oxygen present at the beginning of the experiment. Once this has been consumed, bleaching can still proceed but by way of dye-dye reactions that lead to P2. Solutions were also purged with pure O_2 . This had little effect on the rate of bleaching. According to Equation 3.2, in air-equilibrated water the concentration of dissolved oxygen is already sufficient to ensure quantitative quenching of the triplet-excited state. As such, increasing the

concentration of O₂ should have no additional effect which is confirmed in the inset of Figure 3.14.

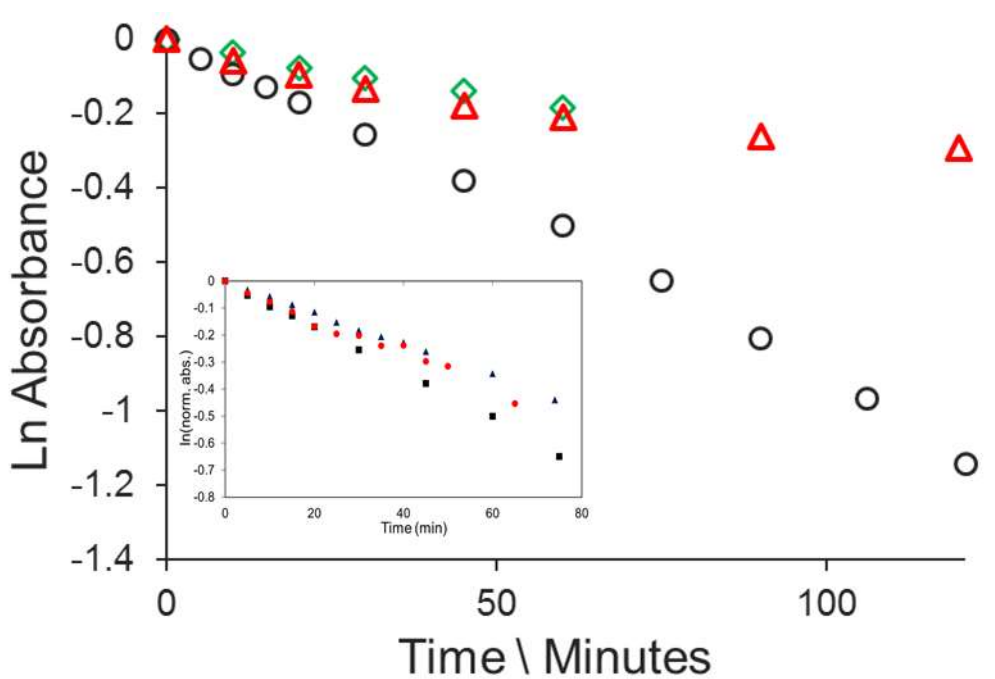


Figure 3.14 – Effect of removing oxygen from samples bleached by 523nm illumination at 20°C and concentration of 20μM. The air equilibrated sample (○) is presented alongside repeat measurements purged with N₂ (△,◇) the inset shows the air equilibrated rate (■) compared to O₂ saturated samples (●,▲).

The bleaching experiment was carried out in air-equilibrated D₂O. As was noted in the introduction, deuterated solvents are less able to promote the non-radiative deactivation of singlet oxygen; in the case of water, the excited-state lifetime is an order of magnitude longer in D₂O than in H₂O^[52]. The bleaching rate in D₂O in figure 3.15 is only two-fold faster than in H₂O, so the increase is modest compared to the increase in excited-state lifetime. The enhanced rate would indicate that free singlet oxygen is now able to bleach Erythrosine unlike in H₂O. The free ¹Δ_g is able to initiate further bleaching of the intermediate such that this species is not seen in D₂O. The same is true for self-catalysis.

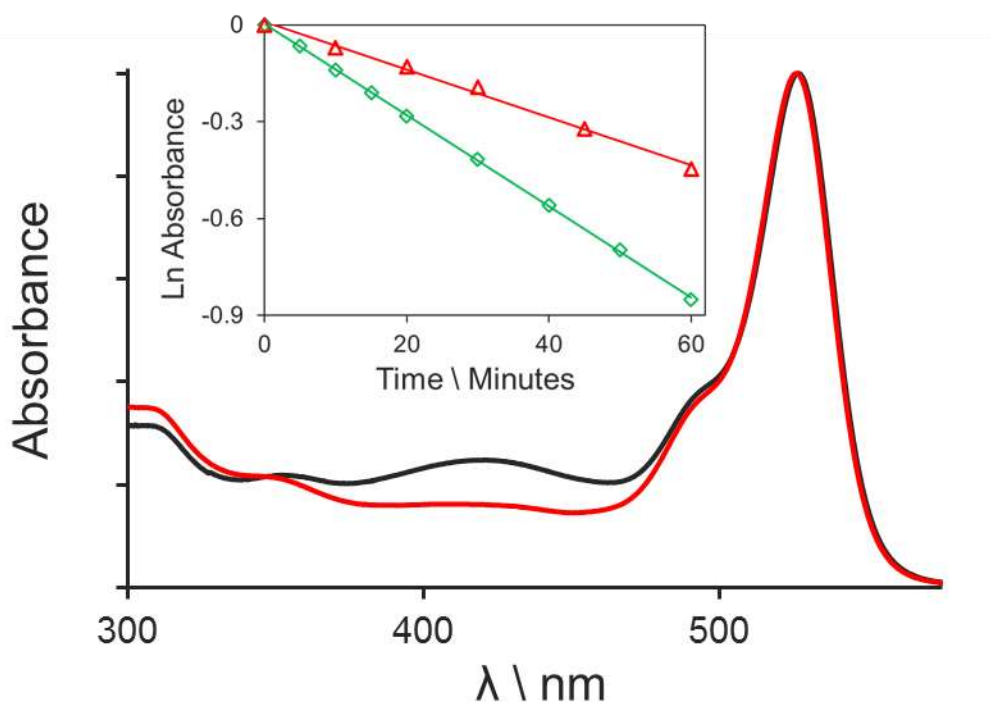


Figure 3.15 – Normalised absorbance after around 70% of loss of initial chromophore of in H₂O (—) and D₂O (—). Inset shows bleaching rates in H₂O (Δ) and D₂O (◇).

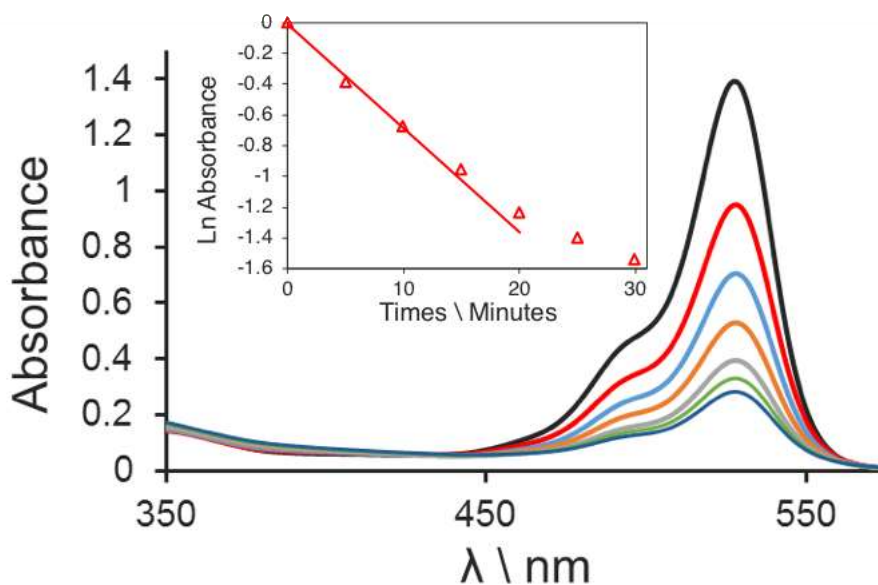


Figure 3.16 - Bleaching overlay in the presence of 50mM furfuryl alcohol, note that the blue absorbing product is not seen.

Furfuryl alcohol is a well-known singlet oxygen trap^[53] and could help elucidate the bleaching mechanism. We might anticipate that furfuryl alcohol will intercept any free singlet oxygen in competition to attack by the latter on the chromophore. In fact, furfuryl alcohol, added at 50mM, was seen to cause an initial increase in the rate of bleaching (Figure 3.16). Fitting the early bleaching data to first-order kinetics gives a rate constant of 0.067 min⁻¹; which is a 10-fold

increase compared to the reaction in the absence of added furfuryl alcohol. The observed rate was seen to decrease as reaction progressed. Interestingly, a partially bleached sample continued to bleach in the dark. Transient absorption spectroscopy was used to show that furfuryl alcohol quenched the Erythrosine triplet state with a bimolecular rate constant of $7.3 \times 10^5 \text{ M}^{-1} \text{ s}^{-1}$. Even at 50mM, direct quenching of the Erythrosine triplet is not competitive with quenching by molecular oxygen. Therefore, the implication is that the substrate subsequently intercepts singlet oxygen formed via the primary photoreaction between Erythrosine triplet and molecular oxygen. This reaction forms an endoperoxide that breaks down in water to form oxidising species which act to quickly degrade Erythrosine. A partially bleached solution of Erythrosine in water was treated with AgNO_3 to produce an instant precipitate. This finding indicates the release of halide ions during the bleaching step. It is known that iodide ions act as good quenchers for singlet oxygen in water. However, addition of potassium iodide, $[\text{KI}] = 1 \text{ M}$, had no effect on the photobleaching of Erythrosine. This finding confirms our suspicions that free singlet oxygen is not the primary cause of photobleaching of Erythrosine.

3.4 Bleaching in the Solid Phase

The usefulness of the rapid photobleaching of Erythrosine in the solid state was demonstrated by recording the illumination area of the LED focussed onto stained paper. To the best of our knowledge, no chemical solid-state actinometer exists that could be used for the measurement of the number of photons absorbed by a system. Erythrosine is used in printing inks for use with foodstuffs and textiles, among other such applications. Because of its ready availability and low toxicity, it should make a good chemical actinometer. To further demonstrate the solid-state bleaching, absorbent artist's paper was soaked in a concentrated Erythrosine solution. Sections of the dried paper were subjected to natural illumination and the colour was seen to fade according to the exposure time. With a suitable measurement protocol, this could make for a useful actinometer. The bleaching rate appeared to be increased when the paper was only partially dried, indicating that the mobility of the Erythrosine is important.

3.5 Conclusion

The bleaching of Erythrosine in H_2O was extensively characterised in terms of the concentration of the sensitiser and the effect of temperature. The dye was previously known to be sensitive toward illumination and to feature significant intersystem crossing to the triplet state. As such, we might anticipate a relatively high rate of photobleaching and the involvement of singlet oxygen. Indeed the involvement of singlet oxygen was confirmed by the increased rate found in D_2O compared to H_2O but, on critical examination, it was concluded that free singlet oxygen does not cause bleaching at the dye concentrations used. Instead,

bleaching arises from chemical reactions within the geminate pair required as part of triplet-triplet energy transfer. Once the geminate pair separates, deactivation of singlet oxygen is too fast for bimolecular reaction with the dye.

Two important features emerge from this study. Firstly, we report activation parameters for the bleaching reaction. We are unaware of any related values for photobleaching of a dye in solution. If a dye is to be used in some exterior light-harvesting application for example, the sample could easily reach temperatures of 50°C in operation. Our work shows that this could have important consequences for the longevity of the device. Secondly, we report on the significance of auto-catalysis at quite modest concentrations of sensitising dye. This situation changes the reaction mechanism, leads to faster rates of photobleaching and (in all likelihood) introduces new products. Such factors amplify the difficulty of extrapolating photostability levels from short-term illuminations under fixed conditions.

Self-catalysis increases both the rate and quantum yield of photobleaching. A net result is that Erythrosine is too susceptible to photodegradation to be proposed as a viable sensitizer for sustainable photochemical processes. It is ideal, however, for use as a sensitizer for any process where the final product distribution needs to be colourless. This was demonstrated by the efficacy with which the products of Erythrosine excitation attacked Merocyanine 540 which is previously quite stable, the Erythrosine can then be removed by further illumination. It is also apparent that a simple chemical actinometer can be formulated by impregnation of the dye onto adsorbent paper.

References

- [1] L. M. G. Antunes et al. *Food Chem. Toxicol.* **2012**, 50, 3447-3451.
- [2] N. P. Lang, E. Østergaard, H. Löe, *J. Periodontal Res.* **1972**, 7, 59-67.
- [3] H. Shindy, *Chemistry International*, **2016**, 2, 29-36.
- [4] D. Metcalf, C. Robinson, D. Devine, S. Wood, *J. Antimicrob. Chemother.* **2006**, 58, 190-192.
- [5] A. O. C. Jorge et al. *Oral Surg. Oral Med. Oral Pathol. Oral Radiol.* **2012**, 114, 67-74.
- [6] A. D. Garg, M. Bose, M. I. Ahmed, W. A. Bonass, S. R. Wood, *PLoS One*, **2012**, 7, 34475.
- [7] J. Weber, *Opt. Comm.* **1973**, 7, 420-422.
- [8] I. Georgakoudi, T. H. Foster, *Photochem. Photobiol.* **1998**, 67, 612-625.
- [9] R. S. Mulliken, *Nature*. **1928**, 122, 505.
- [10] E. A. Ogryzlo et al. *Relaxation and Reactivity of Singlet Oxygen, Vol. 1*, ACS Publications, **1968**.
- [11] P. B. Merkel, D. R. Kearns, *J. Am. Chem. Soc.* **1972**, 94, 7244-7253.
- [12] K. Krumova, G. Cosa, *Overview of Reactive Oxygen Species, Vol. 1*, The Royal Society of Chemistry, **2016**, pp.1-21.
- [13] H. H. Wasserman, J. L. Ives, *Tetrahedron*. **1981**, 37, 1825-1852.
- [14] L. Carlos et al. *ACS Sustain. Chem. Eng.* **2013**, 1, 1545-1550.
- [15] T. B. Amor, G. Jori, *Insect Biochem. Mol. Biol.* **2000**, 30, 915-925.

- [16] A. A. Gorman, M. A. J. Rodgers, *Handbook of Organic Photochemistry*. **1989**, 2, 229-247.
- [17] C. Schweitzer, R. Schmidt, *Chem. Rev.* **2003**, 103, 1685-1758.
- [18] C. S. Foote, R. W. Denny, *J. Am. Chem. Soc.* **1968**, 90, 6233-6235.
- [19] H.-D. Martin et al. *Methods Enzymol. Vol. 319*, **2000**, pp.226-241.
- [20] K. Gollnick, G. O. Schenck, *Pure Appl. Chem.* **1967**, 296.
- [21] P. R. Ogilby et al. *Photochem. Photobiol.* **2011**, 87, 671-679.
- [22] T. Kiesslich, A. Gollmer, T. Maisch, M. Berneburg, K. Plaetzer, *BioMed Res. Int.* **2013**, 2013.
- [23] H. Chao et al. *Angew. Chem. Int. Ed.* **2015**, 127, 14255-14258.
- [24] H. Zhang, Y. Shan, L. Dong, *J. Biomed. Nanotechnol.* **2014**, 10, 1450-1457.
- [25] R. Bonnett, *Chem. Soc. Rev.* **1995**, 24, 19-33.
- [26] M. C. DeRosa, R. J. Crutchley, *Coord. Chem. Rev.* **2002**, 233, 351-371.
- [27] L. Song, E. J. Hennink, I. T. Young, H. J. Tanke, *Biophys. J.* **1995**, 68, 2588.
- [28] M. Imamura, M. Koizumi, *Bull. Chem. Soc. Jpn.* **1955**, 28, 117-124.
- [29] R. A. Lessard et al. *Appl. Phys. B.* **1994**, 58, 73-77.
- [30] H. Görner, *Photochem. Photobiol. Sci.* **2008**, 7, 371-376.
- [31] Y. S. Keum, J. H. Kim, Q. X. Li, *J. Photosci.* **2003**, 10, 219-224.
- [32] W. Caetano et al. *J. Photochem. Photobiol. A*, **2012**, 232, 14-21.
- [33] S. Hossain et al. *J. Haz. Mater.* **2007**, 147, 471-477.
- [34] B. B. Bhowmik, P. Ganguly, *Spectrochim. Acta A*, **2005**, 61, 1997-2003.
- [35] L. Turgeman, D. Fixler, *IEEE Trans. Biomed. Eng.* **2013**, 60, 1571-1579.
- [36] M. Coppey-Moisan et al. *Appl. Phys. Lett.* **2003**, 83, 2471-2473.
- [37] G. W. Robinson et al. *J. Am. Chem. Soc.* **1977**, 99, 4306-4311.
- [38] P. G. Bowers, *Proc. Royal. Soc. Lond. A*, **1967**, 299, 348-353.
- [39] R. Brennetot, J. Georges, *Chem. Phys. Lett.* **1998**, 289, 19-24.
- [40] R. Duchowicz, M. L. Ferrer, A. U. Acuña, *Photochem. Photobiol.* **1998**, 68, 494-501.
- [41] I. M. Issa, R. M. Issa, M. M. Ghoneim, Y. M. Temerk, *Electrochim. Acta.* **1973**, 18, 265-270.
- [42] K. R. Naqvi, J.-P. Behr, D. Chapman, *Chem. Phys. Lett.* **1974**, 26, 440-444.
- [43] W. Francis, W. P. Helman, B. R. Alberta, *J. Phys. Chem. Ref. Data.* **1993**, 22, 113-262.
- [44] Y. Usui, K. Itoh, M. Koizumi, *Bull. Chem. Soc. Jpn.* **1965**, 38, 1015-1022.
- [45] F. Mata-Perez, J. F. Perez-Benito, *J. Chem. Educ.* **1987**, 64, 925.
- [46] A. A. Gorman, G. Lovering, M. A. J. Rodgers, *J. Am. Chem. Soc.* **1979**, 101, 3050-3055.
- [47] P. R. Ogilby et al. *Phys. Chem. Chem. Phys.* **2016**, 18, 22946-22961.
- [48] G. S. Kell, *J. Chem. Eng. Data*, **1975**, 20, 97-105.
- [49] R. Rodríguez, R. Arroyo, P. Salinas, *J. Non-Cryst. Solids*, **1993**, 159, 73-79.
- [50] J. Leszczynski et al. *J. Phys. Chem. B*, **2013**, 117, 2314-2320.
- [51] P. Neta, R. E. Huie, A. B. Ross, *J. Phys. Chem. Ref. Data.* **1990**, 19, 413-513.
- [52] P. R. Ogilby, C. S. Foote, *J. Am. Chem. Soc.* **1982**, 104, 2069-2070.
- [53] W. R. Haag, E. Gassman, *Chemosphere*, **1984**, 13, 631-640.

Chapter 4 – Violation of the Mirror Symmetry Rule in the BOPHY Architecture

4.1 Introduction

The photophysical properties of a new family of chromophores, bis(difluoroboron)-1,2-bis((1*H*-pyrrol-2-yl)methylene)hydrazine (BOPHY) have been investigated. The BOPHY class is a subset of the dipyrromethene group, of which the BODIPY is the most famous. The chemical structure of BODIPY is shown in Figure 4.1 next to the two BOPHY structures studied here. These are the unsubstituted form, hereafter referred to as BOPHY, and a tetramethyl derivative, referred to as TM-BOPHY. The BODIPY family is an extremely popular and successful addition to the library of highly fluorescent chromophores so there is a desire to synthesise related chromophores displaying the benefits of BODIPY but hopefully with new properties.

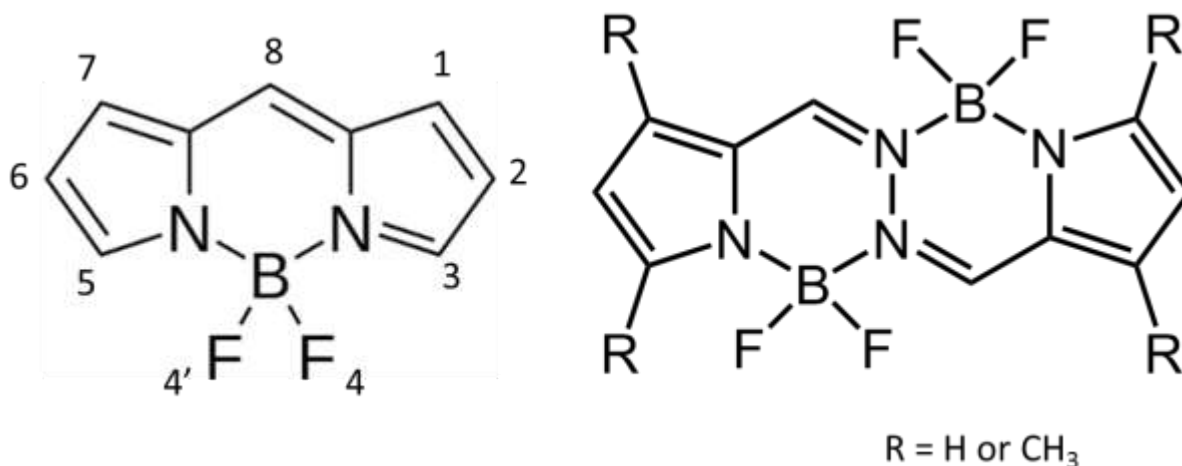


Figure 4.1 – Left, the chemical formula for BODIPY with the numbering system provided, right shows the chemical formulae for the two BOPHY molecules considered here.

Chromophores of the BODIPY type were first reported in 1968^[1] but did not gain popularity until the 1990s, leading to them becoming ubiquitous within the literature. Such BODIPY dyes have a number of desirable photophysical properties. They can be highly emissive, many derivatives feature near-unity quantum yields^[2], and display sharp, intense absorption transitions with molar absorption coefficients of about $80,000\text{M}^{-1}\text{cm}^{-1}$ for simple derivatives^[3]. The absorption and emission spectra show good mirror symmetry with small Stokes' shifts. The radiative lifetime is quite long, typically being ca. 5 ns ^[4] for simple compounds. In general, BODIPY dyes exhibit excellent solubility in most organic solvents and do not tend to form

aggregates. The rate constant for intersystem crossing is of the order of 10^6s^{-1} ^[5] so crossing to the triplet manifold does not compete with singlet emission, unless the molecule is specifically engineered to do so, for example by the introduction of heavy atoms^[6].

The synthetic versatility of the BODIPY class is perhaps its greatest attraction^[7]. The α positions, 3 and 5, are especially active allowing substituents to be added here so as to extend the conjugation path^[8]. At the 2 and 6 positions, the prior insertion of a halide atom allows substitution at this point^[9]. Aryl groups and sensing units^[10] can be added at the *meso* position. Additional aromatic rings may be fused to the structure^[11]. A particularly interesting aspect is that transformations may be made at the boron centre. The fluorine atoms may be removed and replaced, with oxygen^[12] to create strapped BODIPYs for example, or to allow insertion of ethynyl^[13] groups. This allows further derivatisation of the fluorophore, including the addition of long hydrocarbon chains to the BODIPY core.

Interest increased in BODIPY dyes when it was realised that they could be used as dyes for biological imaging^[14], with the spectral profile being similar to that of the popular fluorescein dye but with the advantage of the emitter being more photostable^[15]. A number of commercial BODIPY dyes are now available for microscopy. The tunability of the optical properties makes them effective organic laser dyes^[16] where they are denoted PM567, PM597 etc. Given the versatility of the BODIPY family, it is nowadays possible to synthesise molecules absorbing at any preferred wavelength above about 440nm. The capacity to introduce sensing units at the *meso* position means that BODIPY derivatives have been proposed as sensors^[17] for many analytes including alkali metal ions^[18], biomolecules^[19] and reactive oxygen species^[20]. Addition of amino donors, nitro acceptors, etc. allows electron or charge transfer systems to be developed which can act as pH sensors^[21]. They have been developed to be used in OLEDs^[22] and incorporated into co-polymers for organic photovoltaics^[23] and thin-film transistors^[24]. Rotatable aryl groups at the *meso* position have proven to be effective as indicators for viscosity^[25]. Recent developments include incorporating BODIPY into host-guest systems with mesoporous silica^[26] which can improve stability and allows light to be guided through channels. The procedure described where the fluorine atoms are removed has led to some extremely elegant systems being prepared where a BODIPY acceptor can be made into multi-chromophore system^[27]. In such systems, electronic energy is passed downhill to the final BODIPY acceptor to make light-harvesting molecules with pan-chromatic absorption profiles, systems with up to 21 chromophores^[28] have been developed.

The qualities of the dipyrromethene dyes are well established so the quest to find new chromophores that retain the positive qualities of BODIPY but with new features is ongoing. Some examples of this include the boranil^[29] and BOIMPY^[30] classes. To this end, the BOPHY

class was first reported in 2014 by two groups^[31, 32]. The BOPHY molecules in Figure 4.1 were reported^[31] as were derivatives featuring some small substituents^[32]. The generic BOPHY chromophore absorbs strongly in the near-UV and well into the blue region. The molar absorption coefficient was reported as being $37,500 \text{ M}^{-1}\text{cm}^{-1}$ with a near unity quantum yield for fluorescence. The Stokes' shift is approximately 30nm, which is similar to equivalent BODIPY dyes, although this occurs at higher energy in BOPHY so the energy of its Stokes' shift is greater. The reported molar absorption coefficient is only around half of that of tetramethyl-BODIPY^[33] and the fluorescence lifetime of TM-BOPHY is reported as 2.7ns.

The original paper on the BOPHY architecture noted that there is an apparent violation of Kasha's rule^[34]. In particular, the absorption spectrum was broad and featured two peaks of similar magnitude, while the fluorescence features a typical vibronic progression. Some density functional theory calculations were performed and it was suggested that BOPHY molecules with C_2 and C_i symmetry would have similar energies. Ultimately, the unusual absorption spectrum was assigned to a normal vibronic progression^[31], which is an unsatisfactory explanation.

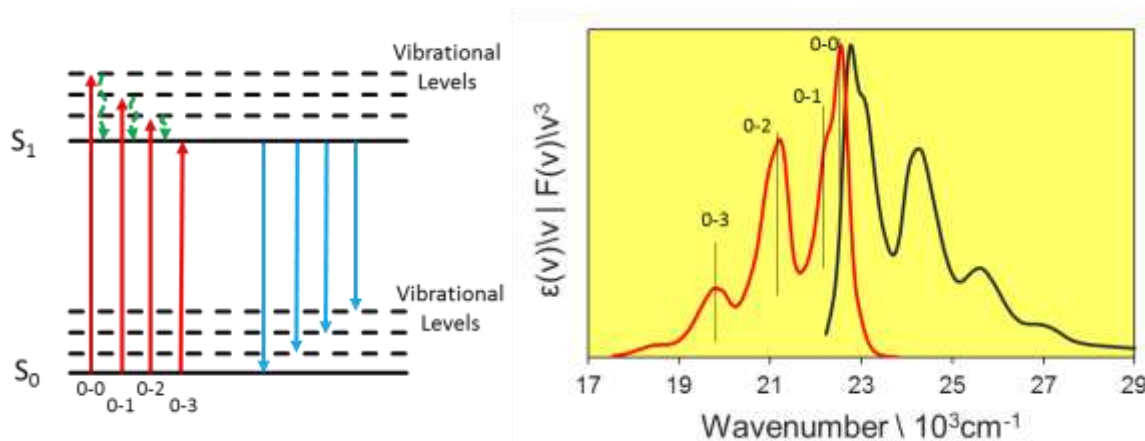


Figure 4.2 – Jablonski diagram showing excitation to S_1 (—) and fluorescence (—) to the ground state, there is internal conversion (—) from higher vibrational levels before emission. Right, the mirror symmetry of absorption and fluorescence perylene, the reduced spectra are presented on an energy scale.

The emission from organic fluorophores in nearly all cases is due to transitions from the lowest vibrational level of the excited state S_1 . This is known as Kasha's rule. Electronic excitation is possible to many different levels, typically into S_1 or S_2 envelopes, including the vibrational sub-levels, but these quickly relax to the lowest level of S_1 as shown in Figure 4.2. This excess energy is dissipated as heat in around 10^{-12} s ^[35], while organic fluorescence typically has a lifetime of the order of a few nano-seconds. As such, the radiative process does not compete with intramolecular vibrational relaxation, and emission has essentially not started by the time

relaxation is complete. A further consequence of this, as noted by Vavilov^[36], before Kasha, was that the quantum yield of fluorescence is usually independent of the excitation wavelength. Due to the Franck-Condon principle (i.e., electronic transitions are vertical with no change in nuclei position^[37]) and the fact that the structures of S_0 and S_1 are not much altered on excitation, transitions between the two states tend to be correlated. As a consequence, we usually see mirror-symmetry between the fluorescence and the S_0 - S_1 absorption profile for an organic molecule. The spectra recorded for perylene are presented in Figure 4.2, on a wavenumber scale. It is important to note that to assess the mirror symmetry of a system, correct representation of spectra is on an energy scale, with the spectra corrected for photons per quanta of energy. This procedure is termed the reduced spectra^[38]; for absorption $\epsilon(\nu)/\nu$ is plotted and for fluorescence, $F(\nu)/\nu^3$, on a wavenumber scale.

There are exceptions to Kasha's rule, an example being the fluorescence of azulene^[39], which emits from the S_2 state. There are other photo-processes that can initiate from higher energy states. It has been reported that the quantum yield for photobleaching of fluorophores can depend on the excitation wavelength^[40] or intensity^[41], with UV illumination causing greater bleaching than visible light. For this to happen, there must be bleaching from higher energy states that can initiate before relaxation to the S_1 state. Processes that can compete with vibrational relaxation, promoting different photochemistry^[42], include photochromic ring opening^[43], excited-state intramolecular proton transfer^[44] and intersystem crossing^[45] (ISC), even in pure organic systems^[46]. This field of research is called anti-Kasha photochemistry and was reviewed as early as 1978^[47]. This is also the basis for the so-called hot-donor systems^[48] where charge injection occurs from excited vibrational levels, which could be a possible route to breaking the Shockley-Queisser limit^[49] in photovoltaics. A further Kasha-violating phenomenon is hot fluorescence whereby emission is seen from excited vibrational^[50] levels of the S_1 state, a scheme for this and for anti-Kasha photochemistry is given in Figure 4.3.

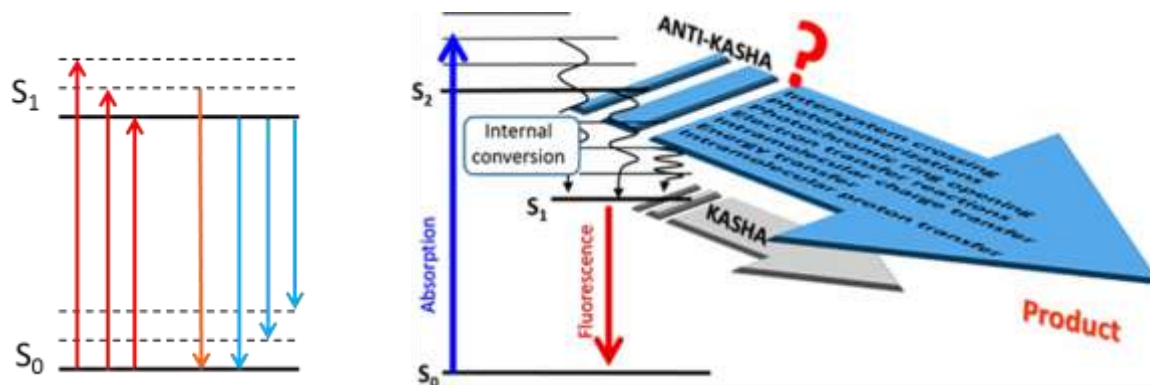


Figure 4.3 – Left shows a Jablonski diagram for hot fluorescence (—), right shows the anti-Kasha scheme adapted from ref [42].

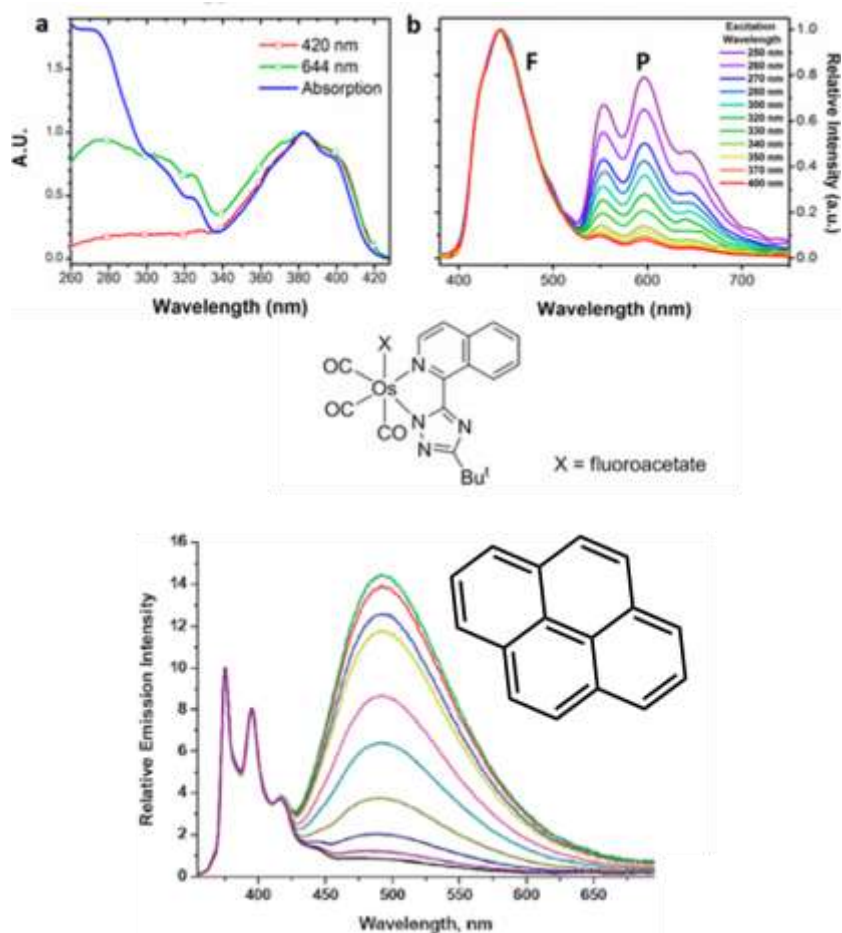


Figure 4.4 – Top panel shows the varying ratio of fluorescence to phosphorescence when an osmium complex is excited at different wavelengths, adapted from ref [45]. The bottom panel shows the changing emission of pyrene as concentration increases.

There are a number of instances where the mirror symmetry between the absorption and emission spectra is violated. It may be the case that there is in fact mirror symmetry but it is hidden. An example of this type of phenomenon is quinine sulphate^[51] where there is structure to the absorption spectrum but not the emission. In this case, the absorption transition is the overlap of transitions to S_1 and S_2 and in fact the emission is a mirror image of S_1 to S_0 . The emission may be compromised, a well-known example is pyrene^[52] which forms excited state dimers, known as excimers, that result in the broad, red-shifted fluorescence seen in Figure 4.4. The emission takes the form of the structured S_1 - S_0 transition, with the broad emission superimposed. Some chromophores exhibit different pK_a values in the excited state, causing ionisation of the species upon excitation and hence an altered spectrum. Pyranine^[53] being an example of such a case. This situation can be described by the Förster cycle^[54]. In Figure 4.4, we see an osmium complex that shows different levels of fluorescence and phosphorescence emission depending on the excitation wavelength^[45]. This is a result of the competitive intersystem crossing. In the ground state, dyes that are not well solvated may form

aggregates or dimers^[55]. Such species can form so-called J- or H-aggregates depending on whether the stacking is end-to-end or parallel, respectively. This effect causes a red or blue shift. If the stacking is oblique, then the absorption spectrum will be altered and excitonic splitting will be observed, the theoretical work for this was also described by Kasha^[56, 57]. The splitting is controlled by a number of factors and is described by equation 4.1 which accounts for the transition dipole moment and the relative orientation of the chromophores. Merocyanine 540 is a sulfonated dye that can be dissolved in water to form a coloured solution of low fluorescence yield, the spectrum of which is given in Figure 4.5. The spectrum shows a clear splitting compared to the monomeric spectrum in ethanol where mirror symmetry is observed.

$$\Delta E = \frac{2|\mu_{ag}|}{r^3} \cdot (\cos\alpha + 3\cos^2\theta) \quad (4.1)$$

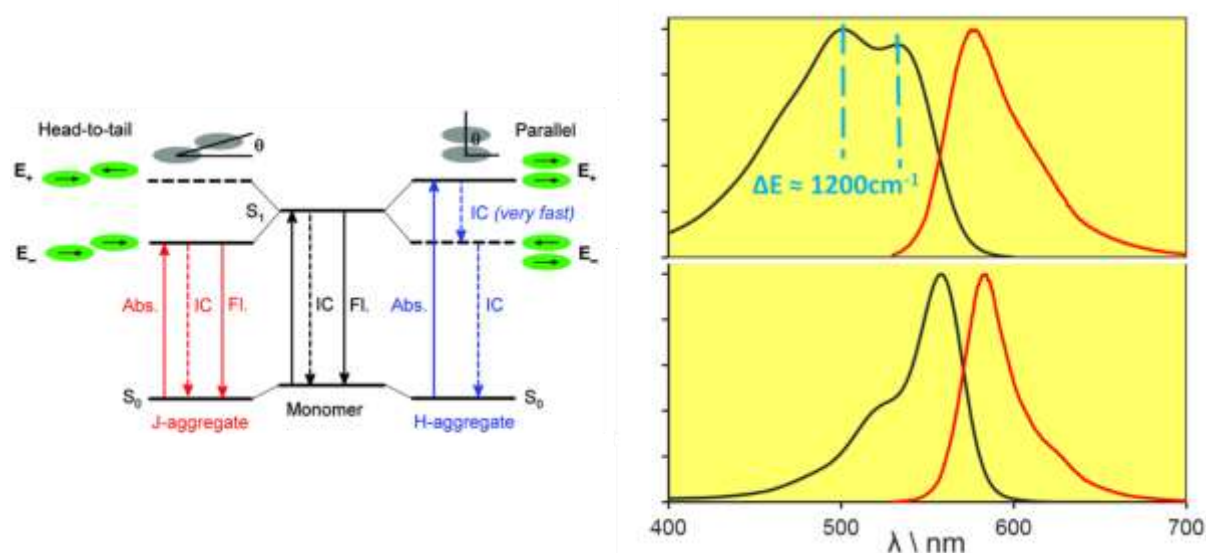


Figure 4.5 – Left, scheme describing the energy changes when a chromophore forms dimers, adapted from ref [55]. Right, upper panel shows spectra of a Merocyanine 540 derivative in water and below in ethanol where the mirror symmetry is restored.

4.2 Photophysical Properties of BOPHY Dyes

The absorption spectra of BOPHY and TM-BOPHY are presented in Figure 4.6, confirming the double peak reported previously in the literature. The substituted version, featuring electron-donating methyl groups, slightly extends the conjugation path thereby causing the maximum absorption to be red-shifted by around 20nm in MeTHF.

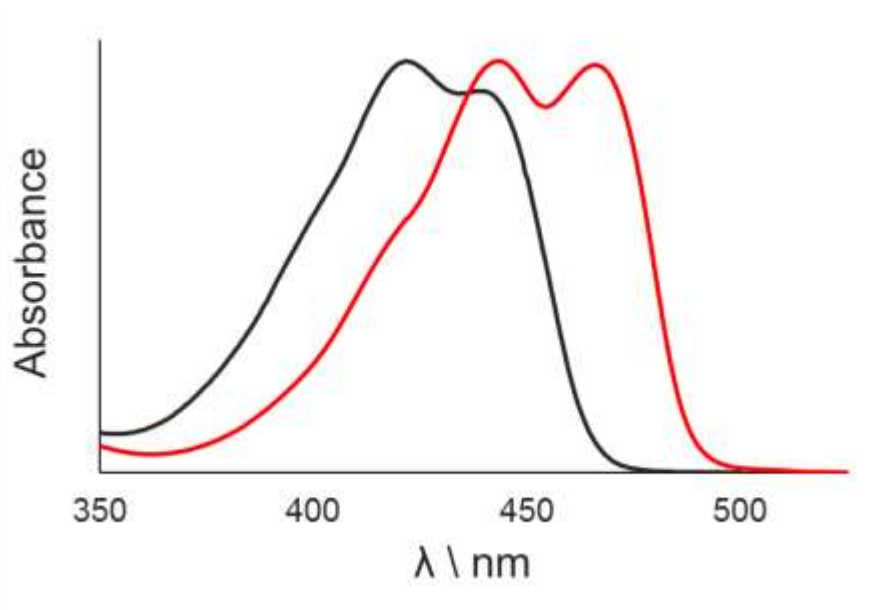


Figure 4.6 - Absorption spectra of BOPHY (—) and TM-BOPHY (—) in MeTHF

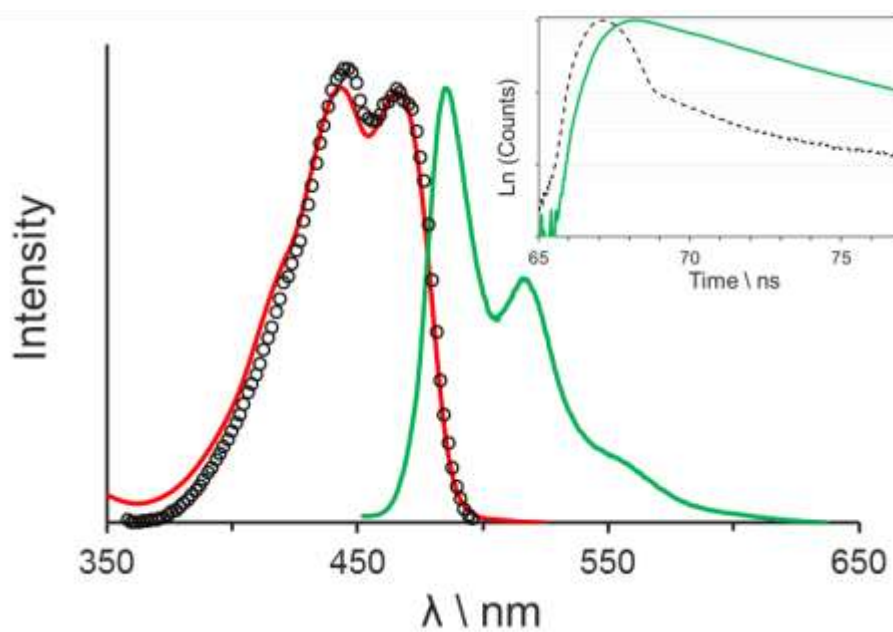


Figure 4.7 – Spectra of TM-BOPHY in MeTHF including corrected excitation spectrum (○). The inset shows time-resolved data, the lifetime (—) is well described by a single exponential decay, (--) is the IRF.

The fluorescence spectrum for TM-BOPHY is confirmed to display a typical vibronic progression in Figure 4.7 so mirror symmetry is violated. The emission maximum occurs at around 490nm, about 25nm from the absorption maximum, representing a Stokes' shift of $1,000\text{cm}^{-1}$. The Stokes' shift occurs over a similar wavelength to tetramethyl-BODIPY^[7] but the band positions are shifted by around 30nm so the energy is greater. Changing the excitation wavelength does not alter the spectral shape of the emission nor the quantum yield.

That is to say, the absorption and excitation spectra are well matched so we are dealing with a single chromophore and the transitions to any level results in fluorescence. The excitation spectrum for BOPHY is also seen to provide an excellent match to the absorption spectrum in Figure 4.8. Indeed, the general forms of the absorption and fluorescence spectra are similar to those of TM-BOPHY, although the absorption spectrum looks to be less structured and the second peak is of slightly more significance than the first band.

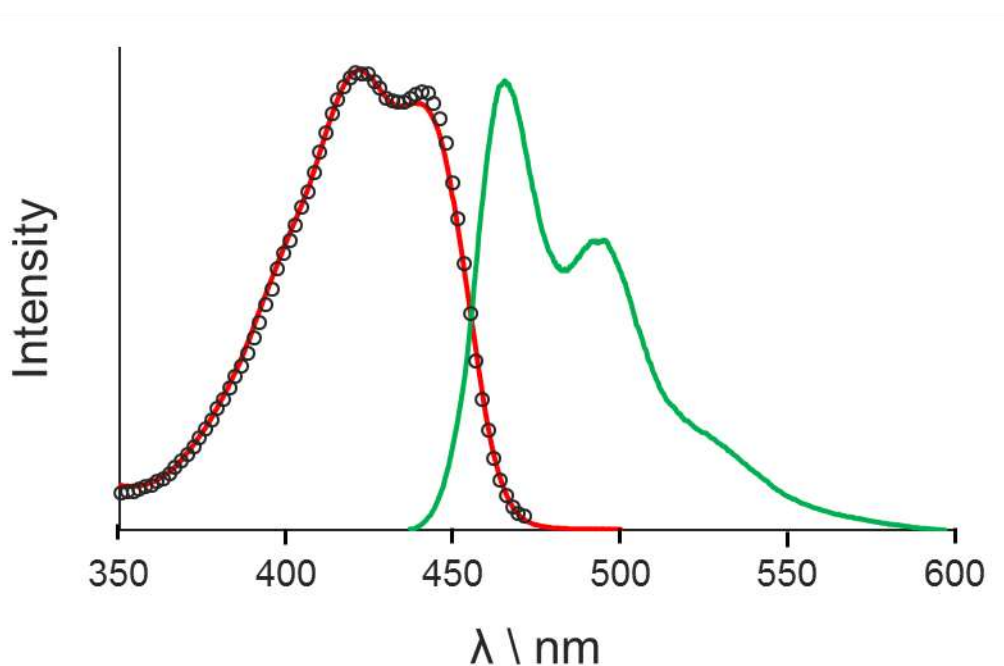


Figure 4.8 – Absorption (—), fluorescence (—) and excitation (○) spectra recorded for BOPHY in MeTHF.

The doubled-peak motif seen for absorption spectral profiles is often associated with dimer formation as set out in the introduction. Since this is related to dissolution of the chromophore, varying the concentration should induce changes in the absorption profile if there is aggregation. Over a concentration range from nearly 300 μ M down to 0.5 μ M, so over a 500-fold reduction in concentration, the Beer-Lambert relationship is seen to hold for TM-BOPHY, as shown in Figure 4.9. There is no change in the shape of the spectrum over this concentration range. To make measurements over such a wide concentration variation requires the use of cuvettes with path lengths from 2mm to 4cm. The absorbance values are then normalised to a 1 cm cuvette. It seems unlikely that the lack of mirror symmetry is due to aggregation. Additionally solutions were filtered to remove any such aggregates. In fact, the solid form of TM-BOPHY is quite fluorescent, as can be seen in the photograph in Figure 4.10. A fluorescence quantum yield of 0.28^[32] has been reported for TM-BOPHY as a solid. The

solid shows orange emission with a maximum at about 600nm. The emissivity of the solid can be used to check for aggregates in a solution, under illumination by a UV lamp. The aggregates would appear as orange dots compared to the bright yellow-green fluorescence of the solution.

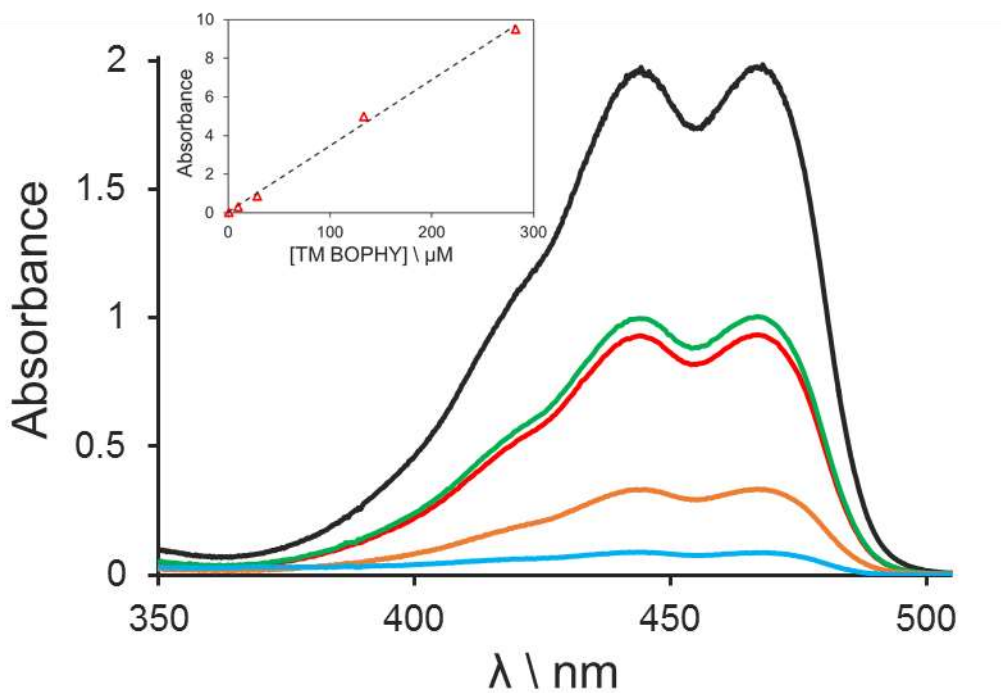


Figure 4.9 – Absorption spectra recorded for TM-BOPHY at concentrations from 0.6 μ M to 280 μ M in CH_2Cl_2 , the inset shows the Beer-Lambert plot where the absorbance values were normalised to a path length of 1cm.

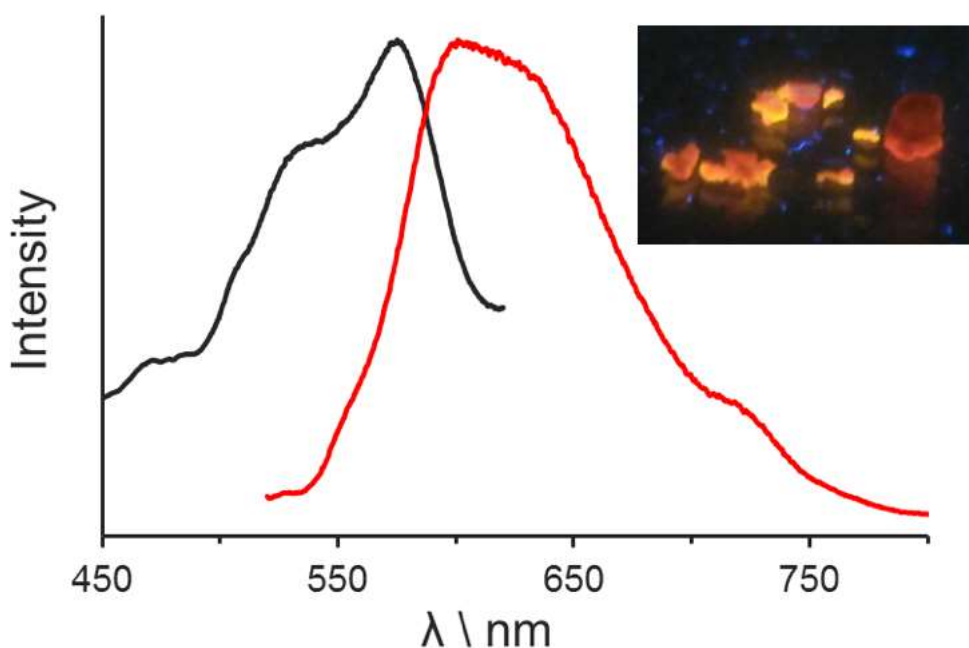


Figure 4.10 – Excitation and emission spectra recorded for solid TM-BOPHY, the inset shows a photograph of the solid under UV illumination.

The molar absorption coefficient for both chromophores was found to be around 35,000 M⁻¹cm⁻¹ in a solution of CH₂Cl₂, in agreement with early reports^[31]. These compounds are evidently highly fluorescent on inspection by eye, which is reflected in the literature. Indeed reports claim that the quantum yield is essentially unity and not affected by changes in solvent polarity. In our hands, the fluorescence quantum yield is not so high. In CH₂Cl₂, TM-BOPHY displayed a quantum yield, Φ_f = 0.75, and BOPHY was a little lower at Φ_f = 0.65. Some of the photophysical properties are collated in Table 4.1. Both emitters have the same radiative rate constant and emission lifetimes are around 2.5 ns. The natural radiative lifetimes, as calculated from the Strickler-Berg^[58] expression (Equation 4.2), are in excellent agreement with the measured lifetimes. It is perhaps a little surprising that the values are in such good agreement as an assumption of the Strickler-Berg relationship is that good mirror-symmetry is observed.

$$\frac{1}{\tau_0} = 2.88 \times 10^{-9} n^2 \langle \nu_f^{-3} \rangle^{-1} \int \epsilon \, d \ln \nu \quad (4.2)$$

<i>Material</i>	$\epsilon \setminus M^{-1}cm^{-1}$	$f^{(a)}$	$\tau_f \setminus ns$	$\tau_0 \setminus ns^{(b)}$	Φ_f	$k_r \setminus s^{-1}$	$k_{nr} \setminus s^{-1}$
BOPHY	38500 ^(c)	0.6	2.4	3.5	0.65	2.7x10 ⁸	1.5x10 ⁸
TM-BOPHY	375000	0.56	2.7	4.1	0.75	2.8x10 ⁸	8.9x10 ⁷

Table 4.1 – Comparison of the photophysical properties of BOPHY and TM-BOPHY in MeTHF, (a) is the oscillator strength and (b) is the natural radiative lifetime as calculated by the Strickler-Berg method, (c) value taken from reference [31].

The fluorescence quantum yield was determined in solution by the ratiometric method. The initial choice of reference for this measurement was Coumarin 153 in ethanol^[59] (Φ = 0.38). This reference material is a good spectral match to TM-BOPHY and allowed the quantum yields to be found in various solvents (Table 4.2). Since we could not replicate literature values for TM-BOPHY, taking account of the fact that Coumarin 153 is not primary standard for quantum yield measurements, further measurements were made. Alternative ratiometric standards were perlyene^[60] in cyclohexane (Φ_f = 0.94) and Rhodamine 123^[61] in ethanol (Φ_f = 0.90). Relative to these additional standards, our value for TM-BOPHY remained at Φ_f = 0.75. As a final check, the fluorescence quantum yield for TM-BOPHY was measured by thermal blooming^[62]. This measurement requires a null reference, which was provided by Brilliant Green (BG). A 405nm laser was used to excite the samples, BG is a red absorbing dye however there is a higher-energy transition available that is convenient for use with this laser. Now, TM-BOPHY and BG were measured in methanol, by this method to give a yield of Φ_f = 0.67. This value is in fair agreement with our ratiometric results and confirms that there is

indeed a non-radiative pathway that helps deactivate the emitting state for TM-BOPHY. Finally, BOPHY was compared to perylene in cyclohexane in order to determine the fluorescence quantum yield (Table 4.3).

<i>Solvent</i>	Φ_f	$\lambda_{abs} \text{ \AA}$	$\lambda_{fluo} \text{ \AA}$	<i>Stokes' Shift</i> \ cm^{-1}
Cyclohexane	0.78	470	485	660
CH ₂ Cl ₂	0.75	468	487	830
MeTHF	0.74	466	485	840
Acetone	0.71	461	483	990
Acetonitrile	0.65	459	482	1040
DMF ^(a)	0.72	463	486	1020
Methanol	0.71	461	482	950
Benzonitrile	0.74	470	492	950
Butyronitrile	0.69	463	484	940
DMSO ^(b)	0.67	464	488	1060
PDMS ^(c)	0.78	467	484	750

Table 4.2 – Variance of photophysical properties of TM BOPHY in solvents of a range of polarities.
(a) Dimethyl formamide, (b) Dimethylsulfoxide, (c) Polydimethylsiloxane

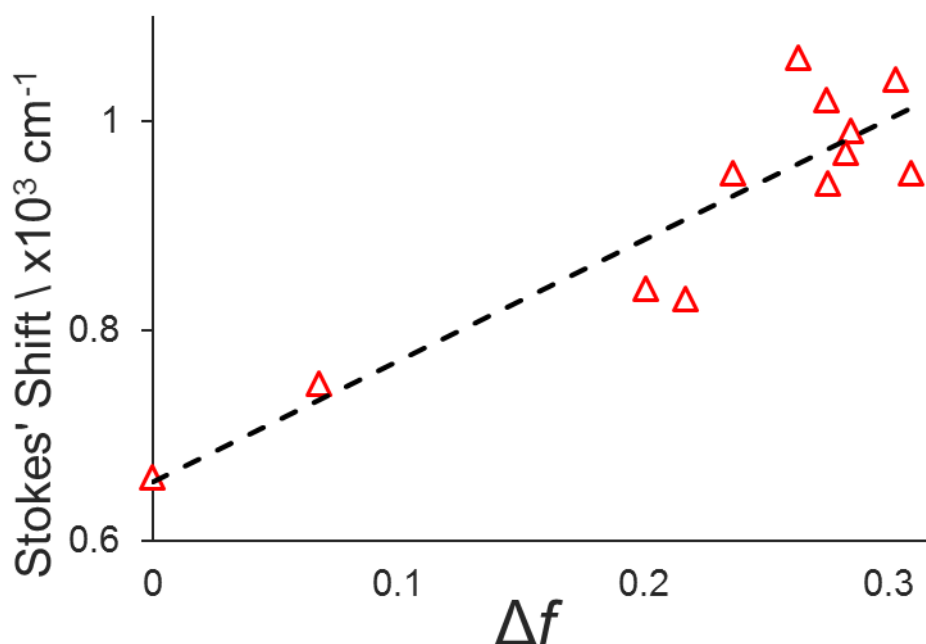


Figure 4.11 – Lippert-Mataga plot for TM-BOPHY.

In Table 4.2 it is shown that TM-BOPHY is not solvatochromic, with the spectra only shifting by about 10nm across the solvent range. This is reasonable given that the dye is non-polar in nature. The Stokes' shift does not increase significantly with increasing polarity of the solvent

and the change in dipole moment on excitation from ground state is approximately 3.5D as calculated by the Lippert-Mataga method^[63, 64] (Figure 4.11). The Lippert-Mataga expression (Equation 4.3) relates the Stokes' shift to the polarizability of the solvent, Δf , which depends on the permittivity and refractive index, as given in Equation 4.4. Here a is the molecular radius, which is assumed this to be 5Å throughout these studies.

$$\nu_G - \nu_E = \frac{2}{hc} (\Delta f) \cdot \frac{(\mu_E - \mu_G)^2}{a^3} + \text{const.} \quad (4.3)$$

$$\Delta f = \left(\frac{\epsilon - 1}{2\epsilon + 1} - \frac{n^2}{2n^2 + 1} \right) \quad (4.4)$$

The emission quantum yield shows only a small change over the solvent range and a plot of solvent dielectric constant against the quantum yield is given in Figure 4.12. This shows that there is a weak trend for loss of fluorescence with increasing solvent polarity. Given the notorious difficulties in measuring accurate quantum yields and the need to correct for differences in solvent refractive index, the changes in quantum yield is probably within the uncertainties of the measurement. In spite of that the trend is clear. The same situation is found for BOPHY, although fewer solvents were tested. Note that the fluorescence quantum yield for BOPHY is reduced slightly compared to TM-BOPHY (Table 4.3).

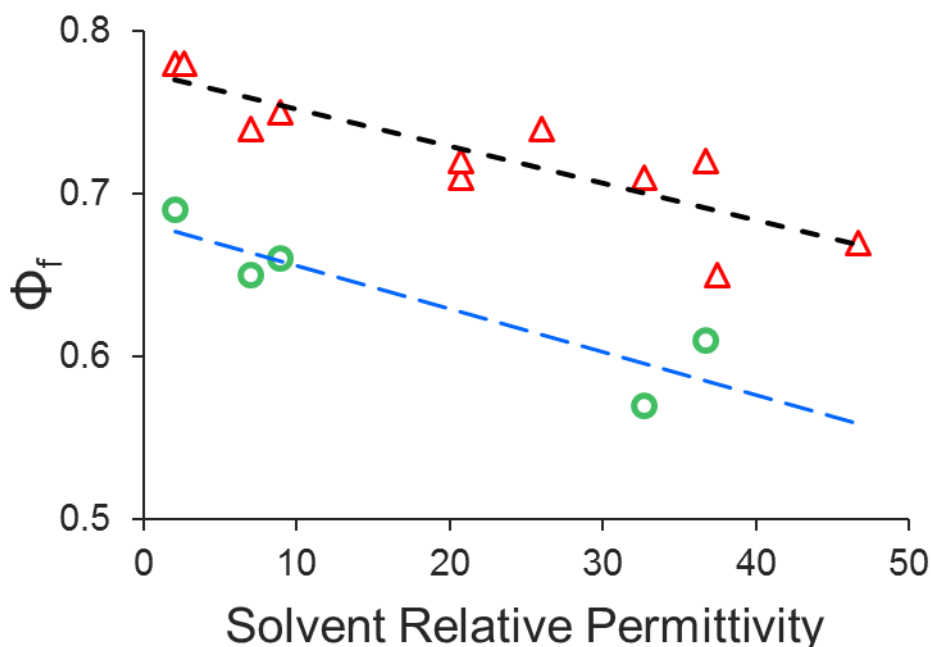


Figure 4.12 - Quantum yield plotted against solvent dielectric constant for TM-BOPHY (Δ) and BOPHY (○), the lines are added for clarity and imply no specific relationship.

Solvent	Φ_f	$\lambda_{abs} \text{ \AA}$
Cyclohexane	0.69	447*
CH ₂ Cl ₂	0.66	
MeTHF	0.65	440
DMF (a)	0.61	434†
Methanol	0.57	435

Table 4.3 – Properties of BOPHY in some solvents * - Band position in carbon tetrachloride, † - Band position in acetonitrile, (a) – Dimethyl Formamide.

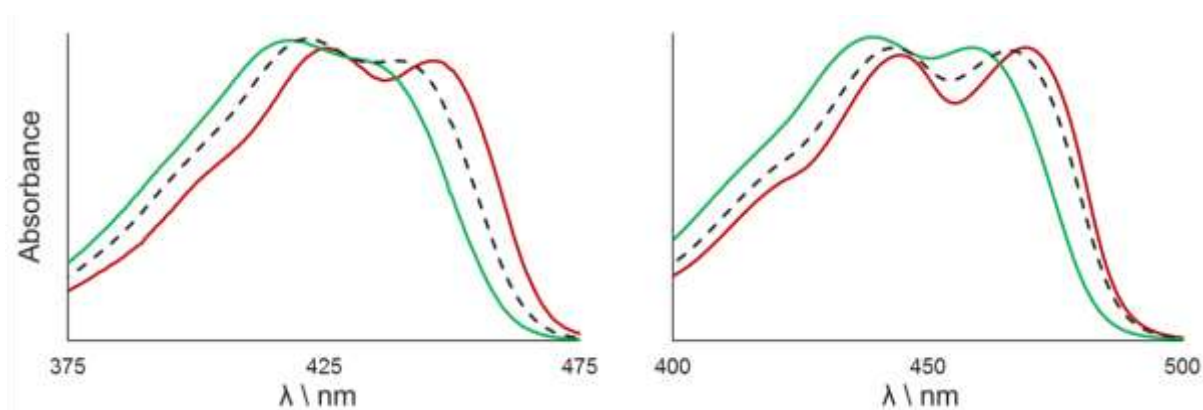


Fig 4.14 - Absorption spectra recorded for BOPHY, left and TM-BOPHY, right, in cyclohexane (—), MeTHF (- -) and acetonitrile (—).

Our work has demonstrated that the BOPHY chromophore is not solvatochromic and there is no indication for the involvement of charge-transfer interactions. There are, however, subtle changes in the absorption spectral profiles recorded in different solvents. In particular the ratio of the two absorption peaks is sensitive to the nature of the solvent and appears to exhibit a crude correlation with the fluorescence quantum yield as demonstrated by Figure 4.14. We express this ratio as the intensity of the second (i.e., the higher-energy transition) divided by the intensity of the first peak (i.e., the lower-energy transition). Thus, solvents, and other conditions such as temperature, that favour the second transition give the lower fluorescence quantum yield. Perhaps, this upper-lying excited state is coupled directly to the ground state. It is also clear that conditions showing less mirror symmetry give rise to lower fluorescence yields.

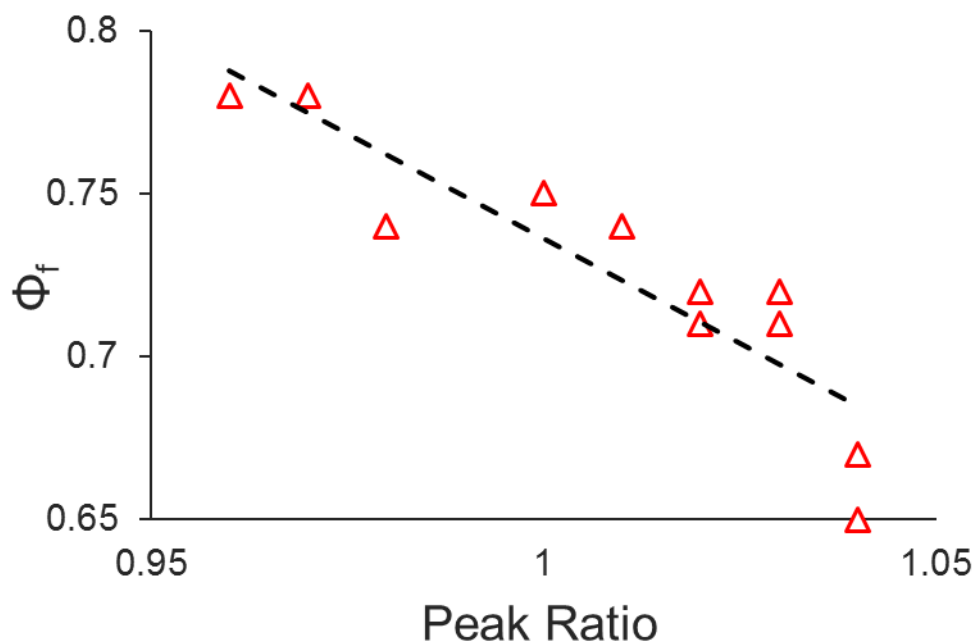


Figure 4.15 – Ratio of the distinctive double peaks in TM-BOPHY versus the fluorescence quantum yield for a small range of solvents, the line emphasises the correlation, but no specific relationship is implied.

Transient absorption spectroscopy was used to further probe the photophysics of TM-BOPHY in solution but no meta-stable species were observed. In deaerated solution, laser excitation did not result in detectable levels of a long-lived excited-triplet state. Addition of iodomethane to BOPHY in a MeTHF matrix at 77K resulted in the appearance of phosphorescence (Figure 4.16), but no such emission was seen in the absence of the spin-orbit promoter. The emission maximum for the phosphorescence is found at 600nm and 630nm for BOPHY and TM-BOPHY, respectively. This corresponds to a singlet-triplet energy gap of some $5,000\text{cm}^{-1}$. The vibronic progression of the phosphorescence is similar to that of the fluorescence so no change in the geometry in the triplet-state is anticipated. This puts the triplet state at a relatively high energy compared to that seen for simple BODIPYs^[65]. It might be noted that fluorescence quenching by iodomethane conformed to Stern-Volmer kinetics as illustrated by Figure 4.17.

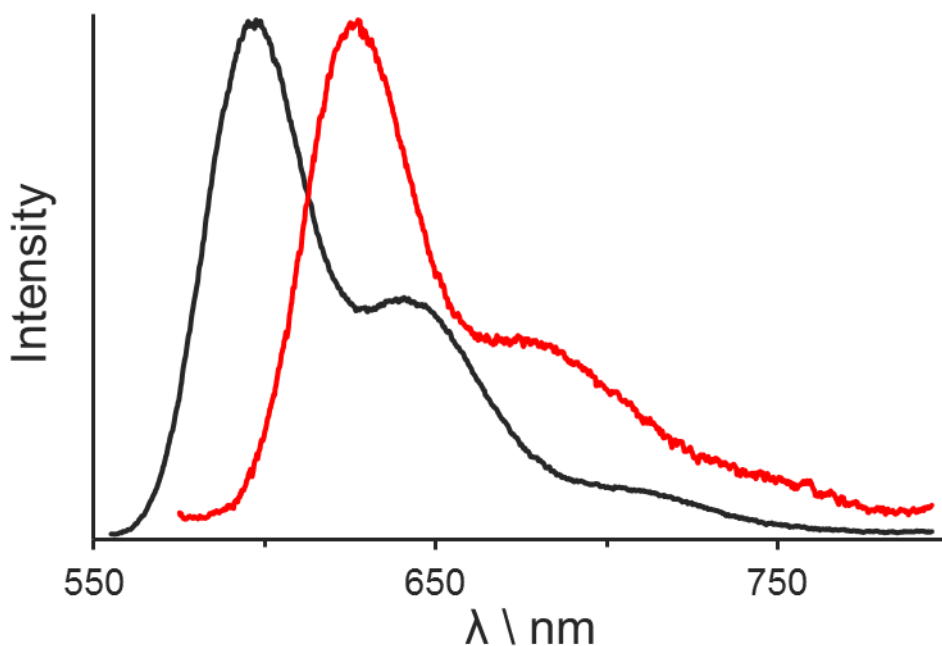


Figure 4.16 – Phosphorescence spectra recorded for BOPHY (—) and TM-BOPHY (—) in a MeTHF glass at 77K after addition of iodomethane.

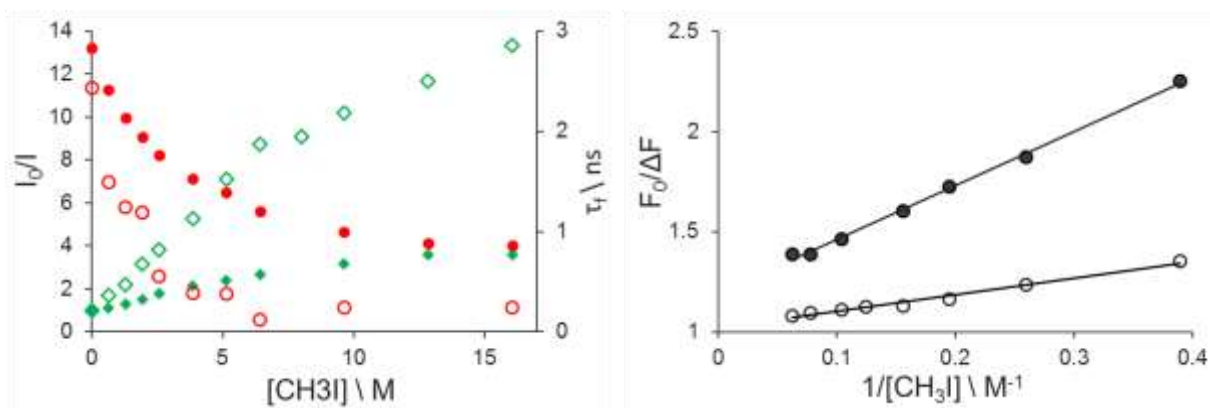


Figure 4.17 – Stern-Volmer plots for the quenching of steady-state and time-resolved fluorescence properties for BOPHY (\diamond , \circ) and TM-BOPHY (\blacklozenge , \bullet), right, fitting to the modified Stern-Volmer equation for BOPHY (\circ) and TM-BOPHY (\bullet).

4.3 Temperature Controlled Spectroscopy

4.3.1 Low-Temperature Spectra Recorded for TM-BOPHY

Both BOPHY derivatives show poor mirror symmetry in fluid solution at room temperature. There appear to be two states lying at rather close energy and small variations in the ratio of the two components can be induced by changes in the nature of the solvent. To further examine this situation we turned to low-temperature emission spectroscopy. To allow critical

comparison of the relevant spectra, corrections were applied for any spectral imperfections of the instrument and all spectra refer to reduced spectra^[38]. Low-temperature spectra were recorded using an optical cryostat operated with liquid nitrogen as coolant.

Firstly, TM-BOPHY was studied in MeTHF from 80K to room temperature. The temperature was eventually raised to 340K necessitating a switch from the cryostat to a conventional cuvette. To ensure that the chromophore was in its lowest-energy configuration, the system was cooled slowly from room temperature to 80K. The effects on the spectra are shown in Figure 4.18. It is evident that at 80K mirror symmetry is restored. Notably, there are only minor changes in the fluorescence spectrum but the excitation spectra change significantly.

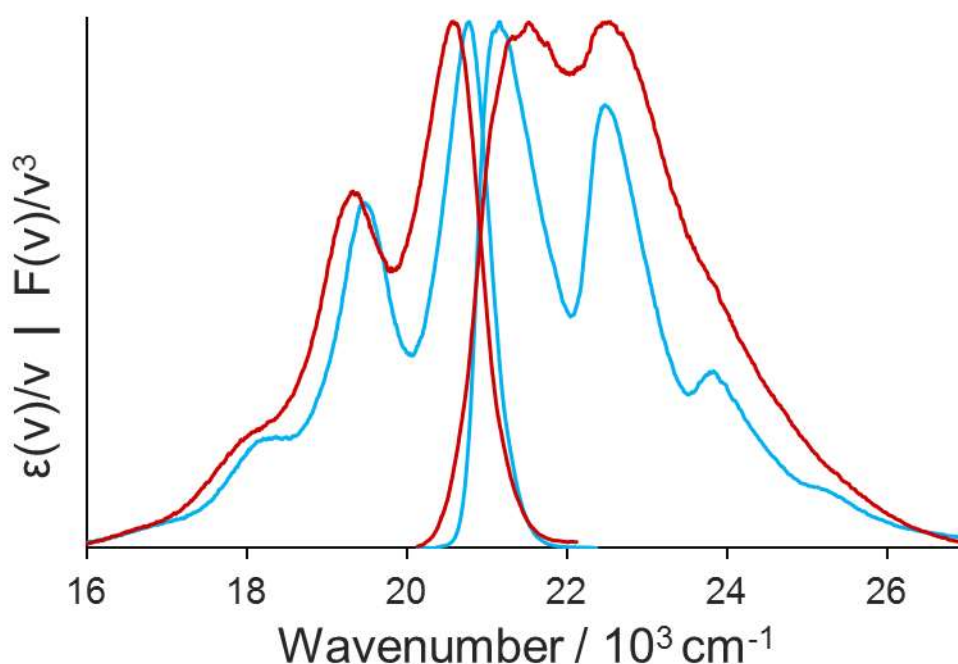


Figure 4.18 – Excitation and fluorescence spectra recorded for TM-BOPHY in MeTHF at 90K (—) and 290K (—), presented on an energy scale.

The effect is replicated in Figure 4.18 for BOPHY although the low-temperature spectrum is not as well-resolved as for TM-BOPHY.

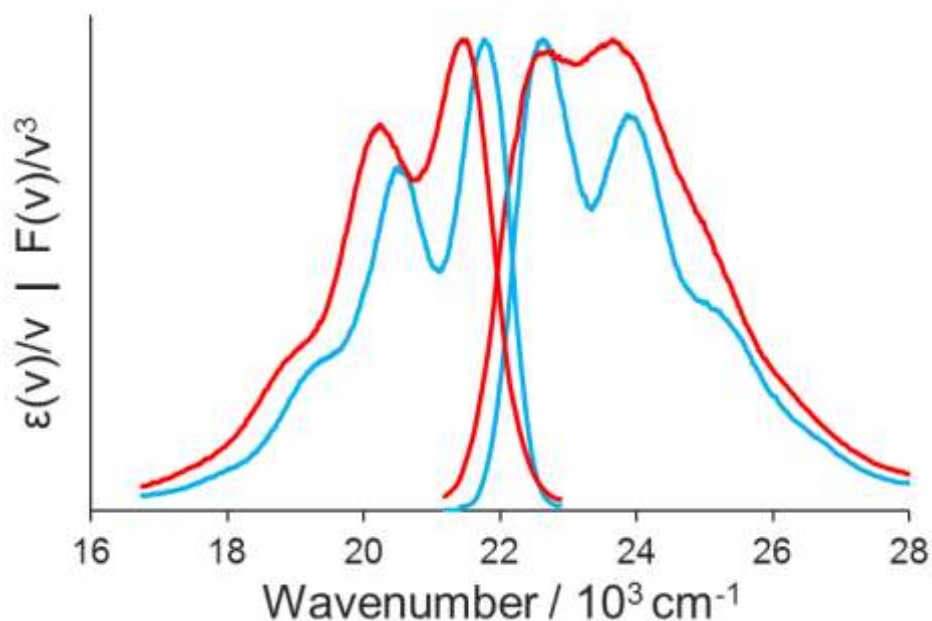


Figure 4.19 - Excitation and fluorescence spectra recorded for BOPHY in MeTHF at 90K (—) and 290K (—) presented on an energy scale.

4.3.2 Analysis of TM-BOPHY Fluorescence Spectra

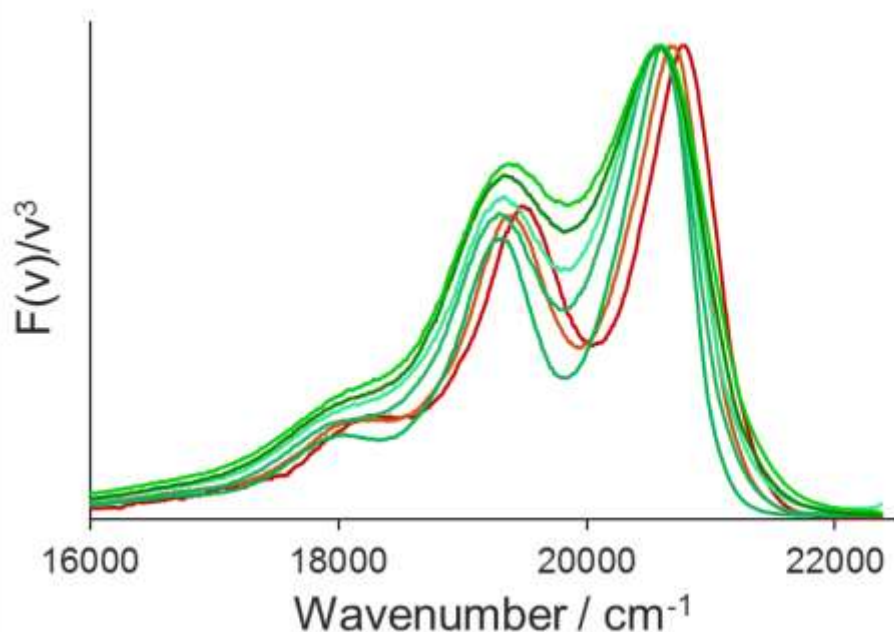


Figure 4.20 – Selected TM-BOPHY fluorescence spectra from 80-125K (—) and 140K-340K (—).

The main finding from this study is that mirror symmetry is restored at low temperature, specifically when the solvent forms a rigid glass. For the fluorescence spectra, it was possible to fully reconstruct the entire spectrum using a series of Gaussian-shaped components to mimic the underlying vibronic progression. The same pattern could be applied across the full

temperature range. This pattern is then applied to the corresponding excitation spectra. First, we can use this analysis to confirm mirror symmetry at low temperature. Then, we can check if the fitting pattern can be maintained across the temperature range. Such fitting is not a unique solution, but a reasonable set of bands was found and maintained for the fluorescence spectra. The scheme is given in Figure 4.21, showing the pattern in the glass and at room temperature. Seven vibronic bands were required to achieve a fit to the data with minimal residuals at 80K. It was also necessary to include a hot-fluorescence band at all temperatures, otherwise the spectra became unrealistically broad and bands are lost. At 80K the hot-fluorescence band is located at about 500cm^{-1} from the ν_{0-0} band and mirrors the first vibrational level so it is likely that this band is due to fluorescence from the first vibrational level to the ground state. We have seen such hot emission in many BODIPY-based fluorophores^[66].

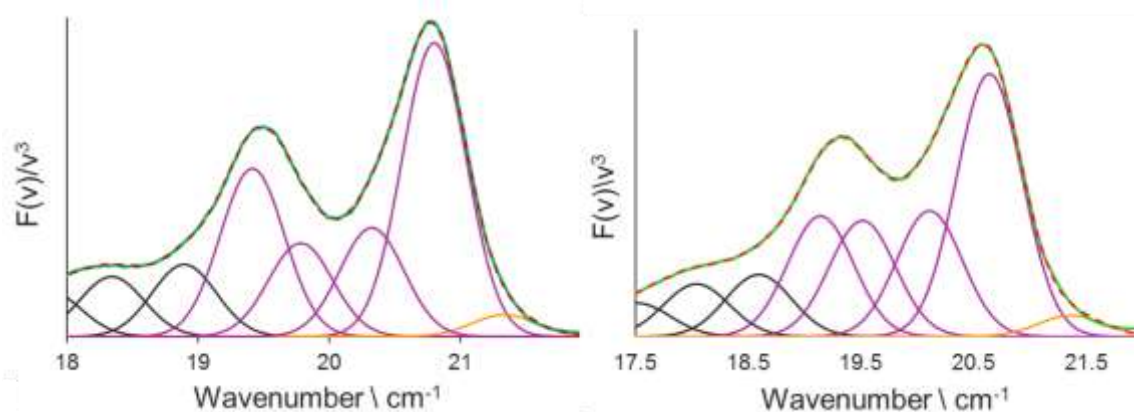


Figure 4.21 - Gaussian fits to the TM-BOPHY spectra recorded at 95K (left) and 290K (right), bands (—), Hot fluorescence (—) is shown. The measured spectra (—) and the fit (- -) are also shown.

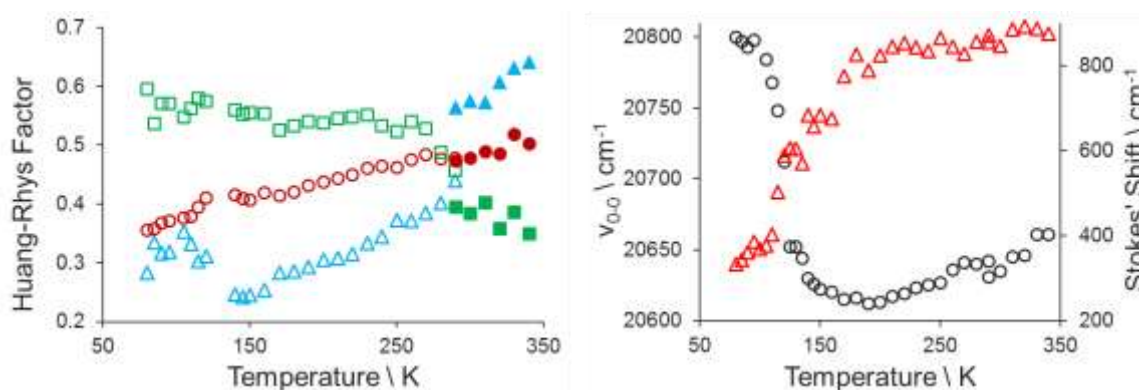


Figure 4.20 – The left-hand panel shows the ratio of the vibronic bands to the ν_{0-0} band, ν_{0-1} (○), ν_{0-2} (△) and ν_{0-3} (□). The filled markers represent the change to a conventional cuvette. The right-hand panel shows the change in the position of the ν_{0-0} fluorescence band (○) and the Stokes' shift (△).

From 80K to 120K, the MeTHF matrix is a rigid glass and throughout this phase there is essentially no change in the fluorescence spectra. The solvent cannot relax before emission so there is only a small Stokes' shift. Above this temperature, the glass begins to melt and an amorphous phase is entered. Throughout this phase, the fluorescence intensity falls considerably, possibly due to precipitation of the dye or loss of the good optical glass. The position of the ν_{0-0} band is shown in Figure 4.20 which red-shifts by about 200cm^{-1} . The temperature effects replicate those seen by Wild^[67] for an oxazine dye, and the full-width at half-maximum (FWHM) of the bands falls to a minimum of 500cm^{-1} . The matrix melts above 150K, the ν_{0-0} band shows a very slight blue shift as the dye tracks the changing properties of the solvent and the FWHM is seen to increase steadily from 500cm^{-1} to 800cm^{-1} . The solvent can now relax before emission so the Stokes' shift barely changes above this temperature. In Figure 4.20, the relative intensities of the vibronic bands compared to the ν_{0-0} transition is given. The ν_{0-3} band is the most significant of the bands analysed in detail. As the temperature increases, the relative intensities of the bands changes and the ν_{0-2} transition becomes the most important which suggests a change in geometry of the excited state above about 260K.

4.3.3 High-Temperature Spectroscopy of TM-BOPHY

To get an improved understanding of the changing properties with temperature, the fluorescence from TM-BOPHY was studied at temperatures up to 500K. For this purpose, the chromophore was dispersed into a transparent KBr disc. The quantum yield was found to drop steadily up to temperatures of about 400K but then dropped precipitously at higher temperatures. The change in k_{nr} resisted simulation by an activationless and activated barrier which may be due to the dye degrading at high temperature.

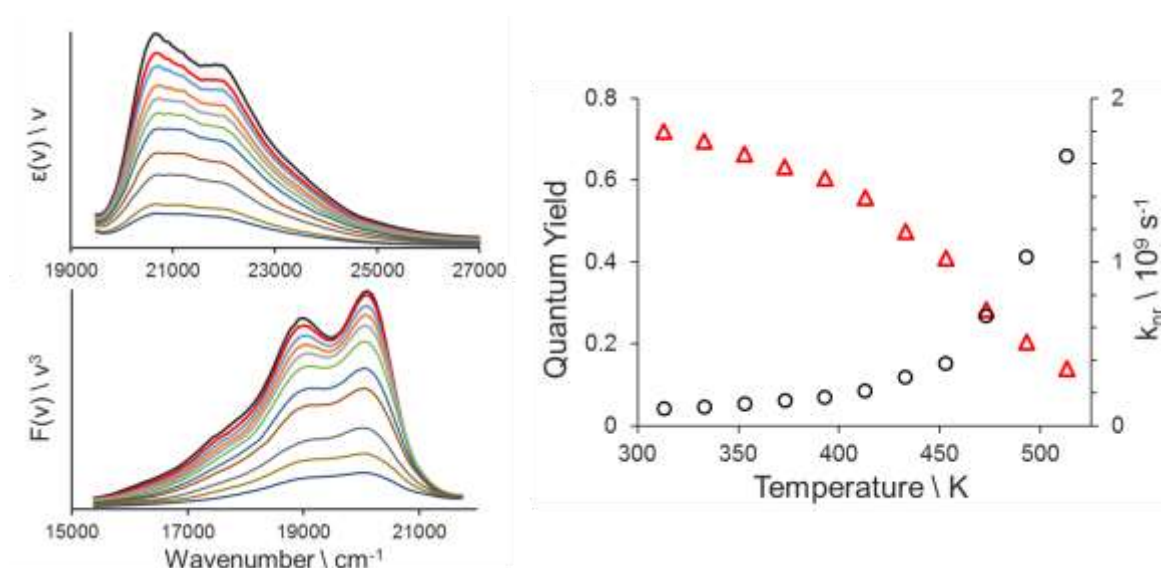


Figure 4.21 – Excitation and Fluorescence spectra for TM-BOPHY from 320K to 520K. The change in quantum yield (Δ) and k_{nr} (\bullet) are plotted on the right.

4.3.4 TM-BOPHY Excitation Analysis

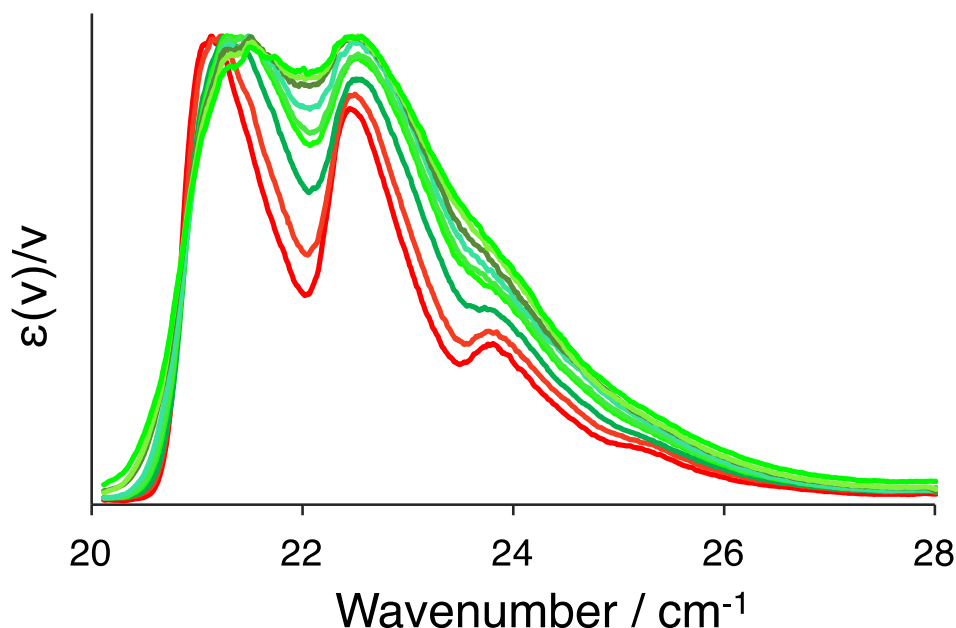


Figure 4.22 - Evolution of the excitation spectra recorded for TM-BOPHY in MeTHF across temperatures ranges 80-140K (—) and 150-340K (—)

Selected excitation spectra are shown in Figure 4.22. The position of the maximum is seen to blue shift as the glass melts, contributing to the change in Stokes' shift. Notably, there is only a small change in the broadness of the spectrum on going from 80K to 140K but there is quite a large change once the glass melts. This finding is taken to indicate that the change in the spectra is related to increased structural perturbation of the chromophore. As the spectra show mirror symmetry in the frozen glass the fluorescence vibronic pattern is applied to the excitation spectrum. In the glass it is possible to use the same set of bands to achieve a reasonable simulation of the excitation spectrum. As the matrix moves through the phase changes, the fit becomes increasingly unrealistic. We see that the broad peaks cannot be fitted to the same number of Gaussian bands as before and bands are lost. This breakdown at room temperature is shown in Figure 4.23. The ν_{0-0} band stops being the most significant band which does not reflect what is seen in the emission. The full width of the bands also increases markedly with temperature. At this stage, it is apparent that the excitation does not follow the scheme as laid out by the fluorescence.

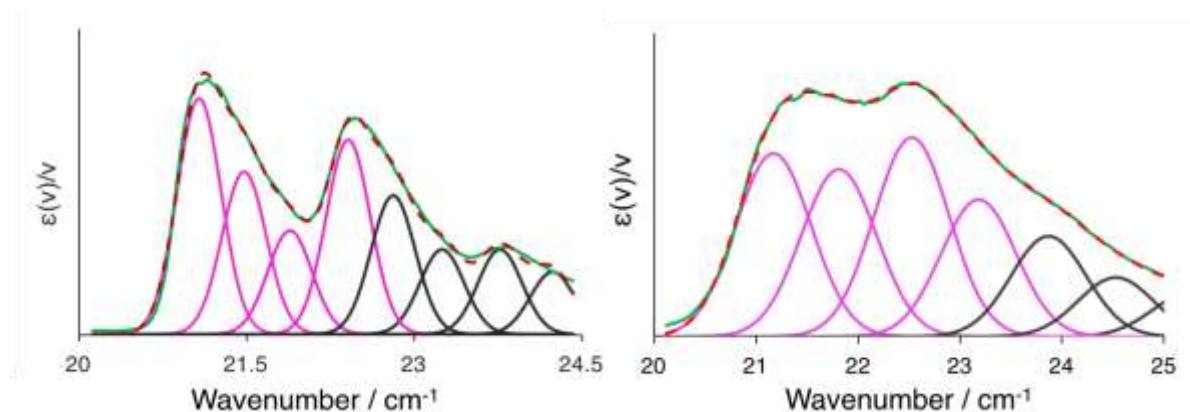


Figure 4.23 – Deconstruction of the excitation spectra at 95K, left, and 290K, right.

4.3.5 Electronic Spectra of TM-BOPHY in a Stretched Film

When trying to measure fluorescence polarisation, a technique to orientate the molecules along a single axis involves the use of stretched polymer films^[68]. Strips of polythene film were steeped in concentrated CHCl_3 solutions of TM-BOPHY and left for 24 hours to allow penetration of the chromophore into the film. The strips were then stretched to approximately five times their original length. In stretching the film, the molecules are forced to align with the processing grooves of the film. The molecules are restricted to a single environment at room temperature. Quite remarkably, TM-BOPHY in the stretched film displayed an excitation spectrum comparable to the spectrum seen in the frozen glass, which is shown in Figure 4.24. It would seem that in restricting the molecular orientation in the polymer groove, access to the state that causes the unusual excitation spectrum is restricted. This effect cannot be fully replicated by dispersing TM-BOPHY into other matrices. Thus, the chromophore was immobilised in a polythene melt, Zeonex 480, which is a nonpolar polymer, and poly(methyl methacrylate) (PMMA). In PMMA films, the excitation spectrum is much the same as in fluid solution at room temperature. In Zeonex and the polythene melt there was some increase in spectral fine-structure but not to the extent seen for the stretched film, this is also demonstrated by the inset of Figure 4.24. It would seem that the stretched film provides the necessary combination of immobilisation, single environment and polarity that results in the molecule being restored to its mirror-symmetry form.

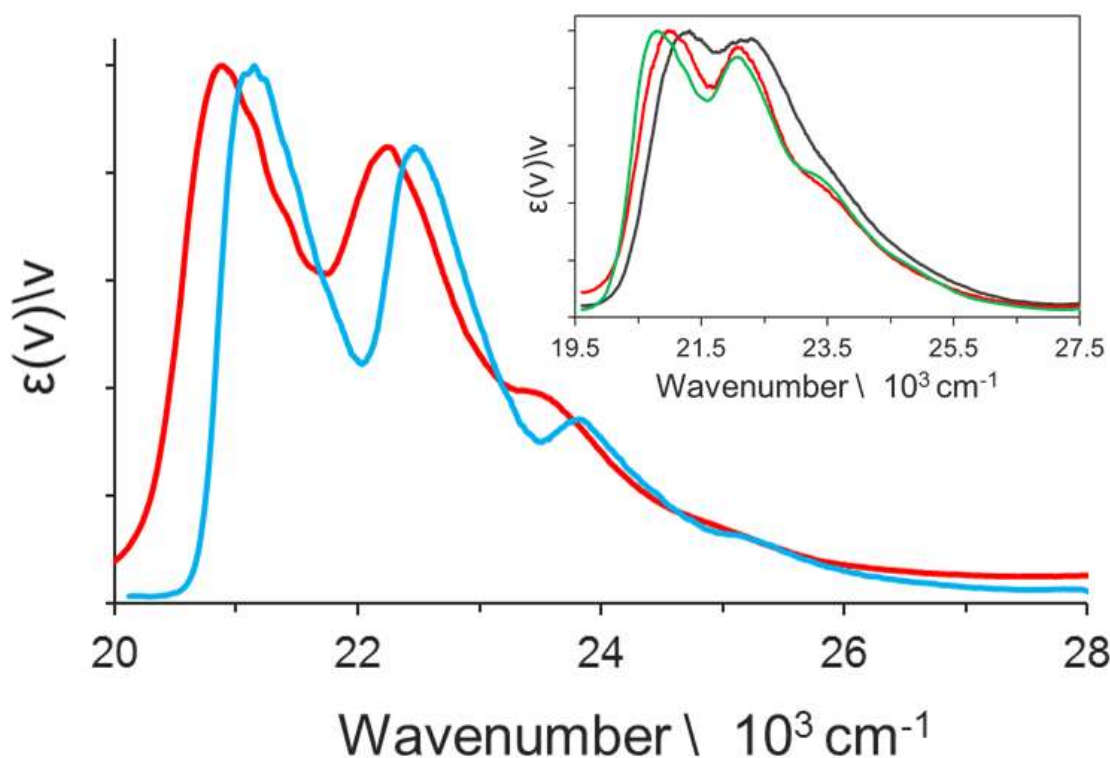


Fig 4.24 - Excitation spectra of TM-BOPHY in MeTHF at 80K (—), and in a stretched polythene film at room temperature (—). Inset shows the spectra in different polymeric media at room temperature PMMA (—), Zeonex 480 (—) and a polyethylene melt (—).

At room temperature, the mirror symmetry seen at low temperatures in the rigid glass is essentially restored. This implies that the loss of mirror symmetry is activated by the mobility of TM-BOPHY. The temperature dependence of the properties of TM-BOPHY restricted to the polythene grooves was studied, again from 80K to room temperature. The same vibronic pattern was fitted to the excitation and fluorescence spectra as was used for the solvent and was found to be an acceptable fit across all temperatures (Figure 4.25). Changes in the excitation are not due to some new state but to the temperature dependent broadening of the vibronic modes.

The fluorescence spectra showed almost no change across the full temperature range with only slight broadening, the properties are displayed in Figure 4.26. The half-widths at full maxima (FWHM) for the fluorescence and excitation spectra both increase by around 150cm^{-1} , which is entirely consistent with the increase in temperature of 200K. There is only a minor change in the Stokes' shift which can be traced to small shifts in the excitation spectrum, the polymer relaxation must always be on a similar timescale to the emission at all temperatures, and stays at around 600cm^{-1} . The significance of the fluorescence vibronic bands does not vary as much as was seen in fluid solution, although, in part, this is due to the restricted temperature range that could be used for the film. The bands do seem to change slightly in

significance, suggesting that the same process seen in the solution is emerging but restricted. This change was interpreted as a small modification of the geometry of the excited state as the temperature changes. The unique environment of the stretched film appears to inhibit this change. The most useful consequence of the stretched film is that it affords us the opportunity to compare the excitation spectra at the various temperatures to the spectra in MeTHF and thereby allows characterisation of the divergence from mirror symmetry.

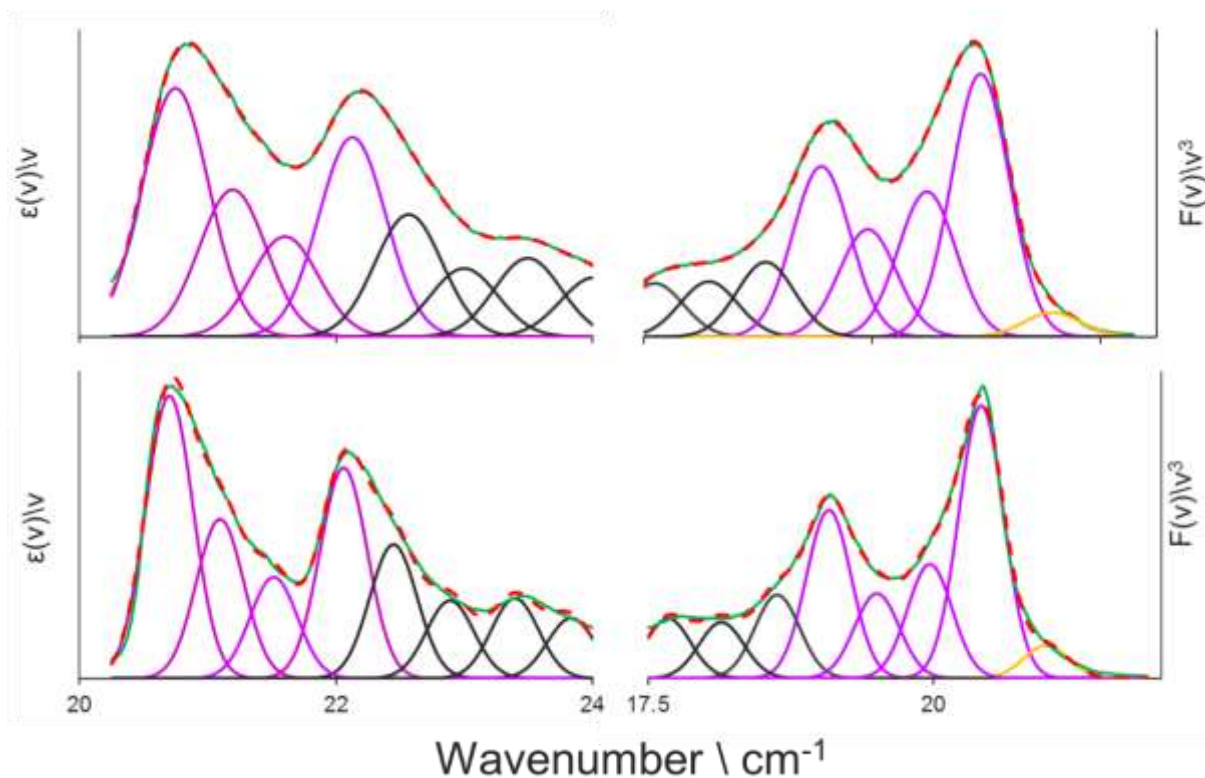


Fig 4.25 - Fitted reduced excitation, left, and reduced fluorescence, right, spectra recorded for TM-BOPHY in the stretched film at 290K (top) and 80K (bottom).

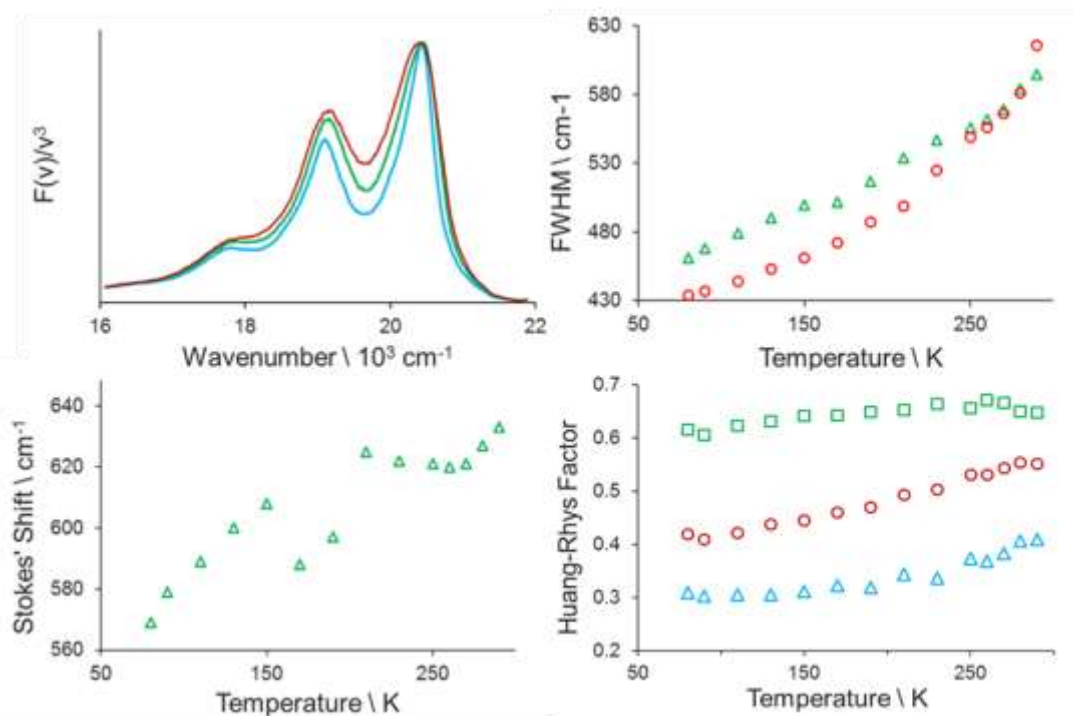


Figure 4.26 – Composite illustration of how temperature affects the various parameters that combine to define the fluorescence spectral profile in the film. Top left shows that there is little change in fluorescence spectrum. Going from 80K (—) to 290K (—). Top right shows the change in FWHM of the excitation (○) and the emission bands (△). The bottom right panel describes the main vibrational bands, the scheme is as per Figure 4.20.

4.4 Revealing the Second Transition

Different environments have been discovered where the mirror symmetry of TM-BOPHY absorption/emission spectral profiles is restored and our analysis of this situation leads to the conclusion that the breakdown of mirror symmetry is related to the mobility of the environment. The most likely explanation for this situation is that, in a fluid environment, the chromophore can access a different conformer with a subtly changed geometry. This second conformer then leads to a second optical transition at a slightly higher energy to the original transition. The second conformer of the molecule does not emit but must be in equilibrium with the standard conformer as the excitation spectrum is a good match to the absorption spectrum.

The simplest way to resolve the appropriate absorption spectrum of the second transition is to subtract the film excitation spectrum from that recorded in MeTHF at the same temperatures. This process can be replicated with the frozen glass spectra being removed from the fluid spectra. A problem was encountered in that the temperature change introduces spectral broadening that is not apparent for the spectra recorded in the rigid glass. As a compromise,

the spectrum recorded at 115K was used as the background and was subtracted from the spectra measured in the fluid (i.e. from 150K onwards). The spectra in the amorphous phase were not considered. In both cases, we are able to reveal the same profile for the second transition. As the temperature increases, we can track the fractional contribution of this second transition. When we remove the frozen glass spectrum we find a clear progression whereby the fractional contribution of the second transition increases in a consistent manner with increasing temperature. As was noted however this does not account for broadening of the underlying first transition nor for the fact that the solvent properties will change systematically with temperature. Thus, the amount of the second transition revealed by this method is considered to be overestimated. Using the method where the film spectra are removed there is an initial rise in the fractional contribution of the second transition as the temperature increases but this then falls at temperatures above 200K.

Neither of these methods is entirely satisfactory, temperature effects for the solvent are not reproduced with the film, of course, and there are differences in band half-widths. In Figure 4.26 we see that the FWHM of the excitation spectrum in the film increases as ambient temperature is approached, the polymer glass transition temperature, T_g , is expected to be at around 150K^[69] which we may expect to represent a different environment, but this region does not contain any significant spectroscopic signature.

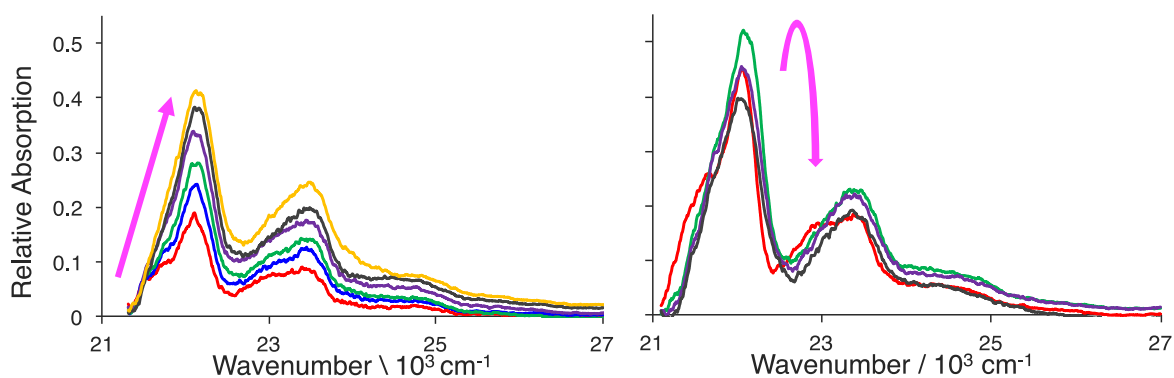


Figure 4.27 - Second electronic transition as revealed by subtracting the frozen glass spectrum (left), and removing the stretched film spectra (right) from 150K (–) to 290K (–) and 340K in the case of left. Pink arrows describe the extent of the new transition as the temperature increases.

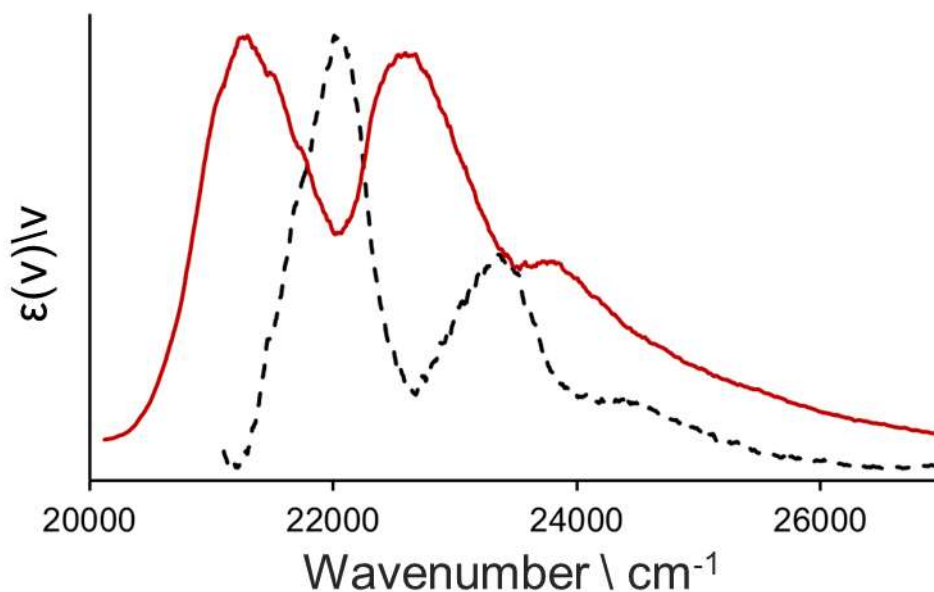


Figure 4.28 – The original optical transition (—) and the activated transition (- -).

The two absorption spectral profiles shown in Figure 4.28 display maxima at $22,100\text{cm}^{-1}$ and $21,200\text{cm}^{-1}$ (i.e., 450nm and 470nm). The energy gap between the two transitions is therefore on the order of 900cm^{-1} , which is above thermal energy at room temperature. The same energy difference between the respective ν_{0-0} transitions should facilitate very fast and irreversible nonradiative decay from upper to lower levels^[70].

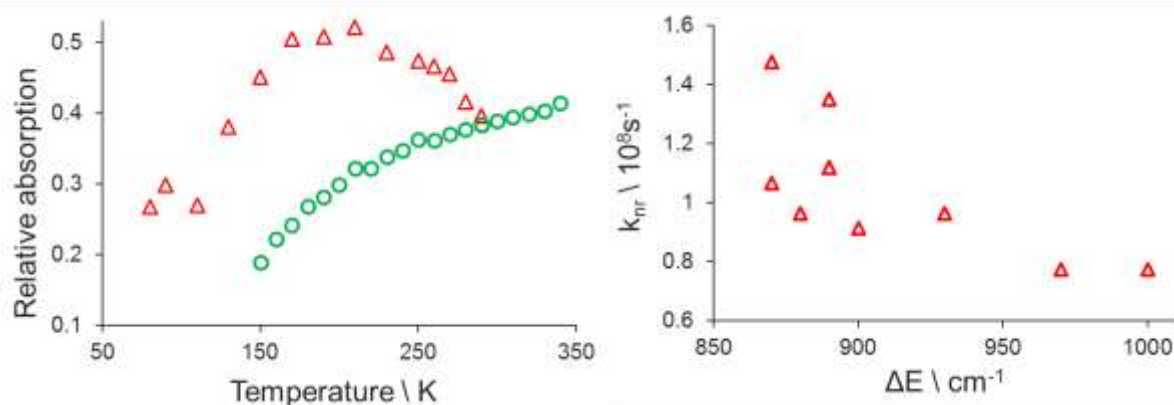


Figure 4.29 - The left panel shows how the fractional contribution of the second transition varies with temperature as derived by removing the spectra from the glass (○) and the spectra from the film (Δ). Right panel shows the correlation between non-radiative rate in different solvents compared to the energy gap between the two transitions.

4.5 Effect on Non-Radiative Rate

There is a weak trend towards a decrease of the fluorescence quantum yield with increasing solvent polarity and, for TM-BOPHY, the quantum yield falls within the range for $\Phi_f = 0.7-0.8$. Values reported in the literature are much closer to unity and declare no solvent dependence. During the temperature controlled spectroscopy, the fluorescence intensity increases as the temperature falls, so the fluorescence quantum yield cannot be unity at room temperature. This was particularly evident when TM-BOPHY was studied in ethanol (Figure 4.30). This raises the question of whether the higher-energy conformer might promote radiationless deactivation to the ground state. To explore this possibility, the temperature dependence of the fluorescence quantum yield was studied in various solvents. Ethanol is known to give a good optical glass at low temperatures so this solvent was used to study TM-BOPHY from 80K to room temperature. The low temperature quantum yield values determined in MeTHF are somewhat complicated, as demonstrated in Figure 4.30. In ethanol the intensity increased progressively in a consistent manner from room temperature to 160K. Once the solvent begins to freeze, the intensity dropped until plateauing at 90K where a rigid glass is formed. In ethanol a maximum value for Φ_f is reached at 0.85. The fluorescence intensity in the different solvents, in the fluid phase, was converted to a non-radiative rate constant and compared with the absolute temperature in Figure 4.30. The kinetic data were fitted to the sum of an activated and a barrier-free process, as described in Equation 4.5.

$$k_{nr} = k_0 + k_a \cdot e^{\left(\frac{-E_a}{RT}\right)} \quad (4.5)$$

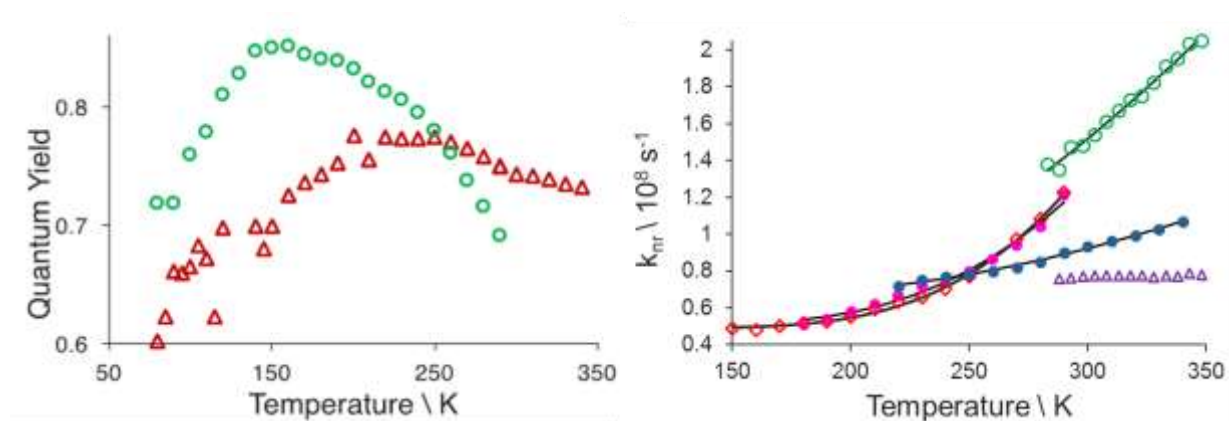


Figure 4.30 – Left panel, Quantum yield in ethanol (○) and MeTHF (△), right panel non-radiative rate in CH₃CN (○), EtOH (◇), MeTHF (●), C₆H₁₂ (△) and BuCN (●)

<i>Solvent</i>	$k_0 \backslash 10^7 s^{-1}$	$k_a \backslash 10^{10} s^{-1}$	$E_a \backslash kJ mol^{-1}$
Butyronitrile	5.1	1.0	12.1
Ethanol	4.9	2.0	13.6
Acetonitrile	5.6	2.6	8.2
MeTHF	6.6	1.1	9.3

Table 4.4 – Fluorescence data fitted to Equation 4.5 for various solvents, data in cyclohexane did not result in a realistic fit.

The activationless rate constant that characterises deactivation of the fluorophore at low temperature is essentially independent of the nature of the solvent (Table 4.30). The average value ($k_0 = 5.5 \times 10^7 s^{-1}$) is quite high and appears consistent with the notion that Φ_F falls short of unity even in the rigid glass. The corresponding activated rate constant shows more dependence of the properties of the solvent but there are too few solvents to draw any real conclusions. In fact, the analysis presented here is rather simplistic and does not take into account changes in the solvent or, more critically, changes in the absorption spectral profile of the fluorophore as the temperature changes. When performing temperature controlled spectroscopy, we use a constant excitation wavelength. This is satisfactory for most compounds since the excitation intensity absorbed, I_{abs} , is essentially constant. In the case of the BOPHY architecture, the absorbance at the excitation wavelength cannot be assumed to remain constant over the full temperature range. As the solvent cools, the density changes causing the concentration of species to increase. In the fluid at least, this is well characterised^[71], so we can employ a suitable correction factor. Corrections for both effects were applied and the results are shown in Figure 4.31. In ethanol, it appears that the emission quantum yield reaches a maximum close to unity in the rigid glass, then falls in a steady manner through the extended phase change and levels off in the fluid before a thermal process causes further loss of fluorescence. In MeTHF, a similar pattern is seen although the quantum yield appears to exceed unity, showing that the treatment is far from complete.

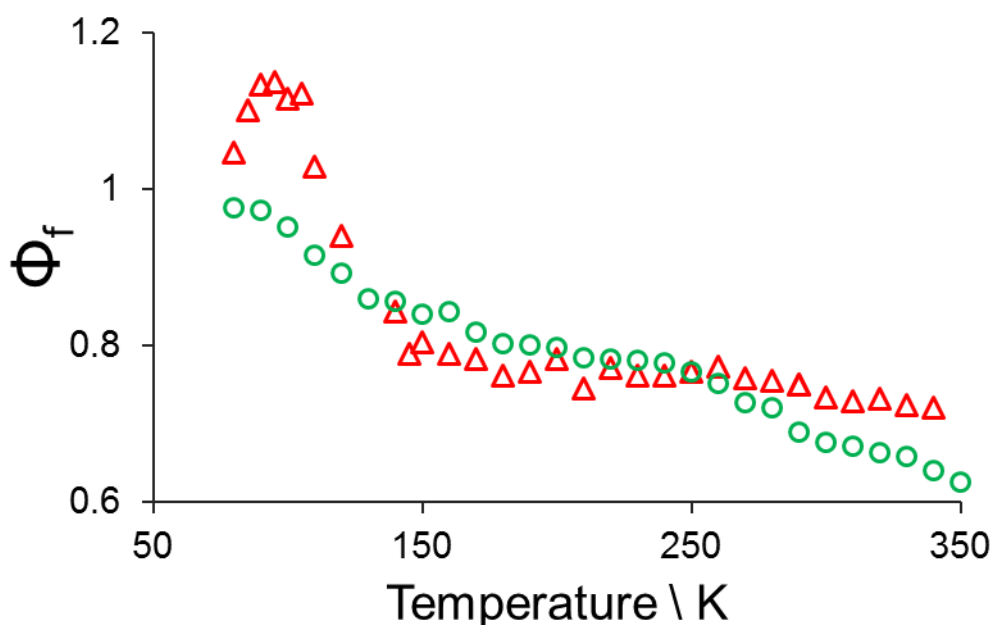


Figure 4.31 – Temperature dependence for the emission quantum yield derived for TM-BOPHY in MeTHF (Δ) and ethanol (○) after both correction factors are applied.

4.6 The second transition in BOPHY

In Figure 4.8 it was shown that mirror symmetry is quite well maintained for the unsubstituted form of BOPHY. To further corroborate our findings for TM-BOPHY, the unadorned BOPHY chromophore was studied from 80K to 340K in MeTHF. It is notable that room temperature absorption spectrum of BOPHY shows the second peak to be at least as high as for the ν_{0-0} band. This is reflected in other situations, such as the rigid glass spectrum where the excitation shows that the second peak is more significant compared to ν_{0-0} than in TM-BOPHY. It is also noted that the overall spectrum seems disproportionately broad.

The optical spectra were deconstructed to a series of Gaussian bands, using the pattern developed for TM-BOPHY. This pattern was found to give acceptable fits for the reduced emission spectra at all temperatures. In the frozen glass, the fitting pattern was also a reasonable approximation of the reduced excitation spectra. However, as for TM-BOPHY, when the solvent passes through the phase change the fitting breaks down. Indeed, the failure was more dramatic than for TM-BOPHY, as the temperature reached 150K the fitting was already becoming unrealistic as can be seen from Figure 4.32. The ν_{0-0} band now no longer represents the most significant transition and is seen to further decrease in significance as the temperature increases further. The bands, in general, start to broaden significantly. The

changes in the fluorescence properties are seen to vary in a similar manner to TM-BOPHY and are given in Figure 4.33.

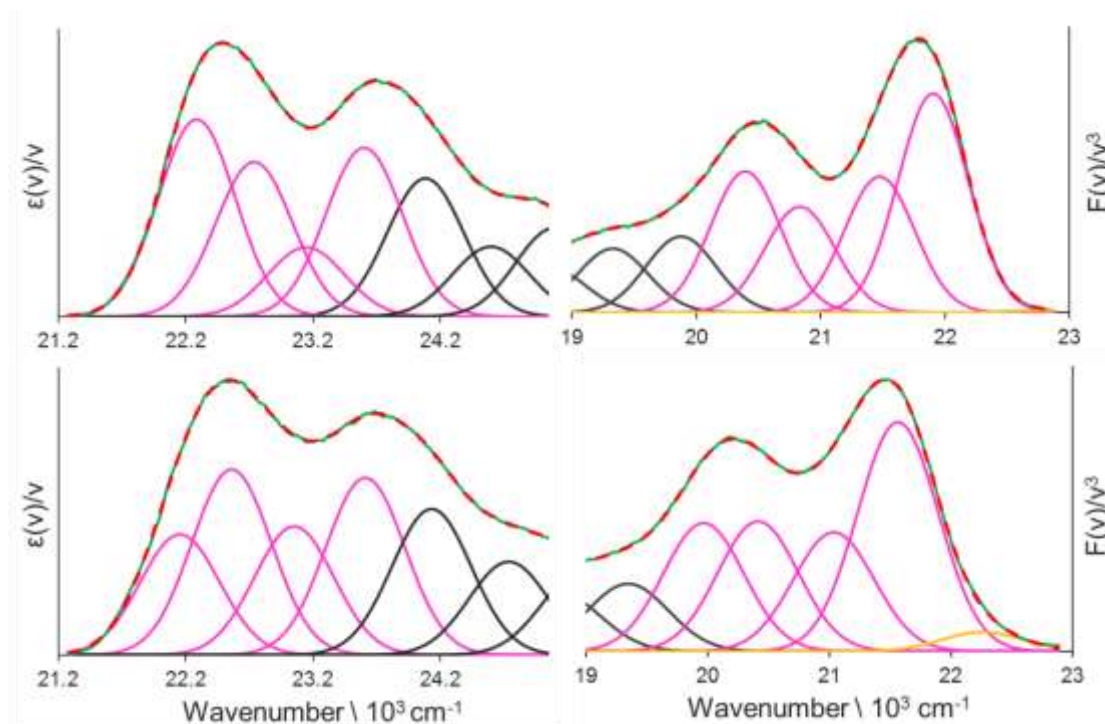


Figure 4.32 – Gaussian fitting of BOPHY spectra at 100K (top row), bottom left excitation at 150K bottom right emission at 280K

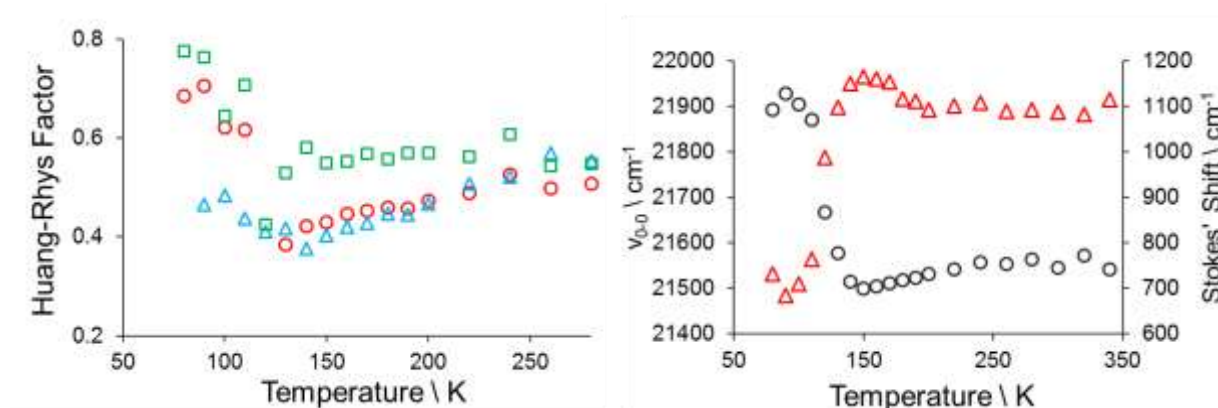


Figure 4.33 – Right, band ratio for the ν_{0-0} transition, ν_{0-1} (●), ν_{0-2} (▲) and ν_{0-3} (■). Left, The position of the ν_{0-0} band (●) and the Stokes' shift (▲).

It was not possible to replicate the stretched film method for BOPHY. Only weak fluorescence was seen when the protocol was repeated, which did not appear to be a good match to the frozen glass spectra. It would seem that the dye was not being properly distributed in the film. It was therefore only possible to reveal the second transition by removal of the rigid glass spectrum from the fluid spectra. For these spectra, an excellent optical glass was maintained at all temperatures. The position of the ν_{0-0} band of the excitation spectrum was seen to be

constant up to 110K but then drops dramatically at 120K. The spectrum at 100K was used as a reference for removal from the fluid excitation spectra. The energy gap between the two transitions for BOPHY is around 700cm^{-1} but no solvent dependence was found. This is lower than the energy gap for TM-BOPHY, which is around 900cm^{-1} , and this might contribute to the lower fluorescence yields for BOPHY. Figure 4.34 shows the gradual evolution of the second transition with temperature, starting from 120K.

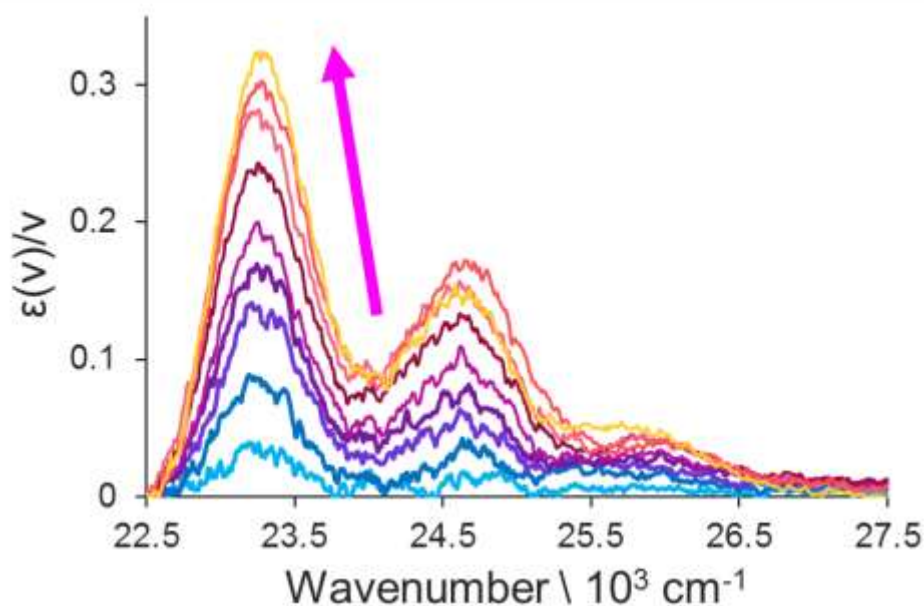


Figure 4.34 - Spectra of the second transition as revealed by subtraction of the frozen glass spectrum from 120K to 340K, the amount revealed increases with temperature as demonstrated by the arrow.

The excitation spectrum derived for the second conformer for BOPHY is well resolved and is shown alongside the original transition in Figure 4.35. The spectral shapes look similar for the two transitions. As for the equivalent analysis of TM-BOPHY, the fractional contribution of the second conformer increases steadily with temperature.

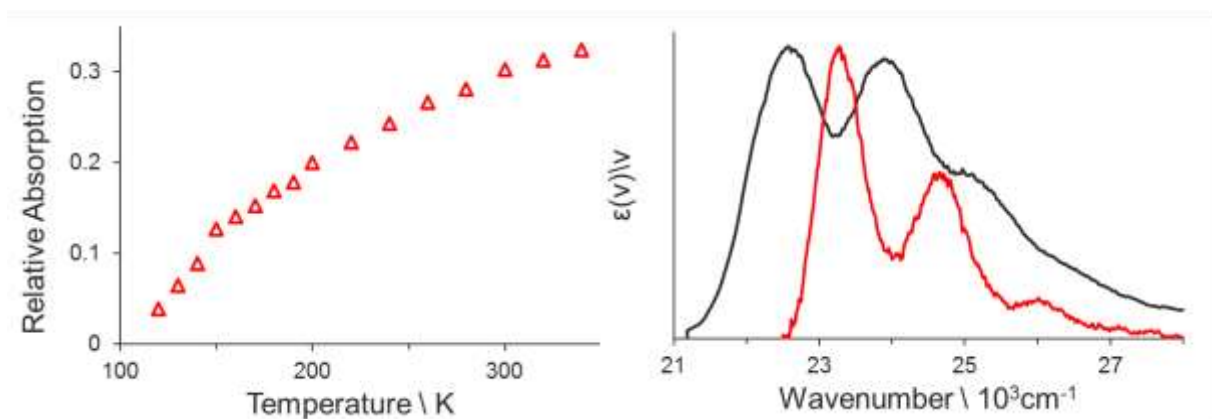


Figure 4.35 - Right, the relative absorption of the second transition increasing with temperature, left the original conformer (—) and the second transition (—) at 300K

4.7 Conclusion

This new class of pyrrole-BF₂ dyes is promising in that it affords structural opportunities not easily available to BODIPY. Substitutions can be made at opposite corners of the core structure, allowing for long, linear molecules. High, although non-unity, fluorescence quantum yields are found, while the absorption spectrum is rather broad. This latter feature is a desirable property for molecules that act as quantum yield standards and for light-harvesting applications. The cause of this broadness has been studied in detail and is ascribed to an equilibrium exchange between two conformers. Access to this second conformer is restricted when the mobility of the molecule is limited, such as in rigid glasses, while in stretched polymer films mirror-symmetry is restored between absorption and fluorescence spectra. Attempts to confirm the second conformer were made by NMR, it is notable that the boron and fluorine NMR spectra of BOPHY are rather less well-defined compared to BODIPY which is illustrated in Appendix 1. Temperature controlled NMR was able to improve our understanding of the conformer.

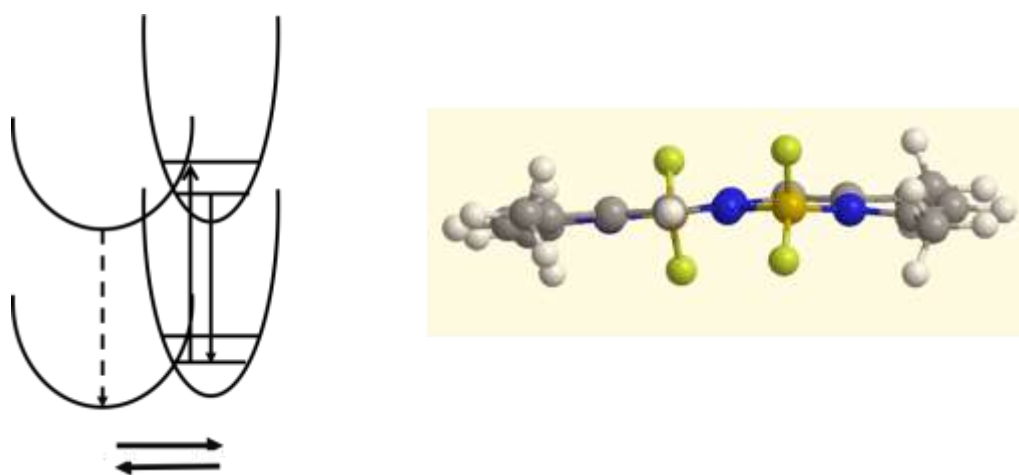


Figure 4.36 – Left, the planar geometry is responsible for the fluorescence but is coupled to the conformer that does not radiate. Right, a calculated, minimised structure suggest some warping of the BOPHY structure. The structure was calculated using the PBE0/6-311G) basis set in a chloroform reservoir using the PCM model and the Mennucci-Tomasi correction applied.

An energy-minimised structure, shown in Figure 4.36, has been calculated for TM-BOPHY that found the core structure to be slightly buckled. This conformation is consistent with the experimental observations. Two conformers are found, one of which is coupled to the ground state. We imagine then, fluorescence comes from a planar geometry and this geometry is in equilibrium with a buckled conformation which disrupts the conjugation and causes non-radiative return to the ground state as shown in the energy diagrams also given in Figure 4.36. It seems that the quantum yield for any molecule featuring the BOPHY core is likely to be limited to $\Phi_f = 0.80$ in solution, which may be considered a downside as many unity quantum

yield fluorophores are available. This loss of fluorescence could be compensated for however in terms of effective photon absorption and in the new structures that could be created. In microscopy, the cyanine dyes still dominate, especially when working in the red part of the spectrum. For such dyes the quantum yield is considerably below unity so there is still scope for bright but non-unity emitting dyes in this area, for example if improved stability is found. In terms of light harvesting applications, dispersing the dye into sol-gel matrices at room temperature could also restore the mirror symmetry while further synthesis at the boron centres could allow strapped-BOPHYs to be created which again may restore the symmetry. The BOPHY motif then, despite this conformer exchange, retains some promising qualities.

References

- [1] A. Treibs, F. H. Kreuzer, *Eur. J. Org. Chem.* **1968**, 718, 208-223.
- [2] B. Ventura, G. Marconi, M. Bröring, R. Krüger, L. Flamigni, *New J. Chem.* **2009**, 33, 428-438.
- [3] J. Bañuelos Prieto, I. López Arbeloa et al. *J. Phys. Chem. A*, **2004**, 108, 5503-5508.
- [4] G. Ulrich, R. Ziessel, A. Harriman. *Angew. Chem. Int. Ed.* **2008**, 47, 1184-1201.
- [5] A. C. Benniston, G. Copley, *Phys. Chem. Chem. Phys.* **2009**, 11, 4124-4131.
- [6] A. Kamkaew, K. Burgess et al. *Chem. Soc. Rev.* **2013**, 42, 77-88.
- [7] G. Ulrich, R. Ziessel, A. Harriman, *Angew. Chem. Int. Edit.* **2008**, 47, 1184-1201.
- [8] V. Leen, M. Van der Auweraer, N. Boens, W. Dehaen, *Org. Lett.* **2011**, 13, 1470-1473.
- [9] V. Leen, T. Leemans, N. Boens, W. Dehaen, *Eur. J. Org. Chem.* **2011**, 2011, 4386-4396.
- [10] S. T. Manjare, J. Kim, Y. Lee, D. G. Churchill, *Org. Lett.* **2014**, 16, 520-523.
- [11] Y. Ni, W. Zeng, K.-W. Huang, J. Wu, *Chem. Commun.* **2013**, 49, 1217-1219.
- [12] D. Sirbu, A. C. Benniston, A. Harriman, *Org. Lett.* **2017**, 19, 1626-1629.
- [13] G. Ulrich, C. Goze, M. Guardigli, A. Roda, R. Ziessel, *Angew. Chem. Int. Ed.* **2005**, 117, 3760-3764.
- [14] A. Entwistle, M. Noble, *J. Microsc.* **1992**, 168, 219-238.
- [15] B. Hinkeldey, A. Schmitt, G. Jung, *ChemPhysChem.* **2008**, 9, 2019-2027.
- [16] I. L. Arbeloa et al. *J. Phys. Chem. A*. **2002**, 106, 7736-7742.
- [17] N. Boens, V. Leen, W. Dehaen, *Chem. Soc. Rev.* **2012**, 41, 1130-1172.
- [18] K. Yamada, K. Suzuki et al. *J. Am. Chem. Soc.* **2005**, 127, 6956-6957.
- [19] N. DiCesare, J. R. Lakowicz, *Tetrahedron Lett.* **2001**, 42, 9105-9108.
- [20] Z.-N. Sun, H.-L. Wang, F.-Q. Liu, Y. Chen, P. K. H. Tam, D. Yang, *Org. Lett.* **2009**, 11, 1887-1890.
- [21] M. Tian, X. Peng, F. Feng, S. Meng, J. Fan, S. Sun, *Dyes Pigm.* **2009**, 81, 58-62.
- [22] C.-L. Liu, Y. Chen, D. P. Shelar, C. Li, G. Cheng, W.-F. Fu, *J. Mater. Chem. C*, **2014**, 2, 5471-5478.
- [23] B. C. Popere, A. M. Della Pelle, S. Thayumanavan, *Macromolecules.* **2011**, 44, 4767-4776.
- [24] H. Usta, J. F. Stoddart et al. *Adv. Mater.* **2013**, 25, 4327-4334.
- [25] I. López-Duarte, M. K. Kuimova et al. *Chem. Commun.* **2014**, 50, 5282-5284.
- [26] F. Cucinotta, B. P. Jarman et al. *ChemPhotoChem.*
- [27] R. Ziessel, A. Harriman et al. *Chem. Eur. J.* **2005**, 11, 7366-7378.
- [28] R. Ziessel, G. Ulrich, A. Haefele, A. Harriman, *J. Am. Chem. Soc.* **2013**, 135, 11330-11344.
- [29] M. Urban, K. Durka, P. Jankowski, J. Serwatowski, S. Luliński, *J. Org. Chem.* **2017**, 82, 8234-8241.
- [30] B. Lee, D. Lee et al. *Chem. Eur. J.* **2016**, 22, 17321-17328.
- [31] V. N. Nemykin, C. J. Ziegler et al. *J. Am. Chem. Soc.* **2014**, 136, 5623-5626.
- [32] C. Yu, E. Hao et al. *Org. Lett.* **2014**, 16, 3048-3051.
- [33] J. H. Boyer et al. *Heteroat. Chem.* **1993**, 4, 39-49.
- [34] M. Kasha, *Discuss. Faraday Soc.* **1950**, 9, 14-19.

- [35] J. R. Lakowicz, *Principles of Fluorescence Spectroscopy*, Springer, **2006**.
- [36] A. D. McNaught, *Compendium of chemical terminology*, Blackwell Science Oxford, **1997**.
- [37] C. E. Wayne, *Photochemistry*, Oxford University Press, Oxford, **1996**.
- [38] G. Angulo, G. Grampp, A. Rosspeintner, *Spectrochim. Acta A*, **2006**, 65, 727-731.
- [39] M. Beer, H. C. Longuet-Higgins, *J. Chem. Phys.* **1955**, 23, 1390-1391.
- [40] S. N. Batchelor, A. Jarvis et al. *Dyes Pigm.* **2003**, 59, 269-275.
- [41] C. Eggeling, J. Widengren, R. Rigler, C. A. M. Seidel, *Anal. Chem.* **1998**, 70, 2651-2659.
- [42] A. P. Demchenko, V. I. Tomin, P.-T. Chou, *Chem. Rev.* **2017**, 117, 13353-13381.
- [43] T. T. Herzog, G. Ryseck, E. Ploetz, T. Cordes, *Photochem. Photobiol. Sci.* **2013**, 12, 1202-1209.
- [44] A. P. Demchenko, P.-T. Chou et al. *Chem. Sci.* **2016**, 7, 655-665.
- [45] C.-C. Hsu, Y. Chi et al. *J. Am. Chem. Soc.* **2012**, 134, 7715-7724.
- [46] O. Yushchenko, E. Vauthey et al. *J. Phys. Chem. Lett.* **2015**, 6, 2096-2100.
- [47] N. J. Turro, V. Ramamurthy, W. Cherry, W. Farneth, *Chem. Rev.* **1978**, 78, 125-145.
- [48] H. Tamura, I. Burghardt, *J. Am. Chem. Soc.* **2013**, 135, 16364-16367.
- [49] W. Shockley, H. J. Queisser, *J. Appl. Phys.* **1961**, 32, 510-519.
- [50] E. R. Menzel, J. S. Polles, *Chem. Phys. Lett.* **1974**, 24, 545-548.
- [51] J. L. Irvin, E. M. Irvin, *J. Biol. Chem.* **1948**, 174, 589-596.
- [52] J. B. Birks, *Rep. Prog. Phys.* **1975**, 38, 903.
- [53] M. Schäferling, T. Lang, A. Schnettelker, *J. Lumines.* **2014**, 154, 458-464.
- [54] Z. R. Grabowski, W. Rubaszewska, *J. Chem. Soc. Faraday Trans.* **1977**, 73, 11-28.
- [55] M. Bayda, A. Wojcik et al. *Dalton Trans.* **2017**, 46, 1914-1926.
- [56] M. Kasha, *Radiat. Res.* **1963**, 20, 55-70.
- [57] M. Kasha, H. R. Rawls, M. A. El-Bayoumi, *Pure Appl. Chem.* **1965**, 11, 371-392.
- [58] R. A. Strickler, S. J. Berg, *J. Phys. Chem.* **1962**, 37, 814-822.
- [59] G. A. Reynolds, K. H. Drexhage, *Opt. Commun.* **1975**, 13, 222-225.
- [60] B. Berlman, *Handbook of Fluorescence Spectra of Aromatic Molecules*, **1972**, 27, 939-940.
- [61] R. F. Kubin, A. N. Fletcher, *J. Lumines.* **1982**, 27, 455-462.
- [62] J. H. Brannon, D. Magde, *J. Phys. Chem.* **1978**, 82, 705-709.
- [63] N. Mataga, Y. Kaifu, M. Koizumi, *Bull. Chem. Soc. Jpn.* **1956**, 29, 465-470.
- [64] E. v. Lippert, *Ber. Bunsenges. Phys. Chem.* **1957**, 61, 962-975.
- [65] A. Harriman, R. Ziessel et al. *J. Phys. Chem. A.* **2006**, 110, 7994-8002.
- [66] A. Harriman, P. Stachelek, A. Sutter, R. Ziessel, *Phys. Chem. Chem. Phys.* **2015**, 17, 26175-26182.
- [67] E. Görlach, H. Gygax, P. Lubini, U. P. Wild, *Chem. Phys.* **1995**, 194, 185-193.
- [68] J. Michl, E. W. Thulstrup, J. H. Eggers, *J. Phys. Chem.* **1970**, 74, 3878-3884.
- [69] J. Brandrup, D. R. Bloch et al. *Polymer Handbook*, Wiley, New York, **1989**.
- [70] J. Jortner, J. W. Verhoeven et al. *Chem. Phys. Lett.* **1993**, 205, 451-455.
- [71] I. S. Khattab, F. Bandarkar, M. A. A. Fakhree, A. Jouyban, *Korean J. Chem. Eng.* **2012**, 29, 812-817.

Chapter 5 - Electronic Communication in a Linear BOPHY Supermolecule

5.1 Introduction

The large, planar, symmetrical core of BOPHY can be functionalised at the α -pyrrolic positions, thereby allowing long molecules to be isolated that are effectively linear. In the event that significant through-bond communication is engineered across such BOPHY-based molecular architectures, it might be possible to accrete many molecules into integrated networks. A molecular device will surely require thousands of molecules working in unison, perhaps with some fixed group structure, and communication between and within molecules will be vital. As a starting point to better understanding of the internal electronic properties of the BOPHY, this being a relatively new entry into the field of organic dyes, we now describe the properties of a BOPHY supermolecule featuring dimethyl-anilino terminals; the molecule is abbreviated as BOPHY-DMA. The primary objective of the work is to establish the extent of electronic communication between the terminal sites. We are still at the stage of examining if BOPHY has advantages relative to the better-known BODIPY and this work forms part of the global project.

The need for dyes absorbing in the far-red region of the spectrum for bio-imaging purposes, as well as devices that can make use of natural light resources is well known. The use of cyanine^[1] dyes and porphyrin-type macrocycles^[2] is well established in this field. The modern BODIPY family is now a very important class of dye that has been modified for imaging purposes, BODIPY dyes are prized for their versatility^[3] as the photophysics can be tuned almost infinitely. Protocols to shift the absorption spectrum include extension of the conjugation path^[4], adding electron-withdrawing groups to the *meso*-position^[5] or attaching electron-donor groups at the α -position^[6]. The related aza-BODIPY^[7] family extends the spectral range by some 100nm whilst still demonstrating desirable photophysical properties, with fluorescence quantum yields of 90% and emission at 680nm^[8]. Generally, the penalty associated with reducing the energy gap will be an increase in the non-radiative decay rate^[9] and thus a loss of fluorescence. If the energy of the HOMO is lowered, then oxidation of the chromophore will become easier so that red-shifted dyes are typically less stable. This situation is exacerbated by the likelihood that the extension of conjugation paths will result in sites where chemical attack can occur. The BOPHY system has been examined to see if it can be tuned to red-shift the absorption and emission profiles. This has been successfully achieved by addition of groups to the α -positions^[10], diagonal^[11] and linear^[12] β -positions,

fusion of extra aromatic rings to the core^[13] and by adding molecular fragments to the *meso*-position^[14]. TDDFT studies^[15] have also looked at how to achieve a red-shifted absorption spectrum in the BOPHY framework. Significant extension of the conjugation path was first reported by Ziesse^[16] with substituents at the α -pyrrolic positions running along a diagonal axis of the BOPHY core. Different types of unsaturated units were appended to the central core and it proved to be possible to tune the emission well into the far-red and near-IR regions. Such molecules therefore could become useful for the applications described previously. Indeed, due to active site substitution being on opposing sites of the core the opportunity to make extremely long, linear molecules presents itself. This is unlike the BODIPY case where V-shaped configurations abound^[17].

The target BOPHY-DMA features anilino terminal groups which are strong electron donors that push charge toward the centre of the molecule. In the literature, a selection of molecules have been reported which are particularly relevant and comparable to the BOPHY-DMA molecule. Xiao et al introduced a BOPHY molecule with a single styryl unit^[18] that was reported to act as a pH sensor in acetonitrile-water mixtures. A recent paper demonstrated a symmetrical molecule^[19] featuring aniline substituents but without the vinyl linker such that aniline group is nearer to the BOPHY core. Again, the photophysics were shown to be pH dependent but no information on the terminal-terminal effects were reported. Nemykin et al reported a BOPHY molecule of similar structure^[20] but terminated with ferrocene rather than aniline units. Typical of such ferrocene-containing chromophores it is non-emissive. These authors found a terminal-terminal distance of 17.2Å and reported that there was significant intramolecular electronic interaction along the full length of the molecule. A later paper by the same group introduced a related ferrocene-BOPHY where further ester and phenyl substitutions were made the β -pyrrolic positions^[14]. In this latter case, electronic coupling between the terminal ferrocene groups was not found. This disparity between the two sets of compounds was assigned to a disruption of the rigidity of the BOPHY core.

Studies in intramolecular electronic communication are particularly prevalent in inorganic chemistry where metal centres are often in different oxidation states. If there is communication between centres, this should manifest itself in the emergence of an intervalence charge-transfer (IVCT) transition as electron transfer between the units can occur. This is a particularly strong phenomenon in the case of metal-metal complexes^[21], the most well-known example being the deep blue colour of Prussian blue^[22] ($\text{Fe}_4[\text{Fe}(\text{CN})_6]_3$) which is due to an intense IVCT band around 680nm resulting from transfer between the Fe(II) and Fe(III) sites. The deep colour of many minerals is often due to IVCT transitions as shown in Figure 5.1. Such intervalence interactions are classified into three groups^[23] as per the scheme of Robin and Day. Class I materials are those where the coupling is weak such that centres A and A⁺ act

as nuclei in isolation. Conversely, Class III materials are those where the coupling is strong and the material will display the properties of a new complex $(A-A)^+$. Where there is some amount of coupling between the mixed-valence species then that is a class II compound and there might be absorption associated with the hopping electron. The theoretical work was derived by Hush^[24] and the critical equations can be found in section 5.4.4.



Figure 5.1 – A microtomed slice of the mineral Kyanite, the green colour originates from ferric ions while the blue band is due to an IVCT transition between Fe^{2+} and Fe^{3+} .

Studies of intramolecular electronic communication are dominated by the realm of inorganic chemistry so a lot of the effort in the study of intramolecular communication concerns metal-complexes^[25, 26]. The theory has been extended into the organic realm in areas such as ferrocene-terminated compounds^[27] on account of the strong electron donating properties but with the drawback that they rarely show any singlet emission. Other compounds displaying IVCT character include those containing multiple repeating units like polymers^[28] or arrays of porphyrins^[29]. Studies concerning electronic communication in pure organic compounds displaying mixed valence states are less common, by definition they must contain redox active sites or exist as stable radicals or ions. Pure organic molecules are of great interest for molecular devices compared to metal-organics as there are no expensive, potentially toxic, metals present. They are usually more flexible in terms of tuning the optical properties while emission yields are higher. Phenothiazinophanes with conjugated bridges^[30] were shown to have additional communication due to through-bond interaction but this geometry will always mean through-space communication is favourable. It has been shown that purely organic systems can be understood by Hush-type treatment and can be considered class II or borderline II/III systems^[31]. A pair of linked 2,5-dimethoxy-4-methylphenyl donors^[32], on one-electron oxidation, were shown to be either class II, II/III or III depending on if there were 0, 1 or 2 phenyl spacers respectively. Bands due to organic IVCT transitions tend to be broad, appear well into the IR region at $6000-3000\text{ cm}^{-1}$ ^[31, 33] and are of low intensity. Molar absorption coefficients^[34] up to $5000\text{ M}^{-1}\text{cm}^{-1}$ are seen so can be difficult to assign, while electronic coupling of up to 3000 cm^{-1} is feasible^[35] for class II systems. A particularly interesting notion lies in the use of photo-switching^[36] mechanisms by external stimuli to control electronic communication. Nisihara et al^[33] used an isomerisable ethynyl-ethene bridge that isomerises

when a charge transfer band is illuminated. This disrupts the geometry of the bridge and brings the donor units into the Z-conformation meaning that the through-bond communication is reduced and through-space communication is favoured. Care must be taken when applying Hush's equation (Equation 5.3) to organic molecules as it depends on the reciprocal of the distance between the mixed-valence sites. Determining this can be hard as delocalisation of the charge will lead to a reduced effective distance.

The energy-minimised structure of BOPHY-DMA is presented below along with the chemical structure in Figure 5.2 and shows that the molecule is essentially linear from terminal to terminal but with rotatable units. The linear nature of the molecule is testament to the rigid, near planar nature of the core. The distance between terminal units was calculated to be 22.6Å, this length is used as the basis for calculations of electrostatic coupling within the molecule. Despite the significant red shift compared to TM-BOPHY, in a non-polar environment BOPHY-DMA is highly fluorescent, the fluorescence quantum yield being much the same as for the parent TM-BOPHY.

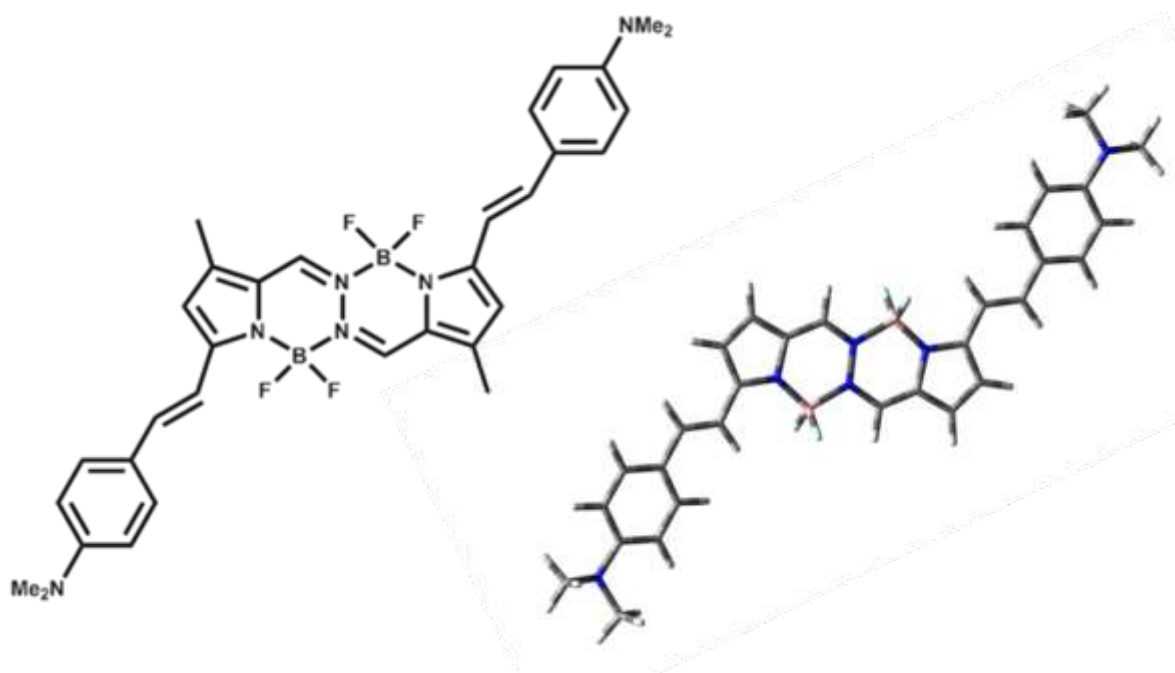


Figure 5.2 – Chemical formula for BOPHY-DMA the energy-minimised structure calculated with the PBE0 functional and 6-311G(d,p) basis set.

5.2 Photophysical Properties of BOPHY-DMA

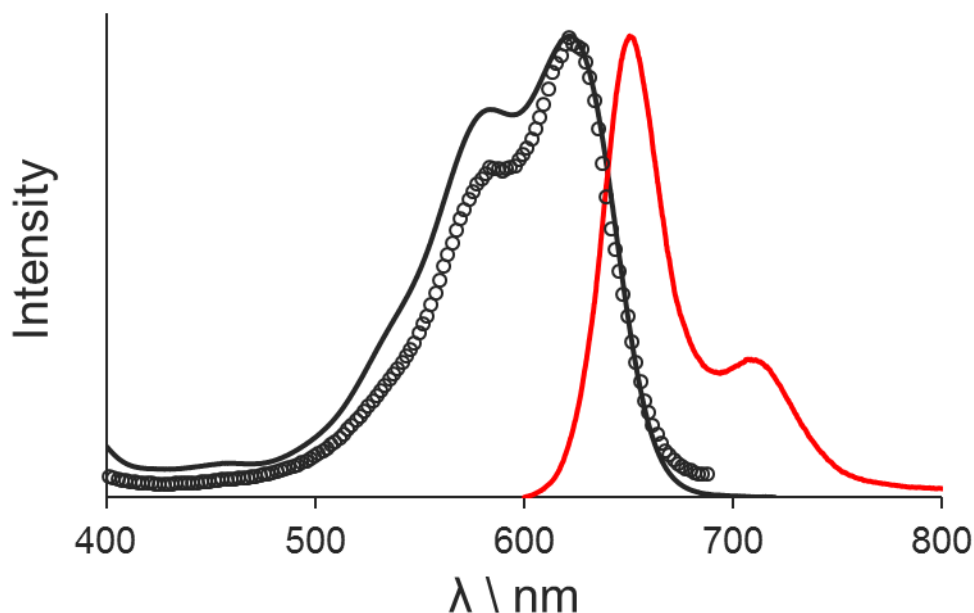


Figure 5.3 – Absorption (—), excitation (O) and fluorescence (—) spectra recorded for BOPHY-DMA in cyclohexane.

For BOPHY-DMA in cyclohexane solution, the absorption and emission maxima occur at 620nm and 650nm, respectively, as shown in Figure 5.3. The molar absorption coefficient is $90,000 \text{ M}^{-1}\text{cm}^{-1}$. The excitation spectrum provides a reasonable match to the absorption profile, with the differences being attributed to the fact that absorption extends well into the region where correction of the excitation spectrum is not reliable, as such only the technical spectrum is presented. The absorption profile corresponds to an oscillator strength of 1.04 and the natural lifetime calculated according to the Strickler-Berg expression is 3.4ns. The experimental natural lifetime for BOPHY-DMA is 2.25ns so the agreement between the values is reasonable but it should be emphasized that there is poor mirror symmetry between absorption and fluorescence spectra and this will affect the calculated natural lifetime. The effects of changing solvent polarity on the emission spectrum can be seen from examination of Figure 5.4. In cyclohexane, the emission profile is quite sharp and structured with a band structure much like that seen for the simpler BOPHY molecules. On moving to toluene, there is already a significant bathochromic shift and band broadening. The existence of an underlying charge-transfer transition is evidenced by the broadness of the spectrum and additional peaks seen in more polar solvents. Solvent related broadening of the absorption

spectrum can be seen in some polar solvents and is described in more detail in Chapter 6 (Figure 6.10).

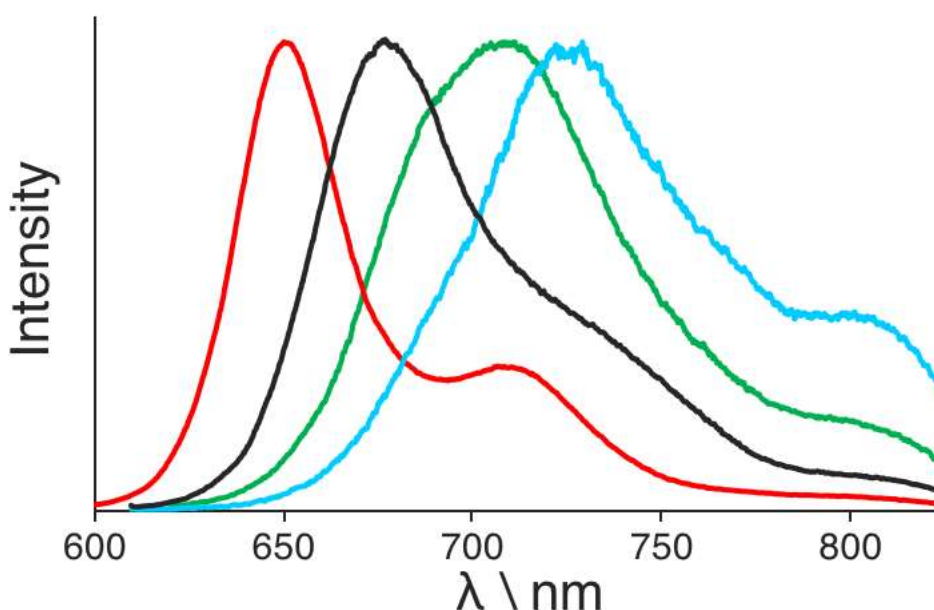


Figure 5.4 – Examples of how the nature of the solvent affects the fluorescence spectrum for BOPHY-DMA: cyclohexane (—), toluene (—), anisole (—) and benzonitrile (—).

In non-polar solvents, the fluorescence quantum yield was found to be high, reaching about 80% in cyclohexane, which is in line with the quantum yield of the parent compound, but it decreases rapidly with increasing solvent polarity. The quantum yield in acetonitrile was found to be <1% so there was a hundred-fold decrease in the more polar solvent. There is a corresponding decrease in the excited-singlet state lifetimes. This effect is in line with observations made with the corresponding BODIPY dyes featuring amino groups^[37]. The changes induced by polar solvents are fully consistent with polar resonance structures contributing to intramolecular charge transfer. It is important to note that the BOPHY-DMA molecule is not only significantly red-shifted in comparison to the TM-BOPHY parent but also compared to the mono-aminostyryl^[18] analogue where an absorption maximum of 550nm in 1:1 v/v mixture of acetonitrile and water is observed. This tells us that the conjugation path must run through the core and to some extent into the arms of the molecule. It is because of the extended conjugation that we anticipate the possibility of terminal-terminal electronic communication.

The charge-transfer character of the molecule causes the greatly increased Stokes' shift seen in the more polar solvents. The calculated k_{rad} values decrease in high polarity solvents, as demonstrated in Table 5.1. The mid-polarity solvents indicate a k_{rad} value in the region of $2.5 \times 10^8 \text{ s}^{-1}$ so the low values seen for high polarity solvents can be attributed to the energy-

gap law. The emission in polar solvents extends outside the region where most spectrometers operate effectively so the fluorescence quantum yield may be underestimated. The fluorescence lifetime in acetonitrile is below the resolution of the TCSPC unit. The fluorescence quantum yield was measured in MeTHF ($\lambda_{\text{ex}}=590\text{nm}$) with reference to Nile Blue in ethanol^[38] ($\Phi_f = 0.27$) and corroborated by reference to *meso*-tetraphenylporphyrin in dimethylformamide^[39] ($\Phi_f = 0.12$). Frontier molecular orbital distributions were computed by TDDFT, with the molecule in a chloroform reservoir, and are shown in Figure 5.5. The calculations support the charge-transfer nature of the molecule, the HOMO being distributed across the core of the molecule and out to the terminating nitrogen atoms whilst the HOMO(-1) resides mainly on the aniline group. The LUMO is, by contrast, located mostly on the core with some extension to the vinyl linker group. Quantum chemical calculations were performed using the GAMESS program with the PBE0/6-311G(d) basis set. Energy-minimised structures were used for all subsequent calculations, with a background reservoir of chloroform molecules. The PCM solvent model was applied with the Mennucci-Tomasi correction. Dipole moment calculations were made using the PBE0/aug-cc-pVDZ basis set.

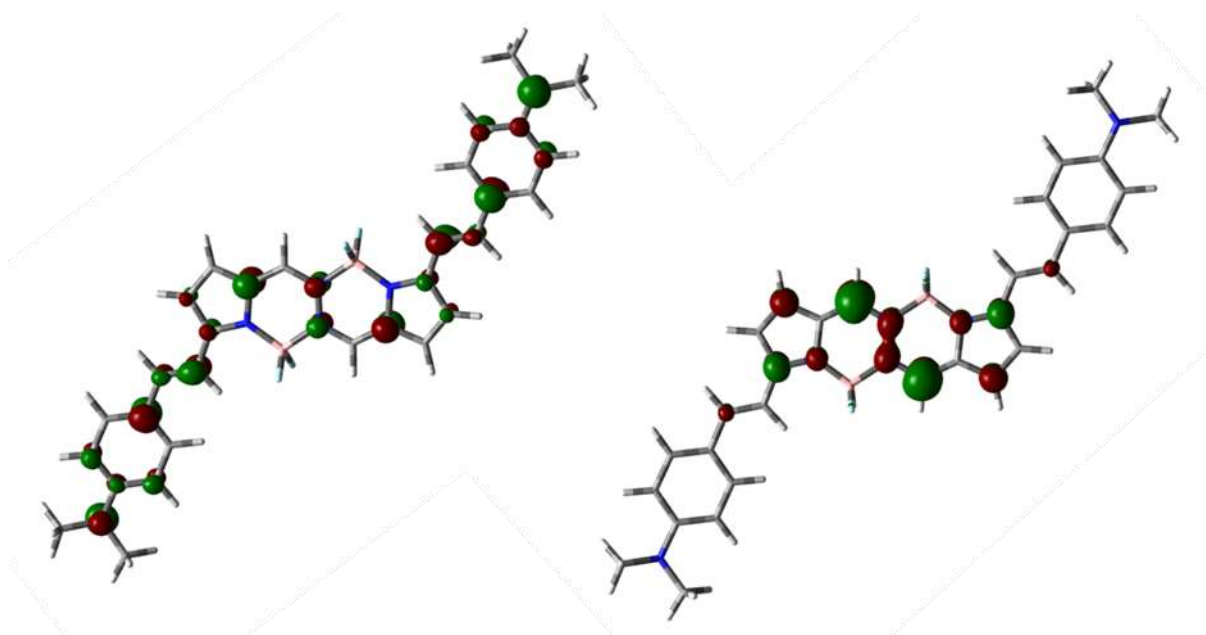


Figure 5.5 – HOMO (left) and LUMO (right) calculated for the BOPHY-DMA in a chloroform reservoir clearly demonstrating the charge transfer between states.

Solvent	ϵ_s	Φ_f	$\tau_f \text{ \textbackslash ns}$	$k_{rad} \text{ \textbackslash } 10^8 s^{-1}$	$k_{nr} \text{ \textbackslash } 10^8 s^{-1}$	$\lambda_{obs} \text{ \textbackslash nm}$	$\lambda_{fluo} \text{ \textbackslash nm}$	$SS \text{ \textbackslash } cm^{-1}$
Cyclohexane	2.02	0.8	1.8	4.4	1.1	620	650	700
Toluene	2.38	0.5	1.6	3.1	3.1	635	675	1000
But ₂ O	3.1	0.62	2	3.1	1.9	620	670	1100
Et ₂ O	4.33	0.42	1.5	2.8	3.9	620	670	1200
Anisole	4.33	0.3	1.3	2.3	5.4	635	710	1600
CHCl ₃	4.81	0.45	1.55	2.9	3.5	630	690	1300
MeTHF	6.97	0.28	1.1	2.5	6.5	625	690	1550
DCM	8.93	0.2	0.86	2.3	7.7	630	720	2000
EtOH	24.5	0.06	0.22	1.9	43	625	715	1900
Benzonitrile	26	0.07	0.48	1.7	19	635	725	2000
Acetonitrile	37.5	0.01	0.12	>1.3	<82	615	725	2400

Table 5.1 – Photophysical properties derived for BOPHY-DMA in solvents of varying polarity

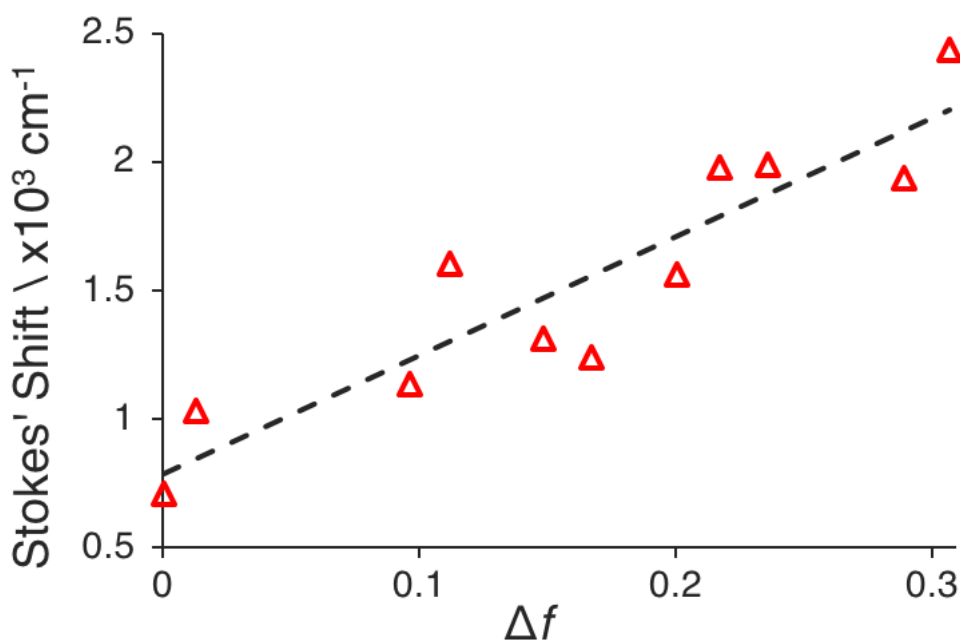


Figure 5.6 – Example of a Lippert-Mataga plot constructed for BOPHY-DMA in a range of organic solvents of differing polarity. The line drawn through the data points is a best fit to the LM equation with a change in dipole moment of 7.6D.

A Lippert-Mataga type plot was constructed for BOPHY-DMA (Figure 5.6) and found to be linear. The calculated change in dipole moment in going from the ground to the excited state was 7.6D, where a spherical molecular radius of 5Å was assumed. It should be noted that the

molecular radius criteria is not expected to hold well for a long flat molecule such as BOPHY-DMA.

5.3 Probing Electronic Communication by Measurement of the pK of the Termini

5.3.1 Protonation of BOPHY-DMA

Dyes displaying charge transfer characteristics and possessing readily accessible protonation sites are referred to as being turn on/off sensors^[40] for monitoring pH changes. Many such molecules appear within the BODIPY family^[41], but the Xiao molecule^[18] is the only one claimed for BOPHY thus far. In reality, the need for pH indicators that are not water-soluble is limited and many options are already available. Thus, we do not feel there is any basis in claims that these dyes might be usable as novel pH sensors. More interestingly, we can exploit the protonation of the two equivalent amino sites to learn more about the extent of electronic communication running through the BOPHY structure. It might be anticipated that electronic coupling, no matter how weak, will cause splitting of the pK_a values for the two amino-based terminals. A similar situation is expected for the removal of an electron from each terminal, where long-range electronic coupling should render the half-wave potentials for removal of one and two electrons to be somewhat different.

Protonation could be achieved by adding small amounts of HCl to the dye dissolved in an organic solvent. There was a dramatic change in the absorption characteristics of the dye, which was apparent by eye. The resultant absorption and emission spectra are given in Figure 5.7 for the compound in benzonitrile. Here, the absorption maximum was seen to blue shift by around 70-80nm to 565nm. The product remains a highly conjugated molecule and the absorption maximum is still significantly red-shifted compared to TM-BOPHY. The fine structure is restored, and the emission is also significantly blue shifted. The Stokes' shift is reduced in benzonitrile compared to the neutral dye from 2000cm^{-1} to approximately 1000cm^{-1} so the initial protonation of the dye has significantly weakened the charge transfer nature of the dye. The emission yield is increased some 8-fold after protonation in benzonitrile, although the radiative rate constant is not changed significantly. Under the conditions of the experiment, a slight excess of HCl has been added so that the product should be the diprotonated species. It can be seen from the entries in Table 5.2 that there is a slight trend for reducing the emission quantum yield with increasing solvent polarity but that the dye did not readily protonate in some low polarity solvents such as tetrahydrofuran, leading to compromised solutions. By treating the protonated dye with NaOH the neutral species was restored with no loss of material.

Solvent	ϵ_s	Φ_f	$\tau_f \text{ ns}$	$K_r \text{ } 10^8 \text{ s}^{-1}$	$K_{nr} \text{ } 10^8 \text{ s}^{-1}$	$\lambda_{abs} \text{ nm}$	$\lambda_{fluo} \text{ nm}$	$SS \text{ cm}^{-1}$
Anisole	4.33	0.42				565	596	920
CHCl ₃	4.81	0.78				563	589	780
THF	7.58	0.28	1.5	0.9	5.7	558	589	940
DCM	8.93	0.72				560	590	910
EtOH	24.5	0.54	1.38	2.0	5.3	556	585	890
Benzonitrile	26	0.56	1.68	1.7	4.3	563	595	960
Acetonitrile	37.5	0.50	1.27	3.9	3.9	546	584	1200

Table 5.2 – Photophysical properties of the diprotonated form of BOPHY-DMA in various solutions after addition of excess HCl.

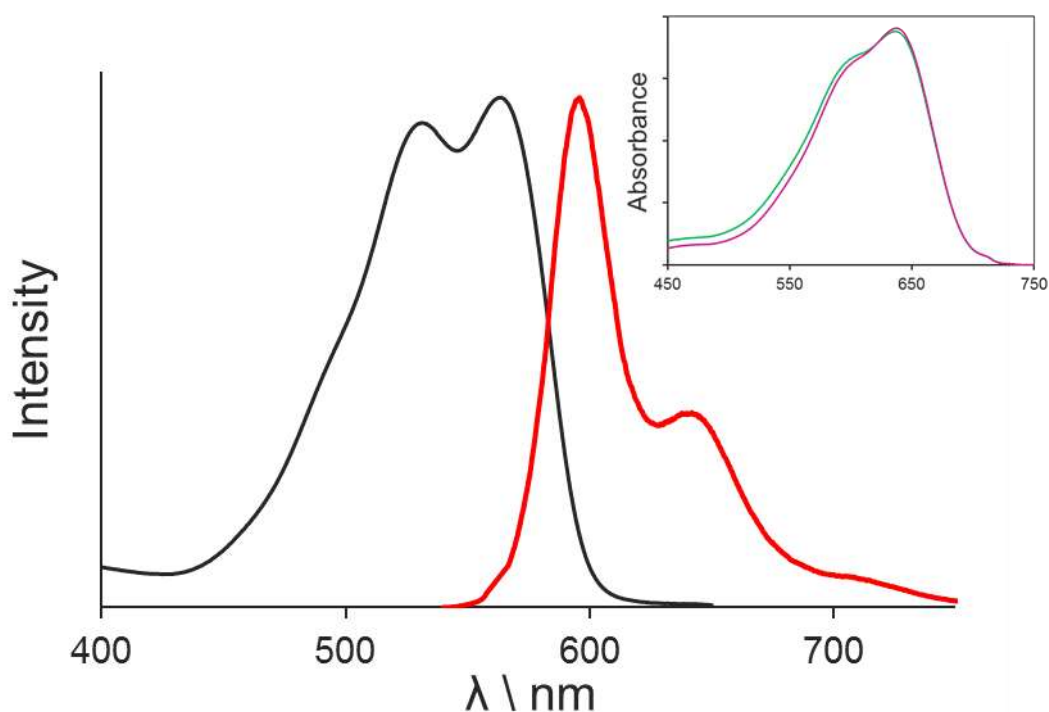


Figure 5.7 - Absorption and emission spectra recorded after diprotonation in benzonitrile. Inset shows absorption spectra for the neutral species after repeated cycling to the diprotonated form by adding HCl/NaOH.

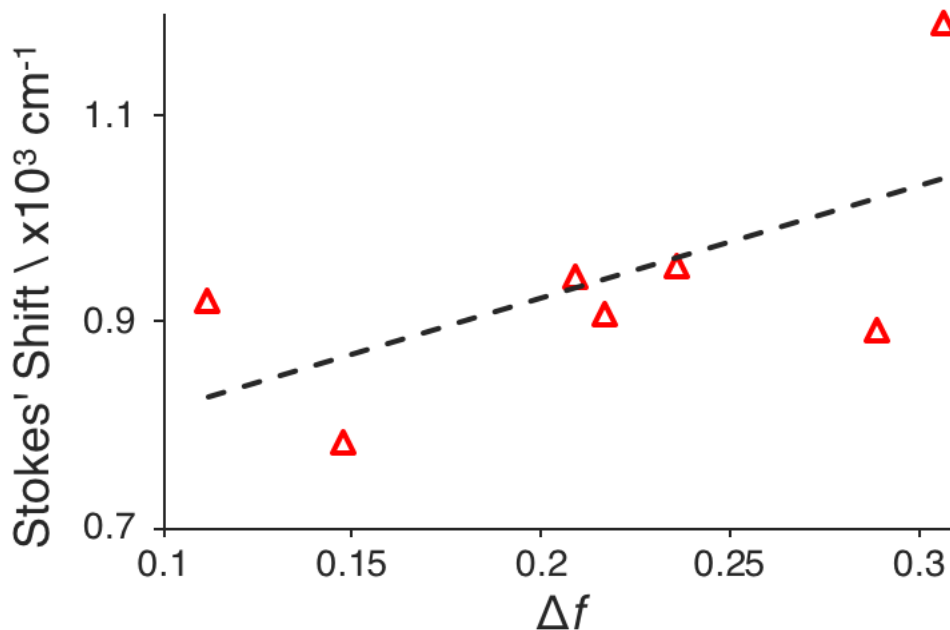


Figure 5.8 – Example of a Lippert-Mataga plot for the diprotonated form of BOPHY-DMA.

A more limited set of solvents was used to construct the Lippert-Mataga plot in Figure 5.8, in part due to difficulties in protonating the dye in solvents of low polarity. The fit is quite poor and does not indicate a significant change in dipole moment on excitation. In the extreme case, using a 5Å radius, the derived $\Delta\mu$ corresponds to 3.7D, but there is a large error associated with this value. The frontier molecular orbital distributions were calculated as for the neutral molecule and are shown in Figure 5.9. In the case of the cation, the HOMO extends only along the vinyl group and the LUMO is slightly more concentrated on the BOPHY core. The aniline moieties do not bear any of the charge once the ammonium cations are present. The HOMO(-1) is distributed over the whole length of the molecule.

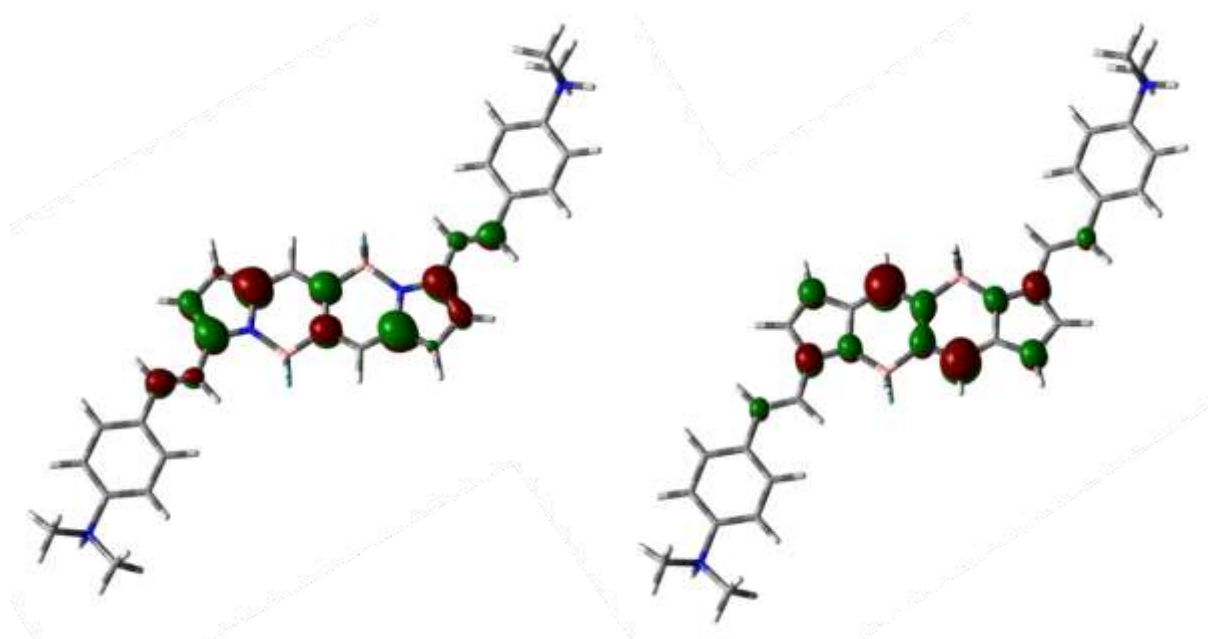


Figure 5.9 – Kohn-Sham distributions calculated for the *HOMO* (left) and *LUMO* (right) for the diprotonated BOPHY-DMA species in a chloroform reservoir; the calculations show that the *HOMO* and *LUMO* are now both largely restricted to the BOPHY core.

5.3.2 Titration of BOPHY-DMA with HCl

We have established that the dye can be protonated under mild acidic conditions and that there is a significant change in the photophysical properties upon the protonation. The next step is to find the pK_a values for protonation of the amino sites. To do this a titration was carried out where small aliquots of HCl in dioxane (40mM) was added to a stirred solution of the dye in benzonitrile. The dye concentration was approximately 2 μ M. The acid was sufficiently concentrated such that the overall volume did not change significantly during the titration but weak enough so that the pH changes allowed the gradual evolution of the absorption spectrum of the protonated species. The chromophore was transformed quantitatively to the diprotonated form but proceeded via a well-defined intermediate species, the absorption spectra of the titration are shown in Figure 5.10.

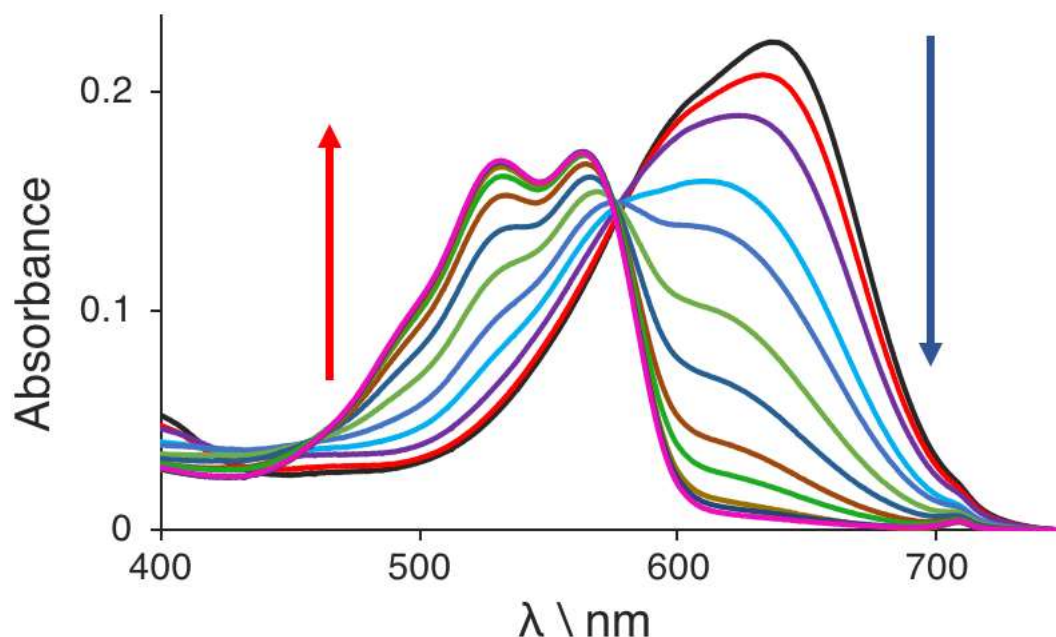


Fig 5.10 - Titration of BOPHY-DMA in benzonitrile with HCl, arrows show the loss of the neutral species and emergence of the protonated species as the pH decreases.

On addition of acid to the solution, the broad peak centred at 635 nm decreases while the structured bands due to the diprotonated species at 545 nm and 565 nm emerge. Addition of HCl was continued until no further change was observed. A precise isosbestic point is not maintained and deconvolution of the spectra show that the spectra cannot be resolved in terms of only the neutral and the protonated species. A third species, with an absorption spectrum occurring between the two limiting forms, must also be present to account for the global spectral changes. This intermediate evolves from the neutral compound and, in the presence of more HCl, transforms to the diprotonated species. Logically we ascribe the intermediate species to the mono-protonated form of BOPHY-DMA. The derived spectra, molar absorption coefficients and oscillator strengths, given as part of Figure 5.11, are in line with a shorter conjugation path. The absorption maximum for the monocation is blue-shifted by around 30nm compared to the neutral species. The derived spectrum is broad and featureless, indicating strong charge-transfer character. The frontier molecular orbital distributions are displayed as Figure 5.12, where the HOMO resides on the styryl arm encroaching onto the core. In contrast, the LUMO is found to reside almost entirely on the core and partially onto the vinyl linkers.

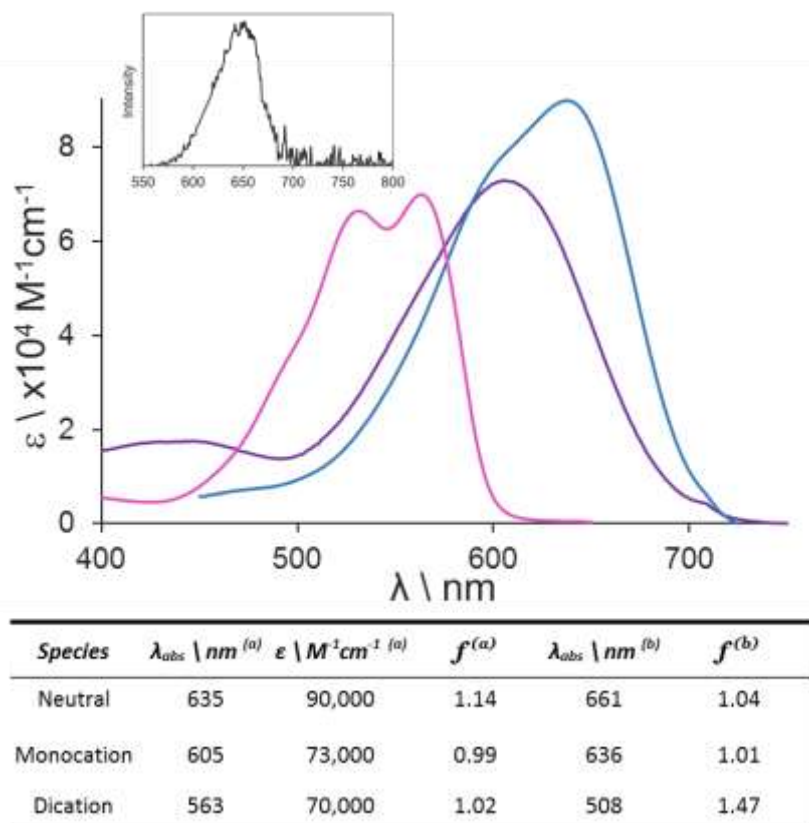


Fig 5.11 - Absorption spectra for all three BOPHY-DMA species, diprotonated (—), monocation (—), neutral (—), scaled by the respective molar absorption coefficients. The table provides photophysical data (a) as measured and (b) from calculations. The inset shows the small amount of emission seen from the monocation in chloroform.

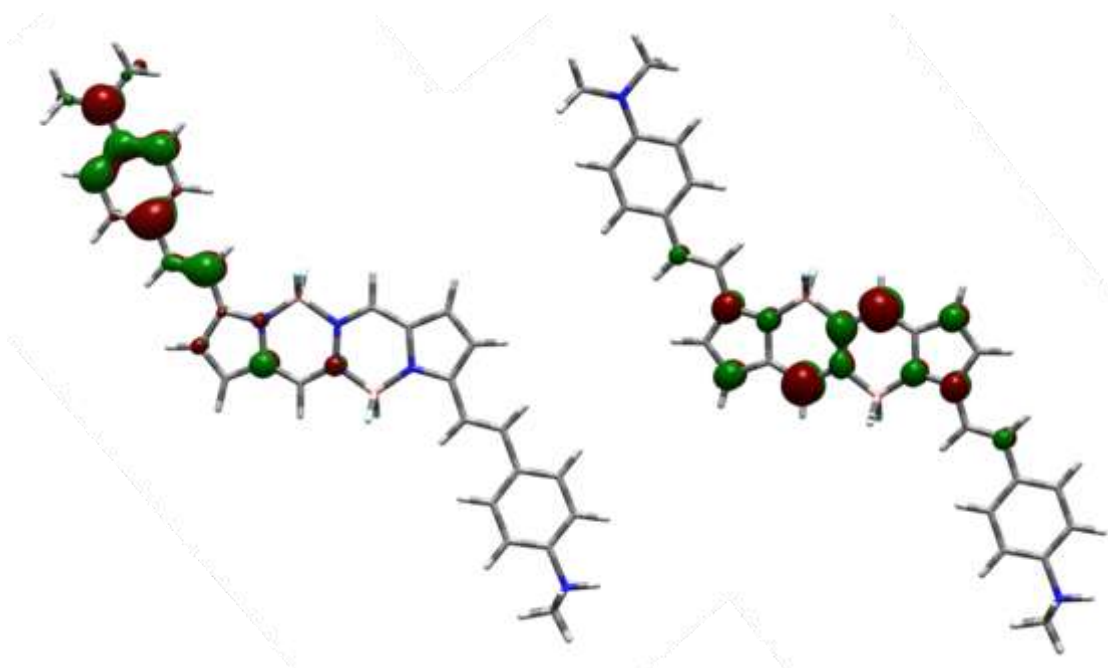


Figure 5.12 – Kohn-Sham distributions calculated for the HOMO (left) and LUMO (right) for the monocationic BOPHY-DMA species in a chloroform reservoir

The absorption spectra are now established, which allows calculation of the concentration of each species at each acid concentration. An equivalent titration was performed monitoring the fluorescence from the sample, the observed emission spectrum is of course dependent on the excitation wavelength selected. At the start of the titration, the fluorescence intensity at 730nm was seen to decrease but no change in profile was found that would correspond to emission from the mono-cation. As the acid concentration increased, strong emission from the doubly-protonated species was seen at 595nm. Thus, it was inferred that the mono-cation has a fluorescence quantum yield that is not of a measurable value in benzonitrile. Protonation was repeated in chloroform, which is the least polar solvent that could be used. Removal of the neutral emission spectrum at the various excitation wavelengths revealed a broad, featureless spectrum, which is probably emission from the monocation (see inset to Figure 5.11). The precise fluorescence quantum yield was not determined but estimated to be less than 1%.

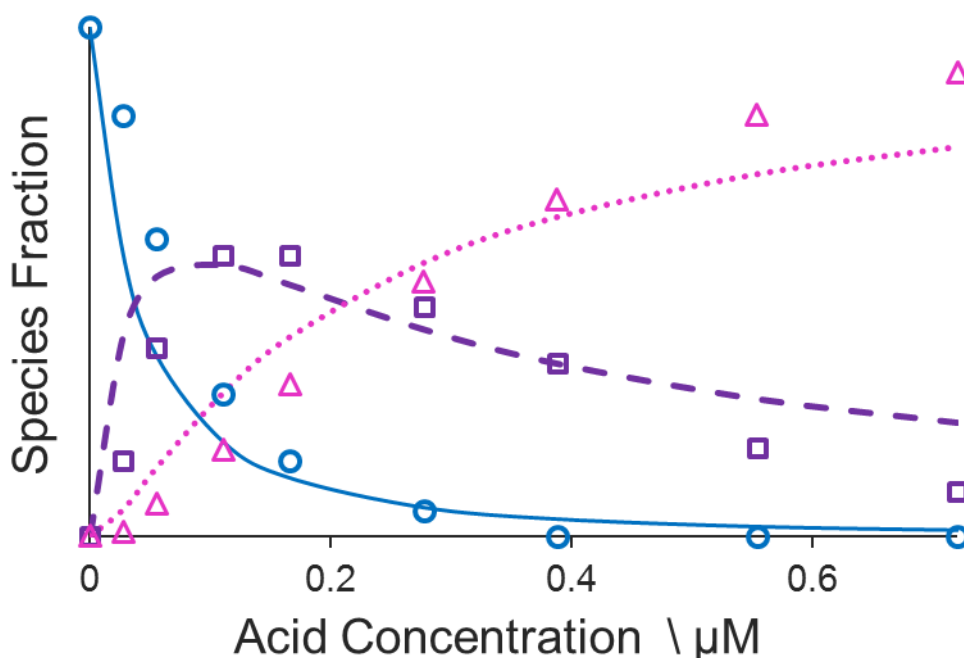
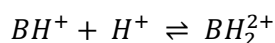
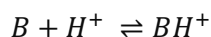


Fig 5.13 - Plot of concentration of acid against fraction of species observed based on spectral decomposition, Points are concentrations as measured from spectral data, and line fits are from NLLS fits to the equations below.

The acid dissociation constant for HCl is well characterised in some solvents, including acetonitrile where the pK_a is 10.3. This value was used for benzonitrile in order to simulate the pK_a values for the successive protonation^[42] steps using the equations in Scheme 5.1. Values of 7.4 and 6.8 were derived for mono-protonation and diprotonation respectively.



$$k_1 = \frac{[BH^+]}{[B][H^+]}$$

$$k_2 = \frac{[BH_2^{2+}]}{[BH^+][H^+]}$$

$$C_{Total} = [B] + [BH^+] + [BH_2^{2+}]$$

$$C_{Total} = \frac{[BH^+]}{k_1[H^+]} + [BH^+] + k_2[BH^+][H^+]$$

$$C_{Total} = [BH^+] \left(\frac{1}{k_1[H^+]} + 1 + k_2[H^+] \right)$$

Scheme 5.1 – Collection of the equations used to calculate the K_a values for the successive protonation steps, B = BOPHY-DMA.

The theoretical pK_a values were calculated by the method set out by Juranic^[43], the optimised geometries were used as inputs with the solute dispersed in a solvent of dielectric constant of 26. The calculations are based on a correlation between the electronic charge on the vicinal nitrogen atom (q_N) and on the amino hydrogen atom (q_H). These electronic charges were computed using the PM6 Hamiltonian with the effect of solvent being taken into account using the COSMO model. Equation 5.1 is used to derive the pK_a values where I is a variable index to distinguish between the amine orders. The coefficients were calibrated using a small range of standard amines. The coefficients were calculated as A = -140.9, B = -11.8, C = -1.25 and D = 52.8.

$$pK_A = Aq_H + Bq_N + CI + D \quad (5.1)$$

$$E = \frac{1}{4\pi\epsilon\epsilon_0} \frac{e}{d_{ab}} \quad (5.2)$$

The theoretical pK_a values were calculated by this method to be 7.3 and 6.8. These are in good agreement with the experimental values. A difference of 0.6 pK_a units is equivalent to an energy difference of 35mV. The field due to a point charge (Equation 5.2) in a dielectric medium with a static permittivity of 26 at 22.6Å is 24.5mV. This simple calculation positions the charges exclusively at the nitrogen atoms, which might be somewhat simplistic. More importantly, no effect of ion pairing at the protonation sites is taken into account. In an organic solvent, we would anticipate that some degree of ion pairing takes place. Such an effect would decrease the splitting energy because of the reduced charges. Even so, the calculation gives

a reasonable representation of the experimental behaviour. In particular, it suggests that the difficulty in adding the second proton to the molecule could be explained in terms of electrostatic potentials, despite the large separation distance of 22.6Å.

5.4 Oxidation of the Dye

5.4.1 Cyclic Voltammetry

The results of the titration suggest there is no long-range electronic communication between the terminal amino groups. To complement the protonation study, oxidation of the dye was recorded. The assumption here is that the first oxidation step for BOPHY-DMA will concern removal of an electron from one of the aniline residues. If there is no communication within the molecule, removal of the second electron will occur at the same potential. On the other hand, electronic communication will cause splitting of the oxidation step

The redox properties of BOPHY-DMA were studied by cyclic voltammetry in dichloromethane as shown in Figure 5.14. A one-electron reduction wave was seen at -1.31V vs Ag/Ag⁺ which is comparable to previously reported values for BOPHY-DMA^[16] where a value just below -1.30V vs Ag/Ag⁺ was seen. The oxidation was quasi-reversible, at least when fast scans were performed but some small loss of the π -radical anion is observed at slow scans rates. The reduction potential is greater than seen for the TM-BOPHY core which occurs at around -0.5V^[44] which again reinforces the charge transfer character of this molecule. A one-electron oxidation peak of poor reversibility is seen at 1.05V vs Ag/Ag⁺ which is attributed to the BOPHY core, again in agreement with previous reports^[16]. At lower potentials, a further process is identified that is related to oxidation of the amino groups. Here two oxidation peaks are seen that are overlapping with peak potentials of approximately 0.48 and 0.58V vs Ag/Ag⁺ when a 150mVs⁻¹ scan rate is used. This section of the voltammogram shows some reversibility, depending on scan rate.

To better resolve the redox processes cyclic voltammetry was performed in anisole at lower temperature. Tetraethylammonium hexafluorophosphate was used as background electrolyte (0.1M) in this case for solubility reasons, with an acetone/dry ice bath used to give a temperature of -78°C. Under these conditions, the low-potential oxidation processes showed much better reversibility and the overlapping peaks were split into two quasi-reversible steps with half-wave potentials of 0.32 and 0.39V vs Ag/Ag⁺. Thus, a splitting of 70mV was found for the two steps when a scan rate of 10mV/s was employed.

This measured value can be compared to a calculated electrostatic field due to a point charge at a distance of 22.6Å. To complete the calculation, it is necessary to know the static dielectric

constant of the solvent system at the relevant temperature. At room temperature, the static dielectric constant of pure anisole is 4.3 but this is likely to increase at low temperatures^[45]. To estimate the dielectric constant we employed a fluorescence sensor that shows exciplex emission in weakly polar solvents. An 8-arylamino-BODIPY derivative^[46] is calibrated using a set of solvents at room temperature. The fluorescence maximum was recorded in our electrolyte solution at -80°C and from the emission spectrum, an estimated relative permittivity of 6.1 was found. The field due to a point charge can then be calculated as being 104mV. This is rather more than the splitting seen in the cyclic voltammograms.

A weakness of the above treatment comes in the notion of point charges. A point charge must be spherically symmetrical and stationary. In Figure 5.15 we see the calculated molecular orbital for the π -radical cation showing that the charge is distributed around the whole of the aniline residue. This will serve to reduce the effective distance between charges. As the distance is decreased an increase in coulombic effects should be seen compared to the protonation case. To improve this situation, we can employ the atomistic approach^[47], this refined method gives a calculated splitting of 108mV. This is significantly greater than the 70mV found by experiment. For the case of CH_2Cl_2 at room temperature, a splitting of 90mV was found at a scan rate of 40mVs^{-1} . This can be compared to a calculated splitting of 78mV. The differences in experimental and theoretical values can be explained with consideration of ion-pairing between the cation and the electrolyte. This is likely to be particularly significant at low temperatures in anisole. It seems then that the splitting observed is consistent with through-space electrostatic interactions with some correction due to ion-pairing and that there is no evidence for additional splitting due to through bond communication between the terminal sites.

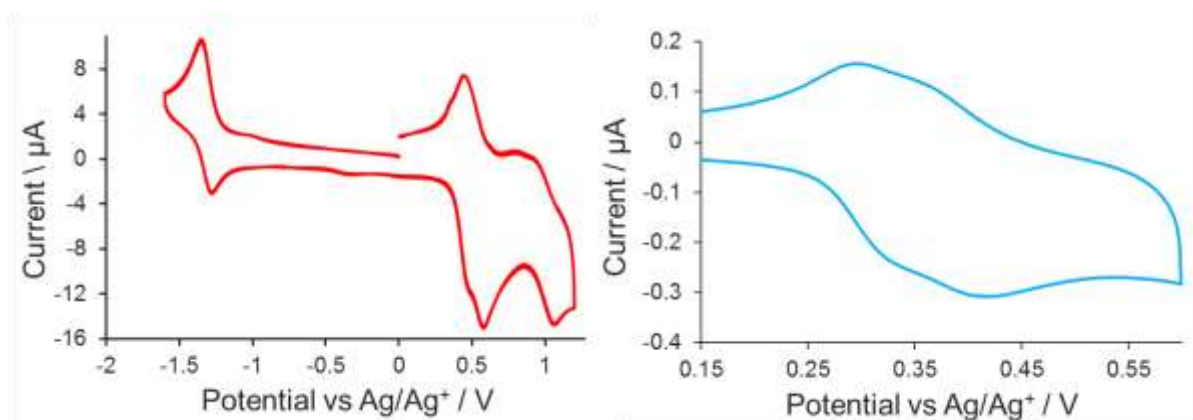
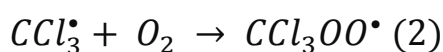


Figure 5.14 – Cyclic voltammograms in CH_2Cl_2 , left, and anisole at low temperature to the right where the splitting of the wave is clearer and reversible.

5.4.2 Photochemical Oxidation

An elegant method to oxidize the molecule is used to further understand the redox properties of BOPHY-DMA. Here, the excited-singlet state of the dye transfers an electron to CCl_4 , resulting in immediate formation of an encounter complex (Scheme 5.2(1)). In competition to geminate charge recombination, the encounter complex can expel a chloride ion. This latter step leads to the formation of a trichloromethyl peroxy radical when molecular oxygen is present. The radical is a potent one-electron oxidant and can oxidize the substrate to the corresponding π -radical cation (Scheme 5.2(3)).



Scheme 5.2 – Outline of the photochemical reactions that can lead to the creation of the BOPHY-DMA cation, here BOPHY specifically stands for the BOPHY-DMA molecule.

Addition of carbon tetrachloride to an aerated solution of the dye caused colour change in the solution, observable by eye on a timescale of minutes once the dye is exposed to white-light. The neutral molecule was readily oxidized under these conditions as outlined in Scheme 5.2 above. The absorption peak at 635nm quickly decreases to reveal a broader structure as the cation develops. The sample was exposed for a total of 30 minutes, eventually leading to excess further oxidation of the molecule. This can be seen by the development of new absorption bands at wavelengths below 600nm in Figure 5.15, which appear to have more defined structure. The method was equally effective in both benzonitrile and CH_2Cl_2 but, in the former case, there was less emergence of the higher energy, structured absorption. Initial studies were conducted in benzonitrile but better behaviour was found in CH_2Cl_2 .

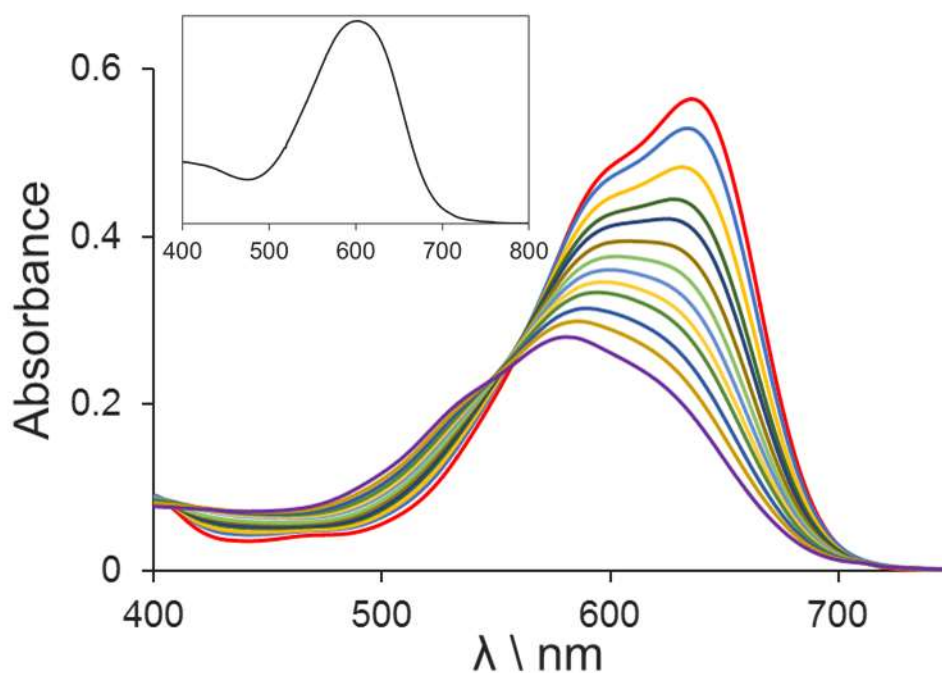


Fig 5.15 - Photochemical oxidation by CCl_4 of neutral BOPHY-DMA to the radical cation in CH_2Cl_2 under white light. Inset shows the recovered cation spectrum

The extracted spectrum is broad and featureless, the maximum occurs at 600nm. The band would appear to have strong charge-transfer character. The singly unoccupied molecular orbital (SUMO) was calculated to be almost exclusively localised on the aniline parts of the molecule. Likely transitions then could be the promotion of the single electron residing in the LUMO or from the HOMO(-1) which is located on the BOPHY core, both of these would be charge transfer in nature. The calculated energy for the HOMO(-1) transition also gives a band at around 600nm so this would appear to be the most likely orbital responsible for the transition.

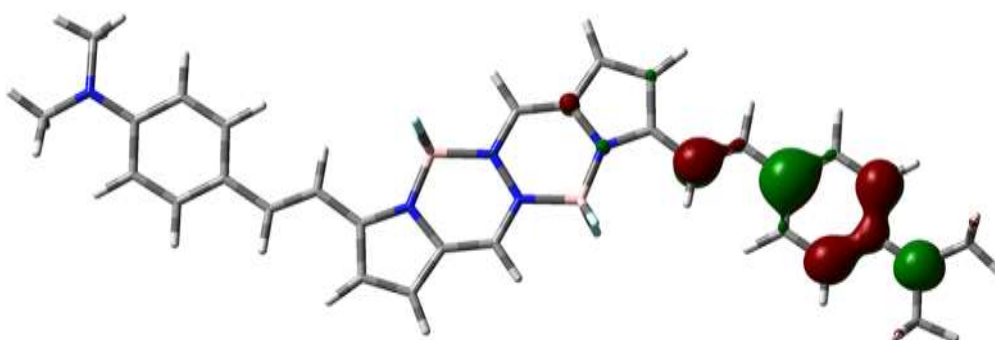


Figure 5.17 - Electron density distribution for the SUMO of the π -radical cation that was formed by the one electron oxidation of BOPHY-DMA

5.4.3 Search for an Intervalence Charge-Transfer (IVCT) Absorption Band

The work of Nemykin^[20] with a BOPHY molecule with ferrocene terminals reported a significant IVCT band centred at around 2000nm. It is interesting, therefore, to see if an identifiable IVCT transition can be seen for BOPHY-DMA. This was first attempted in benzonitrile but there were concerns that sharp bands appearing the IR are associated with overtones of the C-N stretch. The experiment was repeated in CH₂Cl₂. The sharp bands remained and were found to correlate with BOPHY-DMA concentration. The sample was subjected to white-light illumination in solution containing approximately 1M carbon tetrachloride. To have the best chance of finding the IVCT band it is important to maximise the amount of cation present but not to over illuminate the sample or it will be further oxidised to the dication. At a BOPHY-DMA concentration of 16μM, oxidation proceeded as expected. Absorption spectra were recorded at regular intervals until around 70% of the material was oxidized. The absorption spectra in the IR are shown in Figure 5.18. Even at wavelengths up to 2500 nm, no sign of an IVCT band was found.

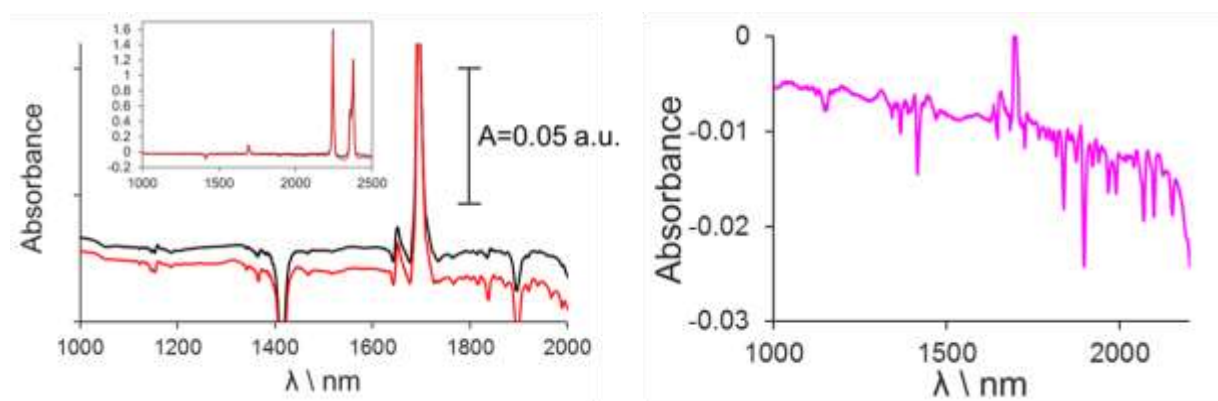


Figure 5.18 – Left panel shows the NIR absorption spectrum recorded for BOPHY-DMA, neutral (—) and part oxidized species (—). The right panel shows the result of a subtraction of the neutral species from that of the most oxidized spectrum. There is no evidence for the appearance of an IVCT band.

We were unable to identify a region of the absorption spectrum that might realistically contain an IVCT transition (Figure 5.18). This disappointing result suggests that there is little, if any, contribution to the electronic coupling due to through-bond interaction. According to Hush theory, the extent of electronic coupling between two sites can be expressed in terms of an electronic coupling matrix element (H_{ab}). This coupling element is calculated from the energy of the IVCT band maximum (ν_{max}), the band half-width ($\Delta\nu_{1/2}$) and the molar absorption coefficient at the maximum (ϵ_{max}) according to Equation 5.3 and it is inversely proportional to the distance (d_{ab}) between the centres. The band half-width is related to its intensity by way of Equation 5.4.

$$H_{ab} = \frac{2.06 \times 10^{-2} \sqrt{\epsilon_{max} \cdot \nu_{max} \cdot \Delta\nu_{1/2}}}{d_{ab}} \quad (5.3)$$

$$\Delta\nu_{1/2} \approx \sqrt{2310 \cdot \nu_{max}} \quad (5.4)$$

From the reported values for the BOPHY-ferrocene compound where an IVCT band is centred at 5500cm^{-1} with a molar absorption coefficient of around $2000\text{ M}^{-1}\text{cm}^{-1}$, we calculate a coupling of at least 150cm^{-1} . For BOPHY-DMA, the separation distance is increased and, therefore, we expect the electronic coupling matrix element will be small^[48]. Approximately 50% of the sample was in the oxidised state so the concentration of the cation was around $10\mu\text{M}$. It is estimated that a band with an absorbance of less than 5 milli-absorbance units may go undetected meaning that $\epsilon_{max} < 500\text{ M}^{-1}\text{cm}^{-1}$. If the band has a full width half maximum (FWHM) of 1700cm^{-1} and is centred at 2500cm^{-1} then an upper limit around 50cm^{-1} coupling between the sites is estimated.

5.5 Use of a Photo-Acid Generator (PAG)

Organic fluorophores that are susceptible to reversible protonation under mild conditions offer the possibility to design advanced devices where the flow of information can be switched by addition of acid or base. A neat way to realise this feat is by the use of a photo-acid or a photo-base. Protonation by a photoacid generator (PAG) is quite straightforward in solution but a more interesting application would be in the area of films^[49]. For this study, N-hydroxynaphthalimide triflate^[50] was used as the proton source. This PAG absorbs in the near-UV as can be seen in Figure 5.19. By use of the pH indicator Methyl Orange it was possible to quantify the change in pH with exposure time to a 365-nm source.

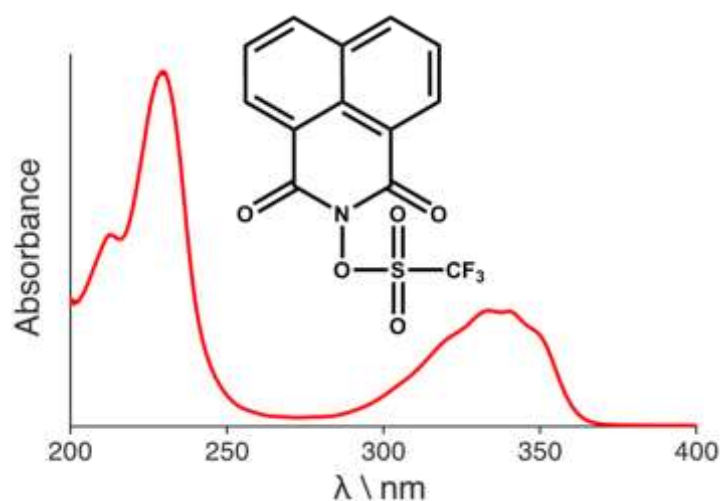


Figure 5.19 – Absorption spectrum and molecular structure of the PAG used.

It was possible to demonstrate that we could drive the protonation of the dye in a solid matrix using the PAG. The cast film containing BOPHY-DMA was prepared as described previously and loaded with an excess of PAG. Once a dried film was available, a 365nm illumination source was used to drive the protonation. After preparation, films were stored in the dark and found to be stable over the course of 10 days. Upon illumination, the exposed section of the film was seen to change colour as can be seen in the photograph in Figure 5.20, and to display strong emission. These effects are attributed to the release of acid and subsequent protonation within the film.

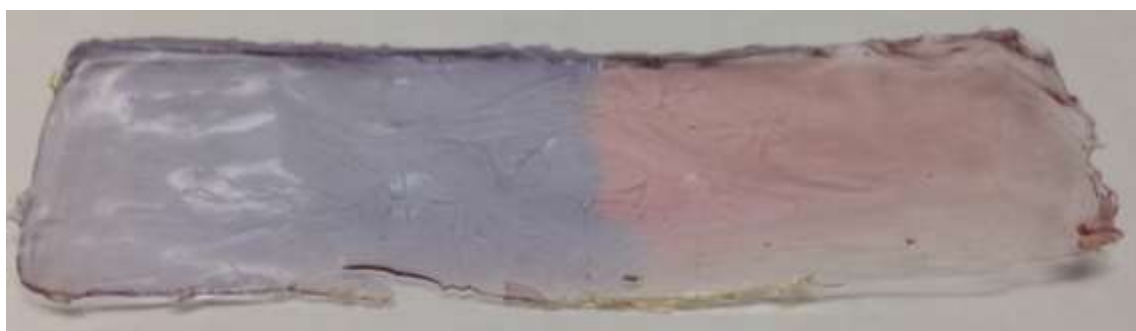


Figure 5.20 – The left hand side of the film is unexposed and displays the colour of the neutral form of BOPHY-DMA, the right hand side is exposed to UV light causing the release of protons from the PAG and subsequent protonation of BOPHY-DMA.

As well as *in-situ* photo-control of chromophore properties, such films present some further opportunities. Chromophores in solution that are sensitive to gases such as phosgene have been proposed as safety mechanisms^[51] for detecting the release of toxic gases. A film is a more practical solution. However, attempts to pass HCl gas over a PMMA film did not yield a colour change film. Most likely, the problem lies in the impermeable nature of the PMMA matrix, so a new carrier would be required.

A further possibility for the solid-bound dye lies in the use of high-resolution microscopy. Where a suitably focused excitation source is used, excellent spatial resolution could be realised. High photon densities would lead directly to the diprotonated species, which should be easily identified given that the emission yield is significantly increased, and that the wavelength of emission is suitably shifted. Photo-lithography has been demonstrated for this particular PAG with two-photon absorption^[50], this would be a particularly effective way to carry out this type of procedure as typical microscopes will be equipped with lasers required for PAG two-photon absorption. With sufficient spatial resolution, electronic energy transfer and a reversible photo-controlled acid/base process, we could envision being able to fabricate intricate molecular-scale devices.

5.6 Conclusion

This work has identified and quantified long-range electrostatic interactions between the charged termini of the target compound following protonation or oxidation. The charges are associated with the aniline termini but, in the case of one-electron oxidation, may be distributed around the terminal group. This leads to an effective fall in the separation distance because of the linear geometry. We have not been able to identify additional interactions, such as through-bond electronic coupling, and the overall magnitude of the electrostatic effects is kept modest by the wide separation. In particular, there is no evidence for the existence of an IVCT transition appearing in the far-red or near-infrared regions. Such optical transitions are invariably weak and difficult to resolve from the baseline but nonetheless the absence of the expected IVCT transition points to weak electronic communication along the molecular backbone.

This finding is in stark contrast to a related ferrocene terminated BOPHY molecule where a relatively strong IVCT band was observed in the NIR region. The structure is given in Figure 5.21, it is interesting that this group did not find electronic coupling in a second derivative with extra substituents, quite why these substituents would turn off terminal-terminal communication is unclear.

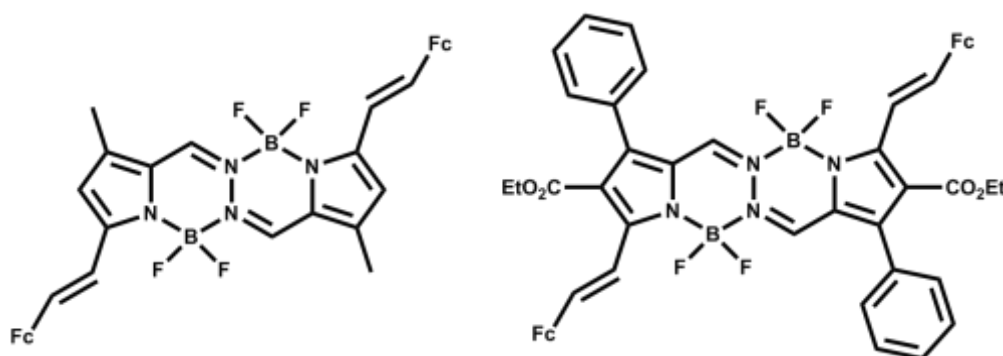


Figure 5.21 – Structure of Ferrocene-BOPHYs, left is the compound with apparent strong communication while on the right is the compound where communication is not found.

This work highlights how difficult it would be to achieve mass-communication in an organic network, long-range communication in pure organic systems is hard to achieve. Additionally, it is an important reminder of the need to consider through-space coulombic interaction between sites, even when large molecules are studied and to consider the effects that ion-pairing can have on observed results.

This work nicely demonstrates the ability to control the photophysical properties of dyes *in-situ* using a photoacid. Despite being something of an aside, this is perhaps the most tantalising aspect of the work undertaken. The difference in colour and emission properties is

evident and well demonstrated by the photograph of the part-exposed film. The potential to combine matrix-bound molecules with microscopy is interesting and could lead to the design of novel molecular devices. The ability to extinguish fluorescence reversibly by release or uptake of protons would allow one to build a protection mechanism into devices when light conditions dictate, for example under conditions of excess photon flux.

References

- [1] J. O. Escobedo, O. Rusin, S. Lim, R. M. Strongin. *Curr. Opin. Chem. Biol.* **2010**, 14, 64-70.
- [2] Y. Kobuke et al. *Chem. Eur. J.* **2009**, 15, 2317-2327.
- [3] G. Ulrich, R. Ziessel, A. Harriman, *Angew. Chem. Int. Ed.* **2008**, 47, 1184-1201.
- [4] D. Zhang, Y. Wen, Y. Xiao, G. Yu, Y. Liu, X. Qian, *Chem. Commun.* **2008**, 4777-4779.
- [5] I. K. Petrushenko, K. B. Petrushenko, *Spectrochim. Acta A*, **2015**, 138, 623-627.
- [6] Z. Shen et al. *Chem. Eur. J.* **2014**, 20, 1091-1102.
- [7] W. L. Zhao, E. M. Carreira, *Angew. Chem. Int. Ed.* **2005**, 44, 1677-1679.
- [8] J. K. G. Karlsson, A. Harriman, *J. Phys. Chem. A*, **2016**, 120, 2537-2546.
- [9] R. Englman, J. Jortner, *Mol. Phys.* **1970**, 18, 145-164.
- [10] C. S. Zhang, J. Z. Zhao. *J. Mater. Chem. C*, **2016**, 4, 1623-1632.
- [11] J.-L. Zhao et al. *Chin. Chem. Lett.* **2016**, 27, 190-194.
- [12] X. Li, G. Ji, Y.-A. Son, *Dyes Pigm.* **2016**, 124, 232-240.
- [13] J. Wang, Q. Wu, C. Yu, Y. Wei, X. Mu, E. Hao, L. Jiao, *J. Org. Chem.* **2016**, 81, 11316-11323.
- [14] V. N. Nemykin et al. *Chem. Eur. J.* **2017**, 23, 14668-14668.
- [15] B. Le Guennic et al. *J. Phys. Chem. B*. **2017**, 121, 10850-10858.
- [16] Q. Hualme, A. Mirloup, P. Retailleau, R. Ziessel, *Org. Lett.* **2015**, 17, 2246-2249.
- [17] G. Ulrich, R. Ziessel, A. Harriman, *Angew. Chem. Int. Ed.* **2008**, 47, 1184-1201.
- [18] L.-J. Xiao et al. *RSC Adv.* **2015**, 5, 16735-16739.
- [19] X. Lv, T. Li, Q. Wu, C. Yu, L. Jiao, E. Hao, *J. Org. Chem.* **2018**, 83, 1134-1145.
- [20] V. N. Nemykin et al. *Chem. Eur. J.* **2015**, 21, 18043-18046.
- [21] C. Creutz, *Prog. Inorg. Chem. Vol. 30*, John Wiley & Sons, **1983**, 1-73.
- [22] M. B. Robin, *Inorg. Chem.* **1962**, 1, 337-342.
- [23] M. B. Robin, P. Day, *Adv. Inorg. Chem. Radiochem., Vol. 10*, **1968**, 247-422.
- [24] N. S. Hush, *Prog. Inorg. Chem. Vol. 8*, John Wiley & Sons, **1967**, 391-444.
- [25] A. Cecon, S. Santi, L. Orian, A. Bisello, *Coord. Chem. Rev.* **2004**, 248, 683-724.
- [26] S. Rigaut et al. *J. Am. Chem. Soc.* **2010**, 132, 5638-5651.
- [27] F. Marken et al. *Inorg. Chem.* **2013**, 52, 4898-4908.
- [28] P. F. Barbara et al. *Science*, **1997**, 277, 1074-1077.
- [29] D. Holten, D. F. Bocian, J. S. Lindsey, *Acc. Chem. Res.* **2002**, 35, 57-69.
- [30] K. Memminger, T. Oeser, T. J. J. Müller, *Org. Lett.* **2008**, 10, 2797-2800.
- [31] J. Veciana et al. *Adv. Mater.* **1996**, 8, 748-752.
- [32] S. V. Lindeman, S. V. Rosokha, D. Sun, J. K. Kochi, *J. Am. Chem. Soc.* **2002**, 124, 843-855.
- [33] R. Sakamoto, S. Kume, H. Nishihara, *Chem. Eur. J.* **2008**, 14, 6978-6986.
- [34] J. Hankache, O. S. Wenger, *Chem. Rev.* **2011**, 111, 5138-5178.
- [35] C. Lambert, G. Nöll, *J. Am. Chem. Soc.* **1999**, 121, 8434-8442.
- [36] J. Yang, W. Zhang, Y. Si, Y. Zhao, *J. Phys. Chem. B*, **2012**, 116, 14126-14135.
- [37] Í. L. Arbeloa et al. *Chem. Eur. J.* **2011**, 17, 7261-7270.
- [38] R. Sens, K. H. Drexhage, *J. Lumines.* **1981**, 24-5, 709-712.
- [39] J. W. Owens, R. Smith, R. Robinson, M. Robins, *Inorganica Chim. Acta.* **1998**, 279, 226-231.
- [40] H. Chao, B.-H. Ye, Q.-L. Zhang, L.-N. Ji, *Inorg. Chem. Comm.* **1999**, 2, 338-340.

- [41] H. Sunahara, Y. Urano, H. Kojima, T. Nagano, *J. Am. Chem. Soc.* **2007**, 129, 5597-5604.
- [42] L. M. Schwartz, R. I. Gelb, *Anal. Chem.* **1978**, 50, 1571-1576.
- [43] I. Juranic, *Croatica Chem. Acta.* **2014**, 87, 343-347.
- [44] C. J. Ziegler et al. *J. Am. Chem. Soc.* **2014**, 136, 5623-5626.
- [45] V. A. Rana, H. Chaube, D. H. Gadani, *J. Mol. Liq.* **2011**, 164, 191-196.
- [46] S. Mula, K. Elliott, A. Harriman, R. Ziessel, *J Phys. Chem. A*, **2010**, 114, 10515-10522.
- [47] C. Li, T.-W. Chou, *Appl. Phys. Lett.* **2006**, 89, 063103.
- [48] J. Bonvoisin, J.-P. Launay, C. Rovira, J. Veciana, *Angew. Chem. Int. Ed.* **1994**, 33, 2106-2109.
- [49] G. Pohlers, J. C. Scaiano, R. Sinta, *Chem. Mater.* **1997**, 9, 3222-3230.
- [50] C. K. Ober et al. *J. Mater. Chem.* **2009**, 19, 505-513.
- [51] P. Stachelek, J. G. Knight, A. Harriman et al. *Org. Biomol. Chem.* **2017**, 15, 7643-7653.

Chapter 6 – The Photostability of the BOPHY Architecture

6.1 - Introduction

The photophysical properties of the BOPHY core, and further conjugated versions, have been described over preceding chapters. It has been stated that for chromophores to be employed in energy-harvesting type devices they will need to be highly photostable. Because we have shown that all photo-processes open to BOPHY must proceed via the singlet state, the triplet is not accessed under normal conditions, this chromophore might be a good model for studying the photostability of potential harvesting dyes. Additionally, we have noted that there are structural opportunities available to BOPHY that make it an interesting platform for adapting into a versatile chromophore. It shows high levels of fluorescence and, due to the presence of the second conformer, the absorption spectrum is relatively broad; this, of course, is a good feature for photonic applications.

Dyes that feature significant intersystem crossing are generally vulnerable to degradation *via* singlet oxygen, as was demonstrated in Chapter 3. There is a large volume of literature concerning the degradation of dyes *via* the triplet state and the effects of singlet oxygen^[1, 2]. Dyes which display only very low quantum yields for triplet formation, in the range 10^{-3} to 10^{-4} , often have the mechanism for chromophore loss ascribed to the triplet state^[3, 4] but the evidence is not so convincing. Studies on the stability of dyes with high fluorescence yields, such as the rhodamine family, are less common. As such the mechanism for dyes that degrade from the singlet state have not been well-established. Indeed, the reverse situation is the much more studied case where the photocatalytic efficacy of various semiconductors such as TiO_2 ^[5] for degrading dyes by the photo-generated holes on the surface has been the subject of innumerable papers^[6].

The bulk of the literature concerning photo-bleaching studies is focused on dyes for bio-imaging purposes, in particular single molecule detection^[7] (SMD), where many photons must be emitted by each molecule to ensure resolution, or in the stability of chromophores as organic laser dyes^[8] which can be in solution, or a variety of solid matrices. In many cases, the stability of the chromophore is probed using intense, pulsed, monochromatic light sources and the change in fluorescence intensity is monitored. Alternatively, fluorescence correlation spectroscopy is used, with bleaching times being rather shorter than would be of interest when considering a light harvesting arrangement. Dyes that have received attention include fluorescein-type species^[9], coumarins^[10], rhodamines^[11], cyanines^[12] and BODIPYs^[13]. In

many cases, despite the low triplet yield for those dyes used in bio imaging, the permanent bleaching of chromophores is regularly attributed to reactions of the triplet state. The bleaching of fluorescein has been of particular interest^[14] as it is a long established dye for imaging purposes. Fluorescein bleaching does not take place via first-order kinetics^[15] in the presence of excess O₂. If dye-oxygen bleaching was the only mechanism, a pseudo-unimolecular reaction would take place and first-order kinetics should be recovered. Removal of oxygen slows down but does not stop the rate of bleaching of fluorescein and it is clear that a bimolecular dye-dye reaction must also proceed *via* the triplet state; O₂ removal will promote this particular reaction since the triplet is no longer quenched. The use of scavengers^[16] or anti-oxidants^[17] and the effect of the density of labelling^[18] was shown to have beneficial effects on stability but such methods do not address the intrinsic stability. Rhodamine dyes have been used as laser dyes^[19] so the stability of Rhodamine 6G in particular has been well studied. Weber found that Rhodamine 6G, while studying various laser dyes, bleached with little change in the spectrum^[11] while acridine orange and dichlorofluorescein formed products absorbing at wavelengths above 350nm. The same author reported^[20] reduced bleaching rates in solutions purged with N₂ compared to air-equilibrated solutions and also that triplet quenchers, such as cyclooctatetraene, could help reduce bleaching. Therefore, it was concluded that crossing to the triplet manifold is the pathway to Rhodamine 6G bleaching. Conversely^[21], Rosenthal found that bleaching of Rhodamine 6G in various solvents could be promoted by solvents where radical attack is prevalent. Bleaching of Rhodamine 6G under continuous illumination and monitoring in methanol revealed a slow initial process followed by a faster rate of chromophore loss. This was believed to be due to some photochemical change involving methanol which then allowed attack of the dye. In this case, O₂ was found to retard bleaching, presumably by intercepting the product responsible for chromophore loss. If this was the mechanism underlying the unusual kinetics it should be simple to avoid such problems since methanol does not absorb light above 240nm^[22]. Nevertheless, this serves as a useful pointer to the fact that studies of chromophore loss accompanied by detailed kinetic profiles are not easily found in the literature. Such studies carried out under broadband or natural illumination are rarer.

Given their high fluorescence quantum yields and that there is minimal triplet observed, BODIPY dyes are considered to be sufficiently photostable to be used as laser dyes^[23, 24] and the proliferation of BODIPYs in the commercial market for bio-imaging would indicate that the photostability is sufficient for such purposes. BODIPY has been shown to have considerably better stability than fluorescein^[13] and, for example the laser dye pyromethene 567 (PM567) in chloroform has a quantum yield of bleaching of 7×10^{-4} ^[25]. The belief that stability is controlled by the triplet still persists^[26, 27] where consideration of BODIPY stability is concerned,

but other researchers have implicated that bleaching occurs from the singlet state^[13] or through interaction with free radicals^[28]. Anti-oxidants that are also triplet quenchers, such as DABCO, were found to stabilise^[29] PM567 but n-propyl gallate did not. The stability in various solvents was shown to correlate with the corresponding singlet oxygen lifetime^[30]. Addition of iodine atoms to BODIPY allows generation of singlet oxygen due to the heavy-atom effect^[31]. Such a compound was shown to be more effective^[32] than the xanthene dye, Rose Bengal, at generating singlet oxygen but was more resistant to photobleaching. This was attributed to the higher oxidation potential of BODIPY. The effect that changing various substituents on the BODIPY framework has on photostability has received some attention^[33]. Substitution of fluorine^[34] or CF₃ groups to the α or β positions was shown to improve the photostability compared to BODIPY with methyl groups in the equivalent positions, without significant changes to the photophysical properties. Similar effects have been noted in cyanines^[35]. The electron-withdrawing property of fluorine serves to stabilise the molecule. Aryl substitution at the 8-position of BODIPY led to comparison of PM567 photostability with three aryl BODIPYs of varying steric hindrance^[27]. All the hindered molecules were more stable than PM567 under pulsed illumination at 532nm. Analysis of the photo-degradation products indicated that cycloaddition of O₂ was one path to chromophore loss, along with direct cleavage of the aryl group. The capacity to generate singlet oxygen was believed to be the reason for the improvement in stability. By calculation, the energy of the triplet of the aryl versions are borderline for sensitizing ground-state O₂ while PM567 has the requisite energy to do so. BODIPY with bicyclo-octa or septadiene fused structures^[26] appended is an interesting case as it is believed to display a regular stacking in solid matrices and have built-in anti-oxidant capacity. The photobleaching of these compounds appears to display some catalytic profile although this is not remarked on in the study. The dyes seem to show inhibition followed by bleaching at rates more rapid than the first-order bleaching of PM567. This finding suggests the possibility of a product that degrades the chromophore.

A study of a selection of eight BODIPY dyes under continuous white-light illumination was reported^[33]. These dyes featured an 8-aryl structure with further substituents on the aryl group. Three feature no α or β groups while the other 5 were tetra-methyl dyes. In toluene, the dyes lacking methyl groups were found to be more stable, the oxidation potential was precisely correlated with the bleaching rate of the various dyes although there was only 3-fold change in bleaching rate across the series. Fluorescence quantum yields varied greatly but the effect of excited-state lifetime was not considered as oxidation by singlet oxygen was explicitly assumed to be responsible for the bleaching.

The photostability of BODIPY immobilised in solid matrices has been reported and is of particular interest as it is anticipated that light-harvesting materials will find use in such media. Doping of a selection of commercially available BODIPY dyes into polystyrene microspheres^[28] was found to improve the photostability. The most red-shifted dyes were the least stable under illumination and doping generally had a small, positive effect on stability. For a certain BODIPY dye absorbing at around 680nm there was an 800-fold improvement in the sphere compared to CH₂Cl₂ solution and over 100-fold improvement compared to the same dye in toluene. The increased stability is postulated to arise from the rigidity of the dye constrained within the sphere and because of protection from molecular oxygen. Although the polymer does not absorb the excitation light, the effect of scattering by microspheres should not be discounted as a form of protection. A variety of common dyes were studied in xerogels^[25] and some dyes compared to solutions. Under constant 532nm illumination in gels, PM567 and PM597 displayed photobleaching quantum yields of the order of 10⁻⁶ while rhodamines were more stable by two orders of magnitude. Perylene Red and Perylene Orange were a further two orders of magnitude more stable. Elsewhere^[36] this relative instability has been attributed to pyromethene dyes residing in the pores of the gels so still being susceptible to oxygen or radical attack. In these gels, PM567 and Rhodamine 6G were again two orders of magnitude more stable compared to when they are in solutions. Interestingly, when the gels were subject to pulsed illumination pyromethene dyes were the most stable. For some of the other dyes bleaching rates correlated with laser repetition rate, the implication being that thermal degradation^[37] must also be considered when materials are bound in solid matrices since deposited heat cannot diffuse quickly.

Reisfeld^[8] studied the different stability levels provided by a host of polymer and inorganic matrices. BODIPY dyes were found to be more stable than Rhodamine dyes. For BODIPY, PMMA was the best host material in terms of stability. Here it was postulated that the relative flexibility of the polymer, when compared to a 3-D crosslinked polymer or organic sol-gels, leads to a pore-free network which inhibits photo-degradation. The bleaching of BOPHY might be expected to show similar properties to BODIPY dyes. The general thinking in terms of BODIPY bleaching is that accessing the triplet state is required for bleaching. Given the extremely low triplet yields this is consensus feels unsatisfactory. It has also been shown that the use of solid matrices generally has a positive effect on photostability which is of considerable interest to us.

Stability studies where lasers are used have advantages in that fluorescence rather than absorbance may be tracked. This could allow for very sensitive measurements. The high power provided by lasers also leads to some differences^[38], of particular note is that high

photon densities may lead to two-photon absorption, promoting the molecule into S_n states which could also cross to T_n states. Indeed, bleaching rates have been shown to be non-linear^[10] with illumination intensity. Higher states may lead to different bleaching routes and the energy may be sufficient for direct ionization^[13] of the molecule, leading to formation of free radicals.

No standard methodologies, illumination sources, or materials exist for establishing levels of photostability. As such, it is unclear how to best compare the stability of different dyes. Typically, photo-processes and photo-reactions are defined by the quantum yield; i.e. for a process x , $\Phi_x = k_x / \sum k_{all}$, the yield should not normally exceed unity. The need to establish quantum yields^[39] for photo-bleaching is clear since this is the only way to compare different materials, environments and excitation sources. This concept has limitations however. In the case of two-photon excitation^[38] for example the denominator of photons absorbed is no longer unity and the situation becomes highly complex. The example of Rhodamine B in methanol demonstrated the fact that the absorption of photons becomes vanishingly unlikely and that reactions can become dormant. Indeed, some have argued^[40] that a fluorescence half-life is a more appropriate measure of photo-stability but this would need correction for excitation intensity and substrate concentration. Putting these concerns to the side for now, it is instructive to compare the bleaching quantum yields found for organic dyes. For coumarin dyes^[41] and fluorescein^[15] the quantum yield is of the order 10^{-4} , for biological porphyrins^[42] it is 10^{-5} , Rhodamine^[43] dyes tend to display yields of 10^{-6} to 10^{-7} while quantum values of 10^{-5} have been reported for some BODIPY dyes^[27].

A cursory investigation was made into the photostability^[44] of BOPHYs by Hao et al. Stability in the case of continuous white-light illumination of BOPHY and a comparable tetramethyl-BODIPY was studied, with both chromophores dissolved in toluene. BOPHY was considerably more stable than BODIPY over the course of one hour. In a DMSO:H₂O (1:1 v/v) mixture, BOPHY was reasonably stable when compared to Fluorescein in a 0.1M NaOH solution. These results suggest that the parent BOPHY should be relatively stable towards prolonged illumination. This report is the starting point for our investigations.

6.2 Photostability of TM-BOPHY

6.2.1 Photostability in a Solid Medium.

The sample of TM-BOPHY used to study photostability was used as received from our collaborators. It should be noted that there is a small amount of impurity seen at around 505nm, highlighted by the star in Figure 6.1. The impurity is clearly present in absorption and

fluorescence spectroscopy but was not seen in NMR spectroscopy. The impurity was seen to bleach rapidly by first-order kinetics. The chromophore was embedded into a PMMA matrix as described in the experimental section and the final thickness of the film was $400 \pm 50 \mu\text{m}$.

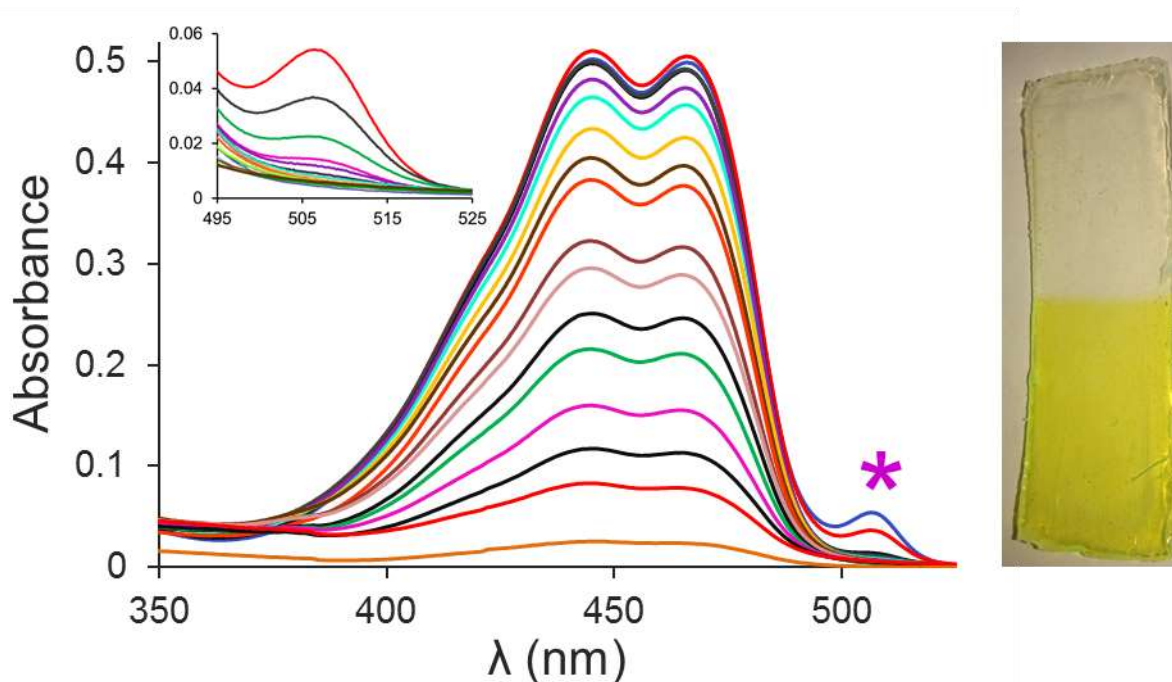
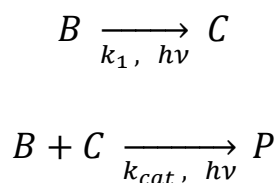


Figure 6.1 – Successive bleaching overlay of TM BOPHY in a PMMA film up to 500 hours, inset 1 rapid bleaching of the impurity, inset 2 shows the film after exposure demonstrating the loss of colour.

Under these conditions it is clear that the absorption profile of the TM-BOPHY chromophore bleaches on a relatively slow timescale. The shape of the profile does not to change during the bleaching process other than the build-up of a UV absorbing product (Figure 6.1). If the kinetic profile of the bleaching is monitored at a selection of wavelengths then the fact that the profile is not changing is confirmed. That is to say, the same decay law is found at different wavelengths so global analysis is used to fit the data. In the solid medium, it transpires that bleaching occurs via an auto-catalytic pathway. This can be seen in the sigmoidal shape of the bleaching curve shown in Figure 6.2. Recognition of the auto-catalytic nature of the bleaching reaction requires us to develop an overall scheme for the process.



Scheme 1 – Outline of the proposed bleaching process for TM-BOPHY in a cast film.

In the scheme, TM-BOPHY, B, is degraded to some product, C, by illumination at a low rate. The product C cannot diffuse appreciably in the film but initiates further bleaching locally to give the final product or products, P. The net result is loss of colour in the film. The second step is characterised by the catalysed rate^[45], k_{cat} , having the units $M^{-1}h^{-1}$. To extract the bleaching rates, Equation 6.1 is used (this was encountered in Chapter 3).

$$\frac{\omega_B}{[B]} = (k_1 + k_{cat}[B_0]) - k_{cat}[B] \quad (6.1)$$

The term ω_B is the time-dependent rate of bleaching, which was determined by a Taylor expansion based on the bleaching data averaged across all wavelengths in the main absorption band. Now [B] is the concentration at which the rate is measured and B_0 is the initial concentration of TM-BOPHY.

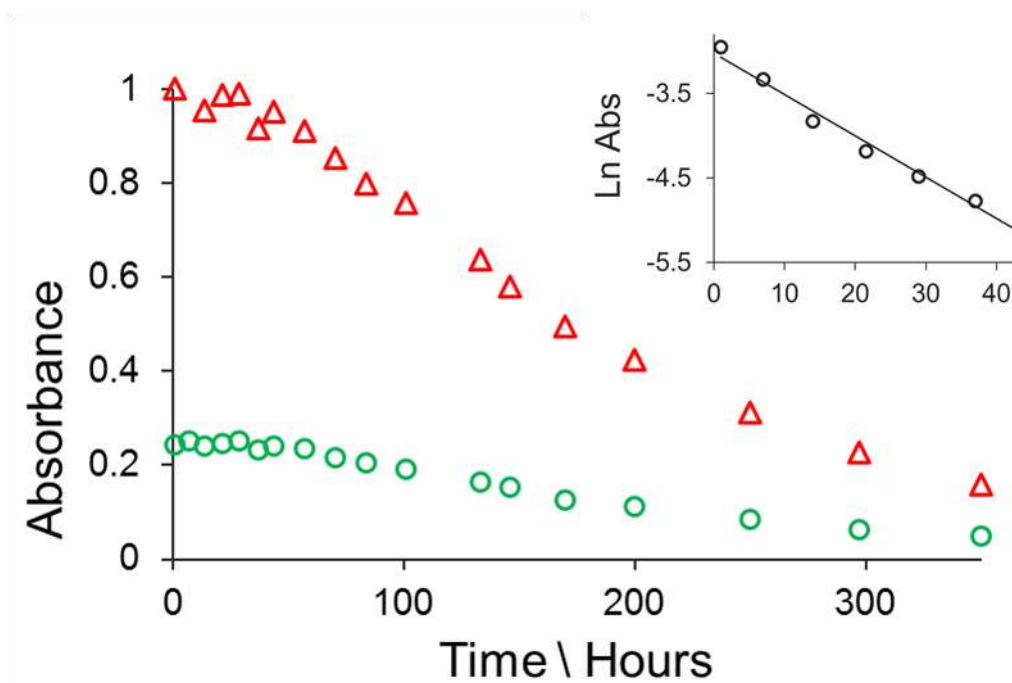


Figure 6.2 – Bleaching kinetics of TM BOPHY in a solid film at 465nm (Δ) and 415nm (\circ), the inset shows the first order bleaching of the impurity.

The data in Figure 6.2 was fitted to a Taylor expansion which allows extraction of the bleaching rate at each concentration. To find the rates it is necessary to convert the data to concentration and plot the data as Equation (6.1). A linear fit, shown in figure 6.3, was found, allowing values to be determined for k_1 and k_{cat} of $3.4 \pm 0.5 \times 10^{-3}h^{-1}$ and $13.5 \pm 1.2 \mu M^{-1}h^{-1}$.

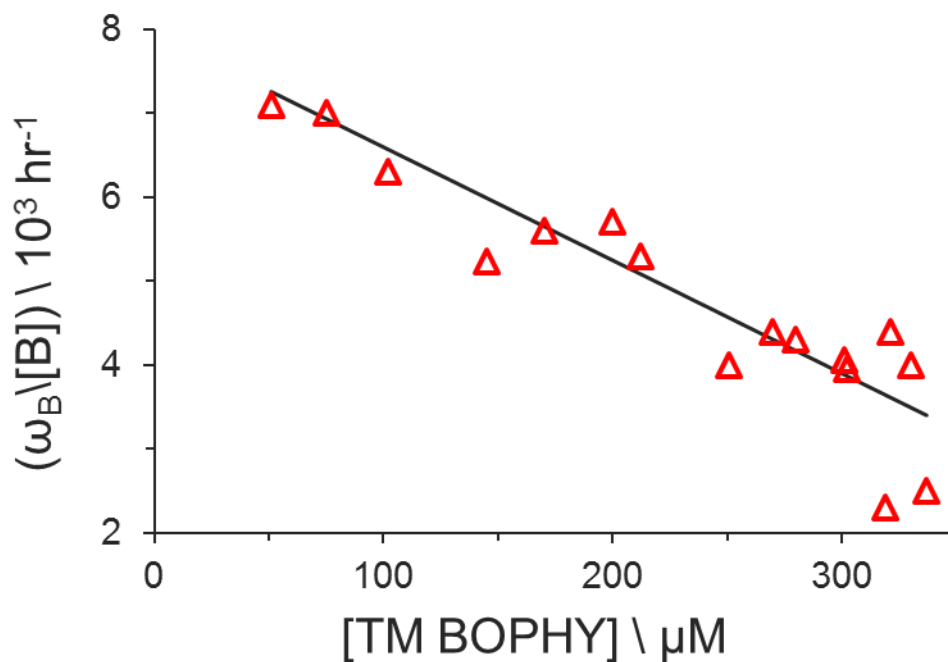


Figure 6.3 - Autocatalysis is confirmed for TM BOPHY in PMMA film as per equation 1. The gradient gives the value for k_{cat} of $13.5M^{-1}h^{-1}$, the intercept is 0.0076 giving a value for k_1 of $3.4 \times 10^{-3}h^{-1}$

Bleaching in the solid film takes place over what is a rather long timeframe for a laboratory experiment. The method requires the sample to be exposed for long periods then removed to record the absorbance. As such, fiducial marks and many repeat measurements are required to find the concentration. This leads to somewhat noisy data, especially during the inhibition period. Even so, for this sample there is a clear inhibition lasting around 50 hours after which bleaching becomes uncontrolled. It should be appreciated that it is feasible for materials to appear highly stable for long periods before rapid loss of colour. The testing of materials for OLEDs necessarily involves extrapolation of the shorter-term stability to provide the claims of 50,000 hours of performance, as mentioned in the introduction. This procedure is not to be recommended.

In the solid media, bleaching of TM-BOPHY is both time-dependent and slow. This means that attempts to characterise the quantum yield would also be time dependent and subject to high levels of error. Illumination of the sample by a 25 mW laser of 405nm allowed bleaching of the sample with a known photon flux. Under these conditions, the best estimate of the turnover number for bleaching with respect to absorbed photons was approximately 10^6 .

6.2.2 Photobleaching in Solution

Understanding the photostability of organic dyes in solid media is useful in terms of potential devices but characterisation of the underlying processes is more readily achieved in solution. Under such conditions, we might expect to better understand reactions mechanisms and to collect more detailed quantitative information about the bleaching rates. A further advantage of fluid solutions arose in the form of faster rates of bleaching. The substrate was studied in a small range of solvents of varying polarity. Moreover TM-BOPHY appears to be soluble in most organic solvents tested and does not show any appreciable fluorescence quenching in the different solvents. There are no obvious effects of solvent on the photophysical properties of this chromophore. All solutions were air-equilibrated so routes to bleaching involving molecular oxygen are active, including reactions from the triplet-excited state. In a typical photobleaching study in solution, the kinetic profiles in Figure 6.3 show a relatively fast degradation process which leads to formation of some stable intermediate. Again, as in the film, no change in the absorption profile is found, which are given for some of the solvents in Figure 6.4. The intermediate undergoes steady bleaching and fitting of the kinetic data shows that bleaching occurs by way of two successive first-order processes. The first lifetime is on the order of 30 minutes while the second lifetime, which is the more significant part, approaches 100 hours. The rates are collated in Table 6.1 and no general trend was observed for the bleaching rate with bulk solvent properties. However, when the photolysis experiment is performed with TM-BOPHY dissolved in toluene, a different kinetic profile is seen. As was observed in plastic films, initial bleaching is extremely slow and it was not until after more than 50 hours of exposure that bleaching began in earnest. Again, bleaching of the chromophore involved auto-catalysis. Surprisingly, toluene provides some stabilisation over short illuminations, but eventually uncontrolled bleaching takes over as product accumulates. The data were analysed in terms of Equation 6.1; the initial rate constant, k_1 , was $1 \times 10^{-3} \text{ hr}^{-1}$, which is of the same order of magnitude as seen in the film, while the auto-catalysed rate constant was $680 \text{ M}^{-1} \text{ hr}^{-1}$ which is some 50 times greater than in the film. In general terms, it appears that the first step is inhibited in toluene but once formed the product is free to diffuse in solution and initiate fast bleaching.

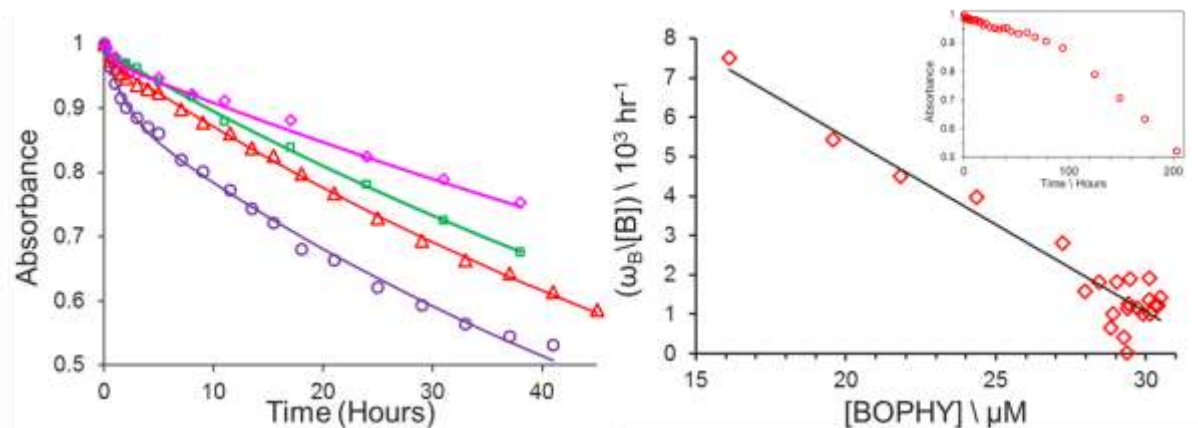


Figure 6.3 – Left panel, kinetic bleaching data for TM-BOPHY in solutions of CH_3CN (\blacklozenge), C_6H_{12} (\blacksquare), DMF (\blacktriangle), and methanol (\bullet). Solid lines represent biexponential fits. Right panel, fit to equation 6.1 for bleaching in toluene, inset: Bleaching data in toluene, note the change in kinetic profile and timescale.

Medium	$k_1 \text{ } h^{-1}$	$A_1 \text{ } \%$	$k_2 \text{ } h^{-1}$	$A_2 \text{ } \%$
C_6H_{12}	5.7	1.1	0.01	98.9
Methanol	11.8	2.5	0.012	97.5
DMF	0.4	9.4	0.014	89.6
CH_3CN	1.2	2.6	0.007	97.4
	$k_1 \text{ } h^{-1}$		$k_{cat} \text{ } M^{-1}h^{-1}$	
PMMA	0.0034		13.5	
Toluene	0.001		680	

Table 1 – Bleaching rates of TM BOPHY in the various media considered.

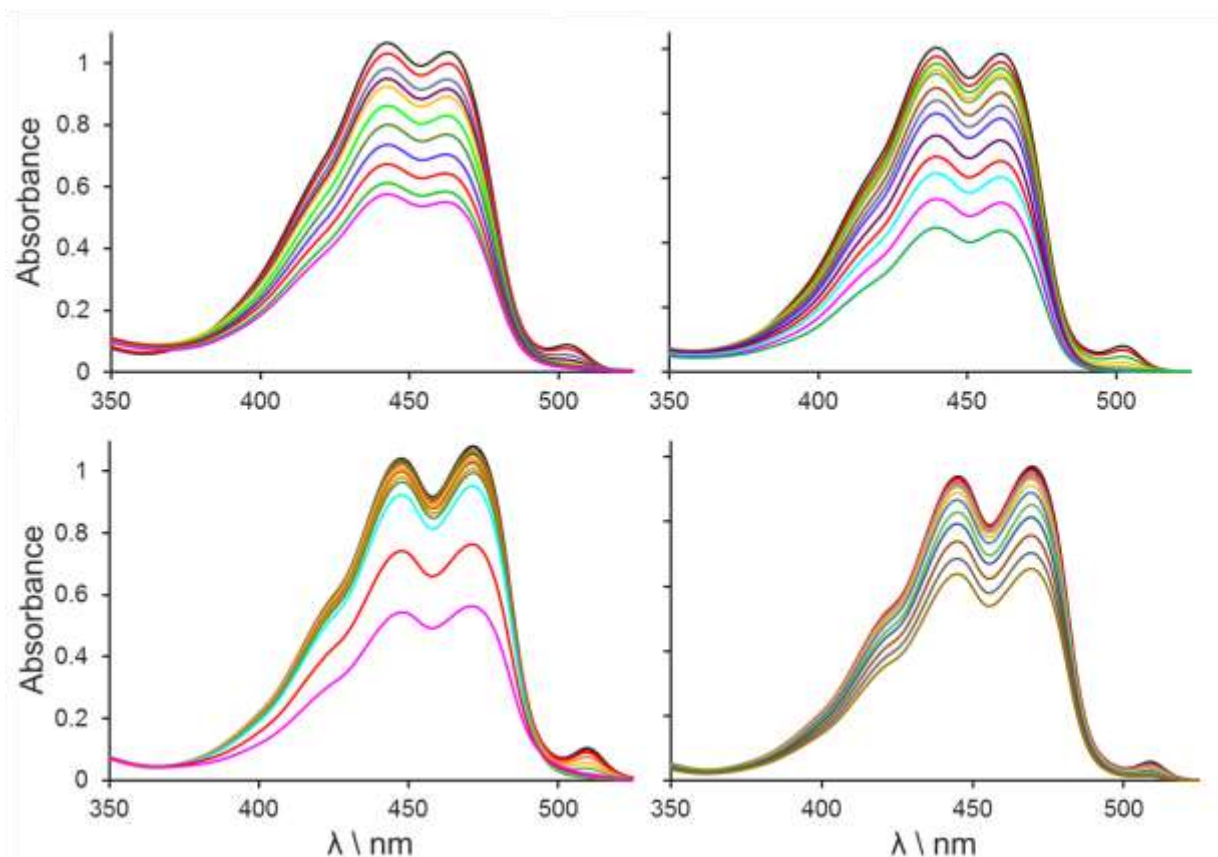


Figure 6.4 - Progressive bleaching overlays for TM BOPHY in various solvents, clockwise from top left DMF, methanol, cyclohexane and toluene, no photo-products are evident in any solvent.

Throughout our work with TM-BOPHY we have stressed that the triplet-excited state of the chromophore is not involved in the bleaching chemistry. This argument is based on the realisation that intersystem crossing is inefficient for this class of compound. Any triplet-excited states formed in aerated solution should react quickly with molecular oxygen to produce singlet oxygen. The latter is well known to bleach organic matter and therefore it seems prudent to check its involvement in the present case. To do this, we take advantage of the fact that the lifetime of singlet molecular oxygen in methanol is only $7\mu\text{s}$ ^[46]. In mono-deuterated methanol, the lifetime increases to $37\mu\text{s}$ ^[47]. The longer lifetime provides more time for the excited state to attack the chromophore and, if involved, we might expect to see more effective bleaching in CH_3OD than in CH_3OH . Solutions of TM-BOPHY were bleached as above but no differences in bleaching rate were observed. It is shown in Figure 6.5 that in both solvents the measured rate constants were identical within experimental error. This observation serves to eliminate singlet molecular oxygen as being involved in the rate-limiting steps.

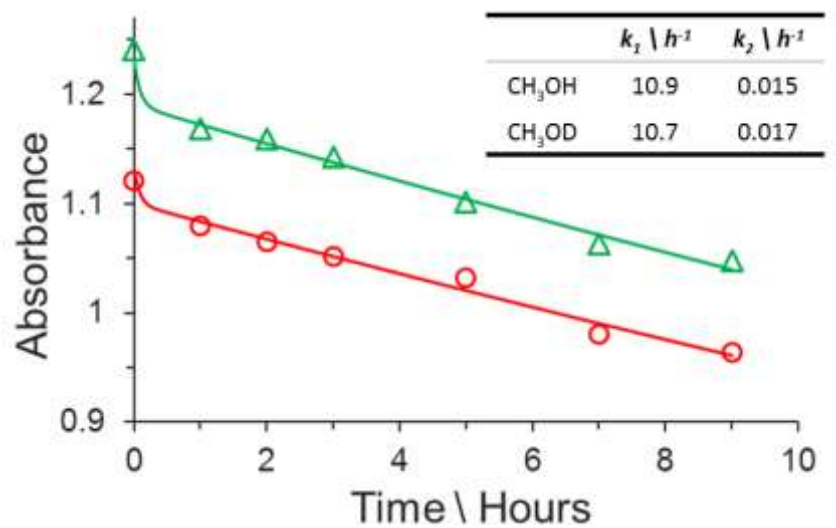


Figure 6.5 – Bleaching kinetics in methanol (○) and mono-deuterated methanol (Δ), no significant difference was found between the solutions, so singlet oxygen is not implicated in the bleaching.

6.3 Photostability of BOPHY-DMA

6.3.1 Photon considerations

The photostability of the extended derivative, BOPHY-DMA is now considered using the same white-light source for excitation. Since the two materials absorb over disparate regions of the spectrum it is important to consider the number of photons absorbed by each sample. The absorption profile of the extended BOPHY is significantly red shifted compared to the parent and the shape is somewhat broader, depending on the nature of the solvent. We must consider these features in conjunction with the output profile of the lamp in order to find the relative number of photons impinging on our samples. As a first step, the spectral power output of the lamp was converted to a relative photon flux. Secondly, the product of the photon flux and absorbance is integrated over the output range of the lamp to give a total relative photon absorbance. This analysis shows that for solutions of the same absorbance value at the maximum λ_{abs} , BOPHY-DMA will absorb approximately twice as many photons as TM-BOPHY.

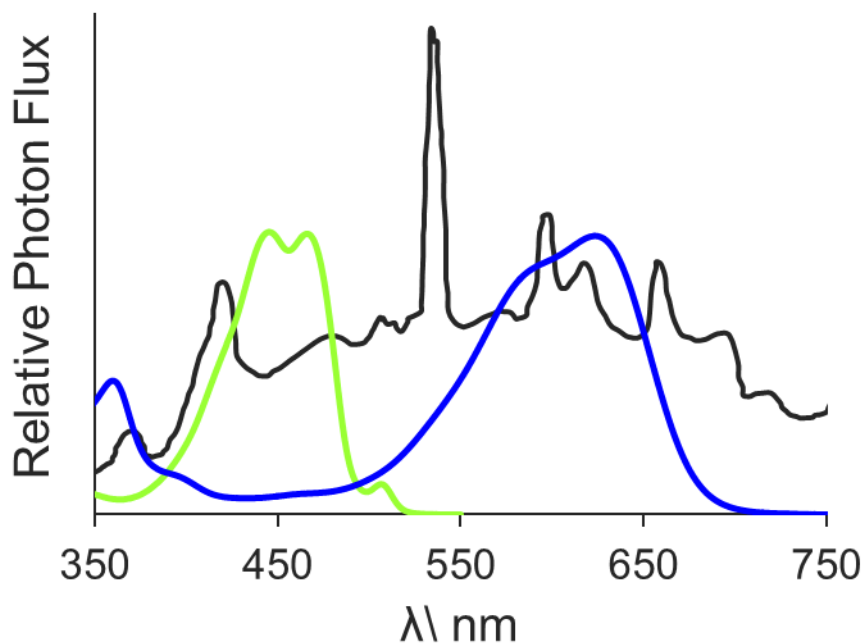


Figure 6.6 – The absorption spectra of the two molecules studied TM-BOPHY (—) and BOPHY-DMA (—). The lamp intensity is adjusted from power to relative photon flux. BOPHY-DMA will absorb approximately double the number of photons per unit time.

6.3.2 Photostability in a Solid Medium

As before, BOPHY-DMA in a cast PMMA film was exposed to broadband illumination. The bleaching is seen to proceed rapidly and in Figure 6.7 there is a clear change in the absorption profile. In fact, the new absorption spectral features emerging during photolysis can be attributed to the monocation. No inhibition of bleaching or auto-catalytic kinetics are seen as demonstrated in Figure 6.8. In this case, it appears that a proton is released during the initial bleaching process. The proton becomes attached to a second molecule of BOPHY-DMA so that the mono-cation is formed as a side product of the bleaching reaction. No isosbestic point is maintained, indicating that the mono-protonated species is itself bleached under illumination. Conversion accounts for around 50% of the loss of the original chromophore. The bleaching rates for the neutral and mono-protonated species are 0.50h^{-1} and 0.017h^{-1} , respectively. That the mono-protonated species is more stable than the parent compound can be explained by the fact that the inherent excited-state lifetime is very short. This particular concept will be expanded by study of the solution-phase bleaching kinetics.

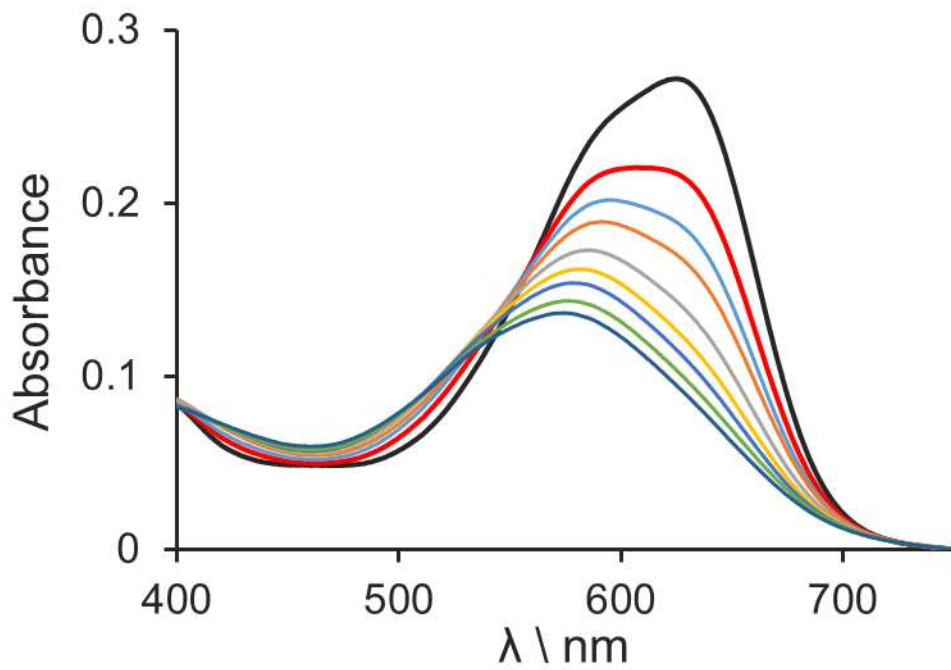


Figure 7.7 – Bleaching overlay of DABOP in a PMMA film.

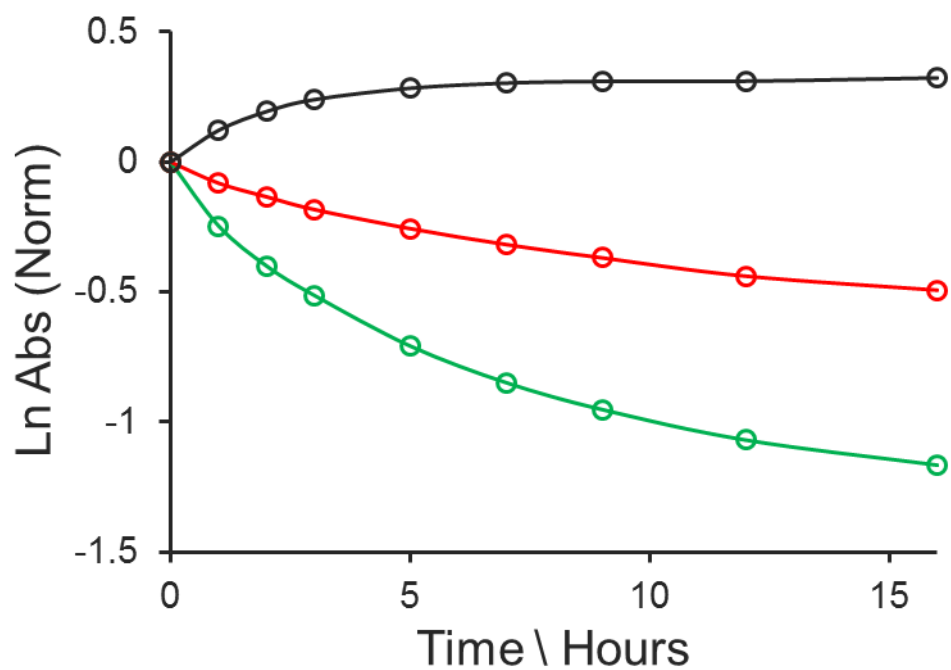


Figure 7.8 - Bleaching progression over time at 500nm (○), 580nm (○) and 635nm (○).

6.3.3 Photobleaching of BOPHY-DMA in solution

Examination of the stability of the BOPHY-DMA allows us to begin to explore some key hypotheses surrounding the photostability of dyes originating from the singlet-excited state. Firstly, we are able to compare bleaching of BOPHY-DMA and TM-BOPHY as a simple means by which to examine how photostability varies with conjugation length. Secondly, it is possible to probe the hypothesis that the excited-state lifetime will play an important role in establishing the bleaching efficiency. Scheme 2 outlines the reasoning behind this claim. The bleaching efficiency is proportional to the bleaching rate constant divided by the sum of all other rate constants leading to deactivation of the excited state. These ancillary processes combine to set the lifetime of the excited state in the absence of photobleaching. Embedded in these terms is the radiative rate constant.

$$\Phi_{bleach} \sim \frac{k_{bleach}}{\sum k_{all}} \sim k_{bleach} \cdot \tau_f \cdot \tau_{other}$$

Scheme 2 – Demonstrates how bleaching should be dependent on time spent in the excited state.

It was shown in Chapter 5 that BOPHY-DMA has significant charge-transfer character. The fluorescence quantum yield drops from 80% in cyclohexane to less than 1% in acetonitrile, with weakly polar solvents giving lifetimes between these two limits. Thus, BOPHY-DMA becomes a good model for probing how the excited-state lifetime relates to the bleaching efficacy. Now BOPHY-DMA was dissolved in a range of organic solvents with all other conditions were kept as before. The bleaching kinetics are shown in Figure 6.9 and the overlays in the various solvents are found in Figure 6.10. It is evident that BOPHY-DMA bleaches very efficiently in cyclohexane. Here, there is clear indication for the involvement of a relatively long-lived intermediate giving an overall bi-exponential process for the observed bleaching. In air-equilibrated cyclohexane, the two derived rate constants are $4.8 \pm 0.3 \text{ h}^{-1}$ and $0.53 \pm 0.05 \text{ h}^{-1}$. Each of these two steps accounts for roughly 50% of the total bleaching but the second step occurs some 10-fold more slowly. Bleaching kinetics were recovered for the other solvents and the derived rate constants are collected in Table 6.2. In each case, despite the kinetic profile, it was not possible to observe any new spectral features that might correspond to a new product. The analysis in cyclohexane establishes a model for the bleaching kinetics and sets a baseline for the speed of chromophore loss. We know that this solvent provides the longest excited-singlet state lifetime for BOPHY-DMA. The polarity of the solvent was found to exert a strong effect on the efficacy of photobleaching.

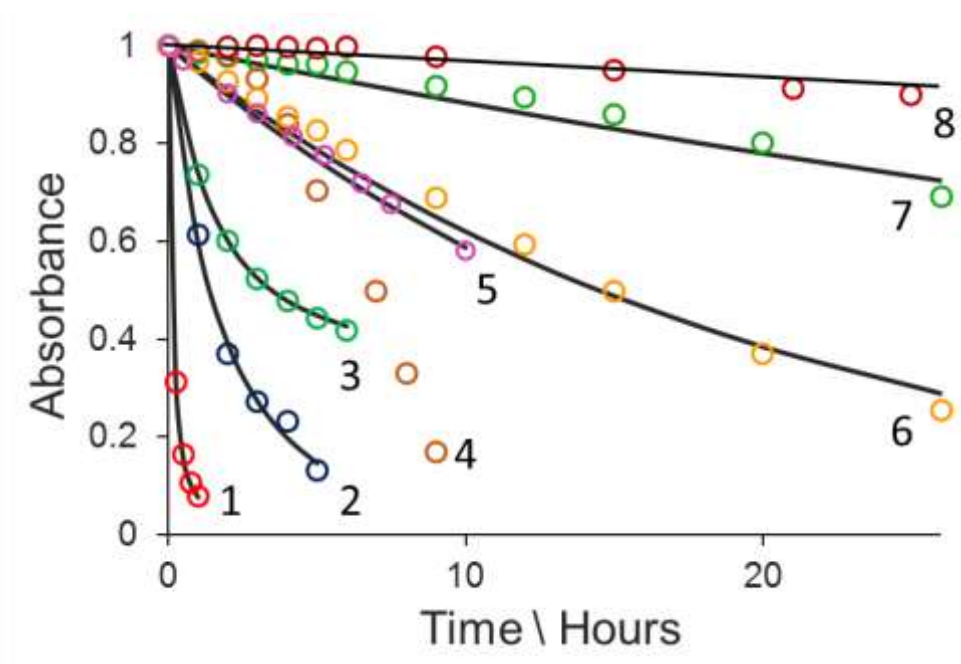


Figure 6.9 – Solution-phase photobleaching of BOPHY-DMA: see Table 2 for key to the graph.

Photobleaching in the more polar solvents tends to follow the same general pattern but the second step is less well resolved. The initial first-order rate constant recorded in benzonitrile is higher than that observed in anisole and MeTHF while that determined in acetonitrile is much lower. Comparing acetonitrile to cyclohexane shows that the bleaching rate is reduced some 100-fold in the polar solvent, which is in line with the change in fluorescence quantum yield. The loss of chromophore seemingly involves the formation of a product that has the same absorption spectrum as the initial BOPHY-DMA with some build-up of unidentified products absorbing in the UV region. There is no evidence for the involvement of a product with a reduced conjugation path. Close inspection of the spectral changes accompanying photobleaching reveals that for the solvents that bleach at a slow but appreciable rate (i.e. anisole and benzonitrile) the monoprotonated cation is formed. This transformation is not quantitative, however, and no isosbestic point is maintained. Those solvents where bleaching is fast and involves bi-exponential kinetics, there is no evidence in the absorption spectra to suggest involvement of the monoprotonated cation.

There is no simple correlation between the bleaching efficacy and the excited-singlet state lifetime, although there are hints that this might be the case in some solvents. Thus, benzonitrile and acetonitrile fit the trend perfectly. For anisole, bleaching is relatively slow but the lifetime is quite long. This finding implies that anisole provides some level of protection against photobleaching (*vide infra*). The fast bleaching observed in ethanol also appears to be anomalous but we can anticipate hydrogen bonding between the chromophore and solvent.

Indeed, the most extreme case of this involves the di-protonated form of the dye as encountered in Chapter 5. It will be highlighted later that protonation of the terminal amine groups results in rapid photobleaching.

The most remarkable result in this series concerns the incredibly slow photobleaching recorded in toluene. In anisole, possible stabilisation was noted and toluene appears to further amplify this effect. Taken in isolation this result seems to contradict the hypothesis that the excited-state lifetime helps control the level of photobleaching. However, there is a general trend that, in the absence of specific interactions between solute and solvent, the hypothesis stands up. This, in turn, would suggest that there is some special situation occurring in toluene (and also in anisole).

<i>Solvent</i>	$\tau_f \setminus ns$	$k_1 \setminus h^{-1}$	$A_1 \setminus \%$	$k_2 \setminus h^{-1}$	$A_2 \setminus \%$
Cyclohexane (1)	1.8	4.8	46	0.53	54
Toluene (8)	1.6	0.001			
Diethyl Ether (3)	1.5	0.61	24	0.018	76
Anisole (6)	1.3	0.021			
MeTHF (4)	1.1				
Benzonitrile (5)	0.48	0.21			
Ethanol (2)	0.22	1.5	11	0.14	89
Acetonitrile (7)	0.12	0.055			

Table 6.2 – Bleaching rates in the solvents tested, bracketed numbers indicate key to figure 6.9. Fits are to either first-order or biexponential kinetics.

Throughout these investigations, the solvent was of the highest available purity. Different batches of solvent were used and all bottles were kept at 4 °C and opened freshly. Studies were made over a six-month period and all measurements were repeated many times. Nonetheless, it is important to remain vigilant to the threat posed by impurities. This situation is exacerbated for ethers, notably MeTHF. For this solvent, the initial bleaching step proceeded as would be expected on the basis of the other solvents but when samples were left to stand overnight in the dark there was an accumulation of peroxides that significantly increased the bleaching rate. There were also differences in the absorption spectral properties in that bleaching in MeTHF led to a coloured product. These results could be rationalised in terms of peroxides attacking the chromophore at sites along the extended conjugation path so as to form BOPHY-based products with blue-shifted absorption maxima.

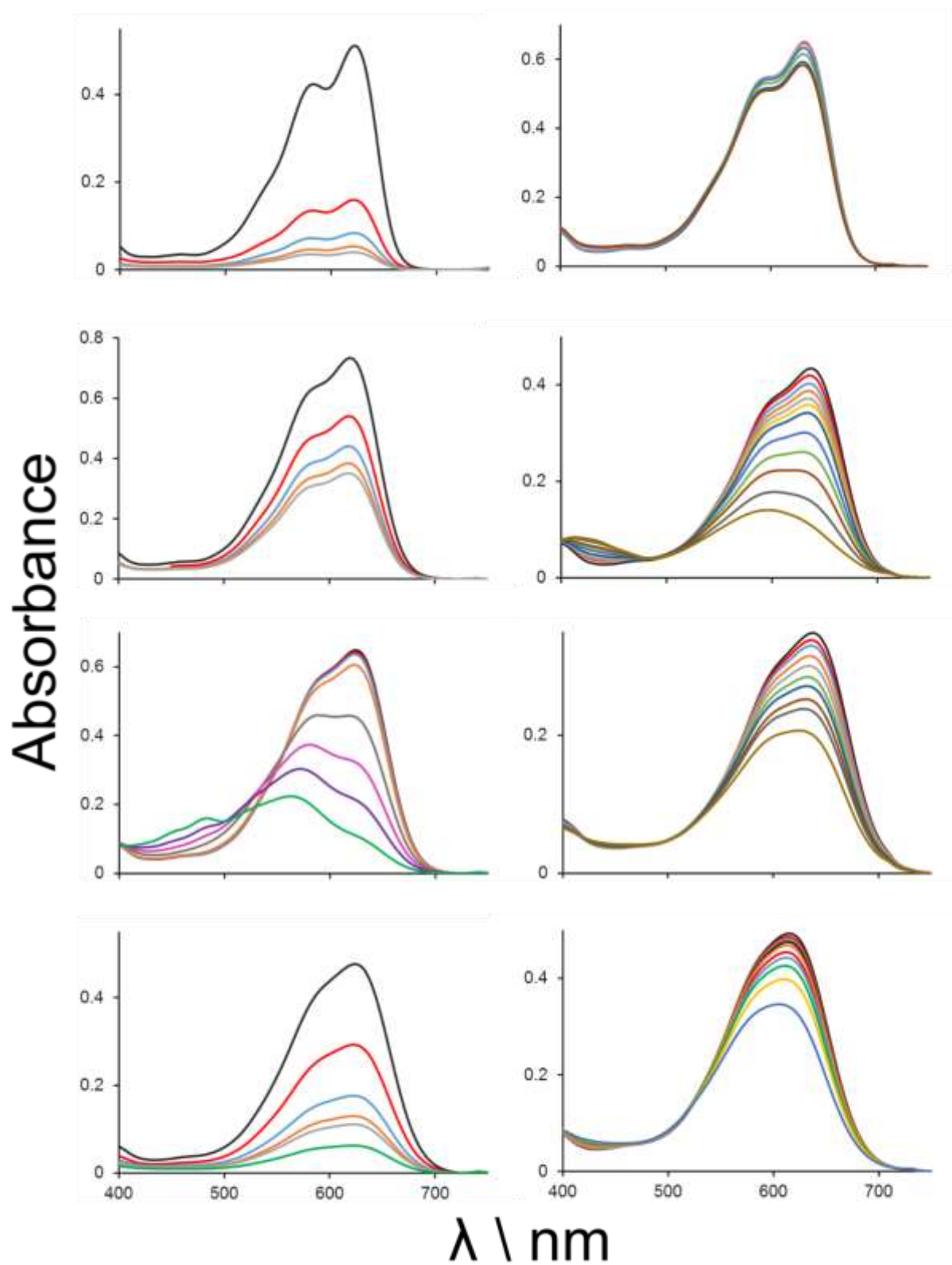


Figure 6.10 – Bleaching overlay for all solvents studied, order is 2 reading from left to right, cyclohexane, toluene, diethyl ether, anisole, MeTHF, benzonitrile, ethanol and acetonitrile.

Additionally, the concentration of molecular oxygen ought to be considered when comparing bleaching rates, in this work rates were not adjusted for oxygen concentration, in Appendix 2 this is given for some solvents used in this work. It is notable that in organic solvents there is not a great difference between solvents that can account for differences. Most notable is that in water the concentration is an order of magnitude lower.

6.3.4 – Photostability of the BOPHY-DMA Dication in Acidic Solution

It was noted that altering the nature of the terminal donors of the chromophore by way of hydrogen bonding can affect the photostability and the extreme case of this situation concerns the diprotonated form of BOPHY-DMA. For this dicationic species, the fluorescence quantum yield in benzonitrile increases some 7-fold compared to the neutral species and the fluorescence lifetime increases 4-fold. The dication was seen to be highly reactive under white light illumination and bleached relatively quickly compared to the neutral compound. When a benzonitrile solution containing excess HCl was illuminated, loss of the characteristic colour occurred. The chromophore is transformed to a product, as seen in Figure 6.11, that bears the characteristic BOPHY absorption profile but is blue shifted by about 50nm. No other product was evident in the visible region but there is an overall loss of material without an isosbestic point being maintained. On prolonged illumination, the new product disappears on a relatively long timeframe.

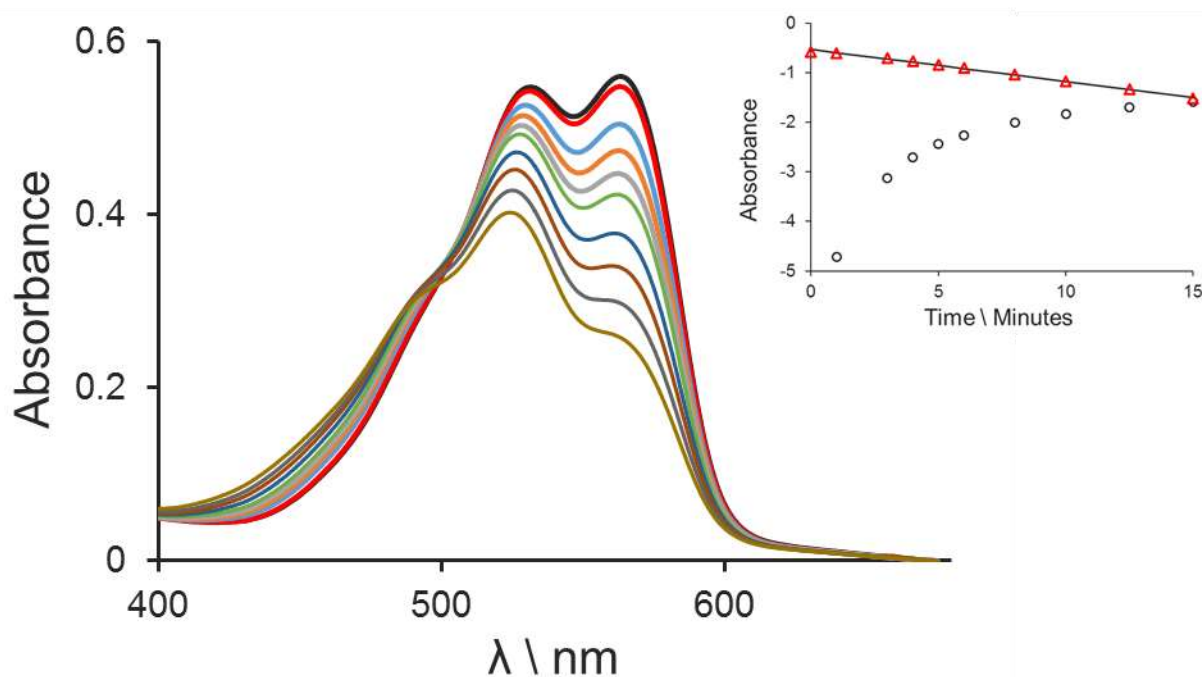


Figure 6.11 – Bleaching overlay and kinetics of the diprotonated form of BOPHY-DMA in benzonitrile. Inset shows the loss of starting material (Δ) and appearance of the product (\bullet).

The sample was exposed to light for a brief period of a few minutes; this is in marked contrast to earlier studies with TM-BOPHY where exposure times were in the region of hundreds of hours. By spectral decomposition, the rate for loss of absorbance attributed to the dication can be found. Bleaching exhibits first-order kinetics with a globally recovered rate constant of 3.8 hr^{-1} . This value is some 20 times higher than that for the neutral form of the dye in benzonitrile and, in fact, is quite similar to the rate constant derived for the neutral species in cyclohexane. The high rate of photobleaching found for the dication is in agreement with the general hypothesis that chromophores displaying inherently long-lived excited states are more amenable to photobleaching. This might be seen as too simplistic, however, since there are other changes between the two chromophores. Nonetheless, the dication adds to our growing list.

6.4 Understanding the Effect of Toluene

6.4.1 Toluene as an Additive Stabiliser and use of Anti-Oxidants

Photobleaching of BOPHY-DMA in toluene proceeds more slowly than in any other solvent studied and understanding this stabilisation would help establish generic mechanisms for the degradation pathway. The measured fluorescence lifetime in toluene is 1.6ns and there is little likelihood of light-induced intramolecular charge transfer in this solvent. Whilst the raised rate of bleaching broadly follows the high fluorescence quantum yield, this anomaly is particularly interesting as it points to mechanisms and environments that stabilise the molecule toward light. It is important to understand whether stabilisation of the molecule by toluene is genuine or if it is accidental, perhaps involving impurities within the solvent. The toluene used was spectrophotometric grade and free of fluorescent impurities. Analysis by gas chromatography revealed that impurities made up less than 0.25% of the total mass and comprised of related aryl hydrocarbons, such as xylenes, benzene and cumene. These materials are similar to toluene and are unlikely to provide stabilisation to the dye by some mechanism other than that open to toluene itself.

Doubts remained that small amounts of impurities with anti-oxidant properties could be present that are able to inhibit the photobleaching. These could be sulfonated compounds residual from the cracking process or butylated hydroxytoluene (BHT), which is a well-known antioxidant commonly added to solvents as an inhibitor^[48] and food preservative^[49]. To

assuage these fears, photobleaching of both BOPHY-DMA and TM-BOPHY in highly purified toluene was performed. The toluene was purified by drying with sodium wire and distilling from sodium under a nitrogen atmosphere. In Figure 6.12 it is shown that no significant difference could be seen in the bleaching kinetics derived for either chromophore relative to that seen in spectrophotometric grade toluene.

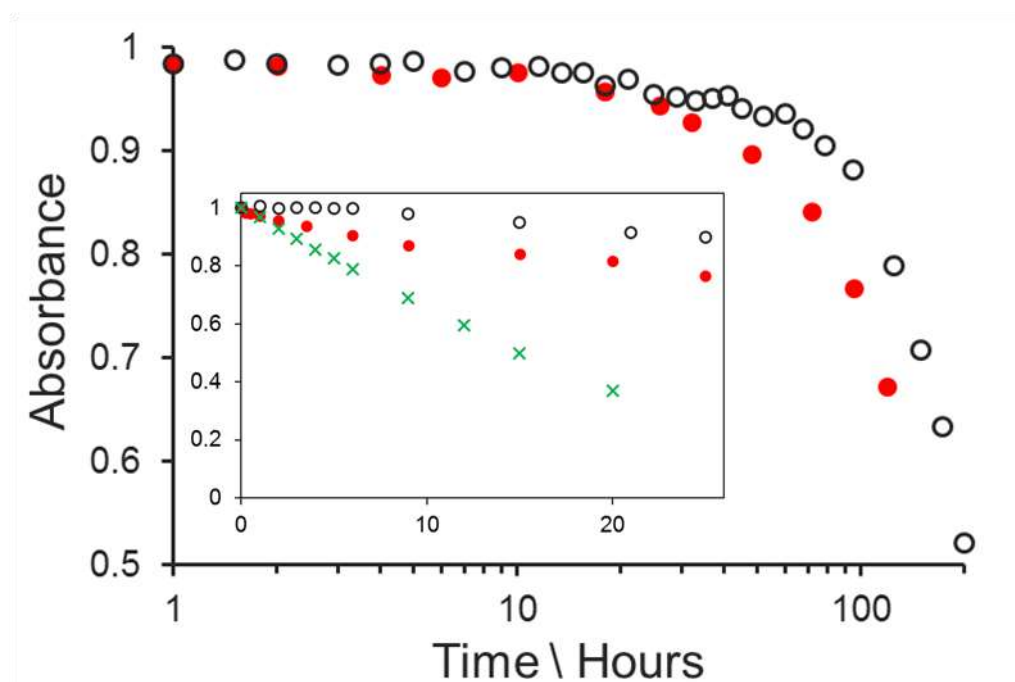


Figure 6.12 - Semi-log plot of bleaching kinetics of TM BOPHY in spectrophotometric grade toluene (O) and highly purified toluene (●). Inset is the equivalent data for BOPHY-DMA, (X) is bleaching in anisole included for reference.

This realisation that the environment provided by toluene is beneficial to the photostability of BOPHY molecules leads us to consider whether we can use the effect to engineer improved photostability in other situations. Toluene was mixed with cyclohexane and white light illumination repeated. At a loading of 10% v/v of toluene, the bleaching kinetics are adequately described by a first-order process in Figure 6.13, with $k_1=1.5 \text{ h}^{-1}$. In this case, the second step was not well resolved. This compares to a k_1 of 4.8 h^{-1} for cyclohexane only. Thus, addition of toluene leads to a 3-fold decrease in the rate of the initial bleaching step. At a loading of 33% v/v toluene, the rate reduces further to $k_1=0.011 \text{ h}^{-1}$ which approaches, although is still an order of magnitude greater than, that seen for pure toluene which is 0.001 h^{-1} . Further increase of the v/v amount of toluene lead to a rate indistinguishable from that seen for pure toluene.

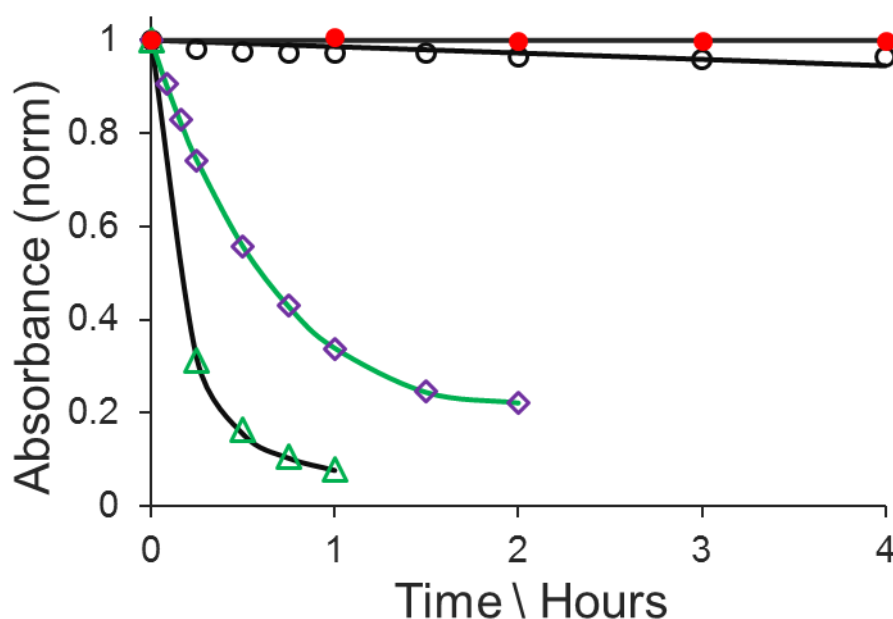


Fig 6.13 – Bleaching kinetics of toluene/cyclohexane mixtures, cyclohexane (Δ), 10% toluene (◇), 33% toluene (○) and toluene only (●).

To check if the presence of anti-oxidants is a viable protocol by which to protect chromophores against photobleaching, BHT was added to methylcyclohexane (MeCHX) solutions of BOPHY-DMA. Bleaching is highly efficient in MeCHX, similar to that found in cyclohexane, so there is plenty of scope for anti-oxidants to provide protection. Addition of BHT does indeed have a significant effect on the initial rate of photobleaching. At a weight loading of 1000ppm, the half-life for loss of chromophore increases from 40 minutes in MeCHX to 160 minutes in the mixture, shown in Figure 6.14. With 20% by weight of added BHT, the initial rate was severely inhibited but after only a short illumination period the rate began to increase and soon reached that seen for the sample in pure MeCHX. Part-bleached samples containing BHT left in the dark underwent total loss of colour due to a thermal reaction.

We can speculate that BHT intercepts whatever intermediates are responsible for bleaching of the chromophore. This, in turn, forms peroxide-containing products which serve to increase bleaching even in dark conditions. This is further borne out by the absorption spectra in Figure 6.15. Products are not seen when illumination is made in pure solvent or in the presence of low concentrations of BHT. In the case of the high loading of BHT, illumination causes the absorption profile to change significantly. Most notably, a blue-shifted product is formed, together with a second product displaying significant UV absorption. The primary product has a broad absorption spectral profile with a maximum at around 590nm. It features the typical BOPHY double-peak motif, suggesting that the chromophore retains the core of the BOPHY

nucleus and that the appendages are attacked first. This is similar to the case for photobleaching in MeTHF where changes in the absorption spectrum were ascribed to reaction with peroxides.

Addition of significant amounts of stabiliser protects the chromophore for a short period but results in catalysed degradation at longer exposure times. To achieve this effect, it is necessary to employ high loadings of the anti-oxidant, so trace impurities cannot be responsible for the stabilisation seen in toluene. Furthermore, the high concentration needed and the onset of dark reactions mean that this approach does not appear to be viable for chromophore protection.

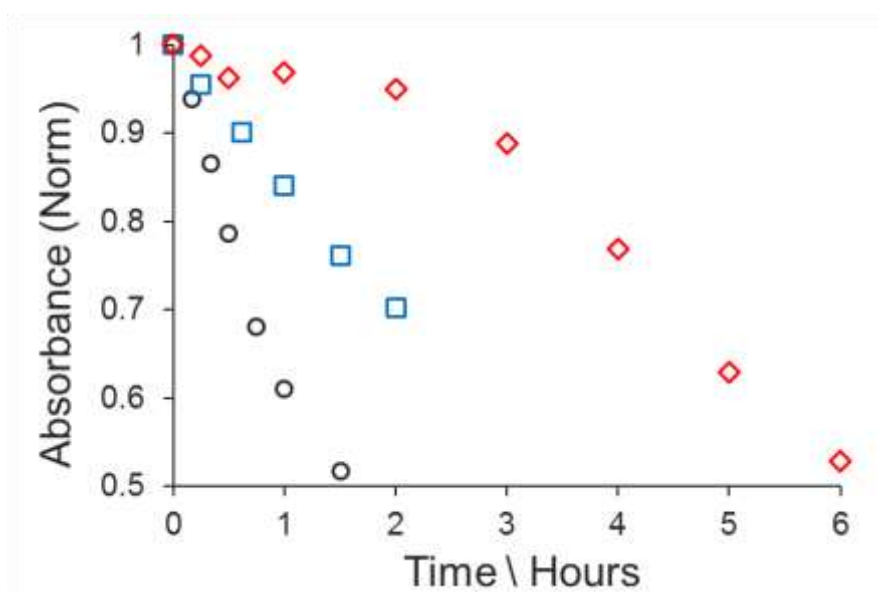


Figure 6.14 - Effect of addition of BHT on bleaching rate of BOPHY-DMA in methylcyclohexane, solvent only (O), 1000ppm (□) and 20% w/w (◇).

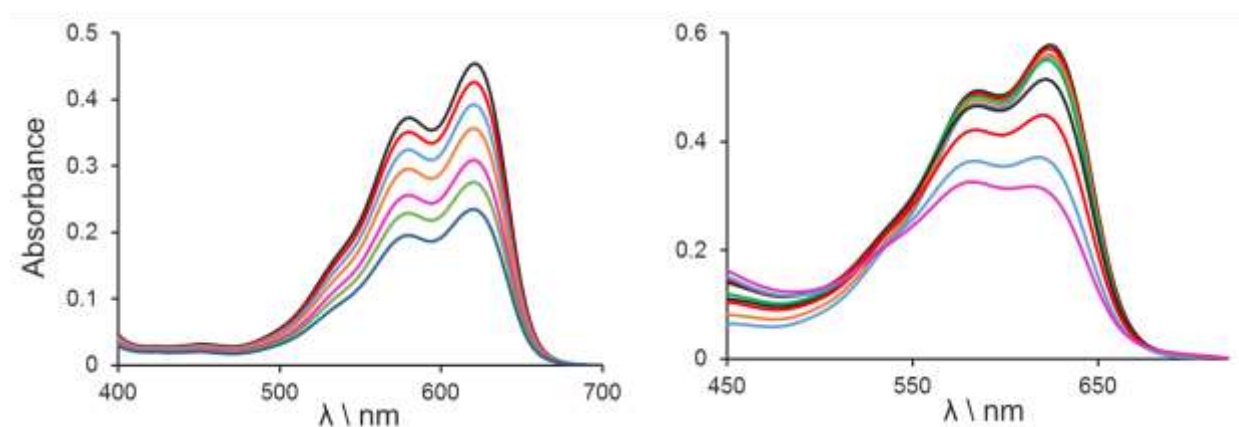


Figure 6.15 – Left, bleaching overlay in MeCHX only, loss of chromophore proceeds with no formation of product. Right, addition of 20% w/w BHT, the formation of coloured products is clear from the spectral changes.

6.4.2 TM-BOPHY-Solvent Interactions Probed by NMR Spectroscopy

The stabilisation effect seen in toluene could not be explained by bulk solvent properties nor is it due to problems with impurities. Thus, it could be the case that there is a specific solute-solvent interaction that does not affect the photophysical properties. To try to understand the molecular environment, high-resolution NMR spectroscopy was used compare the cases where TM-BOPHY is dissolved in aromatic solvents and in chloroform. ^1H and ^{13}C NMR was performed in C_6D_6 and toluene- D_8 and the chemical shifts compared to the shifts seen in CDCl_3 . The results in the aromatic solvents indicate some significant shifts compared to CDCl_3 and are largely similar to each other (Table 6.3), Figure 6.16 gives the numbering system while the spectra are provided in Figure 6.17.

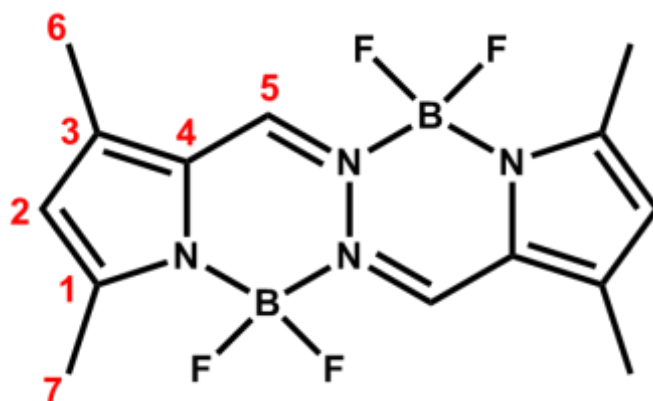


Figure 6.16 – BOPHY structure with atomic assignments

Atom	Chemical Shifts \ ppm				
	CDCl_3	$d_8\text{-tol}$	$\Delta\delta^{(a)}$	C_6D_6	$\Delta\delta^{(b)}$
H6	2.33	1.59	-0.74	1.52	-0.81
H7	2.49	2.32	-0.17	2.34	-0.15
H2	6.18	5.58	-0.6	5.56	-0.62
H5	7.93	7.82	-0.11	7.89	-0.04
C6	11.3	10.2	-1.1	10.3	-1
C7	14.3	13.9	-0.4	14	-0.3
C2	118.7	118.3	-0.4	118.4	-0.3
C4	123.5	123.8	0.3	123.7	0.2
C5	134.7	135	0.3	135.1	0.4
C3	141.2	140.9	-0.3	141.1	-0.1
C1	151.4	150.8	-0.6	151	-0.4

Table 6.3 – Chemical shifts of the protons and carbon atoms in TM BOPHY, (a) is the difference between deuterated chloroform and toluene, (b) is the difference between chloroform and benzene.

Protons H2 and H6, in particular, show a difference in the aromatic solvents compared to CDCl_3 . They are shifted up-field so are more shielded. The carbon shielding other than C4 and C5 shows a similar effect in terms of chemical shift as is seen for the protons. That the shifts are of similar magnitude indicates that the nuclei are exposed to the axial component of the diamagnetic anisotropy of the solvent^[50], or, in other words, the ring current is perpendicular to the molecule, indicating that the solvent and the molecule are parallel to each other^[51]. Such interactions depend on the actual changes in the magnetic field experienced by the relevant nuclei which leads to similar ppm shifts for protons and carbon. If the effects were due to direct electronic causation these would be inductive in nature and the carbon shifts would be expected to be an order of magnitude greater.

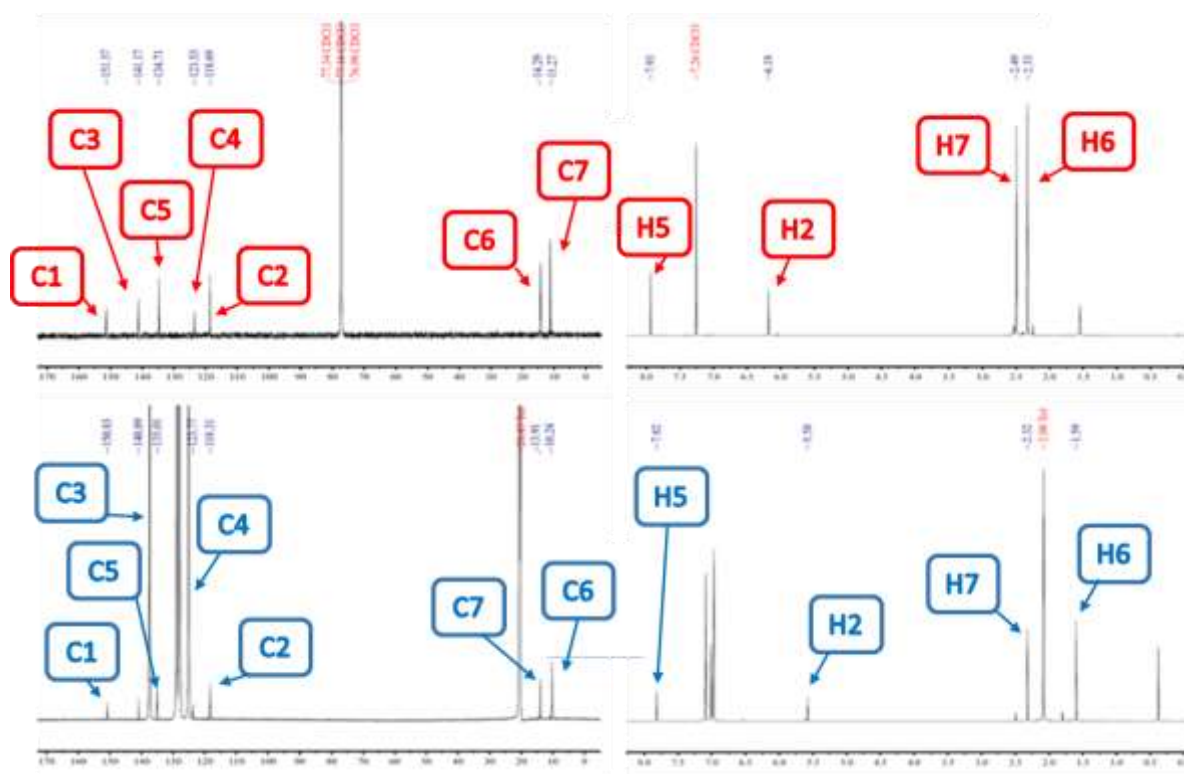


Figure 6.17 – NMR; Top, in CDCl_3 , bottom, in toluene- d_8 . The atoms displaying the important shifts are labelled.

Given the magnitude of the shifts recorded and the values at each atom, a visualization of the dynamic interaction between a benzene solvent molecule and TM-BOPHY is shown in Figure 6.18. As TM-BOPHY is essentially planar and symmetrical, there would be four such interactions per solute molecule in each of the equivalent positions. Such organisation of the

solvent molecules surrounding the solute could quite conceivably inhibit solute-solute stacking or the ability of the solute molecules to come into orbital contact.

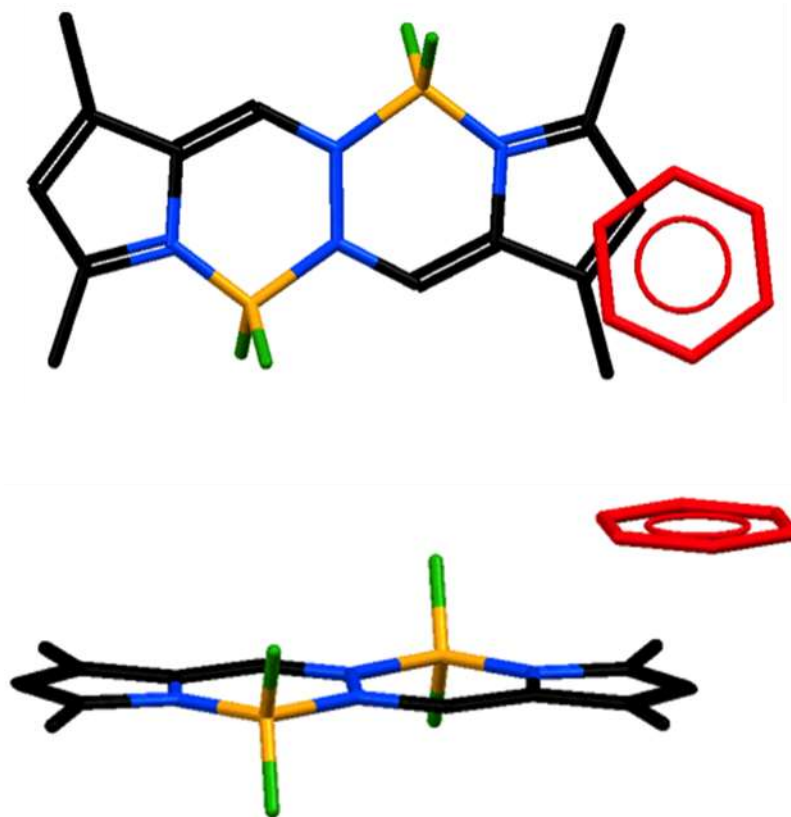


Figure 6.18 – Upper image is a qualitative depiction of the interaction between a benzene molecule and TM BOPHY. It is of course only 1 of 4 benzene molecules that could interact with the solute. The lower panel shows the orthogonal view of the same arrangement. Note the colour scheme, black = carbon, blue = nitrogen, yellow = boron and green = fluorine.

Building on this proposed arrangement allows us to develop a mechanism for the bleaching of TM-BOPHY. Speculatively, it seems that bleaching requires a specific bimolecular reaction. This may be true for the initial bleaching step and must be true for the self-catalysed secondary step. If the solute molecules are stacked in a regular fashion with the solvent molecules, keeping the chromophores apart, then it becomes unlikely that the optimal transient structures needed for photobleaching will occur. This behaviour, which cannot be gleaned from optical methods, is a plausible explanation of the protection offered by toluene and is not generally relevant to other solvents. Anisole and benzonitrile also have aromatic character so are worthy of further consideration. In the less polar anisole, the rate is rather slower than in benzonitrile although the fluorescence lifetime is approximately three times greater in anisole. Anisole is similar in geometry to toluene, so it is fair to assume that stacking between the solvent and

solute will be similar. In benzonitrile, the cyanide group may provide excellent solvency to the molecule disrupting any potential stacking.

6.5 Conclusion

If it is to become possible to routinely use organic dyes for energy harvesting purposes or any of the other myriad uses described beforehand then it is imperative that they show robust stability toward white light illumination. It has been shown that photobleaching can proceed from the excited-singlet state without involvement of the triplet manifold. This is an important point because of the widely held view that it is the triplet-excited state that promotes promiscuous reactions in the presence of molecular oxygen. This generalisation has led to strategies for built-in protection against photobleaching that are selective for the triplet-excited state. In fact, molecular oxygen plays a critical role in the bleaching chemistry. Both the dyes studied here could be stabilised by the simple protocol of their inclusion in a PMMA matrix. This approach minimises diffusional contact between dye molecules and restricts contact with molecular oxygen. Further protection could be introduced through the use of engineering methods such as adding screens or filters, together with the serendipitous identification of “light-fast” dyes. A significant finding from our studies relates to the addition of anti-oxidants as stabilisers. Protection is limited to the early stages of reaction and our results indicate that, over prolonged illumination, auto-catalysis will eventually take over. This is a warning that photobleaching studies should be carried out over inordinately long periods and not rely on long extrapolations.

We have raised the suggestion that dyes possessing extended conjugation pathways are more likely to undergo photodegradation than analogous dyes lacking the unsaturated chains. Indeed, in certain cases, photodegradation was shown to develop blue-shifted BOPHY products arising from attack along the styryl arms. We have not, as yet, provided confirmatory evidence for the claim and the literature is somewhat conflicting in this respect. We have, however, been more successful in establishing a correlation between the rate of photobleaching and the excited-state lifetime of the dye. This has been achieved by using the same dye, thereby making comparisons more easily. The dye in question is subject to intramolecular charge-transfer interactions because of the terminal amino groups. The excited-state lifetime, and the fluorescence quantum yield, are strongly affected by the polarity of the solvent. In polar media, charge-separated resonance forms become more pronounced and offer protection against photobleaching. This is a nice demonstration of the importance of using photophysical data to develop light-fast dyes. It comes at the cost of decreased fluorescence, however, so it might not be a universal solution. The idea of minimising the excited-state lifetime remains valid. This notion leads to the conceptual molecular cascade

devices whereby an array of chromophores is designed to facilitate successive electronic energy transfer steps. The lowest-energy acceptor fulfils the role as terminal site and is the only chromophore with a long-lived excited state. This becomes the vulnerable dye in the circuit and must be set up so as to rapidly offload its excitation energy to the device.

The most striking result reported here refers to the stabilisation of both TM-BOPHY and BOPHY-DMA by toluene and to a lesser extent by anisole. We have attributed this effect to stacking between solute and solvent acting to prevent close approach of two solute molecules. Further engineering would surely present us with the possibility of keeping the molecules very stable. Some form of mass ordering should be possible by use perhaps of aromatic polymers or a specific host that could provide for intercalation. This should not be a difficult challenge to the materials chemist. At the same time, we note that polymer-bound dye could be prepared by *in-situ* polymerisation rather than dispersal in a pre-formed polymer. Work along these lines is underway with Dr. J.G. Knight of Newcastle University.

References

- [1] W. W. Wilson, J. R. Heitz, *J. Agric. Food Chem.* **1984**, 32, 615-617.
- [2] J. Moan, K. Berg, *Photochem. Photobiol.* **1991**, 53, 549-553.
- [3] T. Nagano et al. *Chem. Commun.* **2011**, 47, 10055-10057.
- [4] J. Widengren, R. Rigler, *Bioimaging*, **1996**, 4, 149-157.
- [5] T. Aarthi, G. Madras, *Ind. Eng. Chem. Res.* **2007**, 46, 7-14.
- [6] C. Chen, W. Ma, J. Zhao, *Chem. Soc. Rev.* **2010**, 39, 4206-4219.
- [7] R. Roy, S. Hohng, T. Ha, *Nat. Methods*, **2008**, 5, 507.
- [8] E. Yariv, S. Schultheiss, T. Saraidarov, R. Reisfeld, *Opt. Mater.* **2001**, 16, 29-38.
- [9] P. Meallier, S. Guittonneau, C. Emmelin, T. Konstantinova, *Dyes Pigm.* **1999**, 40, 95-98.
- [10] C. Eggeling, L. Brand, C. A. M. Seidel, *Bioimaging*, **1997**, 5, 105-115.
- [11] D. Beer, J. Weber, *Opt. Commun.* **1972**, 5, 307-309.
- [12] F. Song, X. Peng, E. Lu, R. Zhang, X. Chen, B. Song, *J. Photochem. Photobiol. A*, **2004**, 168, 53-57.
- [13] B. Hinkeldey, A. Schmitt, G. Jung, *ChemPhysChem*, **2008**, 9, 2019-2027.
- [14] E. J. Holborow et al. *J. Immunol. Methods*, **1982**, 55, 231-242.
- [15] L. Song, E. J. Hennink, I. T. Young, H. J. Tanke, *Biophys. J.* **1995**, 68, 2588.
- [16] L. Song, C. A. Varma, J. W. Verhoeven, H. J. Tanke, *Biophys. J.* **1996**, 70, 2959-2968.
- [17] H. Giloh, J. W. Sedat, *Science*, **1982**, 217, 1252-1255.
- [18] T. Hirschfeld, *Appl. Opt.* **1976**, 15, 3135-3139.
- [19] P. C. Beaumont, D. G. Johnson, B. J. Parsons, *J. Chem. Soc. Faraday Trans.* **1993**, 89, 4185-4191.
- [20] J. Weber, *Opt. Commun.* **1973**, 7, 420-422.
- [21] I. Rosenthal, *Opt. Commun.* **1978**, 24, 164-166.
- [22] S. L. Murov, I. Carmichael, G. L. Hug, *Handbook of Photochemistry*, CRC Press, **1993**.
- [23] T. G. Pavlopoulos, M. Shah, J. H. Boyer, *Appl. Opt.* **1988**, 27, 4998-4999.
- [24] F. Amat-Guerri et al. *Chem. Phys. Lett.* **1999**, 299, 315-321.
- [25] A. Dubois, M. Canva, A. Brun, F. Chaput, J.-P. Boilot, *Synth. Met.* **1996**, 81, 305-308.
- [26] W. N. Sisk, N. Ono, T. Yano, M. Wada, *Dyes Pigm.* **2002**, 55, 143-150.
- [27] K. Dasgupta et al. *J. Org. Chem.* **2008**, 73, 2146-2154.

- [28] B. P. Wittmershaus et al. *J. Fluoresc.* **2001**, 11, 119-128.
- [29] M. S. Mackey, W. N. Sisk, *Dyes Pigm.* **2001**, 51, 79-85.
- [30] M. D. Rahn, T. A. King, A. A. Gorman, I. Hamblett, *Appl. Opt.* **1997**, 36, 5862-5871.
- [31] W. Li, L. Li, H. Xiao, R. Qi, Y. Huang, Z. Xie, X. Jing, H. Zhang, *RSC Adv.* **2013**, 3, 13417-13421.
- [32] T. Yogo, Y. Urano, Y. Ishitsuka, F. Maniwa, T. Nagano, *J. Am. Chem. Soc.* **2005**, 127, 12162-12163.
- [33] A. Cui, X. Peng, J. Fan, X. Chen, Y. Wu, B. Guo, *J. Photochem. Photobiol. A*, **2007**, 186, 85-92.
- [34] G. Jung et al. *ChemPhysChem*, **2016**, 17, 433-442.
- [35] B. R. Renikuntla, H. C. Rose, J. Eldo, A. S. Waggoner, B. A. Armitage, *Org. Lett.* **2004**, 6, 909-912.
- [36] G. Qian, Y. Yang, Z. Wang, C. Yang, Z. Yang, M. Wang, *Chem. Phys. Lett.* **2003**, 368, 555-560.
- [37] M. Faloss, M. Canva, P. Georges, A. Brun, F. Chaput, J.-P. Boilot, *Appl. Opt.* **1997**, 36, 6760-6763.
- [38] C. Eggeling, J. Widengren, R. Rigler, C. A. M. Seidel, *Anal. Chem.* **1998**, 70, 2651-2659.
- [39] D. N. Nikogosyan, *Laser Chem.* **1987**, 7, 29-34.
- [40] J. R. Saylor, *Exp. Fluids*, **1995**, 18, 445-447.
- [41] R. L. Atkins et al. *Opt. Commun.* **1974**, 11, 352-355.
- [42] J. D. Spikes, *Photochem. Photobiol.* **1992**, 55, 797-808.
- [43] J. Mohanty, W. M. Nau, *Angew. Chem. Int. Ed.* **2005**, 117, 3816-3820.
- [44] C. Yu, L. Jiao, P. Zhang, Z. Feng, C. Cheng, Y. Wei, X. Mu, E. Hao, *Org. Lett.* **2014**, 16, 3048-3051.
- [45] F. Mata-Perez, J. F. Perez-Benito, *J. Chem. Educ.* **1987**, 64, 925.
- [46] P. B. Merkel, D. R. Kearns, *J. Am. Chem. Soc.* **1972**, 94, 1029-1030.
- [47] J. R. Hurst, J. D. McDonald, G. B. Schuster, *J. Am. Chem. Soc.* **1982**, 104, 2065-2067.
- [48] S. E. Çelik, M. Özyürek, K. Güçlü, R. Apak, *Talanta*, **2010**, 81, 1300-1309.
- [49] J. J. Kabara, *J. Food Prot.* **1981**, 44, 633-647.
- [50] C. E. Johnson Jr, F. A. Bovey, *J. Chem. Phys.* **1958**, 29, 1012-1014.
- [51] W. McFarlane, *J. Chem. Soc. D*, **1970**, 418-419.

Chapter 7 – Covalently-Modified BOPHY Derivatives

7.1 Introduction

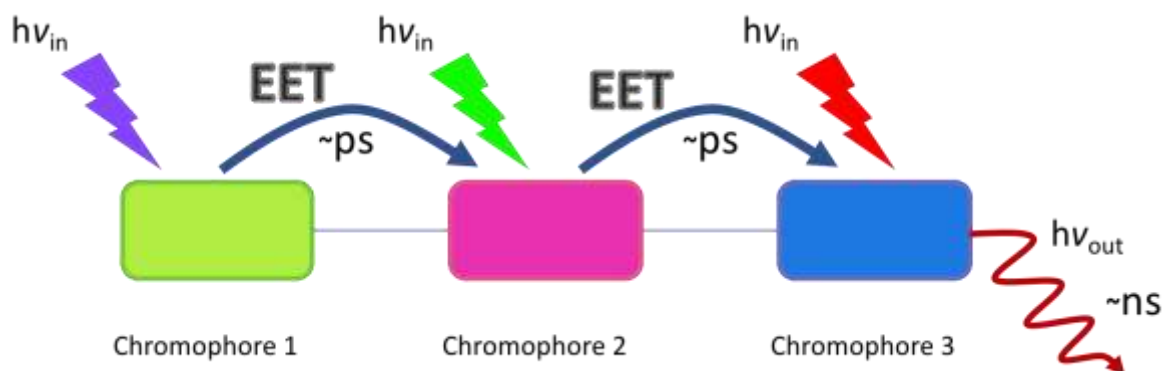
The structure of the BOPHY core allows for both the extension of the conjugation path along a linear backbone but also leaves free the central β -positions so that appendages can be attached at these sites. We have designed a BOPHY-based dyad where the BOPHY molecule is red shifted upon inclusion of styryl functionalised polyethylene glycol chains. A perylene moiety can be attached to the BOPHY so as to form a donor-acceptor dyad. Numerous related derivatives are possible. Here, we simply set out to establish the viability of using BOPHY as the central platform.

The simplest method to make use of organic molecules for harvesting photonic energy is the luminescent solar collector^[1], which can be coupled to some further device. It is not plausible, in such an arrangement, to effectively collect light using a single chromophore^[2]. To harvest sufficient light would require very high densities of the chromophore, this will then incur the well-known penalties associated with high chromophore concentration, most notably excessive self-absorption and the possibility of quenching through aggregation. The design of light-harvesting arrays that to some extent mimic natural light-harvesting systems for photosynthesis has been of considerable interest^[3], particularly since the turn of the century. An effective collector molecule will need strong absorption across the visible-light region of the spectrum^[4], and ideally extending into both the near-UV and near-IR regions. No single chromophore exists that displays such an absorption profile, so systems based on multiple chromophores have been designed whereby electronic energy transfer is used to pass excitons along a gradient. In this way, light may be retrieved by emission at the most red-shifted part of the assembly or the exciton can be used to sensitise, for example, a coupled photovoltaic device. The design of such collectors ranges from relatively simplistic models, like dyads linked by some conjugated bridge, linear arrays and to highly elaborate architectures based on dendrimeric scaffolds^[5] bearing many different chromophores. Early designs were generally based on porphyrins^[6], phthalocyanines^[7], fullerenes^[8] and organometallics^[9]. Given their multiple absorption peaks and their occurrence in Nature, this seems a logical strategy. Notably, the concept of electronic energy transfer can apply to either singlet or triplet states but greater photostability of excited-singlet state systems is anticipated. Other common chromophores used include rylenes^[10, 11], Coumarins^[12] or Rhodamines. The emergence of the BODIPY family has led to many systems^[13, 14] based on this type of chromophore. The main appeal of BODIPY being the tunability of the absorption spectrum,

the intense absorption profile and high fluorescence quantum yields. In the broadest terms, the systems may transfer energy by either through-space or through-bond mechanisms. Through-space systems are controlled by the “FRET” mechanism and covalent attachment allows control of the distance between the chromophores. In contrast, the through-bond systems transfer electronic energy through a conjugated bridge and often involve some type of super-exchange interactions. Electronic energy transfer (EET) in those systems with conjugated bridges can be extremely efficient, indeed it seems that EET probabilities of around 99% are commonplace^[15], but the transfer distances are quite short.

Whilst there are occasional claims for individual parts of the systems being ‘*photostable*’ such notions tend to be unsubstantiated. The role of the physical design of a light harvester bears some important considerations in terms of stability. A dyad is of course a simple system and the absorptivity will not be increased sufficiently compared to individual chromophores for these systems to be anything more than models. It is interesting to consider to what extent dyads act as a pair of chromophores in communication or whether, in cases where there is a high level of conjugation running through the bridge, a new supermolecule emerges. Linear arrays^[16] are fundamentally flawed in terms of practical light harvesting. If any one part of the array becomes damaged then the whole system is put out of operation and the array is dormant. This explains the prevalence of dendrimer or V-shaped arrangements. Here, there can be two or more pathways leading to the terminating unit. This introduces some level of redundancy^[17] in that if there is damage along a pathway the array will remain functional. Elaborate systems therefore have a certain amount of built-in stability.

Some reports have looked at the effects of white-light illumination and found that there was photochemical conversion^[18] of the harvester to new chromophores. This is an elegant, even though serendipitous, solution to the stability problem. Ultimately, there will be loss of efficiency for the system when used with or as a device. Equally worryingly is the possibility that photochemical products^[19] may be catalysts for further chromophore loss. Intrinsically, light-harvesting systems are vulnerable in terms of photostability. By thermodynamic necessity higher-energy chromophores must pass their energy sequentially to the most red-shifted chromophore. Therefore, the final chromophore is the one that will spend the most time in the excited state and will most likely be the least stable unit. This is outlined here in Scheme 1.



Scheme 1 – Simplified 3-chromophore array whereby chromophore 1 passes electronic energy to 2 and then from 2 to 3. Emission will arise from chromophore 3. If EET steps are relatively fast, only 3 is in the excited state for any significant period of time.

In a particularly simple form^[20] the above situation was studied to see the effects of intermolecular energy transfer on photostability. Three different BODIPY dyes were dispersed into a polymer matrix so that the two blue-shifted absorbers can transfer excitation energy to the most red-shifted BODIPY by the FRET mechanism. Interestingly in this case the final BODIPY was the most stable in isolation while the most blue-shifted chromophore was the least stable. Operating the three in unison stabilised the two donor molecules whilst slightly destabilising the acceptor and the overall stability of the system was largely dependent on the properties of the final acceptor molecule. Whilst a disordered system based on FRET between unattached molecules cannot be a viable solution for solar collection, it demonstrates the fact that photophysical and photochemical properties of the final acceptor are important factors in any light-harvesting array. It has also been shown that the photostability of magnesium porphyrin^[21] was found to be significantly stabilised under white-light when attached to a fullerene which is presumably due to the porphyrin excited state being rapidly quenched by way of EET and/or light-induced electron transfer.

In this chapter we introduce a new type of extended BOPHY derivative where increased solubility is assured by the inclusion of poly(ethylene glycol) (PEG)^[22] chains, the structure is in Figure 7.1. These chains are intended to minimise self-association while improving the dispersion characteristics of the dye in plastic films. The terminal units are considered to be weak electron donors^[23]. This allows comparison with systems studied earlier where strong intramolecular charge-transfer interactions run along the molecular backbone. To improve the light harvesting capacity, a second dyad is reported where perylene has been linked to the central BOPHY core also shown in Figure 7.1. It is of particular interest to consider how bleaching proceeds in this latter dyad under conditions of selective excitation. At a naïve level, we might expect quantitative^[24] electronic energy transfer from perylene to BOPHY. This, in

turn, would drastically shorten the excited-state lifetime of the perylene unit and thereby provide increased stability against direct photo-damage.

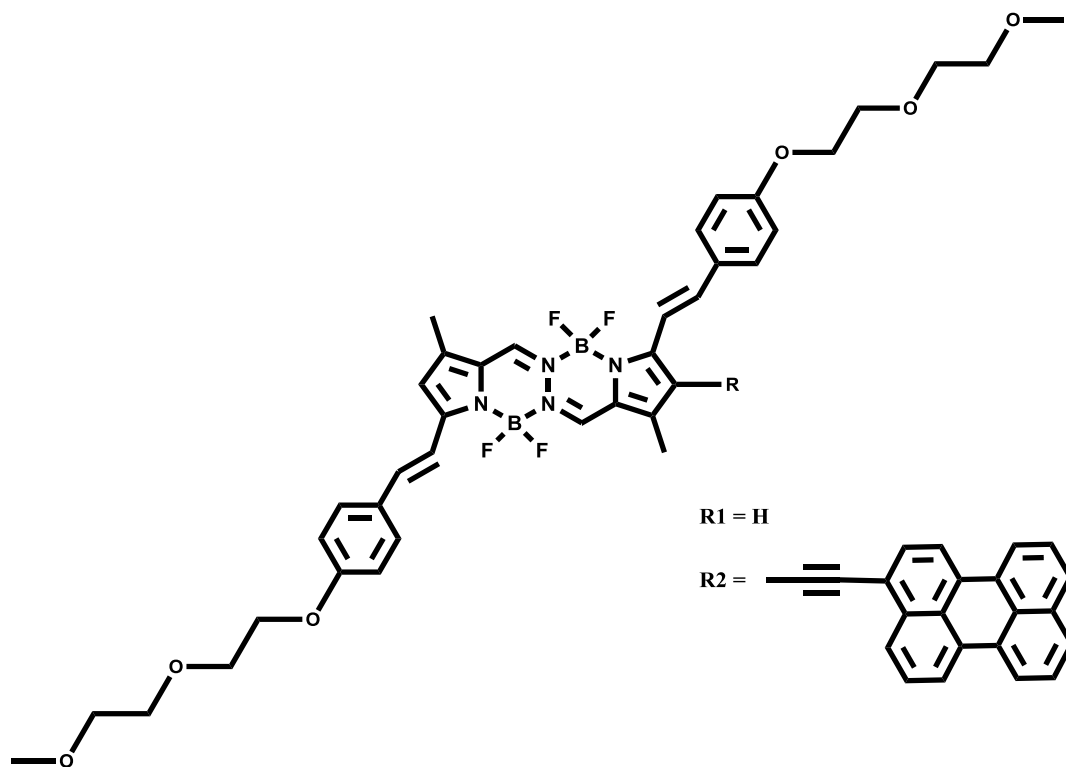


Figure 7.1 – Chemical formulae for PEG-BOPHY and for the perylene-BOPHY molecular dyad studied in this chapter.

7.2 PEG-BOPHY

7.2.1 Photophysical Properties of PEG-BOPHY

The absorption maximum for PEG-BOPHY shows a significant red-shift compared to the parent dye as might be expected on the basis of the conjugation length being extended. The absorption maximum lies at around 585nm and the corresponding emission maximum is at 615nm in MeTHF seen in Figure 7.2. These values correspond to a red shift of approximately 120nm from the position of TM-BOPHY. The molar absorption coefficient is $46,000 \text{ M}^{-1}\text{cm}^{-1}$ at the absorption maximum. From this value, we can derive an oscillator strength of 1.10 and a natural lifetime based on the Strickler-Berg expression of 5.5ns. In MeTHF, the fluorescence quantum yield is 0.34 and the excited-singlet state lifetime is 1.9ns. The increase in dipole moment on excitation is 4.3D as calculated from the Lippert-Mataga plot shown in Figure 7.3. The absorption profile shows the characteristic BOPHY double peak profile and the excitation

spectrum is a good match for the absorption spectrum, the slight difference being attributable to the lack of a reliable quantum counter in this wavelength range^[25].

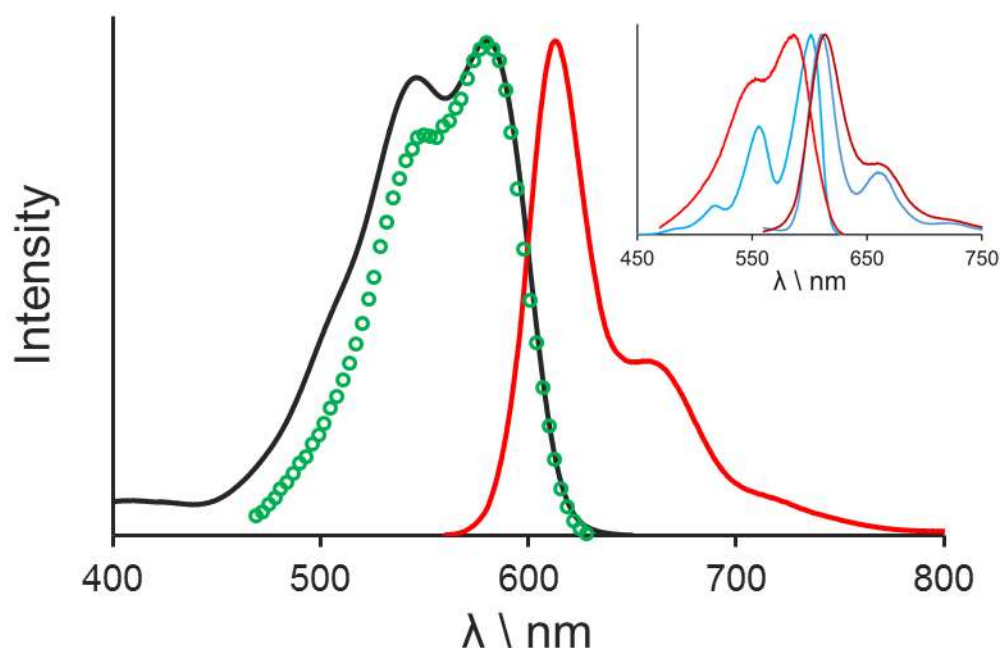


Figure 7.2 – Absorption (—), excitation (○) and emission (—) spectra recorded for PEG-BOPHY in MeTHF. The inset shows the effect of lowering the temperature to 77K. Note that the effect due to the second optical transition is also seen in this dye.

Solvent	Φ_f	$\tau_f \text{ ns}$	$k_r \text{ } 10^8 \text{ s}^{-1}$	$k_{nr} \text{ } 10^8 \text{ s}^{-1}$	$\lambda_{abs} \text{ nm}$	$\lambda_{fluo} \text{ nm}$	Stokes' Shift cm^{-1}
MeCyclohex	0.41	2.0	2.1	3.0	581	605	680
Toluene	0.38				586	612	720
Chloroform	0.34	2.0	1.7	3.4	586	614	780
MeTHF	0.34	1.8	1.9	3.6	580	611	870
Acetone	0.30				572	613	1170
Butyronitrile	0.29	1.6	1.8	4.5	573	614	1170
Acetonitrile	0.22	1.4	1.6	5.5	568	609	1190
Ethanol	0.3	1.7	1.8	4.2	570	610	1150
DMSO	0.23	1.5	1.6	5.2	580	622	1160
Formamide	0.18	1.0	1.9	8.6	575	619	1240

Table 7.1 – Variation of the photophysical properties of PEG-BOPHY in a range of organic solvents.

The fluorescence quantum yields were measured using the ratiometric technique, relative to Merocyanine 540 in ethanol solution^[26] ($\Phi_f = 0.16$), with the usual precautions being taken. The fluorescence quantum yield approximately doubles on going from acetonitrile to methylcyclohexane at room temperature, the properties in various solvents is collated in Table

7.1. From this change in quantum yield, it appears that weak charge-transfer character is present in the molecule. The radiative rate constant does not change notably across the series of solvents but, in general, is higher in the less polar media.

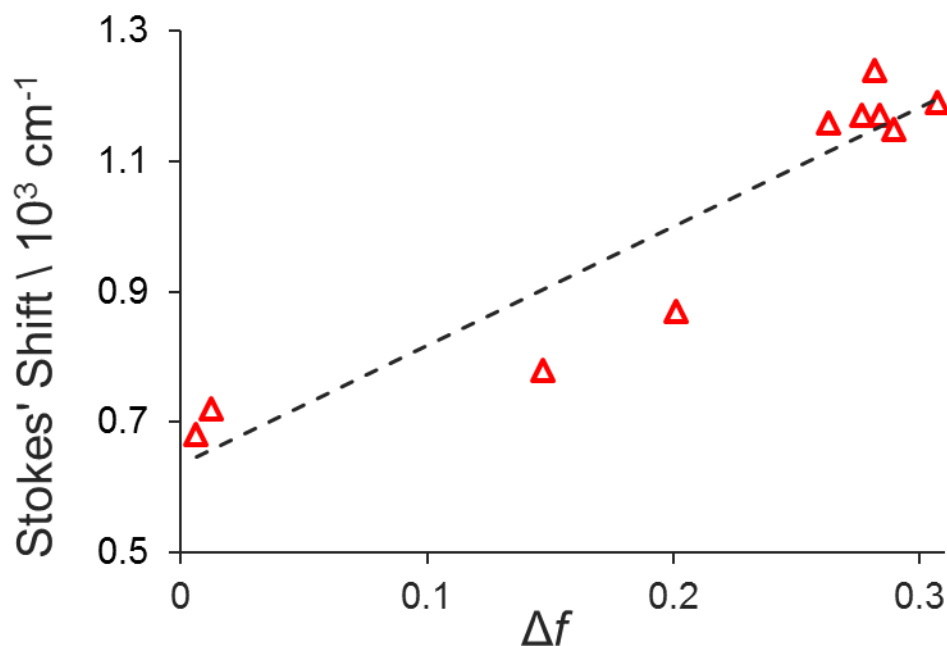


Figure 7.3 – Lippert-Mataga plot for PEG-BOPHY, corresponding to a change in dipole moment on excitation of $\Delta\mu = 4.3D$. The solvent polarity is expressed as the Pekar function, Δf .

As for the parent TM-BOPHY compound, low-temperature phosphorescence was observed in the presence of a spin-orbit coupling promoter. Quenching of the inherent fluorescence is somewhat different than seen for TM-BOPHY in as much as it appears to correspond to a diffusion-controlled process demonstrated in Figure 7.4. The derived bimolecular rate constant for quenching by iodomethane is $2.3 \times 10^8 \text{ M}^{-1} \text{ s}^{-1}$, which is well below the diffusion controlled rate constant of $1 \times 10^{10} \text{ M}^{-1} \text{ s}^{-1}$ as calculated for small organic molecules in MeTHF. The idea that quenching by iodomethane involves dynamic processes was confirmed by the fact that the change in excited-singlet state lifetime mirrors that found for the emission quantum yield.

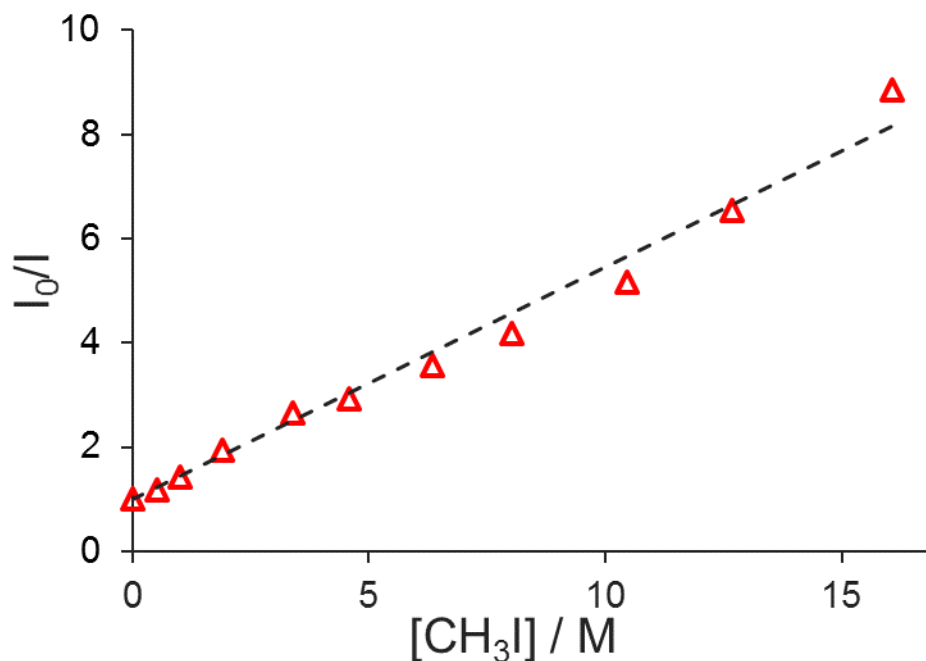


Figure 7.4 – Stern-Volmer plot for the quenching of PEG-BOPHY fluorescence by iodomethane in MeTHF.

7.2.2 Temperature-Dependent Measurements

Our understanding of the PEG-BOPHY chromophore is that the appendage introduces mild intramolecular charge-transfer character that gives rise to a modest solvent dependence. Even in nonpolar solvents, however, the fluorescence quantum yield falls well below unity and it is clear that there is some internal quenching of the excited-singlet state. This inherent quenching is not due to dimerization^[27] since the lifetime correlates nicely with the quantum yield and the absorption spectrum shows no characteristic broadening relative to that of TM-BOPHY. In an effort to better understand the photophysical properties of PEG-BOPHY, the fluorescence yield was recorded at temperatures down to 80K. Studies were made in both MeTHF and butyronitrile; the latter measurements being particularly successful. It is shown in Figure 7.5 that the fluorescence in butyronitrile decreases in intensity and is subject to some broadening. The excitation spectrum, examples of spectra recorded in MeTHF are shown, followed a similar trend to those of the parent, TM-BOPHY, where the low temperature region shows a well-resolved spectrum that appears to come from a single species which quickly changes as the solvent begins to melt.

The fluorescence spectrum recorded for PEG-BOPHY in butyronitrile at ambient temperature is broader and more diffuse than seen in MeTHF, probably because the increased polarity of the solvent favours charge-transfer character. On cooling, the spectral profile undergoes a small red shift and a progressive increase in intensity seen in Figure 7.5. The red shift is a

reflection of the increasing polarity of the solvent as the density increases. This effect continues throughout the liquid phase and can be quantified in terms of the energy of the 0,0 band also in Figure 7.5. Under these conditions, the excitation spectrum is poorly resolved but sharpens and undergoes a red shift on cooling. As the solvent begins to solidify, there is a marked blue shift for the emission maximum, accompanied by fine structure. The excitation spectrum also sharpens quite noticeably and shifts to the red. Thus, the Stokes' shift decreases markedly in the glassy matrix. Intensification of the fluorescence band continues throughout the glassy region. The band half-width decreases steadily with decreasing temperature and mirrors the glass transition temperature and rigidification of the solvent. The intramolecular charge-transfer character is curtailed in the rigid glass, leading to a small Stokes' shift and a much increased fluorescence quantum yield, demonstrated in Figure 7.6, at least in butyronitrile.

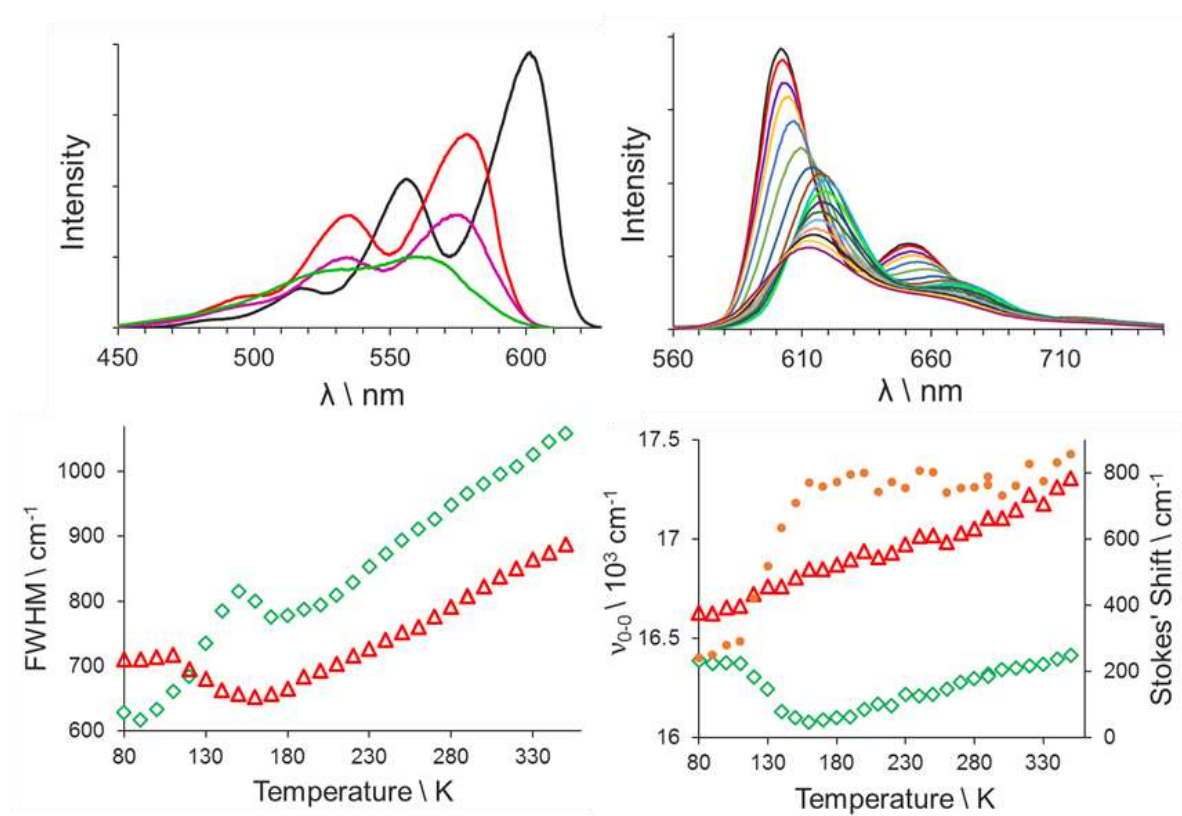


Figure 7.5 – Top left - Excitation spectra at 80K (—), 120K (—), 160K (—) and 350K (—) for PEG-BOPHY in MeTHF. Top right – Fluorescence spectra from 80K-340K in BuCN. Bottom Left, The change in FWHM of deconvoluted fluorescence in MeTHF (Δ), BuCN (\diamond), Bottom right, ν_{0-0} band position in MeTHF of excitation (Δ), fluorescence (\diamond) and Stokes' Shift (\bullet).

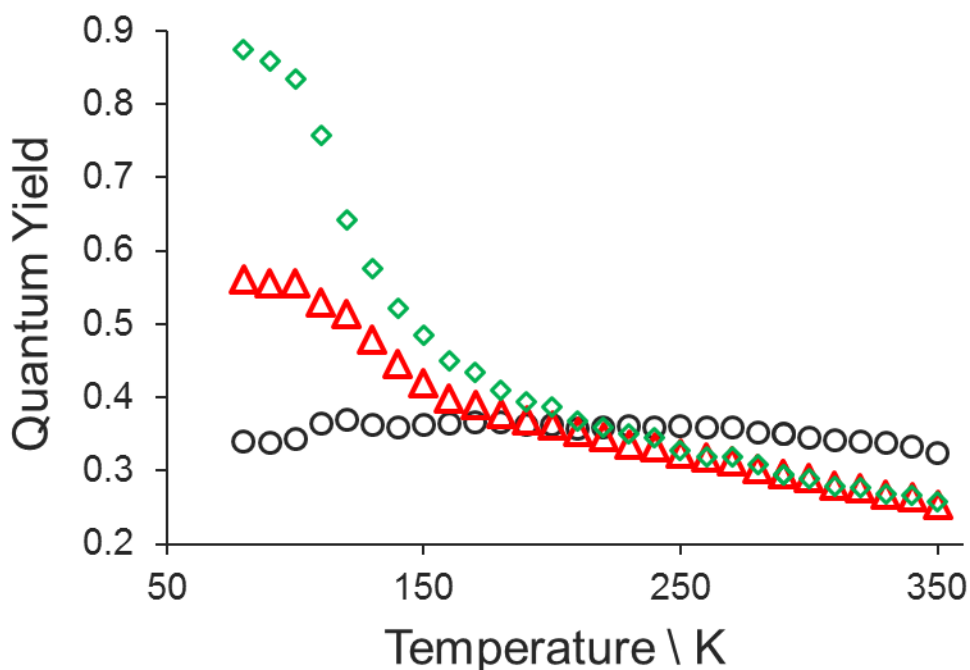


Figure 7.6 - Temperature dependence of PEG-BOPHY fluorescence quantum yield in butyronitrile (Δ) and MeTHF (\circ). Where absorption and density corrections are applied (\diamond) the fluorescence yield tends towards unity at the low-temperature limit.

For PEG-BOPHY in butyronitrile, the temperature was varied from 350K down to 80K. The fluorescence quantum yield recovered from 0.25 at the highest temperature to 0.56 at 80K. After correcting for changes in the density and spectral shifts accompanying cooling of the solvent, it appears that the “true” quantum yield at 80K is close to 0.9 in butyronitrile. Thus, the process that leads to fluorescence quenching at room temperature is shut down in the glassy matrix. The solvent undergoes a phase change at around 160K before forming a rigid glass at about 110K. As can be seen from Figure 7.6, the fluorescence yield tracks these changes. This is not the case in MeTHF where, as for the parent molecule, there could be an issue with limited solubility of the chromophore in the glass. This effect was not obvious in terms of spectral changes.

On the assumption that the radiative rate constant does not change with temperature, at least for the range over which the solvent remains liquid, the fluorescence quantum yields can be used to estimate the corresponding rate constant for non-radiative decay of the excited state. For both butyronitrile and MeTHF, the temperature dependence for these rate constants takes the form of Equation 7.1. Here, there is an activationless rate constant (k_0) that controls decay at low temperature and an activated process that becomes increasingly more important at elevated temperatures. This latter step can be explained in terms of a first-order rate constant (k_a) and an accompanying activation energy (E_a). Figure 7.7 gives the fitting of the data to this expression, allowing derivation of the appropriate rate constants. These values are compiled

in Table 7.2. Also included in the table are the corresponding values observed for PEG-BOPHY in formamide, although here only the high temperature region was covered.

$$k_{nr} = k_0 + k_a \cdot e\left(\frac{-E_a}{RT}\right) \quad (7.1)$$

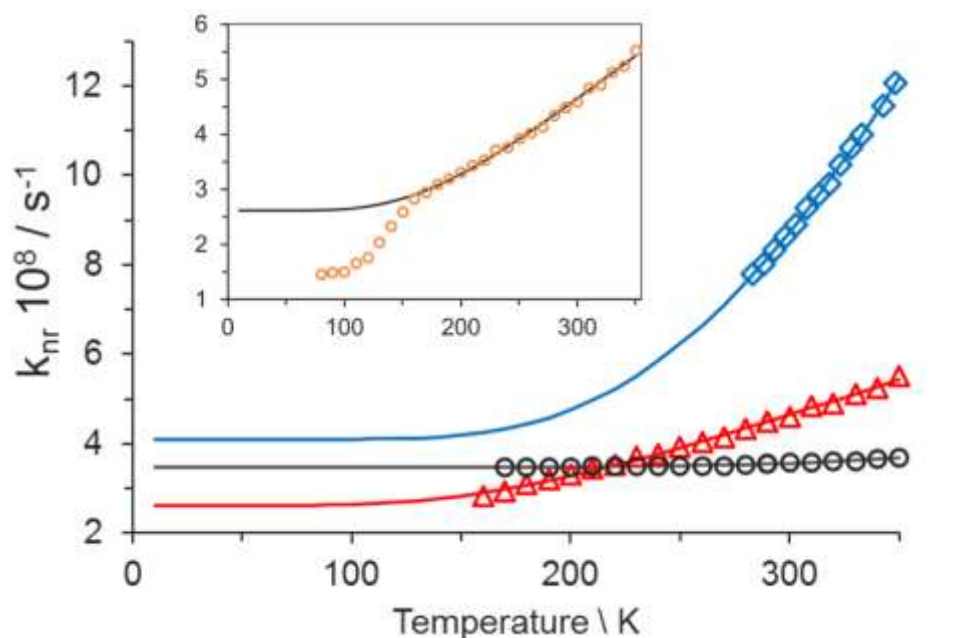


Figure 7.7 - Evolution of the non-radiative decay rate constant with temperature for PEG-BOPHY in BuCN (\blacktriangle), MeTHF (\bullet) and formamide (\blacklozenge) solid lines refer to a fit to Equation 7.1. Inset shows the data collected in butyronitrile at the low temperature region where the solvent solidifies.

Solvent	$k_0 \backslash 10^8 s^{-1}$	$k_a \backslash 10^{10} s^{-1}$	$E_A \backslash kJ mol^{-1}$
MeTHF	3.5	0.4	15.2
Butyronitrile	2.6	0.2	5.6
Formamide	4.1	2.3	9.7

Table 7.2 – Parameters derived from fitting the fluorescence data to Equation 7.1.

7.3 Photobleaching of PEG-BOPHY

The optical properties of PEG-BOPHY can be considered to reside somewhere between those of the two derivatives studied earlier. There is weak charge-transfer character, so we see some reduction of the fluorescent lifetime relative to the parent BOPHY in a polar solvent but the effect is significantly smaller than found for BOPHY-DMA. The expectation therefore is that there might be a modest solvent effect on the rate of photo-bleaching in solution. The absorption maximum recorded for PEG-BOPHY lies between those of the two other BOPHY-based molecules. This allows testing of our assertion that the rate of photo-bleaching will be

faster for compounds with the most red-shifted absorption profiles. This is a crude assumption, based only on the level of conjugation running along the molecular backbone.

7.3.1 Bleaching in Solid Media

As elsewhere in this thesis, the photostability of PEG-BOPHY was probed in a dried film cast from PMMA solution. To our surprise, bleaching was found to be rather efficient under these conditions, where broadband illumination was used. An example of overlaid absorption spectral profiles is shown below as Figure 7.8. Clearly, formation of a stable product accompanies bleaching of the PEG-BOPHY chromophore. The absorption spectrum for this product is blue shifted from that of the original chromophore. Photobleaching was conducted over a total of 34 hours, by which point the PEG-BOPHY was almost fully converted to the product. As there is no maintenance of an isosbestic point during this conversion, we must be losing material in the form of non-absorbing products. The primary product displays the characteristic BOPHY absorption spectrum, thereby indicating to us that the core of the molecule is unaffected. The blue-shifted absorption spectrum suggests that one or both of the styryl arms have been attacked so as to shorten the overall conjugation length. It might be noted that the films were stored in the dark for a week prior to the photobleaching studies but were found to be completely stable.

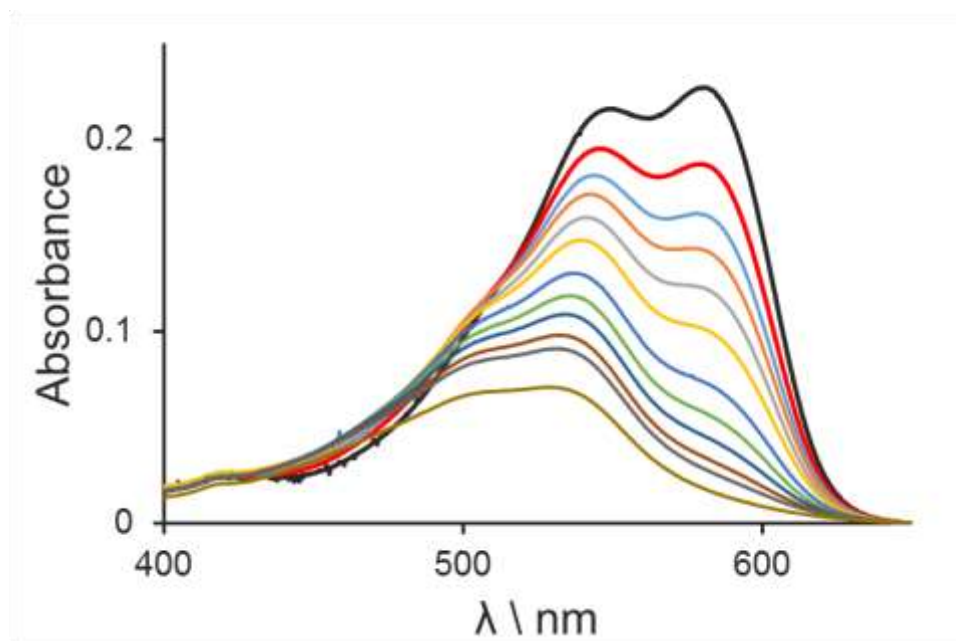


Figure 7.8 – Examples of overlaid absorption spectral profiles recorded during continuous photobleaching of PEG-BOPHY in a PMMA film.

These absorption spectral profiles were deconstructed on the basis of overlapping features due to PEG-BOPHY and the primary product, these are shown in Figure 7.9, with the spectrum of the former being known. This provides us with a good appreciation of the absorption

spectrum for the primary product. The absorption maximum lies between those of TM-BOPHY and PEG-BOPHY, suggesting that only one of the styryl arms has been damaged to the point where it no longer contributes to the conjugation length. Absorbance attributable to this product builds up quickly but reaches a plateau. Without knowledge of the respective molar absorption coefficients, it is not possible to comment on the conversion efficiency without raising some crude approximation. Thus, given the respective absorption spectral profiles, we can argue that the molar absorption coefficient for the primary product will be between the limits set by TM-BOPHY ($\epsilon_{\text{MAX}} = 35,000 \text{ M}^{-1}\text{cm}^{-1}$) and PEG-BOPHY ($\epsilon_{\text{MAX}} = 46,000 \text{ M}^{-1}\text{cm}^{-1}$). This gives us a working range for ϵ_{MAX} for the primary product of $40,000 \pm 6,000 \text{ M}^{-1}\text{cm}^{-1}$. Now, over the early stages of reaction, the rate of change of absorbance at the relevant wavelengths indicates that conversion of PEG-BOPHY to the primary product is less than quantitative. At early stages, the yield of the primary product corresponds to 60% of the amount of PEG-BOPHY lost. This conversion yield remains high for at least 7 hours but falls progressively as reaction proceeds. This finding is supported by the appearance of an initial isosbestic point at 505 nm, which becomes lost on longer illuminations.

At early stages of reaction, loss of PEG-BOPHY gives a good fit to a first-order process with a rate constant of 0.32 h^{-1} . The appearance of the primary product occurs on a comparable timescale (Figure 7.9), confirming that PEG-BOPHY is converted to the primary product. This product is reasonably stable towards illumination but does appear to degrade on long irradiations.

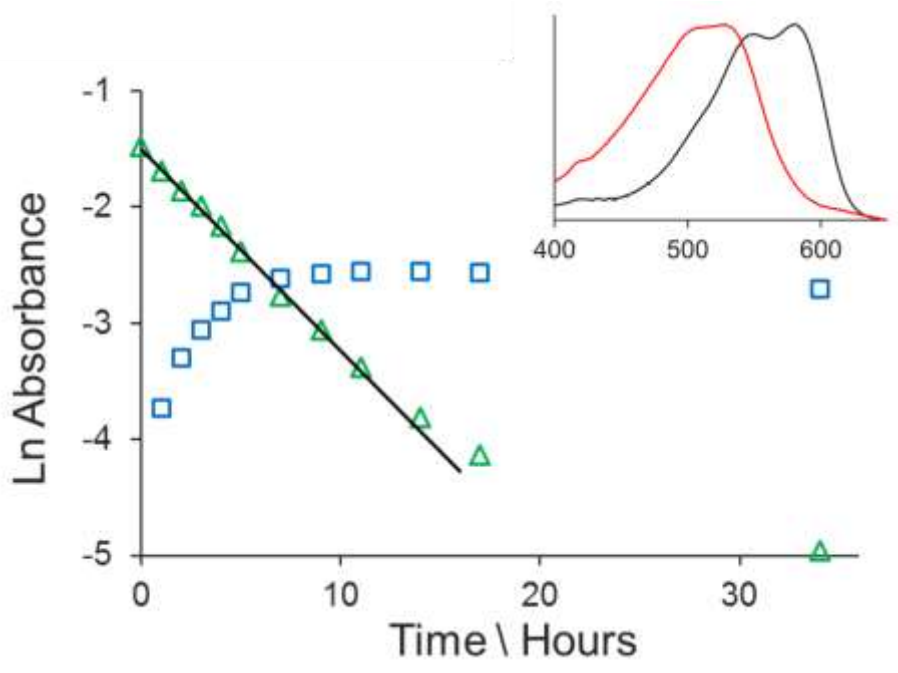


Figure 7.9 – Bleaching of PEG-BOPHY in a PMMA matrix (Δ) and evolution of product (\square) over time. Inset shows the absorption spectrum for PEG BOPHY (\blackrightarrow) and the primary product ($\color{red}\blackrightarrow$).

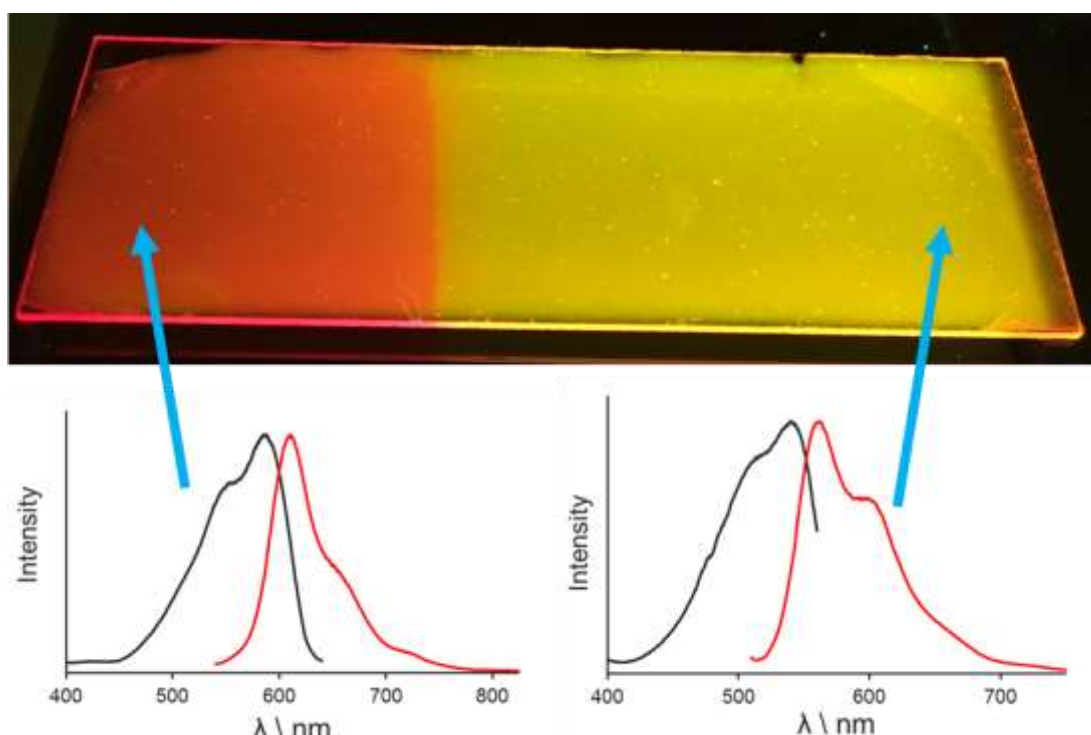


Figure 7.10 – PEG-BOPHY film exposed for different intervals, the left portion is unexposed, and the right portion is close to full conversion. Excitation and emission spectra for the two sections are shown.

Photobleaching of PEG-BOPHY in the PMMA matrix is relatively efficient and gives rise to a distinctive product with well-defined absorption characteristics, a photograph of the two species in Figure 7.10 clearly demonstrates this. Both PEG-BOPHY and the primary product are fluorescent and supported by appropriate excitation spectra. These features could be applied to engineer a practical solid-state actinometer for measuring accumulated exposure to white light. To demonstrate this possibility, a film of PEG-BOPHY was prepared and strips of the films were exposed to the flood lamp for different times. The result is shown as Figure 7.11. On one side of the film, we can see the characteristic pink-red emission of PEG-BOPHY while on the opposite side, after 18 hours of exposure, the yellow emission of the product is seen. Unique patterns can be observed using double-monochromator scanning protocols that allow accurate assessment of the number of photons incident on the film. The high stability of the film in the dark, the combination of absorption and fluorescence spectral changes and the ease of fabrication combine to make this an attractive system. Improvements could be realised by preparing films of precise thickness by, for example, spin coating.

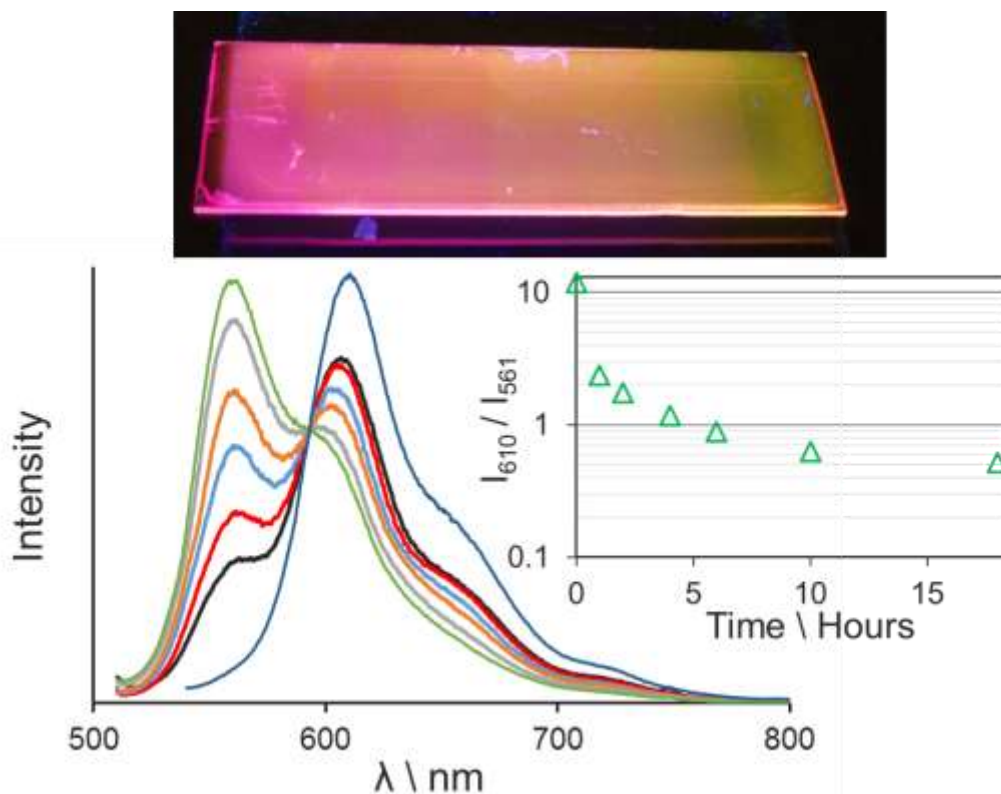


Figure 7.11 – Example of a crude attempt to produce a chemical actinometer with PEG-BOPHY dispersed in a thin film of PMMA. The initial fluorescence peak centred at around 610nm is seen to decrease concomitant with the emergence of a new peak centred at around 560nm. The spectra are normalised at 600nm.

We are now in a position to compare the photobleaching behaviour of the three BOPHY derivatives studied to-date in a film cast from PMMA solution. It is particularly interesting to note that each of these derivatives displays rather different behaviour. Our results obtained with TM-BOPHY indicate relatively slow photobleaching in the solid film at early stages but with auto-catalysis playing an increasing role as photolysis proceeds. The course of reaction shows a pronounced time dependence. In contrast, BOPHY-DMA was seen to bleach quite rapidly and there was a colour change which could be attributed to formation of the corresponding mono-protonated form of the dye. The most interesting effects have been found with PEG-BOPHY which also displays rapid colour changes. Here, the initial photobleaching proceeds smoothly to give a well-defined BOPHY-based product that retains a useful level of fluorescence. This product undergoes photobleaching on longer timescales. Overall, this particular system has the makings of a good chemical actinometer.

7.3.2 Photobleaching in solution

The spectroscopic studies have shown a modest sensitivity towards solvent polarity, especially for the fluorescence quantum yield and excited-state lifetime. This behaviour is

obscured, to some degree, by an activated process that loses fluorescence. It is probable that the two effects are connected. In Figure 7.12 we examine the photobleaching of PEG-BOPHY in air-equilibrated solutions of differing polarity. Typical examples of the accompanying spectral changes are provided in Figure 7.13, while absorbance vs time plots for several solvents are provided in Figure 7.12.

The general scheme for bleaching is the same as seen in the film, with loss of PEG-BOPHY accompanied by build-up and subsequent bleaching of the primary product. In polar solvents, the initial bleaching rate correlates with the fluorescence quantum yield, with faster bleaching of PEG-BOPHY appearing for solvents showing higher fluorescence yields. This is in line with our results described earlier where photobleaching has to compete with other deactivation routes for the excited-singlet state. Toluene provides some level of stabilisation against photobleaching, again similar to the behaviour reported earlier for other BOPHY analogues, and gives the slowest rate of bleaching. In cyclohexane, bleaching was relatively fast but did not form the expected primary product as a meta-stable species. In this latter case, it is possible that the intermediate undergoes relatively fast degradation.

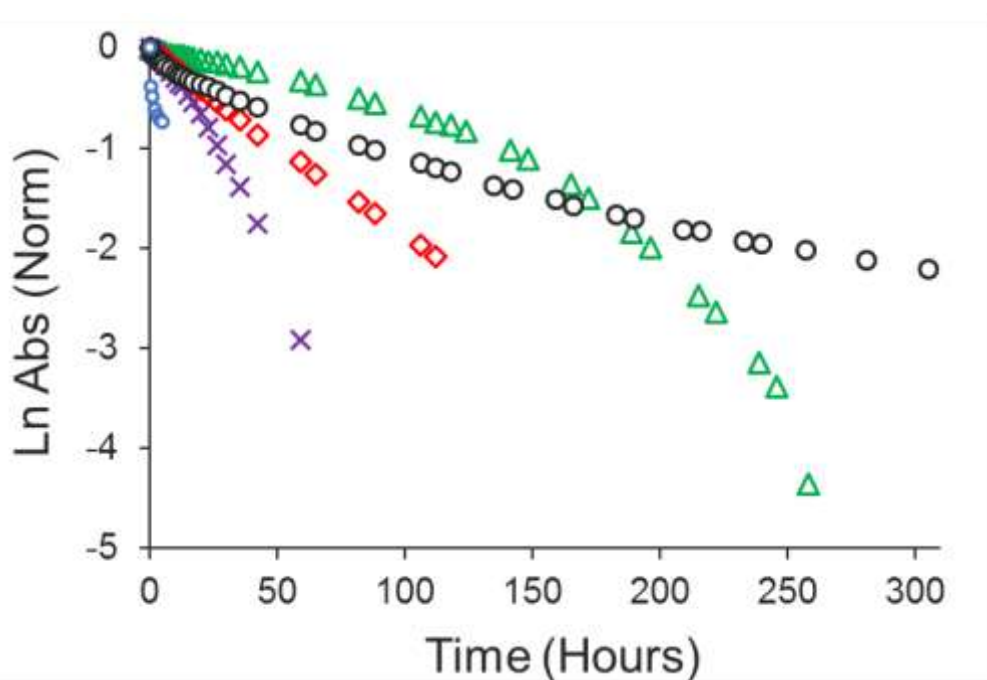


Figure 7.12 – Examples of photobleaching rates recorded for PEG-BOPHY in C_6H_{12} (○), acetone (X), BuCN (◇), MeCN (●) and toluene (△). The course of reaction was followed by absorption spectroscopy and the y-axis corresponds to the change in absorbance at the peak maximum. A white-light source was used for illumination.

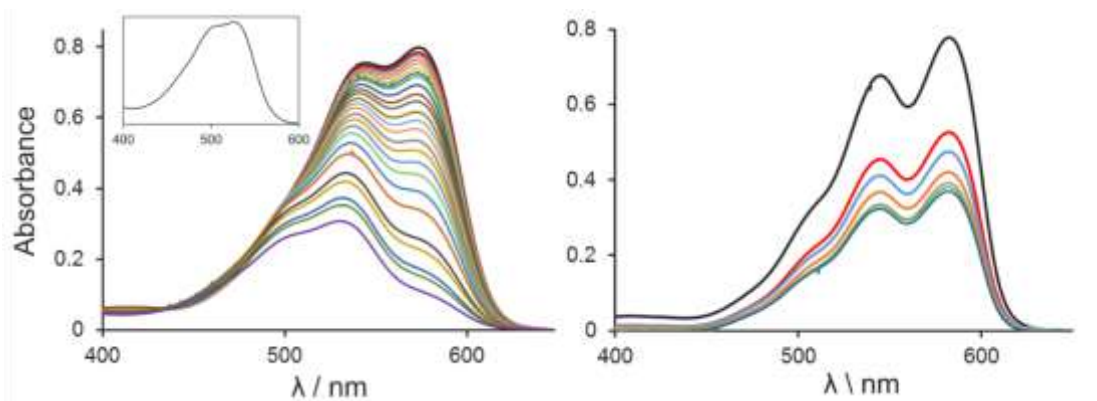


Figure 7.13 – Bleaching overlays recorded for PEG-BOPHY in BuCN (left-hand side) and cyclohexane (right-hand side). Inset shows the spectrum obtained for the product in BuCN.

Apart from cyclohexane, illumination of PEG-BOPHY in air-equilibrated solution leads to the formation of a meta-stable intermediate that absorbs to the blue of the starting compound. The basic absorption profile considered characteristic of the BOPHY chromophore is replicated by this intermediate. Our results obtained for PEG-BOPHY dispersed in thin PMMA films have been interpreted along the lines of this intermediate being a BOPHY-based species with a damaged styryl arm. The same interpretation is carried through to the solution phase studies. Now, we have a simple scheme whereby illumination of PEG-BOPHY results in formation of the primary product (PP), which itself might be susceptible to further bleaching. Except for alkane nitrile solvents, prolonged illumination leads to some kind of self-catalysis which maintains the bleaching rate, shown in Figure 4.15. This is especially evident for toluene and acetone, as indicated by way of Figure 7.14. Photobleaching in acetonitrile and butyronitrile does not involve auto-catalysis but appears to occur by way of dual-exponential kinetics. The primary product is not responsible for auto-catalysis but, of course, it is not the only product. The rates are given in Table 7.2.

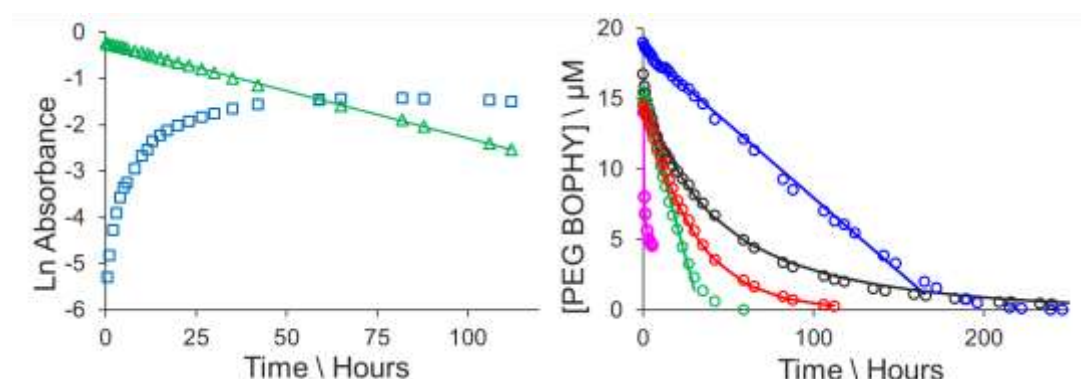


Figure 7.14 – The left-hand panel shows plots of absorbance vs illumination time for PEG-BOPHY in air-equilibrated butyronitrile for the starting compound (Δ) and the primary product (\circ). The right-hand panel shows how illumination affects the concentration of PEG-BOPHY in toluene (\circ), acetonitrile (\bullet), butyronitrile (\bullet), acetone (\bullet) and cyclohexane (\bullet).

Solvent	A1 \ %	$k_1 \setminus h^{-1}$	A2 \ %	$k_2 \setminus h^{-1}$
toluene	-	0.10 ^(a)	-	-
acetonitrile	17	0.037	83	0.011
butyronitrile	-	0.021 ^(b)	-	-
acetone	-	0.45 ^(a)	-	-
cyclohexane	51	2.38	49	0.090
PMMA	-	0.32 ^(b)	-	-

Table 7.2 – Bleaching rate constants derived for PEG-BOPHY in a selection of organic solvents under exposure to white light. Experimental data were fitted to two successive first-order processes. (a) Refers to pseudo-first-order rate constant with units μMh^{-1} , (b) A single first-order fit required.

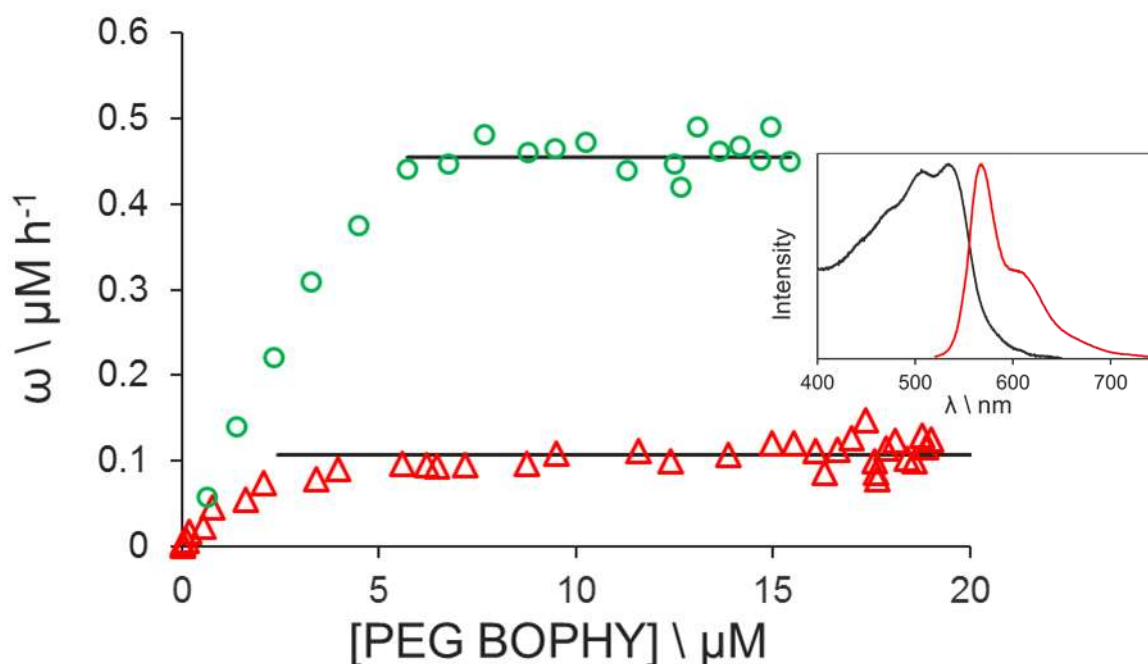


Figure 7.15 – Illustration of how the rate of photobleaching depends on concentration of PEG-BOPHY in toluene (Δ) and acetone (\circ). The straight line drawn through the data points corresponds to a fit to pseudo-zero order kinetics. The inset shows absorption and fluorescence spectra in toluene when there is no discernible amount PEG BOPHY remaining.

In air-equilibrated toluene, photobleaching was continued until the original absorbance due to PEG-BOPHY was completely exhausted. The primary product that remained intact gave a clean emission spectrum with little variation in profile on changing the excitation wavelength. The emission maximum is at 568 nm, indicating a Stokes' shift of 1120 cm^{-1} compared to 720

cm⁻¹ for the starting compound. The fluorescence quantum yield measured relative to Rhodamine 6G^[28] was 0.54.

7.4 BOPHY – Perylene Dyad

7.4.1 Photophysical Properties of the Dyad

An interesting aspect of the results collected thus far with PEG-BOPHY relates to the possibility to construct a simple, solid-state chemical actinometer for the reliable determination of incident photon densities. One way in which this system could be improved is to expand the wavelength range over which the device can operate. This can be done by attaching a secondary chromophore to the BOPHY core that absorbs in the 400-500 nm range. For this purpose, we designed and synthesized a new molecular dyad wherein a single perylene unit has been covalently appended to the expanded BOPHY chromophore. The molecular formula is shown in Figure 7.1 while the absorption and fluorescence spectra are shown in Figure 7.16. Comparison with the spectral features found for PEG-BOPHY shows that the perylene unit amplifies absorption in the 400-500 nm region and also provides a weak fluorescence signal centred at about 500 nm. The sample was further purified by preparative-scale TLC to check that no free perylene is present but this had no effect on the fluorescence spectrum. Most fluorescence is associated with the BOPHY unit and, in line with related BODIPY-based dyads, efficient intramolecular electronic energy transfer from perylene to BOPHY takes place. This process is apparent from the excitation spectrum recorded for the dyad and from the observation that residual emission from perylene is very weak and short-lived. The presence of the conjugated perylene moiety pushes the absorption maximum for the corresponding BOPHY chromophore towards lower energy, accounting for a 20-nm red shift. This represents a further benefit in terms of harvesting the solar spectrum.

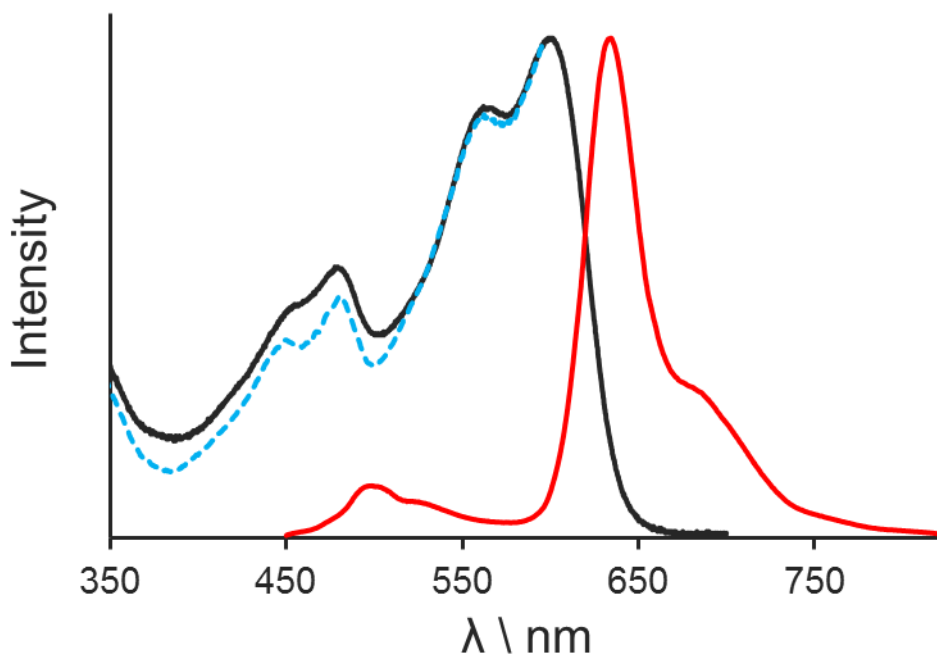


Figure 7.16 – Absorption and fluorescence spectra of the dyad recorded in CH_2Cl_2 , the excitation spectrum (– –) is also provided (recorded at 670nm) and indicates that excitation into the perylene chromophore results in emission from BOPHY.

Although it is not the intention to cover in detail the photophysical properties of the dyad, a few comments are in order. The fluorescence quantum yield and extent of emission from the perylene unit depend on solvent polarity as indicated in Table 7.3. In acetone, fluorescence is very weak and the perylene unit makes the major contribution. In nonpolar solvents such as toluene, more substantial fluorescence is observed with BOPHY being by far the major contributor. This behaviour can be explained in terms of intramolecular light-induced electron transfer competing with radiative decay of the BOPHY excited-singlet state. Emission quantum yields were measured by the ratiometric method relative to tris(2,2'-bipyridyl)ruthenium(II) in water^[29] and confirmed relative to Merocyanine 540^[26] in ethanol.

<i>Solvent</i>	ϵ	Φ_f	<i>p/p ratio</i> ^(a)
Toluene	2.38	0.37	0.02
Ethyl Acetate	6.02	0.23	0.04
MeTHF	6.97	0.25	0.04
Decanol	8.1	0.29	0.02
DCM	8.93	0.09	0.1
Acetone	20.7	<0.01	0.6

Table 7.3 – Selected properties of the perylene-BOPHY dyad, (a) – the ratio of the peak emission from the PEG-BOPHY to perylene.

7.4.2 Photobleaching of the Dyad in Solution

The photobleaching of the dyad was performed as before but band-pass filters were used to select an excitation window for the 420-500 nm region, which is shown in Figure 7.17. Here, the perylene chromophore dominates the absorption spectrum. Selection of an appropriate solvent for this experiment was less straightforward than might be expected. Initial studies were made with acetone but the molecule was too resistant towards photobleaching to make viable kinetic measurements. This result adds to our conviction that photobleaching has to compete with other processes that deactivate the excited state. Shortening the excited-state lifetime serves to reduce the efficacy of photobleaching and these results are fully in line with this doctrine. Chlorinated hydrocarbons and ethers were ruled out because of the problems discussed previously while toluene was not considered due to its protecting nature. Finally, after numerous trials, successful bleaching was deemed to be possible in ethyl acetate.

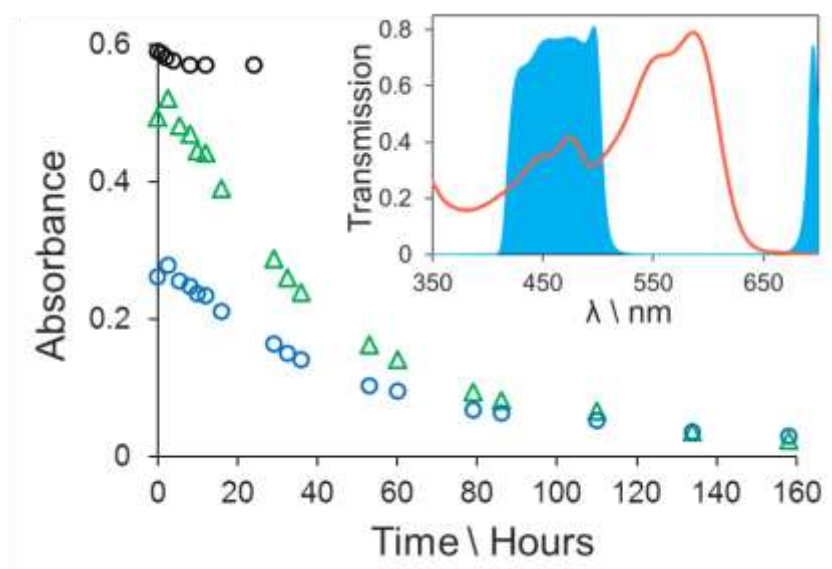


Figure 7.17 – Kinetic traces following photobleaching of the dyad in ethyl acetate, with absorbance changes being monitored at 586nm (Δ) and 475nm (\circ), and also in acetone solution (\bullet) at 585nm. Inset shows the transmitted light by the bandpass filter given by the blue shading, spectral matching with the donor is good.

Excitation into the perylene chromophore results in bleaching of the entire absorption spectral profile. There is no selective loss of the BOPHY chromophore, as might happen if the two units are in electronic isolation. Figure 7.18 demonstrates that photobleaching proceeds smoothly without formation of a coloured intermediate. A product does accumulate but this species absorbs primarily in the near-UV region. We see only limited evidence of the primary product detected for bleaching of PEG-BOPHY. As reaction continues, there is a change in the fluorescence properties, as shown in Figure 7.19, but it is not possible to attribute these to

emission from an isolated version of the perylene. Aside from the improved light-harvesting capability, this dyad does not advance the design of a sophisticated chemical actinometer and, in fact, adds considerably to the synthetic challenge.

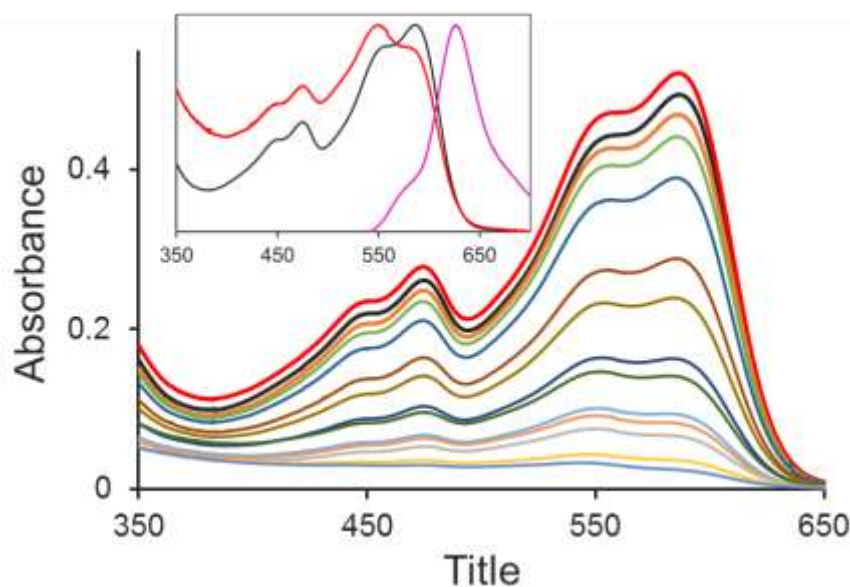


Figure 7.18 – Examples of absorption spectral profiles recorded during the photobleaching of the dyad in ethyl acetate from 0 – 150 hours. The inset shows normalised spectra at the beginning and after 110 hours of continuous illumination. Some change to the acceptor portion of the molecule can be recognised. Excitation at 510nm shows there is emission from a product as well as from the starting material (—).

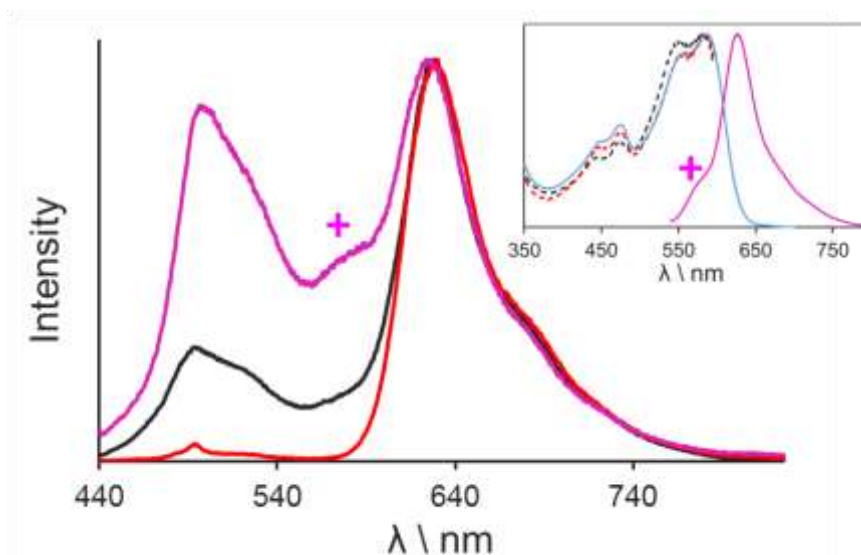


Figure 7.19 – Emission from the dyad at different stages of bleaching; final (—), intermediate time (—) and initial compound (—), excitation at 430nm. + indicates the emergent emission from the bleaching product, also seen for PEG-BOPHY.

7.5 Conclusion

In this chapter, we introduce an expanded BOPHY chromophore equipped with poly(ethylene glycol) chains intended to assist solubility. Spectroscopic properties recorded in solvents of differing polarity are consistent with modest intramolecular charge-transfer character. There is also evidence for an activated channel that competes effectively with radiative decay of the excited-singlet state. This latter process helps to reduce fluorescence at room temperature, even in a nonpolar solvent. The styryl arms lower the HOMO-LUMO energy gap and thereby introduce a significant red shift for the absorption and fluorescence spectra. The compound now absorbs and emits in an interesting part of the visible spectrum. Aided by the PEG chains, the compound disperses easily in thin films cast from solutions of PMMA. These strongly fluorescent films retain excellent optical properties and are extremely stable when stored in the dark. The absorption spectral profile undergoes a further red shift when an ethynyl-*p*-erylene moiety is attached to the BOPHY core. Unfortunately, this strategy does not help in terms of designing useful chromophores since there is a loss of fluorescence from BOPHY. The kinetics for photobleaching also become more complex.

Photobleaching of PEG-BOPHY in thin PMMA films proceeds stepwise and forms a relatively stable intermediate, which is believed to arise because of irreversible damage to one styryl arm. This intermediate is strongly fluorescent and possesses a well-defined absorption spectral profile. The reaction stoichiometry is reasonably well preserved over short illumination periods but becomes distorted at higher conversion of the starting compound. Using double-monochromator scanning techniques, unique signatures from partially bleached films should provide highly accurate chemical actinometers. Such materials would be useful safeguards against accidental exposure to sunlight.

Our work in this area raises serious challenges for understanding the chemistry behind the photobleaching processes. This must involve multiple attacks on the chromophore since it is impossible to imagine that complete loss of colour could result from (for example) addition of a single free-radical. It is interesting to note the loss of colour on transforming the starting compound to the primary product. It is natural to suppose that we should also see the BOPHY derivative with both styryl arms in a damaged condition but this was not observed, although there is increased absorption around 440 nm where the parent compound absorbs. The kinetic measurements go some way towards establishing a pathway for the photobleaching process but do not identify the products.

References

- [1] J. M. Drake, M. L. Lesiecki, J. Sansregret, W. R. L. Thomas, *Appl. Opt.* **1982**, 21, 2945-2952.
- [2] A. M. Hermann, *Sol. Energy*, **1982**, 29, 323-329.
- [3] A. Harriman, *Chem. Commun.* **2015**, 51, 11745-11756.
- [4] S. Kuhri, V. Engelhardt, R. Faust, D. M. Guldi, *Chem. Sci.* **2014**, 5, 2580-2588.
- [5] T. Weil, E. Reuther, K. Müllen, *Angew. Chem. Int. Ed.* **2002**, 41, 1900-1904.
- [6] K. W. Jolley et al. *Coord. Chem. Rev.* **2004**, 248, 1363-1379.
- [7] J.-Y. Liu, H.-S. Yeung, W. Xu, X. Li, D. K. P. Ng, *Org. Lett.* **2008**, 10, 5421-5424.
- [8] J. Köhler et al. *J. Phys. Chem. B*, **2010**, 114, 9148-9156.
- [9] L. Flamigni, J.-P. Collin, J.-P. Sauvage, *Acc. Chem. Res.* **2008**, 41, 857-871.
- [10] J. S. Lindsey et al. *J. Phys. Chem. B*, **2014**, 118, 1630-1647.
- [11] J. S. Lindsey et al. *Chem. Commun.* **2014**, 50, 14512-14515.
- [12] L. He, S. Zhu, Y. Liu, Y. Xie, Q. Xu, H. Wei, W. Lin, *Chem. Eur. J.* **2015**, 21, 12181-12187.
- [13] R. Ziessel, G. Ulrich, A. Haefele, A. Harriman, *J. Am. Chem. Soc.* **2013**, 135, 11330-11344.
- [14] X. Zhang, Y. Xiao, X. Qian, *Org. Lett.* **2008**, 10, 29-32.
- [15] R. Ziessel, A. Harriman, *Chem. Commun.* **2011**, 47, 611-631.
- [16] R. W. Wagner, J. S. Lindsey, *J. Am. Chem. Soc.* **1994**, 116, 9759-9760.
- [17] A. C. Benniston, A. Harriman, *Mater. Today*, **2008**, 11, 26-34.
- [18] A. Harriman, P. Stachelek, A. Sutter, R. Ziessel, *Photochem. Photobiol. Sci.* **2015**, 14, 1100-1109.
- [19] A. Harriman, P. Stachelek, A. Sutter, R. Ziessel, *Phys. Chem. Chem. Phys.* **2015**, 17, 26175-26182.
- [20] B. P. Wittmershaus et al. *J. Lumines.* **2013**, 143, 469-472.
- [21] T. Ichiki, Y. Matsuo, E. Nakamura, *Chem. Commun.* **2013**, 49, 279-281.
- [22] J. Rosenthal et al. *J. Phys. Chem. C*, **2013**, 117, 5599-5609.
- [23] R. Vazquez-Duhalt et al. *Biotechnol. Appl. Biochem.* **2015**, 177, 1364-1373.
- [24] G. Hinze, R. Metivier, F. Nolde, K. Müllen, T. Basche, *J. Chem. Phys.* **2008**, 128, 124516.
- [25] J. R. Lakowicz, *Principles of Fluorescence Spectroscopy*, **2006**.
- [26] A. C. Benniston, A. Harriman, K. S. Gulliya, *J. Chem. Soc. Faraday Trans.* **1994**, 90, 953-961.
- [27] I. L. Arbeloa, *J. Chem. Soc. Faraday Trans.* **1981**, 77, 1735-1742.
- [28] R. F. Kubin, A. N. Fletcher, *J. Lumines.* **1982**, 27, 455-462.
- [29] K. Nozaki et al. *Coord. Chem. Rev.* **2010**, 254, 2449-2458.

Chapter 8 - Photo-Processes of a Chromophore-Quencher Conjugate based on BOPHY

8.1 Introduction

In chapter 6, the remarkable stabilization of BOPHY molecules by toluene was described. There were some concerns that trace amounts of anti-oxidant stabilizers added to the commercial solvent were responsible for this positive effect but these were proven to be unwarranted. Deliberate addition of stabilizers provided some inhibition but resulted in long-term damage of the chromophore. If long-term photostability is to be achieved, some form of self-healing or extraneous protection must be introduced. This seems to be the only realistic strategy for the design (as opposed to the accidental discovery) of photo-stable dyes.

The protection of red-emitting dyes has received considerable attention in the literature^[1]. A driving force for this realisation stems from the need to develop super-resolution imaging^[2] techniques in microscopy. Such dyes must operate in the optical window most suited for bio-imaging, but red-shifted dyes tend to have problems with their photostability. There is a huge variety of different microscopy protocols, particularly single-molecule-based methods such as total internal reflection microscopy^[3] (TIRF), available to the researcher. This fuels the need for new dyes with excellent photostability, especially as many protocols may require prolonged exposure to high powered laser sources. For imaging purposes, there are two distinct problems: Firstly, the chemical conversion of a fluorophore to some non-emissive product (i.e., photobleaching) is a concern for such applications and this has formed the basis of our own research. A second problem often encountered is photo-blinking whereby the fluorophore enters into a transient dark state which is problematic for imaging purposes. This property can be exploited such as in the technique known as stochastic optical reconstruction microscopy^[4] (StORM) where specific excitation wavelengths are used to modulate fluorophore emission. This latter process is referred to as photoswitching. Photo-blinking does not concern us too much here in as much as we are interested in long-term effects, although such states could be of importance to the overall bleaching process.

Cyanine dyes are the most prevalent class of compounds used in imaging, particularly when red-emitters are considered; Alexa Fluor 647 for example is of the Cy5 class of dye and underpins much of conventional StORM. As such, the protection of cyanine dyes has received considerable attention in the literature. The consensus is that both photoblinking and bleaching problems originate from the lowest-energy triplet state. A limitation of cyanine dyes

is their propensity to undergo photo-induced cis-trans isomerization, but this is not seemingly part of photoblinking/bleaching mechanisms. Bleaching is reported to be enhanced when excitation is by a higher energy source, suggesting that higher-energy excited states could contribute to the process^[5] although this is in violation of Kasha's rule. Cyanine dyes are reported to have triplet yields significantly less than 1%^[6] so the so-called 'excursions to the triplet state' are comparatively rare events but would be a function of the density of photons impinging on a sample. Once in a dark state, the fluorophore may stay there for milliseconds, so if the photon collection rate is fast then dark states will be recorded. The concern, when a triplet-excited state is formed, is that there will be subsequent formation of singlet molecular oxygen. This highly reactive transient species might lead to further reactive oxygen species such as H₂O₂, •OH or •OOH. Superoxide ions may also be formed by the interaction of molecular oxygen and the triplet state of the chromophore^[7]. To protect against photobleaching via singlet oxygen formation, typical microscopy experiments will employ the use of enzymatic oxygen scavengers as part of their armoury. The most common system is glucose oxidase and catalase in glucose^[8] (GODCAT), a cocktail which has been shown to improve resistance to photobleaching^[9]. The downside is that as molecular oxygen is removed it can no longer act as a triplet quencher. This has the effect of switching on other triplet-state photochemistry. Generally, when performing bleaching experiments we prefer not to exclude molecular oxygen unless it would afford us further mechanistic insight.

Thus, oxygen scavengers help to solve one problem but exacerbate another so, further additives are usually employed to overcome the photoblinking issue. Commercial packages such as Vectashield may be used or bespoke combinations of additives. The most common mechanism used to do this is a reducing-oxidising system (ROXS)^[10] whereby both a reducing species and an oxidising species are required to return the fluorophore to the ground state. As the triplet state is now long-lived, the reductant may be used to quench the triplet by diffusional electron transfer. This will create a radical pair which may separate with the radical fluorophore sequentially being oxidised or reduced as required by the co-additive and the ground state is restored. A range of anti-oxidants is used, including nitrobenzyl alcohol^[11], ascorbic acid^[12], β-mercaptoethanol^[13], and 1,4-diazabicyclo[2,2,2]octane (DABCO)^[14], while oxidants include methyl viologen^[15] and trolox-quinone^[15]. Trolox, a water-soluble vitamin E analogue^[16], is an anti-oxidant that can be employed singularly. Trolox is not capable of working on its own but it is believed that a small portion of trolox is oxidised to form trolox-quinone^[17] which acts as the counter additive^[17] in ROXS system. The additives used are generically called triplet-state quenchers (TSQs).

It has also been proposed that recombination of the geminate pair created is a possible route to photostability^[5]. The geminate pair is in the triplet state and generally needs to convert via

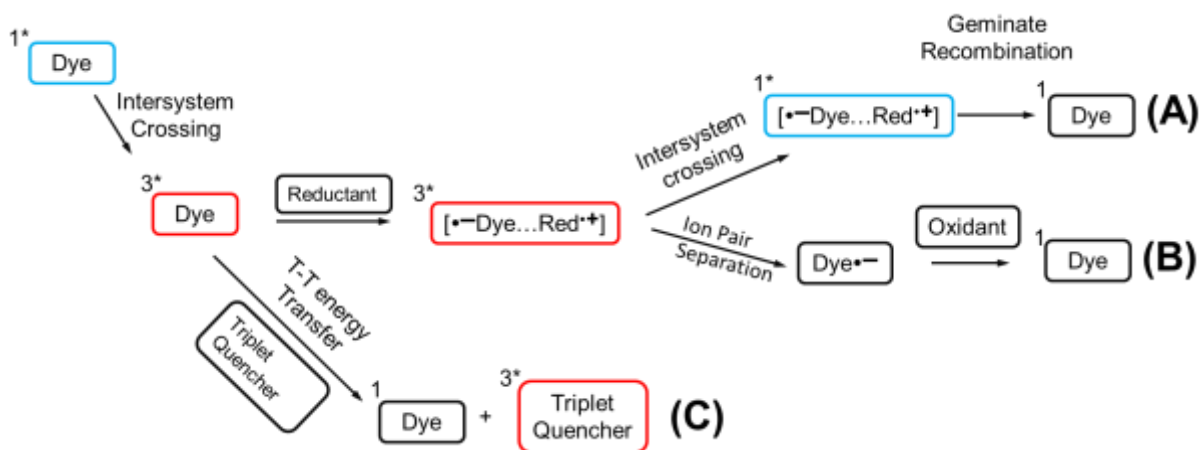
intersystem crossing (ISC) to the ground state. If ISC is slow, the radical pair can escape the solvent cage and then it is necessary for an oxidising agent to return the fluorophore to the ground state. β -mercaptoethanol was shown to promote ISC of the geminate pair^[18] so that free radical ions are not produced in significant quantities. Indeed, certain studies have reported a unity yield for geminate recombination, meaning the oxidant co-solute is redundant. In this case, the proposed mechanism for ISC is hyperfine coupling.

The use of anti-oxidants like Trolox and β -mercaptoethanol as triplet quenchers has been shown to increase the turnover number of dyes used in single-molecule fluorescence spectroscopy by up to three orders of magnitude^[2]. Adding TSQs to solutions for microscopy can present additional challenges, however. Typically, such molecules will have poor water solubility, which is a problem as the stabilising mechanisms are diffusion-controlled and require millimolar concentrations. Such high levels of TSQs have been shown to disrupt lipid bilayers^[19]. Where a solution with an anti-oxidant or redox pair is used there is a subtle interplay between redox driving force, spin conversion and the ability of the ion pair to escape the solvent cage. This means that the optimum combination of photostabilising additives is dependent on the choice of fluorophore.

Whilst engineering solutions to remove oxygen and mixing in additives to protect chromophores could form part of an overall protection package, smarter solutions should be feasible. In a solution for microscopy, it seems reasonable to add light-fast aids but a different approach is needed for solid-state systems. One such approach involves the covalent attachment of a protecting molecule to the chromophores. The first benefit is that high concentrations of quencher are no longer needed as the quencher is already located at the fluorophore. Again, to protect cyanine dyes^[20] from attack via triplet states, Trolox, and nitrobenzyl alcohol groups have been appended^[7] and have been shown to give two orders of magnitude improvement in stability when at least two quenching units are attached to the dye. Since only one part of the redox pair is used, there must be a slightly different mechanism involved. The explanation postulated is a so called 'ping-pong' transfer mechanism^[21]. In the case of an attached anti-oxidant, the partner for the second electron-transfer step is created by the first electron-transfer reaction. The triplet dye reacts with the stabilising agent to form a dye anion and stabiliser cation, which in turn can now act as oxidant. The pair cannot diffuse away from each other so will recombine to restore the ground state. Such dyes are referred to as being 'self-healing'. This approach has also been tried in a form whereby non-natural amino acids^[22] are used as a scaffold to co-locate the fluorophore, bio-target and protecting group. Another triplet state quencher used in microscopy, cyclooctatetraene^[23] (COT), has been attached to fluorophores^[24]. Now, COT is of a different class of TSQ in that acts as a triplet quencher not by electron transfer but via triplet-triplet energy transfer^[25]. Indeed, COT

has a low-lying triplet state related to a buckled conformation^[26], the energy is lower than that of singlet molecular oxygen by 2 kJ mol⁻¹. As a result, when the triplet of COT is formed it cannot react with molecular oxygen, so there is no route to forming singlet oxygen. Generally speaking, the T-T energy transfer solution is a particularly enticing route as there is no ion pair formed as an intermediate. The bridging chain used was either 3 or 13 atoms long^[24]. In the case of appended COT there was found to be a 5 and 60 times reduction in triplet lifetime respectively, similar effects were seen in terms of photostability. The stabilising units need to come into close contact with the triplet state of the dye so locating it nearer to the chromophore is highly advantageous. The effect of either covalent coupling of the stabilising package or the use of solution additives has on the steady state properties of the fluorophore's singlet excited state has received little comment in the literature. In past studies with fluorescein^[25] the majority of stabilising agents used were found to reduce the fluorescence quantum yield. The work of Blanchard^[20] did report a 25% enhancement for Cy5 with COT attached and conversely a 20% reduction of fluorescence intensity for Cy5 with trolox attached which would seem to be modest changes in the properties of the singlet-excited state. In this example, the absorption and fluorescence spectra were reported as being unchanged.

Adsorption of fluorophores and polymers^[9] onto nanoparticles in the presence of anti-oxidants has been shown to have beneficial effects^[27]. In such instances, the nano-particle may confine the fluorophore near the solution of antioxidant. However, electronic coupling of the fluorophore to the surface plasmon^[28] of the nano-particle may reduce the excited-state lifetime and thereby provide stabilisation. A particularly interesting approach involved confinement of Rhodamine 6G within micrometer-sized PDMS wells^[29] which were coated with either polyethylene glycol or bovine serum albumin. It was shown that there was no effect on the triplet properties of the dye and improved stabilisation was attributed to the capacity of the wells to intercept radicals. It is the reaction of these with the surface coating that provides relief from photodegradation.



Scheme 8.1 – Routes that can stabilise fluorophores by restoring triplets to the ground state. (A) geminate recombination facilitated by ISC back to the singlet state, (B) outlines the ROXS system and (C) is triplet-triplet energy transfer to a suitable quencher.

We have been concerned with the properties of the BOPHY class of compound and we now return to this motif. To create the new chromophore-quencher-conjugates (CQCs), the TM-BOPHY molecule was appended with one or two anti-oxidant units. The anti-oxidant selected is butylated hydroxytoluene^[30] (BHT) which is a synthetic analogue of Vitamin E, although it is not water soluble. It is used extensively in the stability of solvents as previously mentioned and as a food preservative^[31] although its toxicity is the subject of debate^[32]. We showed previously that TM-BOPHY bleaches slowly in air-equilibrated solutions with no apparent solvent dependence (other than for toluene) and with auto-catalytic kinetics in a PMMA film. Compared to protection of the red-emitting cyanine dyes, protection of the BOPHY class will bear at least two key differences: First, there is concern that the geminate recombination strategy will not be effective at more energetic wavelengths^[5]. Secondly, we do not believe that the triplet state plays any significant role in the degradation of BOPHY. As such, we do not rely on the TSQ properties of BHT but rather anticipate that it will act to bear the brunt of oxidative stress and mop up any radicals in the system. This approach is based on our prior discovery that auto-catalysis plays an important role in the photo-bleaching of the BOPHY chromophore. As such, the build-up of products is important as they will entertain further reactions under broadband illumination. It might be noted that the absorption spectrum of BHT is rather broad and with a maximum at 280nm ($\epsilon \approx 1500 \text{ M}^{-1} \text{ cm}^{-1}$)^[33]. Since the lamp used has no output at such wavelengths, direct excitation of the BHT units will not occur.

The structure of the CQCs is shown in Figure 8.1, CQCs were prepared by the condensation method^[34] and then hydrogenated to give an ethyl connecting chain. The two parts of the molecule should not exhibit mutual electronic communication so the addition of the BHT is not expected to affect the photophysical properties of BOPHY. In fact, the photophysical

properties are somewhat complex leading to interesting bleaching behaviour whilst opening up the opportunities to use the CQCs for other purposes.

Additionally, the potential for this type of system to act as a photosensitizing catalyst for organic syntheses has been considered. One example^[35] of the current interest in promoting synthetic reactions by photocatalytic means uses a halogenated BODIPY derivative as a sensitizer in conjunction with phenolic anti-oxidants in solution to drive the amidation of aromatic aldehydes by reaction with amines. The anti-oxidants were not covalently attached to the sensitizer. Interception of, presumably triplet, excited states and reactive intermediates is required for this reaction and yields of up to 70% for the chromophore alone and 90% for the combination are reported. It is a logical extension to exploit intermediates involved in our system. Thus, an amidation reaction was attempted where we have assumed that the catalyst is the same intermediate encountered in our photo-stability studies.

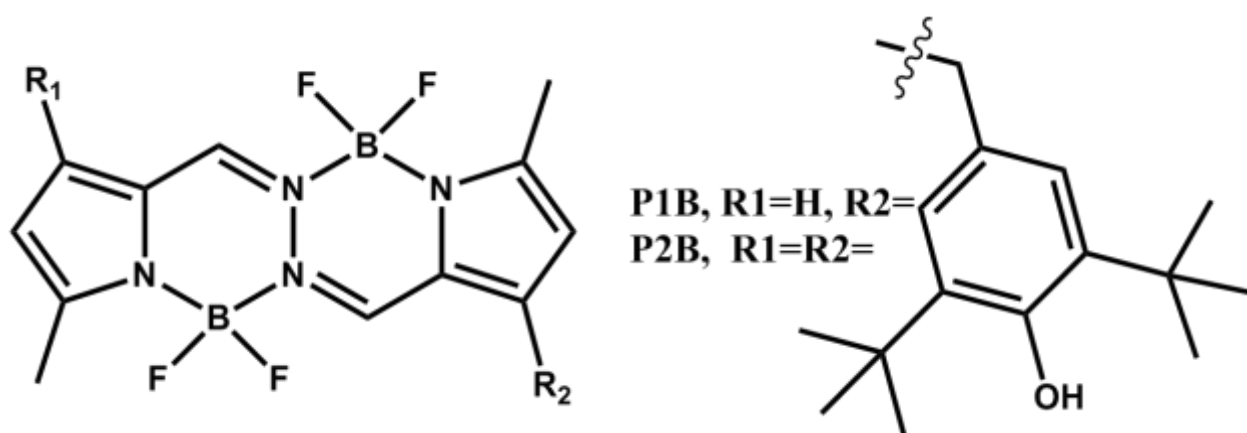


Figure 8.1 – Structure of the CQC compounds P1B and P2B

8.2 Photophysical Properties of CQCs

The addition of one or two BHT units has only a small effect on the absorption spectra, as can be seen in Figure 8.2, compared to TM-BOPHY in cyclohexane. The maxima are shifted by approximately 150 and 300 cm⁻¹ respectively for P1B and P2B; similar shifts are found for the fluorescence maxima. The properties of the dyes are detailed in Table 8.1 found at the end of this section. In nonpolar or low polarity solvents, the fluorescence quantum yield and lifetime of P1B are similar to those of the parent compound. The quantum yield was measured by reference to TM-BOPHY in CH₂Cl₂ ($\Phi_f = 0.76$). As the polarity of the solvents increases, there is a general decrease in fluorescence. This trend is reflected in the reduction of the singlet-state lifetime. The quenching effect is similar, although more exaggerated, in the case of P2B.

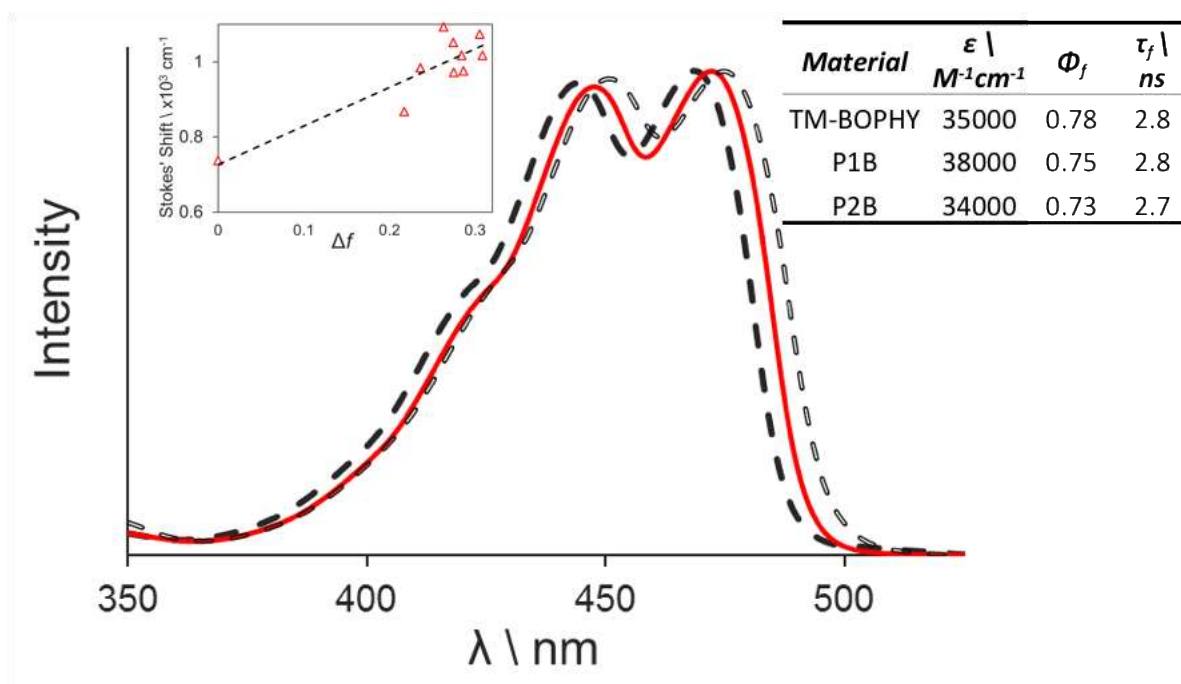


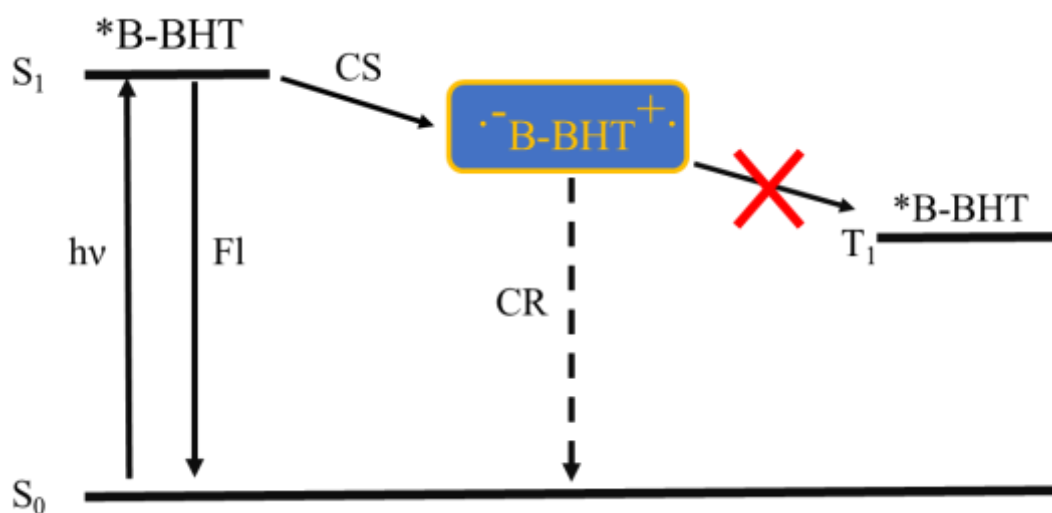
Figure 8.2 – Absorption spectra of TM-BOPHY (— —), P1B (—) and P2B (□ □) in cyclohexane. The spectral profile is only slightly perturbed by the presence of the BHT groups. Inset: Lippert-Mataga plot for P1B, the change in dipole moment is 3.3D which is close to the value for TM-BOPHY.

The quenching can be rationalised as electron transfer from BHT to the excited-state of BOPHY. Cyclic voltammetry was performed in CH_2Cl_2 . A one-electron reduction process for the BOPHY core was seen at -1.49V relative to Ag/Ag^+ for both of the CQCs. This step was not fully reversible in electrochemical terms. Around 10% of the material is lost at a scan rate of 100mV/s. Oxidation peaks are found at 1.32 and 1.28V relative to Ag/Ag^+ for P1B and P2B respectively. These values are in good agreement with the values reported in the literature for the TM-BOPHY core. For both CQCs, a two-electron oxidation wave per BHT unit was observed. In both cases, this peak was at a lower potential than the BOPHY oxidation. Thus, P1B showed an irreversible, two-electron oxidation step at 1.27V relative to Ag/Ag^+ while for P2B a four-electron peak was found at 1.20V relative to Ag/Ag^+ . Scans were performed at up to 5V/s but the oxidation process was still found to be irreversible. This situation is consistent with the redox chemistry seen with related phenolic compounds such as tyrosine^[36] where oxidation results in the loss of the phenolic proton.

Thermodynamically, electron transfer is a good explanation for the observed fluorescence quenching outlined in Scheme 8.2. The driving force cannot be calculated because the electrochemistry is irreversible, but the fluorescence yields do vary with the solvent polarity.

However, the changes in quenching are rather complex. Up to a certain polarity, fluorescence is not quenched (i.e., in CH_2Cl_2 and MeTHF). The molecule was designed such that there is a covalent link between the two redox partners but there is no extended conjugation path for through-bond charge transfer. That this was achieved is borne out by the minimal effect that the BHT groups have on the absorption spectra. In those solvents where the fluorescence is unquenched compared to the parent TM-BOPHY, a single exponential realises a satisfactory fit to the time-resolved fluorescence decay profiles. In Figure 8.3 we see that where the fluorescence is significantly quenched, a two-exponential fit is needed. This finding could indicate some reversibility in the charge-separated state so that repopulation of the S_1 state can occur. However, no simple relationship could be found between excited-state lifetime and temperature^[37].

This leaves us with the likelihood that quenching is related to conformational aspects of the molecule. The quenching must occur when the linker is bent back and the quenching unit is in orbital contact with the BOPHY core. The lifetime then doesn't truly fit a bi-exponential model but rather families of populations. The true lifetime will be a distribution function based around the two sets of populations; a bi-exponential fit becomes a reasonable approximation. Fast electron transfer occurs when a BHT unit approaches close to the BOPHY core, with polar solvents stabilising the charge-separated species. The solvent seems certain to affect the conformational distribution. As such, a simple correlation between solvent polarity and quenching is not followed. For example, in acetonitrile the fluorescence is increased compared to other highly polar solvents such as dimethyl formamide (DMF).



Scheme 8.2 – General scheme outlining processes available to the CQCs upon absorption of a photon by the BOPHY core. The molecule may return to the ground state by emission (Fl) or charge separation (CS) may occur followed by charge recombination (CR) which is a non-radiative path unavailable to the equivalent TM-BOPHY molecule.

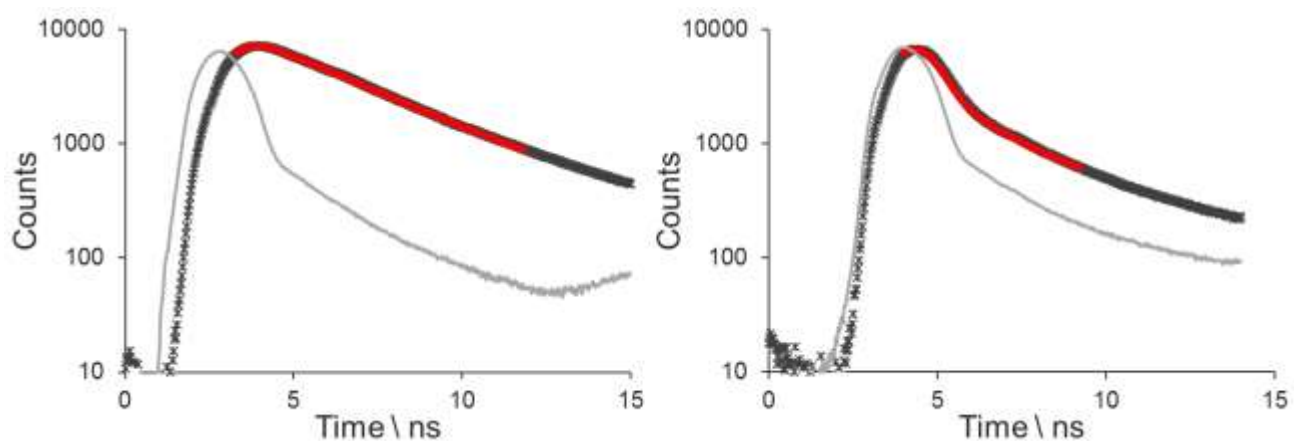


Figure 8.3 - TSCPC data for P2B in CH_2Cl_2 (left) and DMF (right), in CH_2Cl_2 a single exponential fits the data well but the need for two exponentials in DMF is clear.

To test the assertion that the molecular topology is the key to the level of fluorescence quenching, a physical test is required. The ability of the BHT moiety to interconvert between conformations must be viscosity controlled. Therefore, we can measure the loss of fluorescence as the viscosity of a solvent is altered, which can be achieved by a change of temperature. Taking P1B in polar solvents, the fluorescence was recorded as a function of temperature, yielding the Arrhenius plots shown as Figure 8.4.

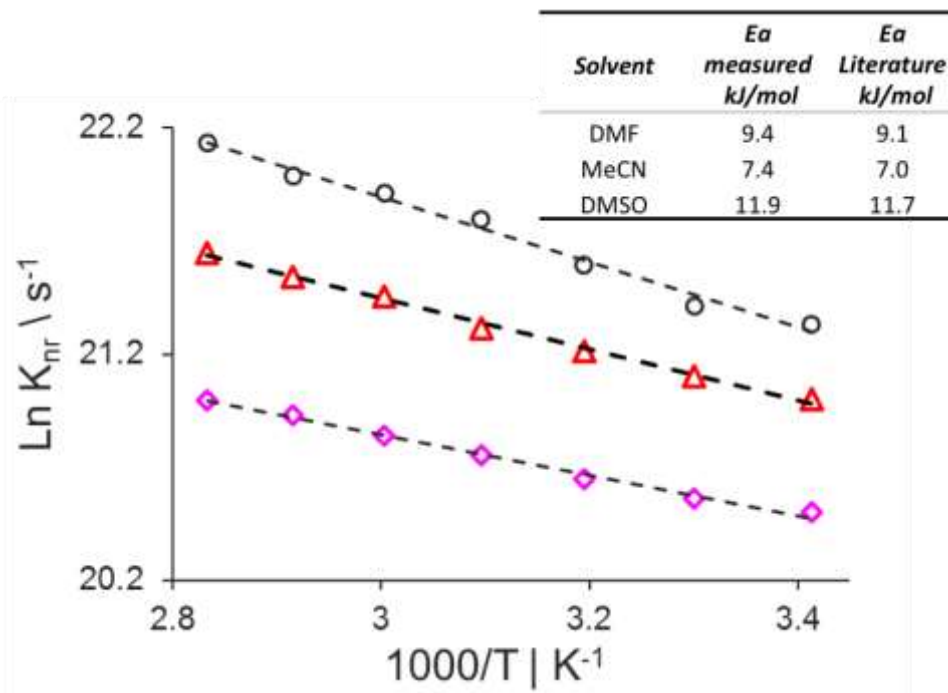


Figure 8.4 – Arrhenius plot of the non-radiative rate constant derived for P1B in polar solvents. The activation energy in acetonitrile (\diamond), DMF (Δ) and dimethyl sulfoxide (DMSO) (\circ) are shown in the attached table

Analysis of the data compiled in the figure gives an Arrhenius-type activation energy (E_a) of 9.4 kJ mol^{-1} in DMF. This compares favourably with a literature value of $E_a=9.05 \text{ kJ mol}^{-1}$ for the viscosity of DMF^[38]. The activation energies in acetonitrile and DMSO also exhibit good agreement with those reported for the viscosity of the solvent over the same temperature range^[39].

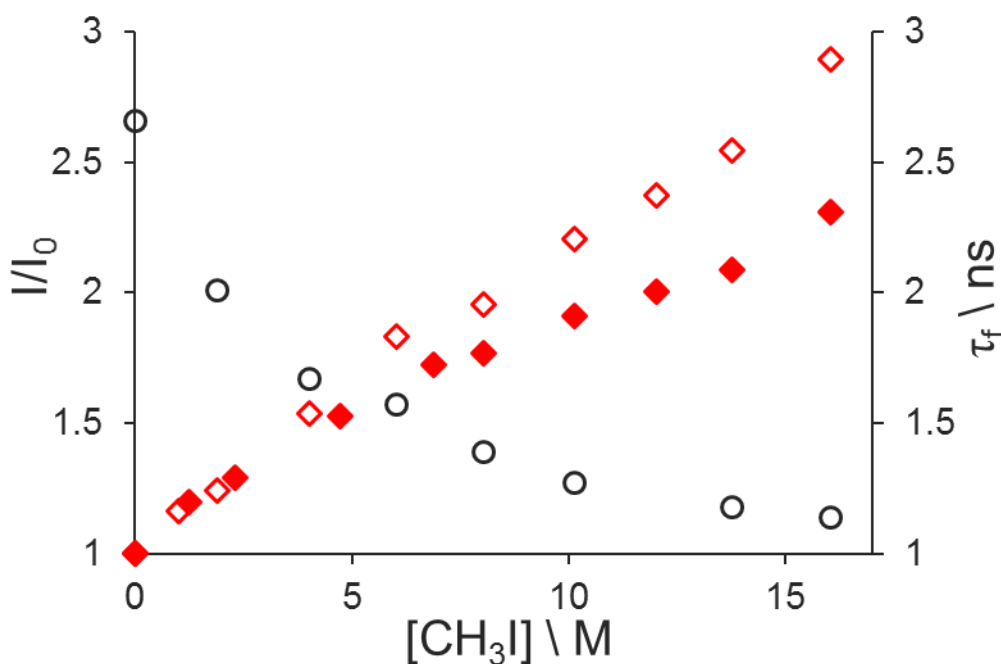


Figure 8.5 - Stern-Volmer plot for P1B (\diamond) and P2B (\blacklozenge) quenching in MeTHF by iodomethane, the excited-state lifetime of P1B (\circ) is also included.

The heavy-atom fluorescence quenching, seen in figure 8.5, and triplet properties of the CQCs are similar to those seen for TM-BOPHY. The total quenching is reduced compared to TM-BOPHY for P1B and more so for P2B which would indicate that the BHT groups block the ability of iodomethane to achieve the required orbital contact with the BOPHY core. The phosphorescence seen at 77K with a 33% v/v addition of iodomethane was much the same as for TM-BOPHY.

Solvent	P1B				P2B			
	Φ_f	τ ns	λ_{obs} nm	λ_{fluo} nm	Φ_f	τ ns	λ_{obs} nm	λ_{fluo} nm
C ₆ H ₁₂	0.75	2.8	472	489	0.73	2.7	475	493
CH ₂ Cl ₂	0.74	2.8	470	490	0.71	2.7	471	493
Butyronitrile	0.44	1.9	465	487	0.35	1.9	468	491
Benzonitrile	0.67	1.9	472	495	0.65	2.6	475	497
Propylene Carbonate	0.3	0.5 1.3 22% 78%	464	486	0.23	0.6 1.2 27% 73%	466	491
Acetone	0.32	0.9 1.7 42% 58%	464	487	2	0.4 1.4 28% 72%	466	490
Acetonitrile	0.25	0.9 2 71% 29%	461	485	0.17	0.4 1.1 37% 63%	463	489
DMF	0.17	0.5 2.5 89% 11%	466	490	0.06	0.3 1.6 92% 8%	468	494
MeOH	0.15	0.4 2.2 89% 11%	464	487	0.08	0.3 2.5 96% 4%	467	490
DMSO	0.13	0.4 3 89% 11%	466	491	0.08	0.3 2.7 94% 6%	468	494

Table 8.1 – Photophysical properties of the CQCs in various solvents. For the polar solvents the two lifetimes and relative A-factors are given.

8.3 Photobleaching of CSCs

8.3.1 Photobleaching of P2B in polar solvents

Attachment of BHT units to the TM-BOPHY chromophore was found to have a significant effect on the kinetics and mechanism of photobleaching of the BOPHY chromophore. In this respect, our design principles were sound but we did not foresee the complication caused by the fluorescence quenching found in polar media. Rather, we had anticipated that the BHT groups would be involved only in mopping up any adventitious free radicals before they could attach the BOPHY core. Since light-induced charge transfer has been implicated as the primary quenching mode, it follows that a charge-separated state must be generated soon after excitation. This species will undergo charge recombination to restore the ground state, in accordance with Scheme 8.2. For photochemical degradation of the chromophore to occur, the system must escape this reversible cycle. One way for this to happen, is for charge recombination to form a long-lived triplet-excited state. The net result, however, is that we might expect to observe some kind of correlation between the fluorescence properties and the

photochemical bleaching kinetics for the CQCs in various polar solvents. Solutions of P2B were bleached following the general protocol employed throughout this work with solution concentrations being on the order of 30 μ M.

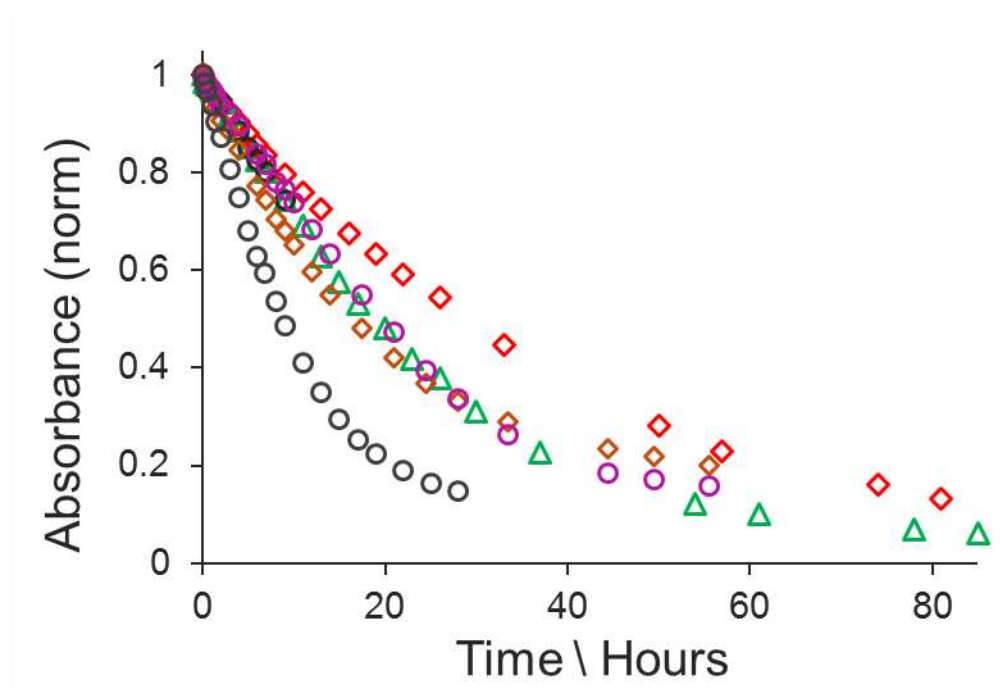


Figure 8.6 -Normalised bleaching data for P2B in polar solvents, DMF (\blacklozenge), Acetonitrile (\bullet), Butyronitrile (\blacklozenge), Acetone (\blacktriangle) and Benzonitrile (\bullet).

The bleaching kinetics are shown in Figure 8.6. Bleaching rates show the anticipated correlation, thereby confirming that the charge-recombination pathway has to be circumvented for effective photobleaching to take place. Much like the situation seen in Chapter 6 where the excited state was quenched, light-induced electron transfer and subsequent charge recombination provides a useful cycle for protection of the dye against photobleaching. Of course, this protection comes at the cost of fluorescence. The bleaching kinetics are complicated and do not fit to simple mono- or bi-exponential models. For polar solvents where a significant concentration persists, the kinetics appear to be zero-order with respect to chromophore. It was observed that the rate of bleaching is linearly proportional to the number of photons absorbed. Indeed, the bleaching rate ω , is controlled by the photon flux according to the Equation 8.1:

$$\omega = I_0 \cdot I_{abs} \cdot k_0 \cdot [P2B]^0 \quad (8.1)$$

Here, I_{abs} is measured by the absorption coefficient ($I_{abs} = 1 \cdot 10^{-A}$) and I_0 is the photon flux of the lamp. We can arbitrarily set this latter value to be unity. We can now determine values for k_0 in the various solvents which are collated in Table 8.2.

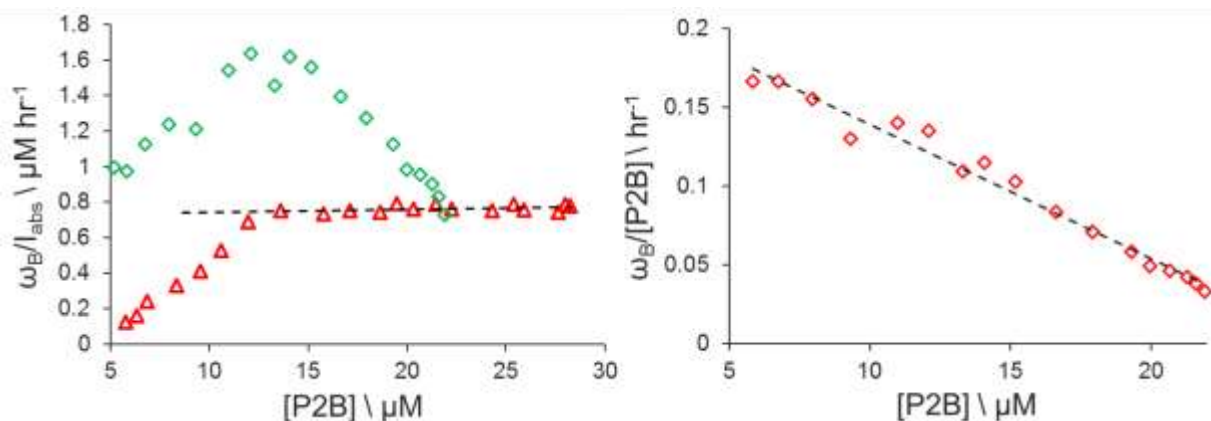


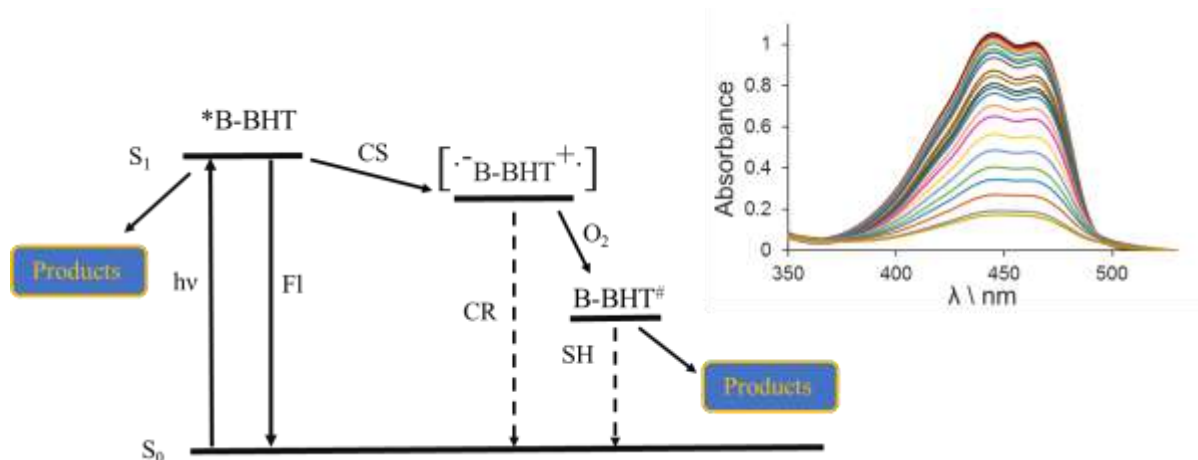
Figure 8.7 Left, the bleaching rate plotted against concentration for P2B in butyronitrile (Δ) the fit is the pseudo-zero order rate, and benzonitrile (\diamond) and right, the fit to the autocatalytic equation for the bleaching in benzonitrile.

Solvent	ϵ	Φ_f	$k_0 / \mu\text{Mh}^{-1}$
Benzonitrile	26	0.65	1.5
Butyronitrile	20.7	0.35	0.78
Acetone	20.7	0.23	0.75
Acetonitrile	37.5	0.17	0.64
DMF	36.7	0.06	0.60

Table 8.2 - Pseudo-zero order bleaching rate of P2B in polar solvents, bleaching rate is correlated, although non-scaling, with fluorescence yield. Rates for P1B followed the same pattern.

The rate of photobleaching correlates with the fluorescence yield although the variation is quite small, as for the parent molecule no coloured product is seen which is demonstrated in scheme 8.3. The rates vary from 0.78 $\mu\text{M hr}^{-1}$ in butyronitrile to 0.60 $\mu\text{M hr}^{-1}$ in DMF which is a small variation, but the fluorescence yield varies 6-fold over that range. With a k_0 of 1.5 μMh^{-1} the case of benzonitrile stands out from the other polar solvents in that both the bleaching rate and fluorescence yield are elevated. The pseudo-zero order fit here is not so satisfactory and it is seen that there is an initial increase in the rate followed by plateauing and then a decrease in the rate. The shape of rate vs concentration profile is reminiscent of that expected for an auto-catalytic process as described in previous chapters. The data can then be fitted to the autocatalytic equation encountered in Chapter 3, yielding $k_1 = 0.042 \text{ h}^{-1}$ and $k_{ac} = 0.0085 \mu\text{M}^{-1}\text{h}^{-1}$. Compared to the other polar solvents, the results in benzonitrile are anomalous but we can begin to understand this by recalling the solvent-chromophore stacking seen in Chapter 6 between toluene and TM-BOPHY, it is reasonable to assume that there might be some stacking between the phenyl ring of benzonitrile and the BOPHY core of the CQCs. If the solvent and chromophore are stacked then the CQC will be in the extended conformation so that the BHT quenching unit will not be in contact with the core and hence the fluorescence

is not significantly quenched. If the electron transfer process is switched off the proposed protection mechanism will also be switched off.



Scheme 8.3 – Outline of the fate of the CQCs following excitation to the S_1 state. The molecule may return unaltered to the ground state by radiative decay (FI), or bleached directly from the singlet excited state (BI), charge separation (CS) may occur followed by charge recombination (CR) again returning to the ground state unaltered. Reaction with O_2 leads to formation of the stable product $B-BHT^\#$ which can promote further bleaching or self-healing (SH). The inset shows the bleaching overlay in butyronitrile, no evidence of coloured products is seen.

Scheme 8.3 outlines an explanation of the bleaching behaviour. Absorption of photons by the BOPHY core leads to the excited state relaxing to populate the radical ion pair after electron transfer from BHT to BOPHY. Recombination of the geminate ion pair will restore the ground state. However the irreversibility of the electrochemistry infers that some small fraction of the BHT group must be chemically transformed on oxidation. The most probable explanation for escape from the recycling step is that the phenoxyl proton is lost from the BHT π -radical cation, leading to formation of an oxy-radical. The remaining BOPHY anion can be re-oxidised by molecular oxygen to restore the BOPHY part of the dye.

8.3.2 NMR spectroscopy for P1B

The bleaching mechanism for the CQCs is likely to differ from that seen for TM-BOPHY and escape from the charge recombination cycle is implicated as a key step. Our understanding is that the attached BHT anti-oxidant is the first part of the molecule to undergo chemical change. Unfortunately, this modification does not affect the absorption spectrum, which is dominated by the BOPHY chromophore. In an effort to monitor loss of the BHT unit, the bleaching reaction was followed by NMR spectroscopy in Figure 8.8, for P1B in a concentrated solution of acetone- d_6 .

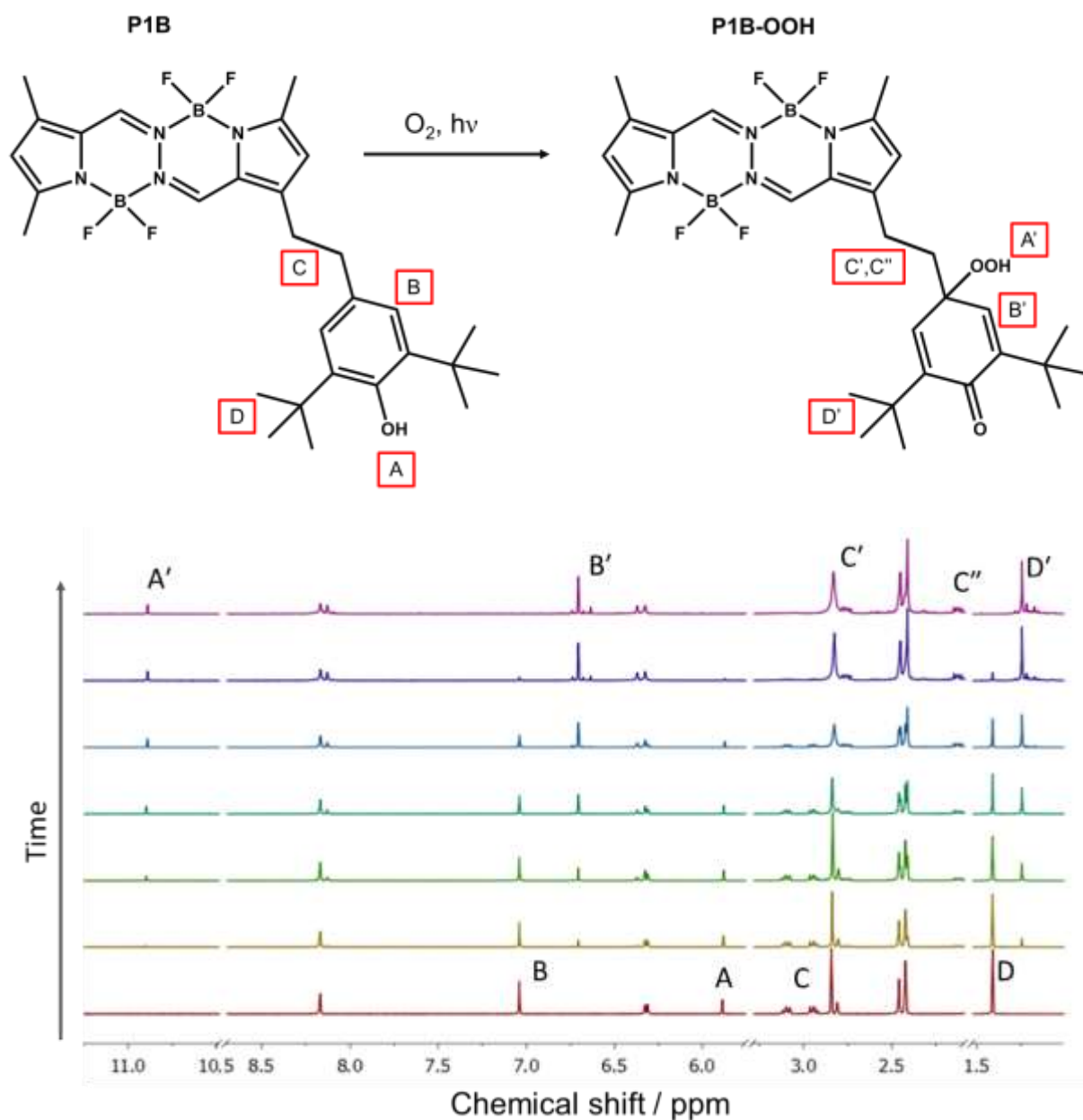


Figure 8.8 – Conversion of P1B to the hydroperoxide radical. Lettering on the diagrams is that used in the description of the reaction, sections for protons A & B are magnified 5 times for clarity.

The conversion from P1B to an intermediate species over a few hours of illumination is relatively clean. Most of the chemistry is related to the BHT moiety as expected. Proton [A] from the hydroxyl group is lost whilst a peak emerges at the same time that is shifted downfield to 10.9ppm, a shift of 5ppm. Protons from the phenyl group [B], the covalent linker [C] and the tertiary-butyl group [D] all show upfield shifts ranging from 0.15 to 0.8 ppm. This agrees with the formation of a 4-hydroperoxycyclohexa-2,5-dien-1-one ring. Mass spectroscopy, seen in Figure 8.9, shows an m/z peak at 611 which matches the $[M+Na]^+$ ion and the corresponding fragment pattern, a full spectrum of the material is given in Appendix 3. The conversion to P1B-OOH is selective, at modest conversion, with a 90% yield. As reaction continues, the

conversion drops to a 70% yield when all the starting compound is consumed. The fact that the intermediate formed is reactive explains the fact that the yield drops with conversion. Indeed, before full conversion is achieved bleaching of the BOPHY chromophore begins to take place. Minimal damage to the BOPHY part of the molecule is recorded during the initial phase of the reaction, which chimes with what is seen in the optical spectroscopy. After extended exposure, there is formation of multiple peaks and general broadening indicating that many breakdown products are formed.

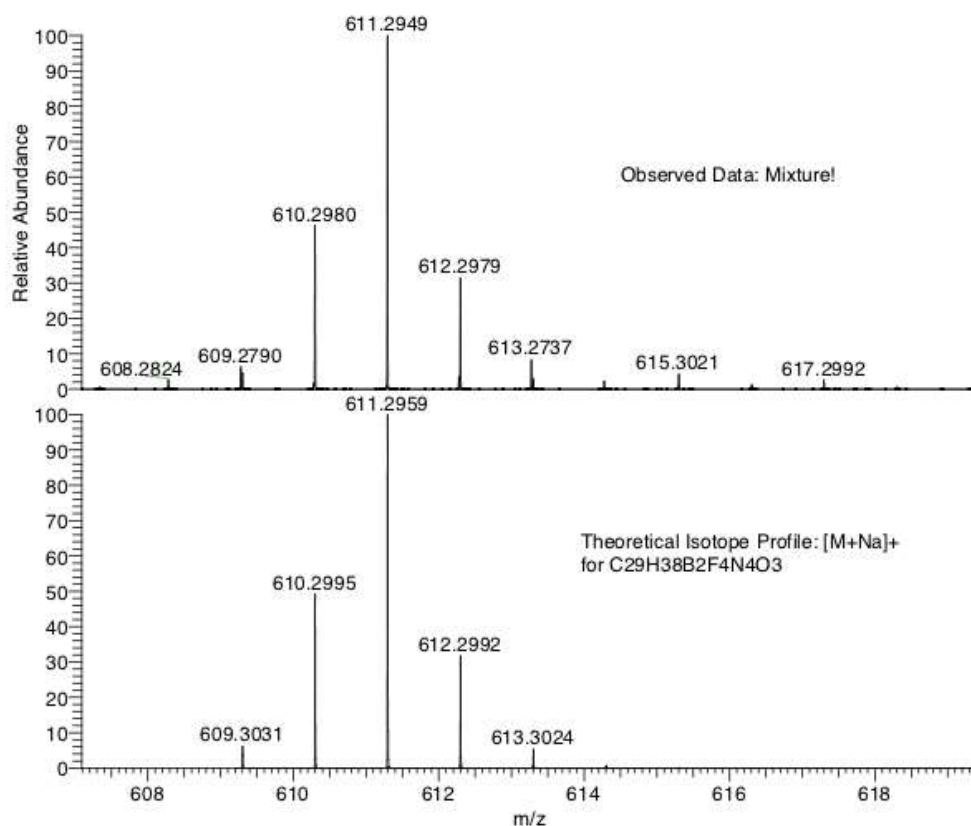


Figure 8.9 – ESI Mass Spectroscopy of the intermediate. The data (top) is a good match to the predicted pattern (bottom)

8.3.3 Photobleaching in Non-Polar Solvents

The photophysical properties of TM-BOPHY were shown to be essentially independent of solvent polarity and this was reflected in the photostability where only the specific interaction with toluene showed a unique photostability. In other solvents, biexponential kinetics were seen. The CQCs exhibit much more pronounced sensitivity to the nature of the solvent because of the conformational distributions and the intramolecular light-induced charge transfer. The latter route is unlikely to occur in non-polar media because of thermodynamic factors. This situation provides an opportunity to examine the photostability in non-polar environments. Cyclohexane was chosen as the initial solvent and photobleaching studies

were carried out with P1B and P2B and with TM-BOPHY as a control. The bleaching kinetics in Figure 8.10 recorded for the CQCs quickly deviate from that seen for the control.

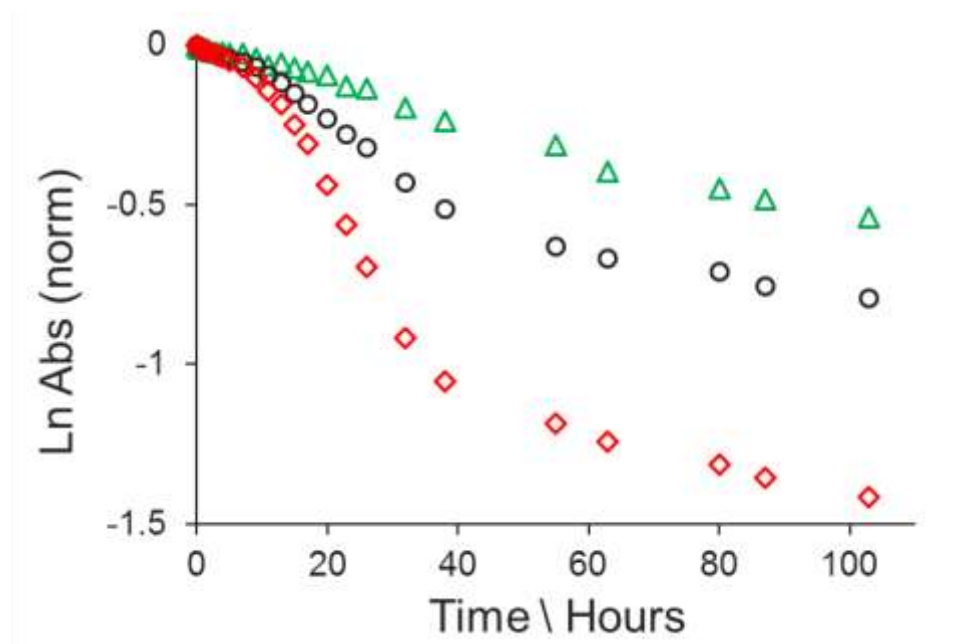


Figure 8.10 - Photobleaching of TM-BOPHY (Δ), P1B (\circ), & P2B (\diamond) in cyclohexane.

The kinetics for photobleaching of the control compound were well explained as dual-exponential processes, as reported before. Specifically, the bleaching chemistry involves successive first-order steps. The bleaching behaviour is more complicated for the CQCs. An initial fast rate was seen for all three compounds followed by a somewhat slower step. Unlike with the control compound, the CQCs showed a subsequent acceleration of the rate of bleaching. The BHT units apparently catalyse the photodegradation and a sigmoidal shape is realised.

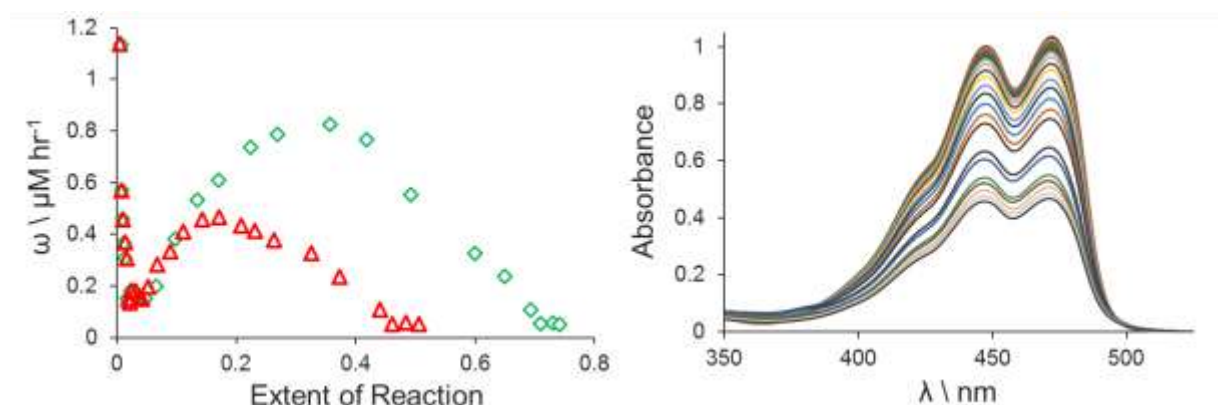
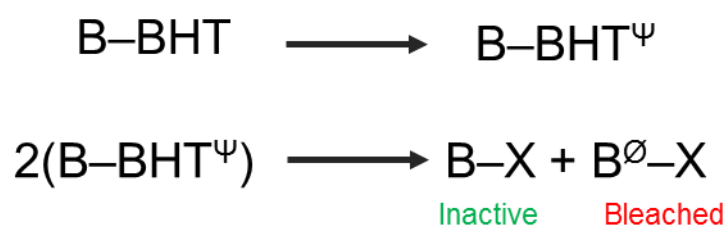


Figure 8.11 – Left, the extent of the photodegradation plotted against bleaching rate in cyclohexane for P1B (Δ) and P2B (\diamond). Right, overlaid bleaching spectra for P1B demonstrates that there are no spectral changes over the course of bleaching.

Photobleaching in cyclohexane proceeds at a relatively fast rate under conditions where light-induced electron transfer is unlikely. As was seen in polar solvents, the CQCs bleach without formation of a product absorbing in the visible region although a minor amount of UV build-up is seen for P2B. The initial fast part of the bleaching is found for both CQCs and this fits to first-order kinetics with rate constants of $k_1 = 0.015$ and 0.008 h^{-1} for P1B and P2B, respectively. For P2B, this first-order behaviour lasts significantly longer, around 7 hours, compared to 2 hrs in P1B. From this observation it is inferred that the BHT plays an important part in the bleaching process. This initial first-order reaction has no apparent effect on the spectral profile of the CQCs. After this initial reaction, an increasing rate is observed that slows until a semi-dormant phase is entered. In Figure 8.11, when the rate is plotted against fraction converted the majority of the profile is described by a parabola indicating autocatalytic bleaching as was seen for P2B in benzonitrile. The parabola is more exaggerated in this case. It can be seen in the overlay (Figure 8.12) that a large proportion of the compound remains when the illumination was ended. The bleaching rate was seen to decrease without fully coming to a halt. Particularly notable is the fact that a greater proportion of the P2B compound was bleached before entering the dormant phase than is seen for P1B. Since the only difference is the number of BHT moieties this strongly implies that the stoichiometry of the reaction with reference to BHTs is key. For P1B it is at around 50% conversion that this phase is reached while for P2B 75% bleaching is seen at this point. Exposure of P1B to light results in conversion to a product whereby the anti-oxidant moiety has been chemically altered. The chemically modified form is designated B-BHT Ψ but optically we cannot distinguish it from B-BHT. Two of these new products can then react together which bleaches one of the chromophores, this product is denoted B \emptyset -X, and leaves the second chromophore intact but with the BHT now inactive, denoted B-X. This leaves 50% of the chromophore intact which is now in some form that is stable compared to the initial CQC (Scheme 8.4). This scheme represents a unique form of self-healing or self-stabilisation whereby some of the chromophores enter into a sacrificial reaction to allow the formation of stable products.

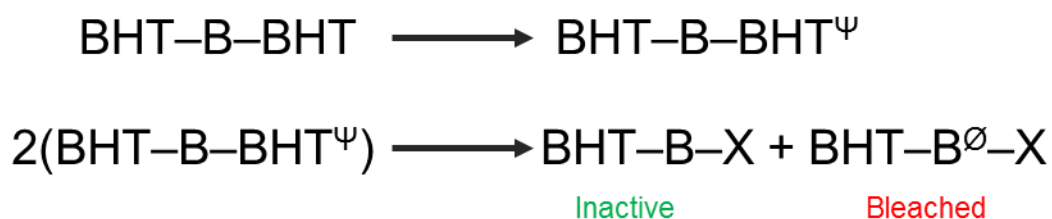


Scheme 8.4 - Reaction accounting for the observed 50% consumption of the P1B.

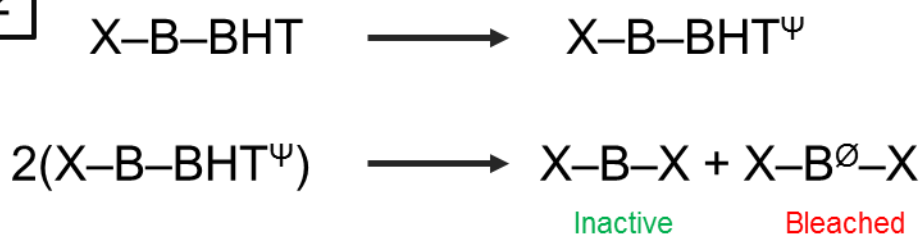
By this same logic, we can then account for the extent of bleaching of P2B. Now, the BHT units can be modified sequentially and therefore P2B is able to enter twice into a reaction

whereby a bleached and an inactive chromophore result. This would then mean that 75% of the chromophore is lost (Scheme 8.5). If synthesis of CQCs with further BHT groups were feasible then presumably a stoichiometry with 4 units would result in a 94%, i.e. near total, loss of chromophore before this dormant region is entered.

1



2



Scheme 8.5 – The successive bleaching mechanisms invoked for P2B, step 1 can account for 50% loss of the chromophore while the second step account for the loss of 50% of the remaining chromophores.

While TM-BOPHY needs a specific bimolecular reaction between two BOPHY molecules, the CSCs seem to bleach via a mechanism where a reactive product is first formed. In toluene it was seen that stacking with the solvent is able to inhibit the bleaching of TM-BOPHY for a long time until enough product has accumulated. Given that the mechanism is different for the CSCs, no inhibition period is expected in toluene solutions. Given that the BHT units should be well solvated in toluene it is not expected that the units will disrupt the chromophore-solvent stacking. Figure 8.12 shows that the bleaching proceeds rather rapidly in toluene compared to cyclohexane, again showing a form of auto-catalytic behaviour but crucially we do not see the inhibition period of TM-BOPHY. An intramolecular bleaching mechanism is still preferred in toluene. As for polar solvents and cyclohexane, no coloured product is seen and global analysis was used to quantify the bleaching rate. Similar extents of bleaching were seen as for in cyclohexane.

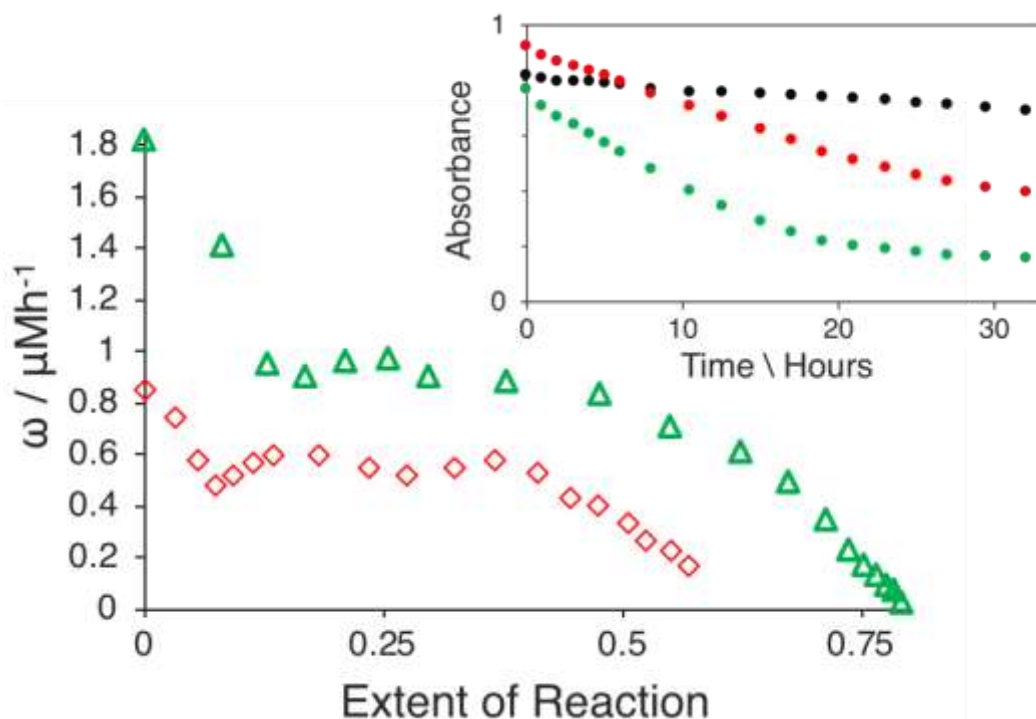


Figure 8.12 – Bleaching rate plotted against extent of reaction for the CQCs in toluene, Inset shows the bleaching kinetics of TM-BOPHY control (●), P1B (◇) and P2B (△) in toluene.

8.3.4 Quantum Yield of Photobleaching

In single-molecule fluorescence microscopy it is possible to count the number of photons emitted by a molecule before it is degraded and no longer emits^[24]. This protocol is averaged over a large ensemble of molecules. This is akin to a quantum yield for photobleaching. To be able to compare different chromophores under different conditions we need to establish a quantum yield for bleaching i.e. $\#molecules\ degraded / \#photons\ absorbed$. As the bleaching kinetics in all media are complex, the quantum yield is time dependent, but we can still estimate an initial bleaching yield. A weakly focussed, high-powered LED centred at 390nm with a luminous power of 2.1W was used to illuminate the sample. The absorbance is measured over time so we can integrate the number of photons absorbed over time and then the number of molecules lost per photon absorbed. Yields were estimated in acetonitrile and cyclohexane and fresh samples of P2B were bleached until around 80% of the material remained. The derived initial quantum yields for photobleaching are as follows:

$$\text{CH}_3\text{CN}, \Phi_{\text{bleach}} = 0.1 \times 10^{-6}$$

$$\text{C}_6\text{H}_{12}, \Phi_{\text{bleach}} = 0.2 \times 10^{-6}$$

8.3.5 Photobleaching in a Solid Medium

Practical outlets for organic chromophores are likely to involve the dyes present in the solid state. Such systems can be modelled easily by using thin films of the chromophore cast from solutions containing a large concentration of a polymer such as poly(methylmethacrylate) (PMMA). Here, the CQCs and a control sample of TM-BOPHY were dispersed in cast PMMA films using the method described previously. The films were subjected to broadband illumination under fixed conditions. The absorption spectra recorded for the CQCs in these PMMA films showed no evidence for aggregation of the dyes. The dielectric constant of PMMA is low so we do not expect there to be light-induced intramolecular electron-transfer under these conditions. Indeed, the fluorescence lifetime of all three emitters is around 2.7ns implying that, at low concentration at least, the fluorescence quantum yield is unquenched. As in solution, the CQCs were seen to bleach with a loss of colour across the spectral range but without evidence for formation of a product with significant absorption in the visible region, demonstrated in Figure 8.13. The figure shows that bleaching kinetics in the films are different again to the solution-based studies. Both P1B and P2B bleach by way of biexponential kinetics but at rates significantly different to that seen for TM-BOPHY where auto-catalysis occurs. When adjusted for photon absorption, the fast rate accounts for 12% of the total bleaching for both materials with k_1 values of around 0.5h^{-1} . The residual signal bleaches with a first-order rate constant of ca. 0.005h^{-1} , the rates are compiled in Table 8.3.

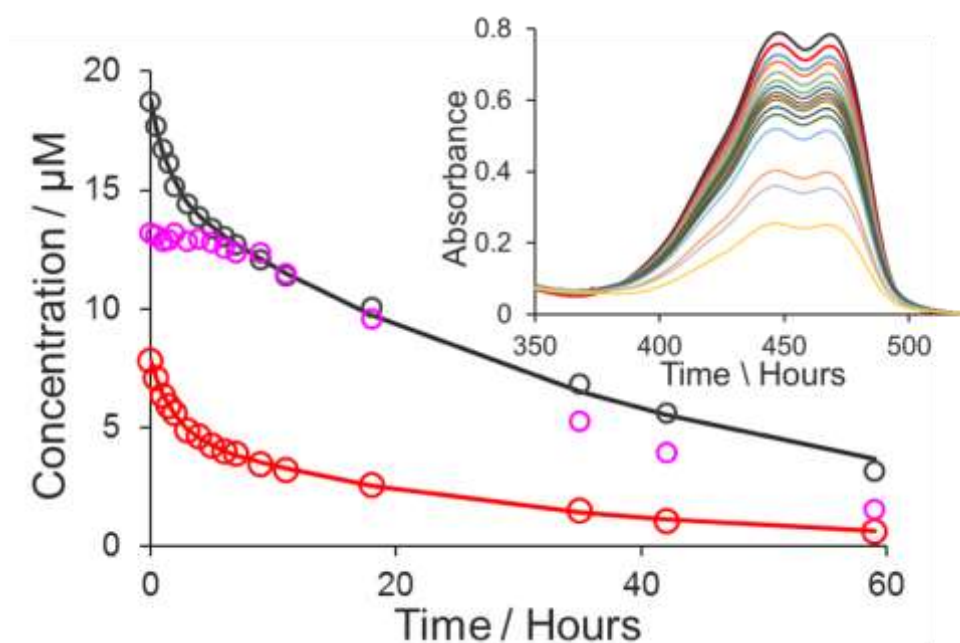


Figure 8.13 – Bleaching of P1B (○), P2B (△) and TM-BOPHY (○), exposed simultaneously in PMMA matrix, the inset shows the sequential bleaching overlay of P1B, demonstrating that no coloured product develops.

Material	A1	$k_1 \setminus h^{-1}$	A2	$k_2 \setminus h^{-1}$
P1B	20.6	0.63	79.4	0.024
P2B	39.3	0.51	60.7	0.035

Table 8.3 – Bleaching rates for the CQCs in PMMA films.

8.4 Effects of additives

A common practice used to identify putative mechanisms for the photobleaching of chromophores and/or substrates relies on the addition of specific additives intended to trap selected intermediate species. The singlet oxygen scavenging^[40, 41] property of 1,4-diazabicyclo[2,2,2]octane (DABCO) is well-known although it can also act as an anti-oxidant. From the photobleaching results and the confirmation provided by the NMR spectroscopy we have implicated an O-centred radical as being the key to the process. 5,5-Dimethyl-1-Pyrroline-N-Oxide (DMPO) is commonly used as a spin trap^[42] in EPR spectroscopy and it was considered that this substrate might be able to intercept the radical in our systems. These two agents were added at 1mM concentration to air-equilibrated solutions of P2B in acetonitrile prior to illumination.

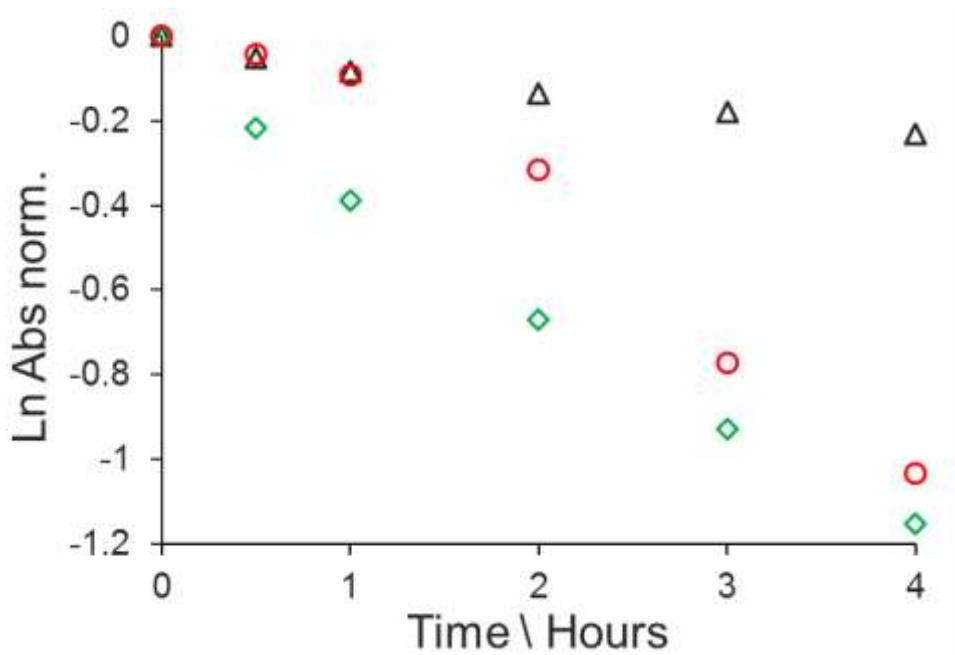


Figure 8.14 – Photobleaching of P2B in acetonitrile, control (Δ), DABCO (◇) and DMPO (○).

Addition of the DABCO has no inhibitive effect and is seen in Figure 8.14 to greatly accelerate the rate of bleaching. In contrast, DMPO seems to have some initial benefit but catalyses the bleaching as some new product is formed. Presumably DMPO intercepts the phenoxy radical to form a reactive product. To confirm the effect, DMPO was added at higher concentrations.

In Figure 8.15 it is shown that at 10mM the inhibition period increases 2.5-fold while at 40mM the sample remained protected. Using a radical scavenger is an effective means to provide temporary protection to the substrate but high concentrations are required and ultimately products formed may destroy the chromophore.

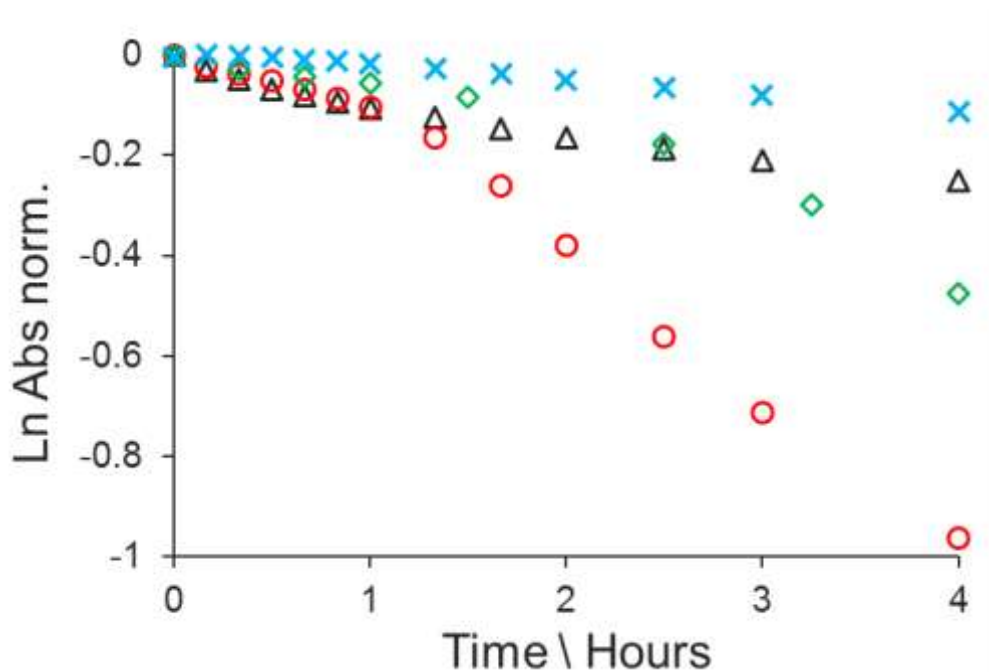


Figure 8.15 – Concentration effect of adding DMPO to P2B in acetonitrile solutions, control (Δ), 1mM (○), 10mM (◇) and 40mM (X).

The presence of DABCO was found to cause dynamic fluorescence quenching for the CQCs. At a concentration of 0.1M, transient absorption spectroscopy shows the radical anion is quenched to the ground state in acetonitrile while without DABCO the lifetime of this transient species is around 300ns. Under these conditions, intramolecular charge transfer is superseded by intermolecular light induced electron transfer between BOPHY and DABCO. Stern-Volmer plots are given in Figure 8.17 for addition of DABCO to P1B in acetonitrile and also in DCM were linear. In acetonitrile the fluorescence lifetime is not well defined, so it is not possible to find if the quenching is truly diffusion controlled but this was found to be the case in CH₂Cl₂ solution.

The radical ion products formed from the bimolecular quenching event recombine quickly as shown by the transient spectroscopy in Figure 8.16, without separation so that protection against photodegradation will be provided, as outlined in Scheme 8.6. However, this comes with the penalty of significant fluorescence loss and requires an unrealistically high concentration of DABCO. At concentrations where the fluorescence is essentially unquenched, even on very short timescales, no photostability is provided

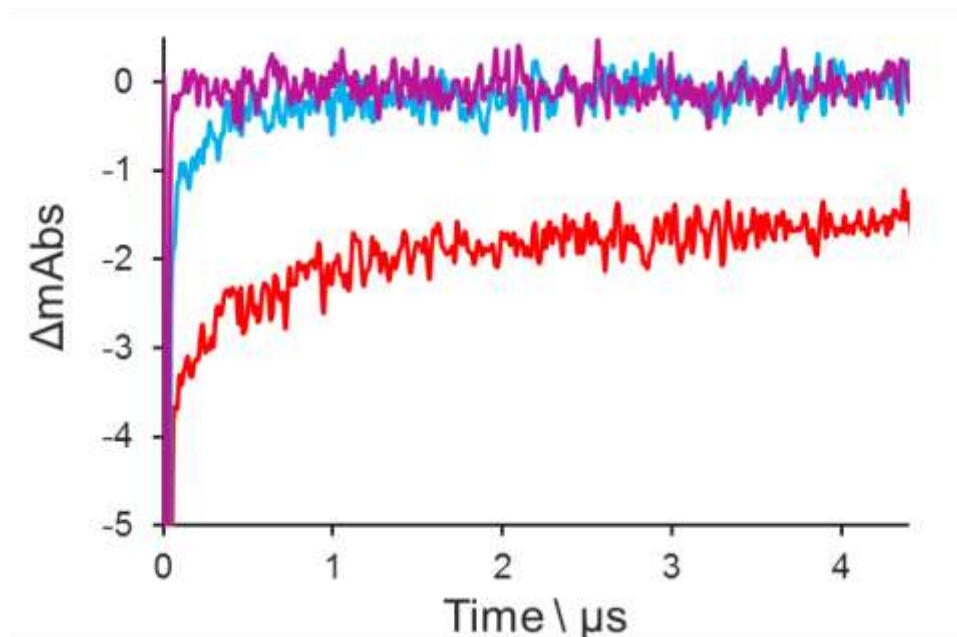
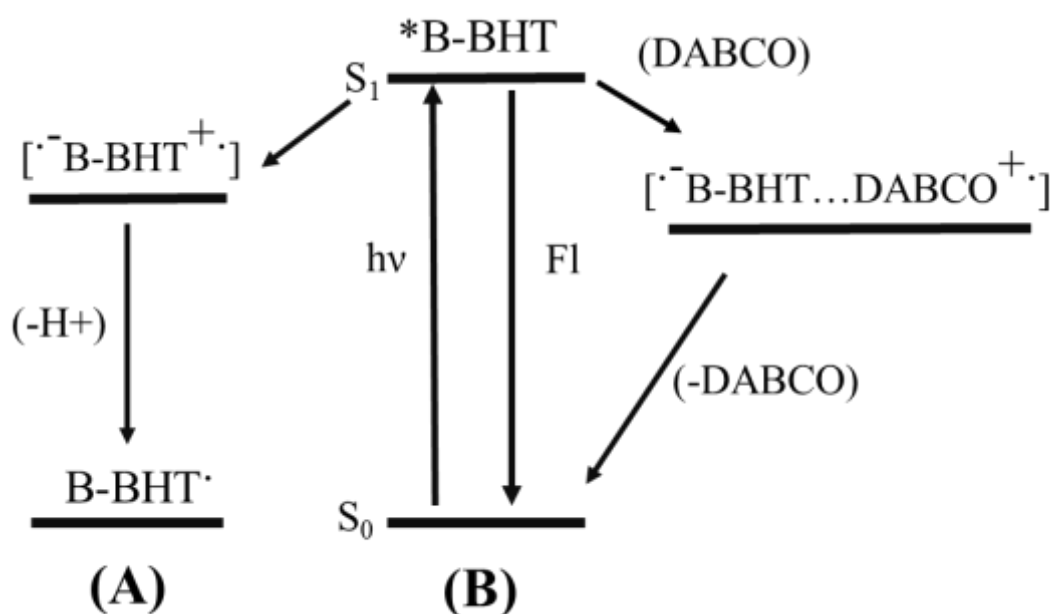


Figure 8.16 - Transient spectroscopy showing the ground state bleach of P2B in DCM (—), MeCN (—), and MeCN with 0.1M DABCO (—), (excitation at 355nm), showing the existence of a small amount of meta-stable BOPHY anion, in MeCN the anion has a lifetime of around 300ns. With DABCO added the charge separated state is quenched immediately.



Scheme 8.6 – Addition of DABCO leads to quenching of the excited state by electron transfer to the DABCO, the ion pair then returns to the ground state. Path (A) can lead to bleaching while path (B) allows the chromophore to be recycled

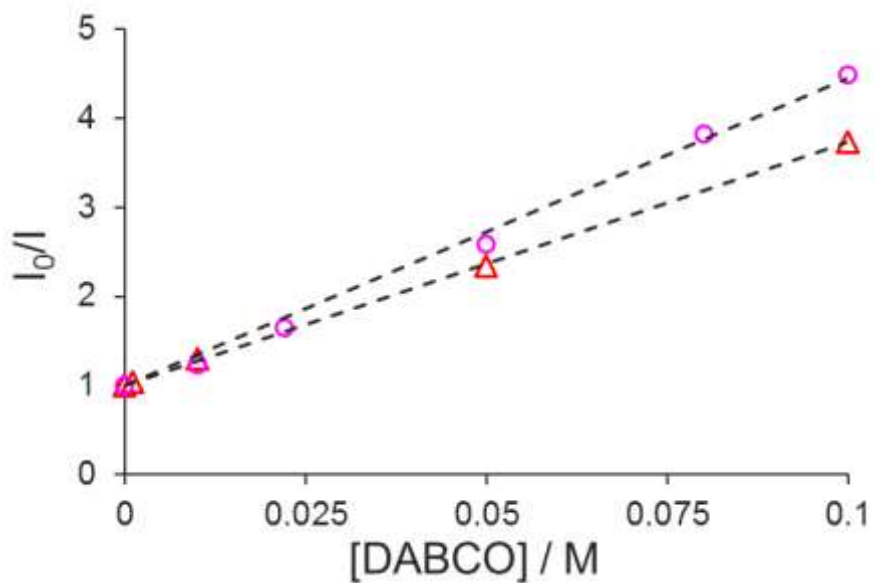


Figure 8.17 – Stern-Volmer plot of the quenching of P1B fluorescence in DCM (●) and CH₃CN (▲) by DABCO, over the limited concentration range studied the relationship is linear, the derived rate is $10^{10} \text{ M}^{-1}\text{s}^{-1}$ so the mechanism is diffusion controlled.

8.5 Properties of Condensed P1B

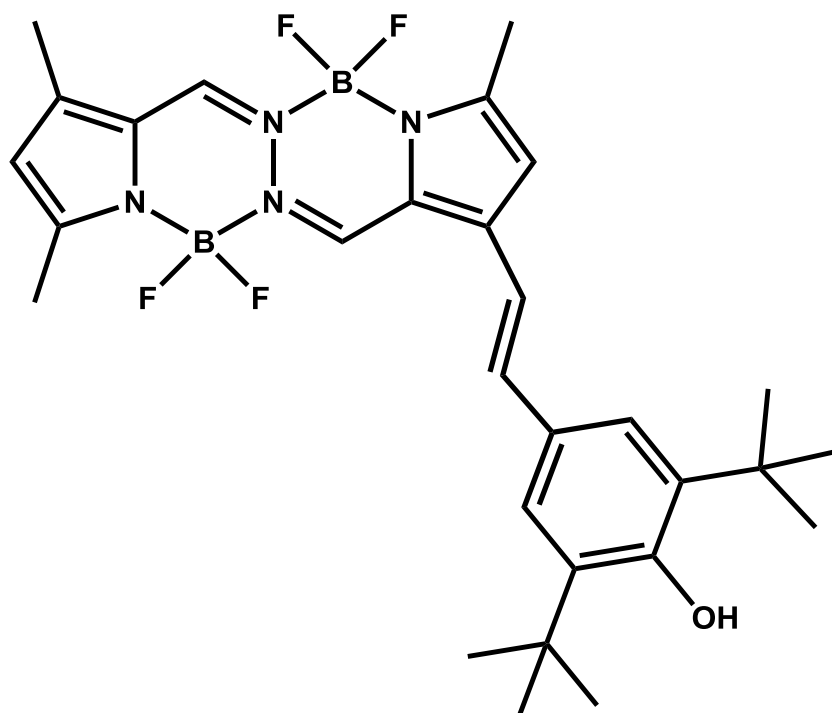


Figure 8.18 - Structure of the condensed precursor to P1B, made with reference to figure 9.1.

To assist understanding of the non-conjugated systems a brief study was undertaken of the conjugated derivative, the structure being given in Figure 8.18, used to synthesize P1B. The effect of conjugation is apparent with the absorption maximum being red-shifted by around 80nm. The compound showed poor solubility, particularly in polar solvents. This situation is illustrated in Figure 8.19 where the absorption profile in DMF is dominated by high energy aggregates. Figure 8.19 shows that the fluorescence yield is seen to decrease across the range of solvents (Figure 8.19), suggesting weak charge transfer character. The change in dipole moment is approximately twice that found for P1B, although only a limited selection of solvents was possible. The time-resolved measurements are adequately described by a single exponential for the fluorescence decay in both cyclohexane and acetonitrile. Photobleaching of the condensed P1B was performed in acetonitrile and found to proceed rapidly. The compound is lost, and a product forms that has a broad spectrum lacking fine structure. The product has a similar profile to that seen for the aggregates in DMF, seen in Figure 8.20, suggesting that the photo-product undergoes self-association to a relatively photo-stable species. This adds to the understanding of the situation of the CQCs in polar solvents as it demonstrates that the BHT unit is not well solvated favouring the conformation that allows electron transfer

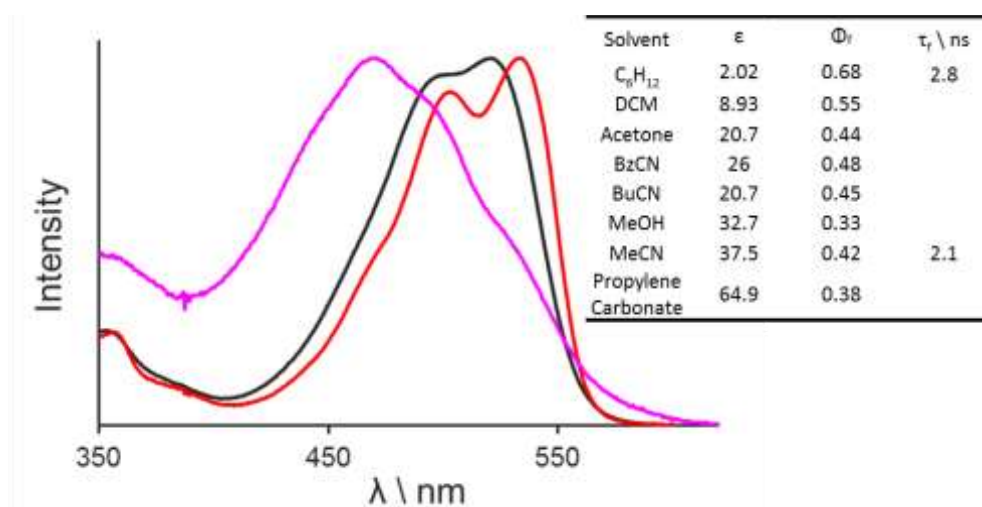


Figure 8.19 – Absorption spectra of condensed version of P1B in Cyclohexane (—), CH₃CN (—) and DMF (—). The table shows the fluorescence quantum yield variation with solvent which follows a clear trend demonstrating that the conjugation and quenching, presumably by electron transfer.

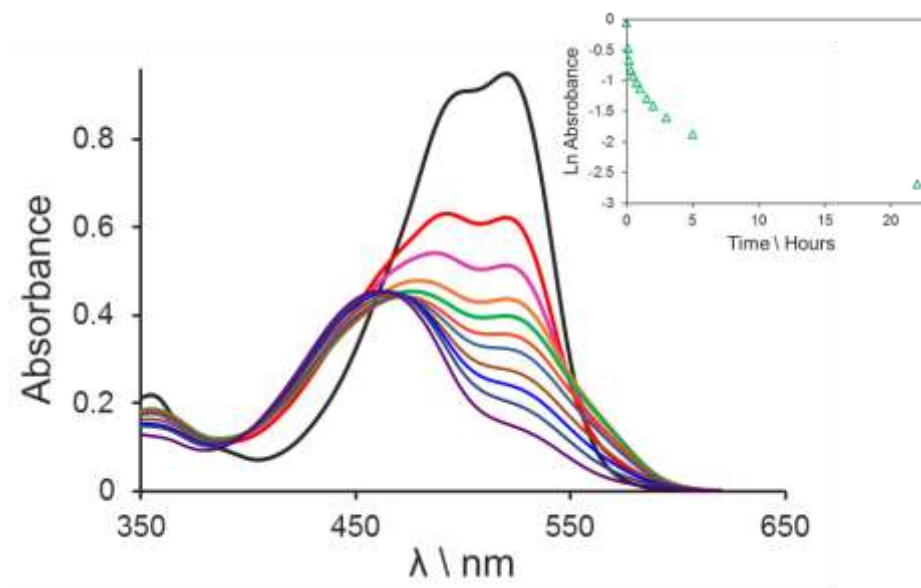
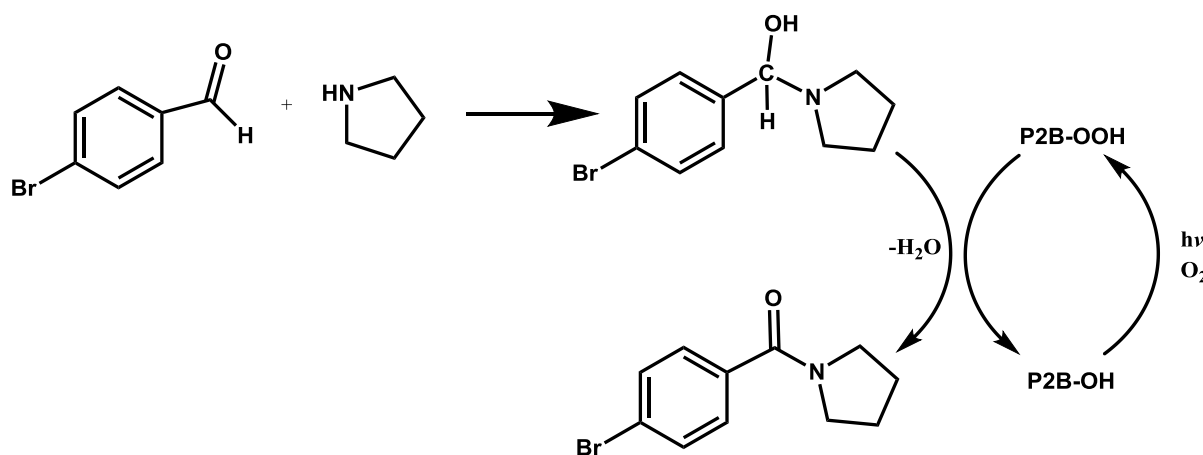


Figure 8.20 - Bleaching overlay of P1B Condensed in acetonitrile, the inset shows loss of chromophore at 530nm.

8.6 - CQC as a Photocatalyst

These CQC derivatives present an opportunity to create organic hydroperoxides that could be useful as photocatalysts for organic transformations. This possibility was explored using the BHT-OOH species to promote amide synthesis by reaction between an aldehyde and an amine. The intention is to use the hydroperoxide to oxidise the intermediate hemiaminal^[43]. Direct amidation of aldehydes by such sensitizers allows the elimination of metal-containing catalysts or hazardous reagents and in principle could be powered by sunlight giving them strong 'green' credentials. The proposed reaction is outlined in Scheme 8.7.



Scheme 8.7 – Outline of the proposed amidation reaction performed using P2B as the catalyst.

The photobleaching method was employed in the presence of 4-bromobenzaldehyde and pyrrolidine with 1 mol% P2B as the catalyst. The product was identified as (4-bromophenyl) (pyrrolidi-1-yl)methanone. In acetonitrile, only 5% conversion was achieved before the stock of P2B was bleached. Changing the solvent to 1,4-dioxane increased the yield to nearly 50% relative to the starting aldehyde. An excess of pyrrolidine leads to heightened bleaching of P2B so yields are lowered. From absorption and fluorescence spectroscopy it is seen that depletion of P2B is the cause of the premature end of reaction. Increasing the amount of photocatalyst to 2 mol% leads to total consumption of the starting material in 24hr and with 75% selectivity for the formation of the product (Scheme 8.7) as determined by NMR spectroscopy. Creation of *in-situ* hydroperoxides could have many applications.

Separately, the CQCs were shown to act as photo-initiators for the radical polymerisation of methyl methacrylate to render a clear plastic as seen in Figure 8.22. Additionally, the CQCs have been shown to be effective at removing NIR-absorbing dyes from solution such as Chlorophenol Red and Indigo by selective illumination of the CQC. This demonstrates the potential to photochemically remove dyes that have been previously used as disinfectants or for the removal of toxic waste.



Figure 8.22 – PMMA photo-polymerised in the presence of P2B which itself is bleached to leave a clear solid. Conditions were not optimised.

8.7 Conclusion

The need for light-fast dyes with strong fluorescence has been fuelled by recent developments in the field of super-resolution microscopy. Fading of the chromophore under the microscope is exacerbated by the high photon densities, favouring two-photon absorption, and by the use of redox buffers in conventional biomedical screening. There appears to be an almost universal acceptance that photofading is the result of a long-lived triplet-excited state, even for chromophores known to be resistant to intersystem crossing. Ways to stabilise the chromophore are beginning to emerge, although these invariably target the triplet state. The two most popular stabilisation protocols involve adding an anti-oxidant and deactivating the triplet state by the presence of redox-active species. Mostly, the additives are separate from the chromophore such that quenching requires diffusional contact. Our approach has been to attach the anti-oxidant to the chromophore via covalent spacer groups. This strategy overcomes limitations imposed by diffusion but introduces new problems. These can be summarised as (i) light-induced charge transfer between chromophore and anti-oxidant and (ii) secondary reactions between damaged anti-oxidant and the chromophore.

Despite these issues, the new materials are useful in terms of mechanistic studies. In particular, we have been able to use NMR spectroscopy to identify a hydroperoxide as the intermediate species. It has also been possible to quantify the reaction stoichiometry and to account for the observed kinetics. This is a marked improvement over most other photobleaching studies.

The hydroperoxide is a key intermediate in the overall process and offers the opportunity to pursue alternative types of photochemistry. For example, organic hydroperoxides are used in many areas of chemistry as general oxidants and as oxidant catalysts. We have shown the utility of our peroxide as a catalyst for amidation of an aldehyde. Other transformations should be possible. It is likely that water-soluble forms of the CQC could be prepared for use in biological or medicinal applications. One obvious advantage is the built-in propensity for self-destruction after the sensitisation is complete.

References

- [1] S. C. Blanchard et al. *Chem. Soc. Rev.* **2014**, 43, 1044-1056.
- [2] P. Tinnefeld et al. *ChemPhysChem.* **2010**, 11, 2475-2490.
- [3] D. Axelrod, *J. Cell Biol.* **1981**, 89, 141-145.
- [4] M. J. Rust, M. Bates, X. W. Zhuang, *Nat. Methods*, **2006**, 3, 793-795.

- [5] P. Holzmeister, A. Gietl, P. Tinnefeld, *Angew. Chem. Int. Ed.* **2014**, 53, 5685-5688.
- [6] M. Levitus, S. Ranjit, *Q. Rev. Biophys.* **2011**, 44, 123-151.
- [7] S. C. Blanchard et al. *Photochem. Photobiol.* **2014**, 90, 448-454.
- [8] M. Schlierf et al. *ACS Nano.* **2012**, 6, 6364-6369.
- [9] C. F. Calver, B. A. Lago, K. S. Schanze, G. Cosa, *Photochem. Photobiol. Sci.* **2017**, 16, 1821-1831.
- [10] P. Tinnefeld et al. *Angew. Chem. Int. Ed.* **2008**, 47, 5465-5469.
- [11] R. Dave, D. S. Terry, J. B. Munro, S. C. Blanchard, *Biophys. J.* 96, 2371-2381.
- [12] J. Widengren, *Abstr. Pap. Am. Chem. Soc.* **2007**, 234, 1.
- [13] E. A. Christensen, P. Kulatunga, B. C. Lagerholm, *PLoS One*, **2012**, 7, 8.
- [14] P. A. Bryon et al. *J Histochem. Cytochem.* **1993**, 41, 1833-1840.
- [15] P. Tinnefeld et al. *Phys. Chem. Chem. Phys.* **2011**, 13, 6699-6709.
- [16] R. Albertini, P. M. Abuja, *Free Radic. Res.* **1999**, 30, 181-188.
- [17] T. Cordes, J. Vogelsang, P. Tinnefeld, *J. Am. Chem. Soc.* **2009**, 131, 5018-5019.
- [18] V. Glembocyste, G. Cosa, *J. Am. Chem. Soc.* **2017**, 139, 13227-13233.
- [19] Jose L. Alejo, Scott C. Blanchard, Olaf S. Andersen, *Biophys. J.* **2013**, 104, 2410-2418.
- [20] S. C. Blanchard et al *Nat. Methods.* **2011**, 9, 68.
- [21] P. Tinnefeld, T. Cordes, *Nat. Methods.* **2012**, 9, 426.
- [22] T. Cordes et al. *Nat Commun.* **2016**, 7, 10144.
- [23] S. C. Blanchard et al. *Photochem. Photobiol. Sci.* **2016**, 15, 196-203.
- [24] S. C. Blanchard et al. *J. Phys. Chem. Lett.* **2012**, 3, 2200-2203.
- [25] L. Song, C. A. Varma, J. W. Verhoeven, H. J. Tanke, *Biophys. J.* **1996**, 70, 2959-2968.
- [26] P. G. Wenthold, D. A. Hrovat, W. T. Borden, W. C. Lineberger, *Science.* **1996**, 272, 1456-1459.
- [27] J. L. Audino, C. D. Geddes, *Biophys. J.* 104, 349a.
- [28] S. El-Molla, A. F. Mansour, A. E. Hammad, *J. Nanomater.* **2017**, 2017, 13.
- [29] L. Guo, F. Gai, *J. Phys. Chem. A*, **2013**, 117, 6164-6170.
- [30] O. Brede, H. Orthner, V. Zubarev, R. Hermann, *J. Phys. Chem.* **1996**, 100, 7097-7105.
- [31] B. Prakash, P. Singh, A. Kedia, N. K. Dubey, *Food Res. Int.* **2012**, 49, 201-208.
- [32] R. Kahl, H. Kappus, *Z. Lebensm. Unters. Forsch.* **1993**, 196, 329-338.
- [33] E. Turkan et al. *Spectrochim. Acta A*, **2011**, 79, 562-569.
- [34] Q. Huailme, A. Mirloup, P. Retailleau, R. Ziessel, *Org. Lett.* **2015**, 17, 2246-2249.
- [35] X.-F. Wang, S.-S. Yu, C. Wang, D. Xue, J. Xiao, *Org. Biomol. Chem.* **2016**, 14, 7028-7037.
- [36] A. Harriman, *J. Phys. Chem.* **1987**, 91, 6102-6104.
- [37] M. E. Michel-Beyerle et al. *J. Phys. Chem.* **1989**, 93, 5173-5179.
- [38] C. Wohlfarth, *Viscosity of the mixture (1) N,N-dimethylformamide; (2) diethyl malonate*, Vol. Springer Berlin, **2009**, 1641-1641.
- [39] A. H. Hamzaoui et al. *J. Chem.* **2015**, 2015, 12.
- [40] E. Lengfelder, E. Cadenas, H. Sies, *FEBS Lett.* **1983**, 164, 366-370.
- [41] S. Beutner, B. Bloedorn, T. Hoffmann, H. D. Martin, *Methods Enzymol.* **2000**, 319, 226-241.
- [42] G. R. Buettner, *Free Radic. Res. Commun.* **1993**, 19, S79-S87.
- [43] X. Liu, K. F. Jensen. *Green Chem.* **2012**, 14, 1471-1474.

Appendices

Appendix 1

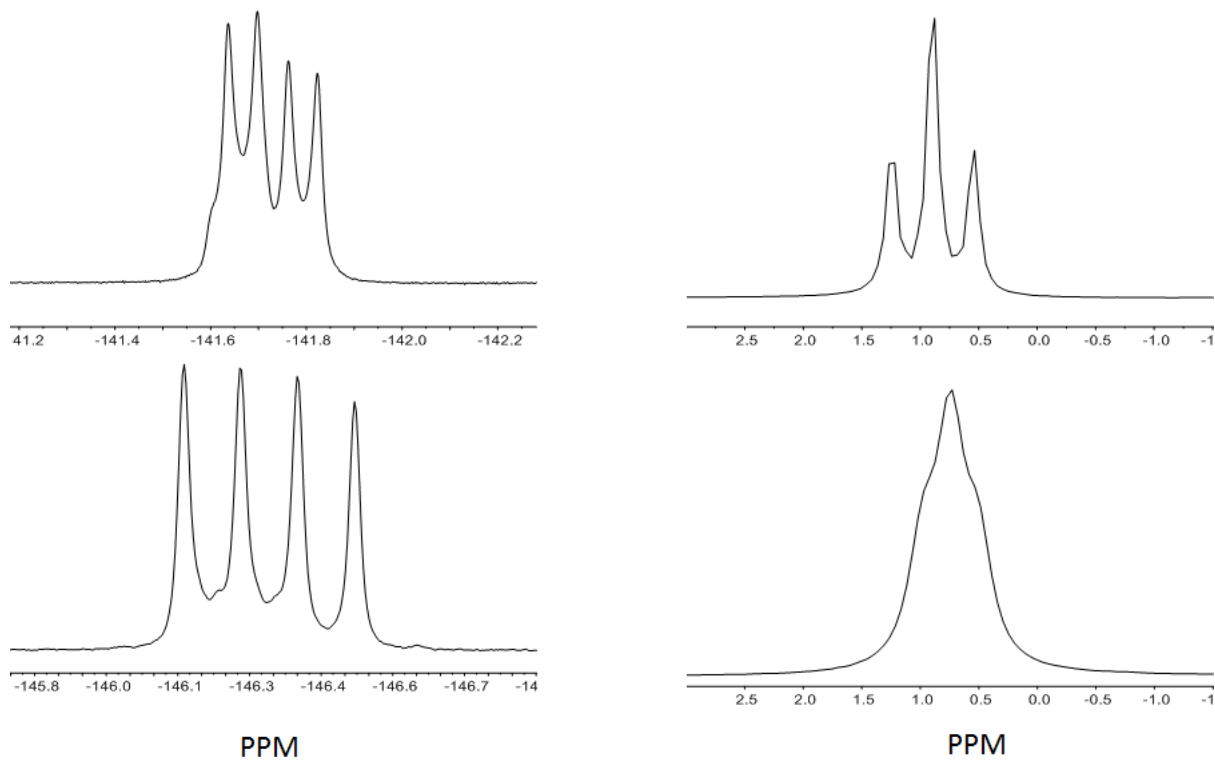


Figure A1.1 – Left upper panel shows the ^{19}F NMR for TM-BOPHY (upper) and a BODIPY (lower). Right shows the ^{11}B NMR, again for TM BOPHY (upper) and a BODIPY (lower). The specific BODIPY structure is shown below.

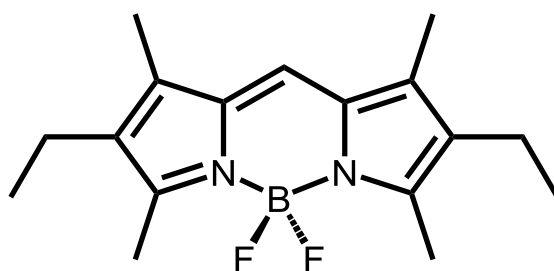


Figure A1.2 – BODIPY structure for which the NMR are compared to a similar BOPHY molecule. NMR were kindly supplied by Dr. Dumitru Sirbu (Newcastle University).

Appendix 2

<i>Solvent</i>	<i>[O₂] \ 10⁻³ M</i>
Acetone	2.4
Acetonitrile	1.9
Cyclohexane	2.4
diethyl Ether	3.1
DMSO	0.46
Ethanol	2.1
Methanol	2.2
Toluene	1.8
Water	0.24

Table A2.1 - Oxygen concentration in some solvents used throughout these studies at 0.21 atm O₂.

Appendix 3

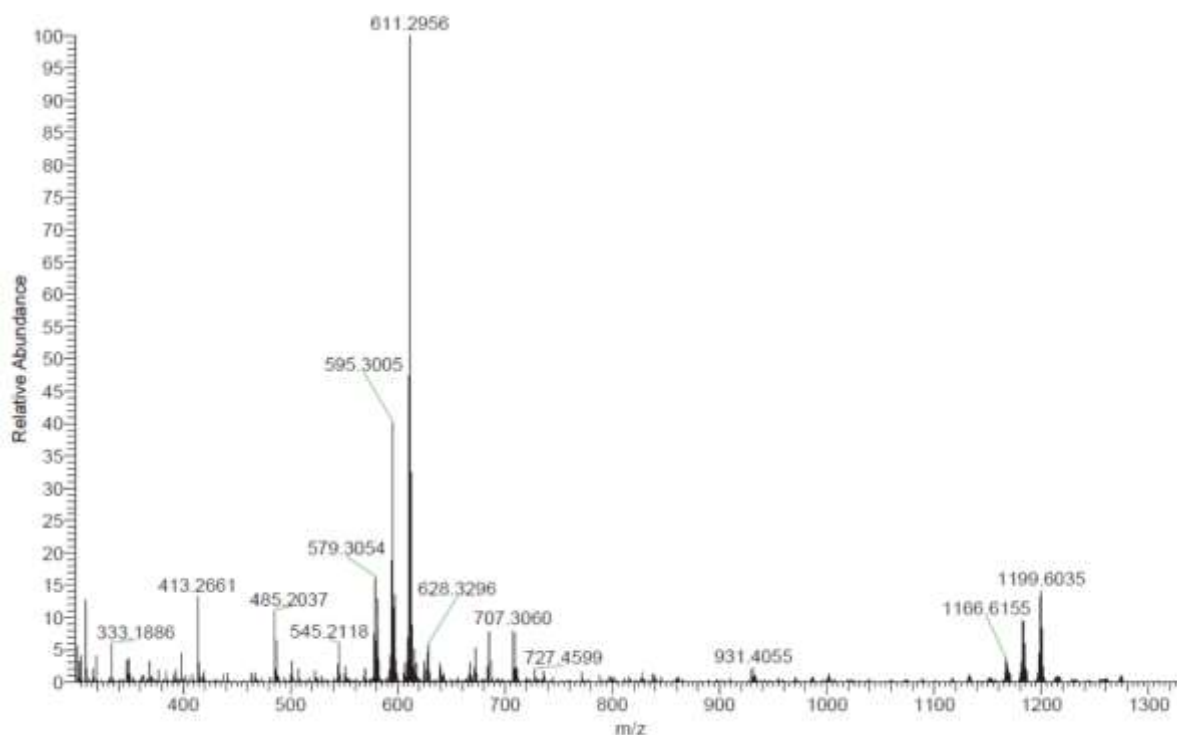


Figure A3.1 – Full mass spectrum for the P1B-OOH intermediate, the intermediate is the most abundant species at m/z of 611 while a significant amount of the starting material at 595 is seen.